The Use of Rocking Walls in Confined Masonry Structures: a Performance-Based Approach

A thesis submitted in partial fulfilment of the requirements for the

Degree of Doctor of Philosophy in Civil Engineering

at the University of Canterbury

BY

LUIS ALBERTO TORANZO-DIANDERAS

SUPERVISED BY

ATHOL J. CARR

JOSE I. RESTREPO

JOHN B. MANDER

University of Canterbury,

Christchurch, New Zealand

2002

Abstract

Excessive economic loss and large social impact, due to extensive damage and operational problems in aseismic structures, has been observed following recent earthquakes. This situation is leading to the formulation of a new design paradigm in seismic-engineering. Performance-based design, addressing life-safety, damage-control and functionality issues, is expected to supersede in the near future the current prescriptive serviceability/life-safety approach. In this context, the observed extent of damage in masonry structures, as a consequence of recent moderate and strong earthquakes, seems to disqualify this traditional material in a performance-based environment.

Masonry-structures with low density of lateral-force-resisting masonry-walls are among the buildings most likely to be damaged by moderate and strong earthquakes. The use of rocking walls is proposed here as an alternative to improve the seismic performance of these kind of buildings without having to give up the masonry as an integral part of the structure. It was found that rocking confined-masonry walls with hysteretic-energy-dissipators at their base can be reliably designed to match target drifts, which are closely correlated to the extent of the damage in a building. It is shown in this thesis that hysteretic-energy-dissipators can provide a reliable energy-dissipation source that allows the seismic design of this sort of structures with any of the new methodologies proposed to meet seismic performance-objectives.

A design procedure adapted from the Direct Displacement Method is developed in the core of this thesis. A prototype structure is designed with the proposed method and a reduced-scale model is built and tested dynamically in a shake table. The experimental results confirmed that rocking walls can be successfully adapted to confined masonry structures. A numerical analysis is also conducted here, with good matching of the experimental results, providing a new tool to deepen the understanding of this system.

Acknowledgements

I want to start acknowledging the welcoming and supporting environment that the Department of Civil Engineering, headed by Professor Andy Buchanan, offers to its students. This is something I had never experienced before and I guess has to do with the warmness of the kiwi people. Part of that encouraging environment were my supervisors, Dr. Athol Carr and Professor John Mander and my former supervisor Dr Jose Restrepo, to whom I also thank for their time, guidance and assistance in my work.

I am deeply thankful to the Ministry of Foreign Affairs of New Zealand that sponsored my studies through a NZODA scholarship. Without their financial support, it would have been impossible for me to carry on my studies here at Canterbury. Thanks to Dr. John Pickering for taking the difficult job of managing our scholarships as a determined but always encouraging advisor.

The idea of undertaking this piece of research was born after discussions with Dr. Jose Restrepo, on the way how we could contribute in a problem that had been observed in recent earthquakes in Peru with school-buildings over there. Although he moved to California before the conclusion of this thesis he has been involved in the research all the way through. I am especially thankful for his support.

The experimental work was an aspect of my work in which I needed a lot of support. All technicians that I met at the Structures Laboratory in the Civil Engineering Department were very supportive when help was needed. I deeply appreciate their help. Kevin Wines, John Maley and Stuart Toase were particularly close and involved with my work and my special thanks go to them.

I also should mention the support of my fellow graduate students that made my stay at the Department even more pleasant. Special thanks to Brian Adams, Caroline Francois, Tony Holden, Mathew Lander, Nagui Bishay-Girges, Baher Zaghlool, Dean Saunders, Guillaume Charton, Linus Lim, Hsueh Lyn, Jeff Matthews and Dong Ping. The friends that I do not mention here should know that this is an incomplete list. Only now I realise how many good friends I made here!

The support of my wife Tatiana here, the support of my parents, Luis and Rosa, my brother and sisters and all my family back in Peru, were perhaps more decisive than any other thing in the completion of my thesis. Without their encouragement to further my studies and look for new opportunities I would not have got here. Thanks a lot family.

Notation

a_{hi}	=	absolute horizontal acceleration at level i
A	=	area
A_{cc}	=	area of cross section of confining column
A_{ext}	=	total rectangular area enclosing hysteresis loops
A_{hl}	=	total area enclosed by a hysteretic loop
$A_{m\theta}$	=	area of cross section of masonry diagonal strut
B	=	base of rocking wall
C_1	=	correction factor for hysteretic loops due to non-perfect rigidity of dissipators
C_2	=	correction factor for hysteretic loops due to actual curved shape of dissipators
C_3	=	experimental correction factor for equivalent viscous damping
d_m	=	diagonal length of masonry infill
e	=	coefficient of restitution
E	=	modulus of elasticity
E_m	=	modulus of elasticity of masonry
E_{mo}	=	initial modulus of elasticity of masonry
E_{k1}, E_{k2}, E_{k3}	=	kinetic energy at stages 1, 2 and 3 respectively
E_{p1}, E_{p2}, E_{p3}	=	potential energy at stages 1, 2 and 3 respectively
E_{s1}, E_{s2}, E_{s3}	=	strain energy at stages 1, 2 and 3 respectively
f_1	=	compressive stress in masonry diagonal strut
f_2	=	tension stress normal to masonry diagonal strut
f_{cc}^*	=	design stress in confining column
$f_{m\theta}$	=	axial uniform stress in masonry diagonal strut
$f_{m\theta}^*$	=	design stress in masonry diagonal strut
$f'_{m\theta}$	=	compressive strength in masonry diagonal strut
f_d	=	diagonal compressive strength of masonry infill
f_{imp}	=	impact factor
f'_m	=	compressive strength of masonry
f_n	=	normal stress in masonry
f_p	=	lateral stress in masonry

f'_t	=	tensile strength of masonry
F_{cc}	=	axial force in confining column
F_{cc}^*	=	design axial force in confining column
F_h, F_v	=	horizontal and vertical forces at the base of a rocking wall
$F_{v\,imp}$, $F_{h\,imp}$	=	horizontal and vertical forces at the base of a rocking wall amplified by impact
$F_{m\theta}^*$	=	design axial force in masonry diagonal strut
$F_{m\theta}$	=	axial force in masonry strut
F_y	=	yielding force of hysteretic dissipators
g	=	acceleration of gravity (9.81m/s/s)
G_m	=	shear modulus of masonry
h_{cg}	=	height of the centre of gravity of an oscillating system
h_{eff}, h_{eff2}	=	effective height of an oscillating system
h_i	=	height of level *i*
H	=	height of a rocking wall
I_{cg}, I_{cg1}	=	moment of inertia about centre of gravity of a single rocking wall
I_o, I_{o1}	=	moment of inertia of a single rocking wall about a point *O*
$I_{o\,comb}$	=	moment of inertia of a combined system about a point *O*
k_x, k_y	=	stiffness of impacting regions in a rocking wall
k_d	=	initial stiffness of hysteretic dissipators
K_{eff}	=	effective stiffness of an oscillating system
K_{fb}	=	lateral stiffness of a rocking wall as if it was fixed at the base
m	=	number of complete cycles of oscillation
m_i	=	lumped mass located at a level *i*
m_d	=	slope of a straight line representing a displacement spectrum
$m_{d\text{-}475,5\%}$	=	slope of a straight line representing the displacement spectrum for a 475 years return period earthquake for a system with an equivalent viscous damping of 5%
M, M_1	=	mass of a single rocking wall
M_{eff}, M_{eff2}	=	effective mass of an oscillating system
n	=	number of half-cycles of oscillation
P	=	axial load
PF	=	performance factor
Q_1,	=	constant calculated with Eq. 4.11
r	=	kinetic reduction factor
R	=	radius

R_c	=	axial force in diagonal strut
R_{eff}	=	effective radius
RF	=	risk factor
S_A	=	similitude ratio for acceleration
S_E	=	similitude ratio for modulus of elasticity
S_F	=	similitude ratio for force
S_L	=	similitude ratio for length
S_M	=	similitude ratio for mass
S_T	=	similitude ratio for time
S_V	=	similitude ratio for velocity
S_{area}	=	similitude ratio for area
$S_{density}$	=	similitude ratio for density
S_{drift}	=	similitude ratio for drift
$S_{frequency}$	=	similitude ratio for frequency
S_{moment}	=	similitude ratio for moment
S_{volume}	=	similitude ratio for volume
t	=	time
T	=	period of oscillation
T_{eff}	=	effective period of oscillation
u_i	=	initial uplift at the base of a rocking wall
v	=	total velocity of the centre of gravity (*c.g.*) of a rocking wall
v_{eff}, v_{eff2}	=	effective velocity of the effective centre of a rocking wall
v_x, v_y	=	x and y components of the velocity of the *c.g.* of a rocking wall
V	=	base shear
V^*, V_1^*, V_2^*	=	design base shear
V_{eff}	=	effective base shear
V_u	=	ultimate load of masonry
V_{cr}	=	first crack load of masonry
w	=	equivalent width of masonry diagonal strut
$w_{cracked}$	=	equivalent width of cracked masonry diagonal strut
$w_{uncracked}$	=	equivalent width of uncracked masonry diagonal strut
W, W_1	=	total weight transferred to a rocking wall
W_{1-2}, W_{2-3},	=	work done by dissipators from stages 1 to 2 and 2 to 3, respectively
α	=	slenderness angle of a wall

α_{eff}	=	effective slenderness angle of a rocking wall
$\alpha_{eff\,comb}$	=	effective slenderness angle of a combined system
β	=	ratio $2F_y/W$
δ_{st}	=	static deformation in the impact region
δ_{imp}	=	deformation due to impact in the impact region
δ^*_{imp}	=	maximum deformation due to impact in the impact region
Δ	=	lateral displacement
Δ_o	=	initial lateral displacement
Δ_m	=	amplitude of the lateral displacement at the m^{th} cycle
$\Delta_{RP=475\,years}$	=	spectral deformation for a 475 years return-period earthquake
ε'_m	=	strain at maximum compressive strength of masonry f'_m
φ_w	=	angle of the diagonal of the masonry panel with the base
μ	=	coefficient of friction
ξ	=	total equivalent viscous damping of an oscillating system
ξ_h	=	equivalent viscous damping due to hysteretic behaviour
$\xi_{h\text{-}ideal}$	=	equivalent viscous damping due to ideal hysteretic behaviour
ξ_i	=	equivalent viscous damping due to impact
ξ_o	=	equivalent viscous damping intrinsic to the structure
θ	=	rotation
	=	angle of diagonal-masonry-strut with the horizontal
θ_o	=	initial rotation
θ_n	=	rotation at the n^{th} half-cycle
$\dot{\theta}$	=	angular velocity
$\dot{\theta}_1$, $\dot{\theta}_2$	=	angular velocity at instants 1 and 2
$\ddot{\theta}$	=	angular acceleration
τ	=	shear stress
τ_o	=	shear bond strength of masonry

Table of Contents

Chapter 1 Introduction

1.1 Introduction

In the last decade, the approach for the design of aseismic structures has evolved towards a more strict design regime. It is becoming common to acknowledge that, currently, the social and economic impact of earthquakes in regions struck by them is unacceptable (Bertero et al. 1996). To some extent, the perceivable damage can be attributed to more demanding public expectations rather than to design deficiencies. What could have been acceptable 50 or more years ago may not be good enough nowadays (Langenbach, 1994). Nevertheless, most of the time, these higher expectations have reasonable grounds in the fact that building-contents as well as the services they deliver are becoming more and more valuable than the building itself. In this new context, the conventional prescriptive serviceability/life-safety design methodology of earthquake-engineered-buildings is no longer enough. Control of damage, definition of operational levels and other performance parameters are expected to be incorporated in the future in seismic codes to define the required seismic performance of earthquake-engineered-buildings. The trend has become to be known as Performance-Based Design PBD, (SEAOC, 1995), a practice also established in other civil engineering fields such as pavement design and fire engineering, which focuses in the final desired performance rather than in the prescription of design-rules.

Perhaps the most comprehensive attempt to establish this practice in earthquake-engineering so far is the work done by the Structural Engineers Association of California SEAOC (SEAOC, 1995). Sensibly, the SEAOC proposes that the process not only should address the design procedures but also all the aspects related to the building, from the selection of the site to the maintenance during its life time. The SEAOC embodies the process in what they call Performance-Based Seismic Engineering. This new development is not only limited to California. A number of other countries in seismically active regions are also involved in the upgrading of their design and construction practices into a performance-based scheme (Mander, 2001, Otani, S., 1997). It is comforting to see that many developing countries are also getting involved in the trend. Even though the amount of research is limited there, the problem has been identified (Gallegos, 1994) and the design procedures are expected to move towards a performance-based scheme.

Changing the focus of the seismic-design from prescriptive to performance criteria has also changed the appreciation about some conventional structural systems. Masonry structures have been among the "victims" of this trend. The behaviour of masonry structures in recent moderate earthquakes has been regarded as poor from the performance-based perspective (Langenbach, 1994). From a number of reports intended to shape a new generation of codes incorporating PBD, it is clear that these new codes will restrict the use of masonry well below its current limits (SEAOC, 1995). This is not necessarily a fair conclusion.

It is true that the main problem with masonry is its brittle nature, something inherent to the very material, however, it is also true that the conventional masonry structural systems were not intended to meet a performance-based environment. The systems proposed, so far, were enough to meet schemes based on working-stresses and ultimate-strength. Moreover, their ability to dissipate energy protecting other elements of the structure was, and is still, highly appreciated in the conventional serviceability/life-safety context (Kappos, 1998). A fairer conclusion would be, therefore, that the conventional masonry structures engineered to meet the two-level scheme succeeded in that, but the brittle nature of the masonry makes these structures very sensitive to intermediate performance levels that were not taken into account in its design.

There are two ways to upgrade the designing practice into a performance-based scheme. The first one is just to take the conventional structural systems, and constrain their design to meet the required performance-objectives. The second way is to search for alternative structural systems whose behaviour is more suited for a performance-based environment. This second option is explored in this thesis through the adaptation to confined masonry of an alternative aseismic system that is being used with other structural materials, mainly reinforced concrete. The main feature of this system is that it has rocking walls as the main lateral load resisting structural elements.

It is shown here that the use of rocking walls can be a solution for buildings with a low density of walls and low to medium total height. With the conventional structural systems, many of these buildings would present damage even under a moderate seismic demand. The use of rocking walls can be an alternative to meet performance-based demands without giving up masonry as an active structural component of the building.

As part of the research a design procedure has been developed based in the Direct Displacement Method (Priestley and Kowalsky, 2000) and a prototype building has been designed using this methodology. The research is complemented with the dynamic testing of a reduced scale model, which was based on the prototype building. The research ends with the numerical modelling of the system, a tool that hopefully will further deepen the understanding of this system.

1.2 Objectives and Scope of the Research

The main objective of this research is to expand the possibilities of masonry structures, particularly masonry infilled frames (MIF) and confined masonry (CM), as reliable structural systems in a performance-based scheme. Due to the variety of masonry-structures that can be found, it was decided to focus the research on a particular case. Masonry buildings with a low-density of masonry-walls were chosen to that effect. Their relevance comes from the fact that they are frequently built and used as classrooms in developing countries. A new structural system, based on rocking masonry walls as the main lateral load resisting elements, is adapted as an alternative to improve the seismic performance of these buildings.

The research will focus on the in-plane loading of the rocking walls without any attempt to establish the response of the system for out-of-plane loading. The study of the out-of-plane load mode is one of the points recommended for further research at the end of this thesis. It was observed in the preliminary literature review that one of the main problems that one may face with rocking walls is the reduced energy dissipation capacity that they have. A second objective of this research is, therefore, to complement the system with elements capable of providing a reliable source of energy-dissipation for the system. Once this is done, it will be possible to use any of the newly developed design-methodologies able to meet seismic performance-objectives.

A third main objective is the testing of the proposed system. It was decided that only dynamic tests would provide reliable results and, therefore, it was expected to undertake them on the shake table of the structures laboratory of the Civil Engineering Department at the University of Canterbury.

A final objective is the provision of a reliable numerical model, able to reproduce the observed behaviour of the system in the dynamic tests. It is expected that such a numerical model can be later used to conduct parametrical analysis of the system allowing a deeper understanding with limited cost.

1.3 Organisation of this Thesis

The organisation of the thesis reflects the work done to achieve the above-mentioned objectives. A rather chronological sequence was established as it also clearly presents the objectives that were being achieved at each stage.

Chapter two presents a review of the state-of-the-art and state-of-the-practice of aseismic masonry infilled frames (MIF) and confined masonry (CM) and assesses their possibilities and limitations in a performance-based context. In the same chapter a review of the nature of the performance-based philosophy is also undertaken. This will be especially important when dealing with the proposed

alternative systems since the performance-based frameworks proposed so far (SEAOC, 1995, FEMA, 1997) are oriented mainly to the design of conventional structural systems.

A second section explores the possibilities of implementing rocking walls in masonry buildings. Chapters three and four are part of this section. Chapter three studies the different elements of this system and how they should be handled to result in a reliable aseismic structure. Chapter four focuses on the development of a seismic design-methodology able to meet seismic performance-objectives. This last chapter finishes with the design of a prototype structure using the developed design-methodology.

The third section presents the experimental work done to verify the behaviour of the rocking walls. It comprises Chapters five and six. The specimen to test is a reduced scale model of the prototype that was designed in Chapter four. Chapter five exposes all the preliminary aspects of the experiments, including the development and design, and the cyclic test of the hysteretic energy dissipators to be used in the specimen. Chapter six presents the experimental results. The experimental results are also analysed here and the assumptions made in the elaboration of the design procedure are assessed as well.

The fourth section shows how the system can be numerically modelled. The experimental results are used as a source for the calibration of the numerical model until the observed behaviour is matched reasonably well. The results are also compared with the ideal model and the model is used to discuss some improvements in the system, suggested for future research.

This thesis ends in Chapter 8, where the conclusions drawn from this work and recommendations for future research are presented.

Chapter 2 Review of the State-of-the-Art and State-of-the-Practice of Aseismic Masonry Infilled Frames and Confined Masonry

2.1 Introduction

This review assesses the potential and limitations of Masonry Infilled Frames (MIF) and Confined Masonry (CM) with particular emphasis in its suitability to meet a seismic performance-based (PB) environment. It was decided to elaborate on this issue because the author has not found a comprehensive study that shows why and how conventional masonry structures are to be limited in a PB environment. It is also expected that this review will show that there are more constructive alternatives to this issue than the simplistic dismissal of masonry structures when PB design is adopted.

Both, MIF and CM, combine masonry with structural frames. In MIF the frames are built first and then the bays are infilled with masonry panels. In CM, the masonry panel is built first and then confined with columns and beams. Much of the available information in the literature, especially experimental, has been derived from models corresponding to MIF. For the purposes of this study, CM will be considered as a special type of MIF. The justification for this is that confined masonry presents many of the features of typical masonry infilled frames, and may be placed at the top of a hierarchical classification for MIF as defined in Table 2-1.

Most of the aspects that will be discussed here have to do with the in-plane seismic response of masonry shear walls as this is the mode which they are relied upon to provide an adequate seismic response to the building where they are being used. The analysis presented here is rather qualitative. A deeper insight of the theories and past experimental work presented here can be found in other works devoted entirely to that purpose (Crisafulli, 1997, Drysdale et al, 1994; Hendry, 1990, Sahlin, 1971). Regarding the frame members, they are assumed to be only of Reinforced Concrete (RC). Extensive coverage of the mechanical behaviour, as well as analytical models for RC elements, may be found somewhere else (CEB, 1996). The combined behaviour of reinforced-concrete frames and masonry panels is also reviewed in this chapter. The features of the numerical model that will be used to represent masonry infills in the subsequent chapters are presented as well. The quantitative definition of the relevant mechanical parameters, therefore, will be emphasised in the corresponding sections.

Table 2-1 Some General Mechanical Characteristics of Masonry Infilled Frames

Structure Type	*Capacity to Transmit Vertical loads through the Masonry Panel*			
	Weak Earthquake	*Moderate Earthquake*	*Strong Earthquake*	*Catastrophic Earthquake*
Partially infilled frame	Not able	Not able	Not able	Not able
Loosely infilled frame	Not able	Not able	Not able	Not able
Tightly infilled frame	Able	May not be able	Not able	Not able
Confined masonry	Able	Able	May not be able	May not be able
Structure Type	*Interaction between the Masonry Panel with the Frame*			
	Weak Earthquake	*Moderate Earthquake*	*Strong Earthquake*	*Catastrophic Earthquake*
Partially infilled frame	No Interaction	May Interact	Interacts	Interacts
Loosely infilled frame	No Interaction	Interacts	Interacts	Interacts
Tightly infilled frame	Interacts	Interacts	Interacts	Interacts
Confined masonry	Interacts	Interacts	Interacts	Interacts

This chapter ends with an analysis of the conventional design procedures for confined masonry, and the possibility of upgrading masonry buildings to meet performance-based criteria. A discussion of performance-based design (PBD) philosophy is included as well in this last section

2.2 Unreinforced Masonry (URM)

Masonry is a brittle composite material, strong in compression but weak in tension. To understand its mechanical behaviour one has to learn about its constituent materials and the way they interact. Masonry units and mortar present large variability in the observed values of their mechanical characteristics. However, the major complexity in the behaviour of masonry lies in the interaction of its units with the mortar; and the complexity increases with increased deformation. In this section the masonry units and the mortar are first explored individually and then as a composite, with emphasis on their behaviour under typical load conditions.

2.2.1 The Constituent Materials

2.2.1.1 Masonry Units

A large variety of masonry units can be found. In shape terms, they can be divided into solid and hollow units. Solid units are those whose effective area, parallel to the bed joints, is 75% or more of the gross area. Hollow units have an effective area of less than 75% of their gross area. Horizontally perforated units, referred sometimes as tiles, are also manufactured (Yamin and Garcia, 1994; FEMA, 1997). Masonry units can also be divided according to their material as clay bricks, concrete blocks, sand-lime bricks, natural stone units and adobe units (Yamin and Garcia, 1994; Tomazevic, 1999). Only the first three types of unit are used in masonry infills.

In a performance-based design scheme, however, only a comprehensive evaluation of the mechanical characteristics of masonry-units can lead to a reliable classification of masonry units. Fortunately, code makers have already addressed that task and the existing standards reflect that fact (ASTM, 1995). ASTM C-62 covers the minimum requirements for clay or shale bricks intended for use in both structural and non-structural masonry. The standard addresses physical properties (appearance, durability, freezing and thawing, absorption, saturation coefficient, strength and rate of absorption), size and coring and visual inspection. Part of the physical requirements is presented in Table 2-2. The normal structural brick is the MW, whereas SW is specified for extreme conditions and NW for non-structural applications. The ASTM C-62 also refers to other standards for the sampling and testing of the bricks. Similar specifications for Concrete Blocks are addressed in ASTM C-55 whereas Sand-Lime Bricks are addressed in ASTM C-73. Similar classifications can be found in other countries (Gallegos, 1994), and they usually reflect the type of masonry-units that can be found in the particular country.

Table 2-2 Physical Requirements for Clay or Shale Bricks according to ASTM C-62 (ASTM, 1995)

Designation	*Minimum Compressive Strength on gross area (MPa)*		*Maximum Water Absorption by 5-h Boiling (%)*		*Maximum Saturation Coefficient*	
	Average of 5 Brick	*Individual*	*Average of 5 Brick*	*Individual*	*Average of 5 Brick*	*Individual*
Grade SW	20.7	17.2	17.0	20.0	0.78	0.80
Grade MW	17.2	15.2	22.0	25.0	0.88	0.90
Grade NW	10.3	8.6	No limit	No limit	No limit	No limit

The quality of masonry units is mainly controlled by the manufacturing process and the materials. Clay bricks present greater difficulty in their manufacture than do concrete blocks. Concrete blocks may be manufactured following simple standards, BS 6073 in the UK, for example. Unfortunately, that is not the case for clay bricks. The processes vary from region to region, however, complete references on optimum manufacture process and selection of materials for clay bricks can be found in the literature (Lynch, 1994).

2.2.1.2 Mortar

The purpose of the mortar is to bond the masonry units to form the composite that is referred as masonry. It can be made out of any binding material and aggregates mixed with water. In general, mortars can be designed by naming their solid components, usually stressing the cementitious ones. Thus, Yamin and Garcia (1994) list Portland Cement-Lime mortars, Masonry Cement mortars, Portland Cement-Boulder Sand mortars and Ready Mixed mortars. The most common mortar is the one made out of Portland cement, lime and sand, mixed with water. In general, cement provides the

bonding and the strength, whereas lime increases workability. The classification of the mortar is mainly based on the volumetric proportioning of its solid components. The amount of water is defined rather qualitatively as to be enough to yield a workable mix. ASTM C-270 defines four types of mortars: M, S, N and O, either by proportion specifications or property specifications. A guide for the selection of the type of mortar (M, S, N or O) suitable for a particular circumstance is also included in ASTM C-270. The first classification, the one that prescribes proportions, is shown in Table 2-3.

Table 2-3 Proportion Spec. for the Classification of Mortars according to ASTM C-270 (ASTM, 1995)

Mortar	*Type*	*Proportions by volume (cementitious materials)*					*Aggregate ratio (measured in damp, loose conditions*
		Portland cement or blended cement	*Masonry cement (types defined in ASTM C-91)*			*Hydrated lime or lime putty*	
			M	*S*	*N*		
Cement-lime mortar	M	1	-	-	-	¼	Not less than 2¼ and not more than 3 times the sum of the separate volumes of cementitious materials
	S	1	-	-	-	Over ¼ to ½	
	N	1	-	-	-	Over ½ to 1¼	
	O	1	-	-	-	Over 1¼ to 2¼	
Masonry cement mortar	M	1	-	-	1	-	
	M	-	1	-	-	-	
	S	½	-	-	1	-	
	S	-	-	1	-	-	
	N	-	-	-	1	-	
	O	-	-	-	1	-	

The second classification, based on the mechanical properties of the mortar, is not common. Most of the codes only specify the proportion of the materials in the way presented in Table 2-3. The American standards present Properties Specification Requirements (Table 2-4), which may be used alternatively, instead of the Proportion Specification requirements presented in Table 2-3. They are intended for laboratory prepared mortar only.

Table 2-4 Properties Spec. for the Classification of Mortars according to ASTM C-270 (ASTM, 1995)

Mortar	*Type*	*Min. Average Compressive Strength at 28 days (MPa)*	*Min. Water Retention (%)*	*Max. Air Content (%)*	*Aggregate Ratio*
Cement-Lime	M	17.2	75	12	Not less than 2 ¼ and no more than 3 ½ times the sum of the separate volumes of cementitious materials
	S	12.4	75	12	
	N	5.2	75	14*	
	O	2.4	75	14*	
Masonry cement	M	17.2	75	--**	
	S	12.4	75	--**	
	N	5.2	75	--**	
	O	2.4	75	--**	

** When structural reinforcement is used in cement-lime mortar, the max. air content shall be 12%*
*** When structural reinforcement is used in masonry cement mortar, the max. air content shall be 12%*

Good quality mortar is defined as the one that produces sound masonry. Unfortunately, to get this so-defined good mortar, is not enough to match the characteristics described in Table 2-5 alone. Other issues, such as the nature of the masonry units or local temperatures, might force a modification of the basic recommendations for mortar. Ultimately, expertise of the masons and good site supervision are the factors that lead to a good quality of the mortar.

2.2.2 Basic Properties of Masonry

Its composite nature makes it difficult to represent masonry in a single comprehensive model. A more rational understanding of masonry is achieved through the study of its behaviour under different load conditions. The analytical models developed to that end, have made use of mechanical parameters related not only with the interaction of their components but also to characteristics of the individual components of masonry: bricks and mortar. Next, the parameters related with the individual components and the ones defined by their interaction, are exposed. Then, the masonry as a composite is analysed.

2.2.2.1 Masonry Unit Related Parameters

a) Compressive Strength of the Masonry Unit

This is one of the most important parameters in the structural response of masonry. Unfortunately, there is a large numerical variability in the compressive strength of the units. In concrete units it varies from 10 to 40 MPa and in sand-lime and clay units from 8 to 50 MPa (Crisafulli, 1997). The variability is not only dependent on the type of materials used but also on the manufacturing procedure. Quality control in the production-line also has a significant influence on the average compressive strength as well as on reducing the extent of the variability of this parameter (Meli, 1994). Therefore, the compressive strength of masonry units should be established by the manufacturer after sampling and testing its production. It is of great concern that manufacturers seldom specify this characteristic.

b) Tensile Strength of the Masonry Unit

The tensile strength of masonry units is small compared to their compressive strength. It has been observed, however, that the tensile strength tends to increase as the compressive strength increases Researchers have attempted to relate the tensile strength linearly to the compressive strength (Sahlin, 1971) or to the square root of the compressive strength (Hamid and Drysdale, 1982). But, because it is always a small fraction of the compressive strength, a value of 10% of the compressive strength is usually recommended for practical purposes (Crisafulli, 1997). There are practical difficulties in testing the tensile strength of masonry units. Stress concentrations at the end grips are difficult to

avoid. That is why indirect procedures are preferred to calculate this parameter. Thus, apart from a direct tensile test, one can use a flexural test and a splitting test (Drisdale et al., 1994). Flexure tests usually yield larger values than do the splitting tests. Crisafulli (1997) states that the splitting test represents the actual stress-state of masonry loaded in-plane better than does the flexure test.

c) Geometry: Dimensions and Shape of the Masonry Unit

Large variability in dimensions is found in masonry units. There are attempts, made by the industry, to control the dimensions in order to fit a "planning grid". If the dimensions are thus defined, they are referred as "modular dimensions". A planning grid of 600mm x 600mm (or 24in x 24in) is widely accepted internationally (Drysdale et al., 1994). In perforated units, the pattern of the holes is also different, varying from round to square holes. As stated earlier, solid units may have perforations provided they comply with the definition in section 2.2.1.1. The regularity of the shape is also a factor taken into account. Brick's "warpage" and "out of square" are the two standard parameters used to define the regularity of the shape. Lack of regularity in the geometry may induce stress concentrations leading to local failures that may trigger the collapse of the whole masonry assemblage. The quality control in the production of the masonry units is the main factor defining these geometry-indexes.

d) Other Masonry-Unit Properties

The above-mentioned parameters are probably the most critical to define the quality of masonry units. There are, however, other characteristics whose control could be vital for the production of good masonry as well as for their analytical modelling. These are briefly discussed next. More detailed descriptions can be found in the literature (Sahlin, 1971; Drisdale et al., 1994; Crisafully, 1997).

- Strength of Masonry Units under Bi-Axial Stress. This is a basic definition used to model the interaction of masonry units with mortar in masonry assemblages. A combination of compression in the vertical direction and tension in the horizontal one represents the state in the masonry unit that is expected in the composite. There are a number of equations recommended by different authors to define the failure criteria in a bi-axial state of stresses (Crisafulli, 1997). As expected, these equations acknowledge a reduction in the compressive strength of the unit when it is subjected to tension in the orthogonal direction.

- Modulus of Elasticity of Masonry Units. It also has a large variability. Values reported in the literature (Drysdale et al., 1994; Crisafulli, 1997) range from 5000 to 25000 MPa. The way the elastic modulus is defined may vary as well, Drysdale et al. (1994) reports that the typical practice is to take a secant modulus from the origin to 33% of the brick strength. Best-fit equations that relate the secant modulus of elasticity to the compressive strength of the brick have also been proposed by some researchers (Sahlin, 1971; Kirtschig, 1985). Although with

different relationships, these equations establish an increasing modulus of elasticity with increased strength.

- Absorption and Saturation Coefficient of the Masonry Unit. These indexes define the total amount of water that is absorbed by the masonry unit to reach saturation. They are a measure of the porosity of the unit. Lower values of the Saturation Coefficient (more extra pore space) are specified for greater durability because the free pore space will let the unit accommodate volumetric changes of the water due to extreme changes in temperature.

- Initial Rate of Absorption (IRA) of Masonry Units and Moisture Content of the Masonry Unit. The IRA defines the amount of water that can be absorbed by a dry masonry unit when partially immersed in water for a specified period of time. This parameter is used to learn how fast the unit can suck water from the mortar immediately after being laid. Along with the moisture content of the unit these properties help to define the optimum water content of the mortar.

2.2.2.2 Mortar Related Parameters

a) Uniaxial Compressive Strength of the Mortar

Drysdale et al. (1994) comment that long experience has shown that, when proportioning according to ASTM C-270, one can expect values above those required by the ASTM C-270 properties-classification. These minimum values presented in Table 2-4, therefore, can be taken as lower limits for those standardised proportions. The reliability of this correlation is also confirmed by an extensive experimental program reported by Meli, (1994) as it can be seen in Table 2-5. In the same table, mortars without lime are also presented. Mortars without lime are common in some countries in Latin America (Meli, 1994; Gallegos, 1994) and, therefore, the values presented by Meli are valuable as a practical reference.

Table 2-5 Compressive Strength for different types of Mortars designed according to the Mexican practice (adapted from Meli, 1994)

Type		*Number of samples*	*Average Comp. Strength* (MPa)*	*Coefficient of Variation (%)*
*Proportion by volume cement : lime : sand***	*ASTM C-270 equivalent denomination*			
1 : 0 : 3	-	211	20.0	24
1 : ½ : 5	S	70	10.7	19
1 : 0 : 6	-	55	10.3	31
1 : 1 : 6	N	26	7.4	38

** The type of test is not mention in the reference.*
*** This definition of the proportions of the mortar is to be used along this chapter*

b) Workability of the Mortar

The degree of workability is important in getting good quality mortar joints. It also strongly affects the productivity of the mason. The workability of the mortar largely depends on the grading of the sand, material proportions and air content, but it is the water content what controls the final adjustment. The conventional laboratory test in the American standards to measure workability is the flow test. It is described in ASTM C-91.

c) Other Mortar Properties

As with the masonry units, there are other less important characteristics of the mortar but whose awareness provides a better understanding, control and modelling of mortars and masonry. They are briefly discussed below.

- Compressive Strength of Confined Mortar. This parameter is important for the formulation of failure models for masonry because the mortar in the actual masonry joint is confined to a variable extent. As expected, experimental work has demonstrated that the confinement increases the compressive strength of the mortar. A number of empirical equations relating the compressive strength of confined mortar to its uniaxial compressive strength and the lateral confinement stress can be found in the literature (Crisafulli ,1997; and Hendry, 1990).

- Modulus of Elasticity of the Mortar. In a general sense, the stress-strain relationship in mortar has been reported to be similar to that for the concrete. No reliable equations, however, have been formulated to define the initial modulus of elasticity. However, some attempts have been made in the past to relate empirically the Modulus of Elasticity to the uniaxial compressive strength (Sahlin, 1971).

- Water Retentivity of the Mortar. It defines the ability of the mortar to retain water, preventing the water from getting sucked by the masonry units or going elsewhere. Failure to hold the water would weaken not only the mortar but also the bond with the masonry unit.

- Air Content of the Mortar. Mortars made with masonry cement typically have air contents ranging between 12 to 18% (Drysdale et.al. 1994). Larger amounts of air are some times incorporated to produce a more workable mortar and on expectation that it will increase its durability, as occurs with concrete. Practices based in analogies of mortar with concrete may be dangerous since both structural materials are intended for different purposes and placed in different environments.

2.2.2.3 Composite Related Parameters

a) Bond Shear Strength between Mortar and Masonry Unit

The character of the bond strength is very intricate, having a complex mechanical and chemical nature (Hendry, 1990). It is known that the mechanical nature of the bond is due to the formation of crystals in the mortar, a product of the hydration process, that penetrate the pores in the bricks (Sinha, 1983). Attempts to understand the fundamental nature of the bond are reported by Hendry (1990), however, experimental work is the one that has yielded most practical results. Values ranging from 0.1 to 1.5 MPa were found in many experimental programs reported by Crisafulli (1997). These values reflect, again, a large numerical variability of this property. The way different conditions affect the shear bond strength can also be found in the literature (Sinha 1983; Hendry 1990; Drisdale et al. 1994; and Crisafulli 1997).

b) Bond Tensile Strength between Mortar and Masonry Unit

The bond tensile strength is generated by the same mechanical interlock that develops the shear strength in the brick/mortar interface (Sinha, 1983). Again, large numerical variability is found. For example, average values ranging from 0.03 to 0.38 MPa are reported by Sinha (1983) using 1:¼:3 (cement:lime:sand) mortars and a variety of bricks. However, for normal conditions, with a reasonable supervision, Sinha (1983) got average values ranging from 0.16 to 0.31MPa. Simple empirical equations have also been recommended to relate the tensile bond strength and the shear bond strength (Crisafulli, 1997). As the parameters that govern the bond tensile strength are the same as the ones that generate the shear bond strength, the same above-mentioned references are recommended to understand what influences bond tensile strength.

c) Coefficient of Friction between Mortar and Masonry Unit (μ)

Large variability and contradictory results have been reported in the definition of the coefficient of friction. Extensive test data collected by Hendry (1990) suggests a broad spectrum for the values of μ. The values range from 0.13 to 1.04. However, as Hendry points out, the values may not be realistic in some cases because the reported values of μ were not measured directly. They were derived assuming a failure mode, the Mohr-Coulomb shear failure criteria, that may not be the actual failure mode. As discussed later in this chapter, this failure model can be expected only for low values of the normal stress. The values reported, therefore, are "equivalent coefficients of friction" that may be used in a Mohr-Coulomb shear failure model rather than "actual coefficients of friction" between the unit and mortar joints. Paulay and Priestley (1992) recommend for design purposes a value of 0.3 whereas Atkinson et al (1989) concluded that a value of 0.7 could be a lower bound after testing 56 specimens and comparing his results with previous tests.

2.2.2.4 Behaviour of Masonry under Compression

Compression is the type of load under which masonry performs better. It is mainly referred to the compression applied perpendicularly to the direction of the bed joints. The most significant parameters in this load condition are the compressive strength of the masonry, its initial modulus of elasticity and its strain stress relationship. From them, the compressive strength of the masonry is the most studied characteristic. The compressive strength is also used as a main reference in the definition of other mechanical characteristic of the masonry.

Many experimental programs have been conducted aiming to relate the masonry compressive strength to the individual mechanical properties of the masonry unit and the mortar, resulting in some simple equations (Crisafulli, 1997). Although the resulting equations can be used as a reference, their generalisation is not advisable. This is because the particular characteristics of other parameters, not taken into account in the formulation of the empirical equations, might affect the outcome in other conditions. This empirical way of defining the strength of masonry, however, may be reliably used in limited geographical zones, where the raw products and construction practices may be expected to be similar to the ones used in the original tests (Meli, 1994).

Compression Failure Theories have been developed based on simplified models that study the interaction of the elements participating in the composite. These theories after being corrected with empirical factors are more capable of being used broadly. A number of failure theories have been developed to explain the strength of masonry. The theories describe the interaction of masonry units and mortar joints in different ways, the criteria for the triggering of the failure also varies. Several of these theories may be found in Crisafulli (1997) and Hendry (1990). One of the simplest theories is a strength-based one proposed by Hilsdorf, (1969). Hildorf's is also the widest accepted because, despite its simplicity, it matches reasonably well experimental results.

For the Modulus of Elasticity of Masonry under compression, it is common to calculate it using an equation assuming a linear elastic behaviour of the masonry constituents. However, the elastic properties of the mortar and masonry units must be known to calculate it. Alternative, using experimental results, other researchers have attempted to correlate E_m to other significant parameters in the masonry. Most of them relate E_m to the masonry compressive strength f'_m, mainly linearly (Paulay and Priestley, 1992; Crisafulli, 1997) or to a root of the compressive strength (Crisafulli, 1997). It has also been found that there is no major variation in E_m when the stresses are applied perpendicular or at a 45-defree angle of the bed joints (Alcocer and Klinger, 1994)

Regarding the Stress-Strain relationship in Masonry under Compression, not much experimental work has been conducted since the usual design parameters were only the initial modulus of elasticity and

the strength of the masonry prism. Crisafulli (1997) reports that no reliable relationship between the maximum stress f'_m and the corresponding strain ε'_m has been found. In a dimensionless basis, however, it has been found that the strain-stress curves are very similar. A number of equations have been developed to represent this non-dimensional curve (Crisafulli (1997), all of them being similar from a practical point of view.

Drysdale et al. (1994), Sahlin (1971), Hendry (1990) and Crisafulli (1997) list a number of parameters that affect the performance of masonry under compression. The list is rather long, being the most significant: masonry unit strength, mortar strength, mortar joint thickness (inversely proportional), bond strength between masonry units and mortar joints, ratio height/length of the masonry unit, variations in dimensions of the bricks and workmanship. Other parameters that may also affect the performance but to a lesser extent are the masonry units coring, patterns and methods of bonding, aging and cycling loading.

Table 2-6 is presented as a reference for typical values of some of the parameters that characterise the behaviour of masonry under compression. It is interesting to note that although strength and modulus of elasticity varies considerably, the magnitude of the strain at maximum strength is consistently found to be close to ε'_m = 0.002. This is perhaps the only property that has been found reasonably independent of any other characteristic of masonry.

Table 2-6 Some Measured Mechanical Properties of Masonry Prisms under Compression (Hidalgo, 1994)

Masonry Unit	*Grouting*	*Compressive Strength f'_m (MPa)*	*Strain at Maximum Strength, ε'_m (mm/mm)*	*Modulus of Elasticity (MPa)*
Hollow Clay Brick	No	5.8	0.0020	5354
	No	7.0	0.0024	5264
Concrete Block	No	4.3	0.0023	2801
	Full	15.5	0.0017	15354
	No	4.4	0.0023	3040
	Full	12.2	--	11053
	No	4.5	0.0024	3613
	Full	13.7	0.0029	10908

2.2.2.5 Behaviour of Masonry under Tension

From a practical point of view, understanding the tensile behaviour of masonry is important in the definition of the behaviour of masonry under flexure. Although tension in masonry is usually neglected when the masonry receives in-plane loads, that is not the case for out-of-plane loads that generate a flexural dominant action.

Experimental programs make use of direct, flexural and splitting testing procedures. A reliable direct test, however, is difficult to set up. Flexural and splitting tests, therefore, are preferred. The modulus of rupture of the masonry, which is the tensile strength of masonry drawn from a flexural test, may be reliably used for the out-of-plane loading of the masonry. Hendry (1990) comments that the modulus of rupture for bending in a plane parallel to the bed joints is several times greater than in a plane normal to the bed joints. Table 2-7 shows some experimental values reported by Henry (1990). Although splitting tests have also been conducted, the results may be not reliable since the heterogeneous characteristics of the masonry may largely disturb the elastic state assumed in the model.

Table 2-7 Experimental Results for Flexural Tensile Strength of Masonry obtained (Reported by Hendry, 1990)

Mortar	*Flexural Tensile Strengths (MPa)*					
	Bending in a plane normal to bed joint		*Bending in a plane parallel to the bed joint*			
			3-course specimen		*4-course specimen*	
	Mean	*COV (%)*	*Mean*	*COV (%)*	*Mean*	*COV (%)*
1 : 2 : 9	0.390	23.3	2.08	20.6	1.78	26.1
1 : 1 : 6	0.594	22.9	2.40	15.5	2.03	18.5
1 : ¼ : 3	0.984	25.4	2.74	18.0	2.29	16.5

No specific failure theories have been formulated since it is widely accepted that the tensile failure is mainly governed by the tensile bond strength between units and mortar joints. Although this failure pattern is the most common, other patterns, featuring tensile failure of the bricks, may be expected depending on the relative tensile strength of the masonry unit compared to the tensile bond strength (Drysdale et al., 1994).

2.2.2.6 Behaviour of Masonry under Shear

In most cases, the action of masonry under shear is accompanied by compressive loads of variable magnitude. For this reason, the response of masonry under shear has been studied when it is combined with compressive loads. In these conditions, at least three failure modes are reported (Crisafulli, 1997; Paulay and Priestley, 1992):

- *Shear Friction Failure*: Occurs for low normal stresses, with a stepped pattern following the mortar joints. Cracks due to debonding of the mortar-brick interface are observed.
- *Diagonal Tension Failure*: It occurs for medium to large compressive stresses. In this case the cracks appear in the bricks. They become the weak regions because the strength of the mortar joints is increased by the compressive field.

- *Compressive Failure*: This mode is observed for very high values of the compressive field compared to the shear stresses. The pattern is similar to the observed in pure compression.

The experimental measure of the shear strength of masonry has been conducted using different procedures. Some of the procedures include the test of arrangements of two to four bricks, but their results are more representative of the strength of the bed joints rather than the overall piece of masonry. Testing masonry panels is a better way to learn the behaviour of masonry under shear. Several arrangements for masonry panels have been proposed and tested. Two main trends may be identified: a) the one that tries to reproduce the actual load pattern applying simultaneously compressive and shear loads and b) the one that applies compressive loads with an inclination relative to the bed joint expecting to reproduce the actual biaxial stress field in the masonry. San Bartolome (as reported by Crisafulli 1997) compared the results of the two above mentioned procedures with the behaviour of full-size models of infilled frames and concluded that the diagonal compressive load represented better the pattern observed in the full-size infills. The diagonal compressive strength of masonry f_d, therefore, was the subject of numerous experimental studies and used as a reference for the definition of the shear strength of masonry.

With regard to failure theories, a Mohr-Coulomb criterion has been adopted widely in the past. This approach, however, only represents reasonably well the failure caused by debonding of the brick-mortar interface. However, this failure pattern is only observed in masonry with low compressive stresses. The approach fails to predict the other failure modes, over-estimating the shear capacity of masonry with medium to high values of axial compression. The main challenge of any failure theory is, therefore, to represent properly the failure patterns observed in masonry in this load condition. Mann and Muller (as reported by Crisafulli, (1997) developed a theory to represent the three modes. Crisafulli also proposes a modification of this theory to improve it.

In relation to the shear modulus of masonry, an approximate value can be calculated assuming an elastic behaviour of the masonry. According to the classical elastic solution, the ratio G_m/E_m may be in the range of 0.40 to 0.45, (taking usual values for the Poison Ratio from 0.10 to 0.25). Experimental results reported by Crisafulli agree with this range. Alcocer and Klinger (1994), however, state that G_m/E_m may vary from 0.10 (for high strength bricks) to 0.30 (for weak bricks).

The parameters that have been found to affect the performance of masonry under shear are the masonry compressive strength (f'_m), brick tensile strength, coefficient of friction (μ), shear bond strength (τ_o), ratio height/length of the brick. In general, it was found that the level of influence of each of them varies depending on the level of compressive stress.

2.3 Masonry Infilled Frames (MIF) and Confined Masonry (CM)

As it was exposed in the introduction of this chapter confined masonry (CM) will be regarded as a particular type of masonry infill frame (MIF), with the reasons exposed there as well. Many of the results drawn for masonry infills, therefore, are going to be used in this section. Because the chief interest of this research is the seismic response of these structures, this section will focus in the aspects of MIF and CM that are related to its seismic response.

The behaviour of unreinforced masonry walls can be significantly improved when combined with reinforced concrete frames to form MIF and particularly CM. The resultant strength is greater than the sum of the two components separately; and the resultant ductility, due to the composite action, is also larger than that of the masonry alone (see Table 2-9). The bare frame system may also benefit from the presence of the masonry infills. The masonry panel increases the stiffness of the bare frame, reducing lateral deformation. Energy dissipation through friction and slip in the masonry-frame interfaces may also improve the dynamic response of the building.

The disadvantage of this system, on the other hand, is the likely degradation of the system's stiffness, strength and energy dissipation capacity during cyclic loading of moderate to large amplitudes. This may lead to the occurrence of unexpected load paths in the structure, that may cause large stress concentrations and local, partial or total failure of the structure. The degradation of the mechanical properties is mainly due to the progressive damage of the masonry infill, and the deterioration of the panel-frame interface conditions. In some cases, degradation of the frame can also be observed. Some of these aspects are explored next in more detail.

2.3.1 Masonry Infilled Frames under Lateral Loading

Because of the likely deterioration of masonry with cyclic loading, the response of MIFs to lateral loading can vary depending if the load is applied monotonically or cyclically. Obviously, in a seismic context, one should be interested in the system's response to cyclic loading. There is, however, a bulk of experimental information dealing with MIFs that has been drawn from monotonic tests. These results are explored first and then we move on to analyse the response of the system to cyclic lateral loading.

Three stages can be identified in the response of the masonry infilled frames when they are monotonically laterally loaded (Tomasevic, 1999, Kappos et al., 1998). They are:

- *Pre-cracking stage*, which corresponds to the initial branch of the load-deformation curve until the first crack appears. At this stage the infill behaves rather elastically showing the largest stiffness;

- *Post-cracking stage*, with a lower but still significant stiffness. This branch of the load-deformation curve takes the infills up to its maximum or ultimate strength after which one can say that it begins to yield; and
- *Post yielding stage*, where the stiffness is negative and the infill is driven to failure

From the above description, three main points are identified, the first cracking limit, the ultimate strength of the infill and the ultimate state determined by the maximum displacement and the corresponding shear reaction of the wall. The first two points are clearly identifiable in almost any monotonic loading test in confined masonry. When discussing the in-plane behaviour of confined masonry, however, it has been customary to set up the ultimate load as the one that causes the first diagonal cracking rather than the actual maximum load carried by the masonry. Alcocer and Klinger (1994) list some of the reasons for this practice:

- The cracking load was found to be less variable than the maximum load for repeated tests
- The cracking load is not greatly affected by the reinforcement in the wall and therefore is easier to predict than the ultimate load in such conditions, and
- Even though it was found that when monotonically loaded, the walls could sustain greater loads, that is not significant during cyclic loading

It is a common practice, with other structural types, to define the strength envelope of a cyclic test equal to its monotonic load-deformation curve. But one needs to be cautious in incorporating this practice when dealing with masonry infilled frames. The reason being that, as stated at the beginning of section 2.3, masonry infills show degradation of some of the mechanical parameters with cyclic loading of moderate to large amplitude. For instance, concerning the strength, it was commented above that in cyclic-loading the ultimate strength may be not significantly larger than the cracking strength, whereas larger ultimate loads can be expected in monotonic tests (Alcocer and Klinger, 1994). But again, there is no general agreement in this point: Crisafulli (1997) and Tomasevic (1999) suggest that this may be true only when a number of moderate to large cycles are applied to the system, and this is not the case of seismic loading, where only very few moderate to large cycles are expected. Some experimental results are presented in Table 2-8. Note in this table that in the cases when more than two cyclic tests have being conducted the minimum value of V_u/V_{cr} is, invariably 1.00, meaning that in at least one of those tests the first crack load was the maximum load that the specimen could sustain.

The deformation capacity of the system has been found to be less variable than its strength capacity. Magenes and Calvi, (1997) and Rodriguez and Rodriguez, (2000) state that consistently ultimate-drift levels of about 0.5% are found experimentally. Contradictory results, however, can be found in the

literature. See for example the storey drifts in Table 2-9, drawn from a reference different than the ones mention above (CEB, 1994). In the same reference, surprisingly large ductility ratios are reported for masonry infill frames (Table 2-9). These ductility ratios are commonly associated with energy dissipation capacity of the structure, because of the hysteretic loops that are usually linked to the ductile behaviour of structures. In masonry infill frames, however, the hysteretic loops are not as consistent as they would be in other type of structures because masonry infilled frames present significant pinching when cyclically loaded. What is certain though is that, due to its relatively large stiffness, masonry infilled frames are able to develop their maximum energy dissipation capacity at an earlier stage than other more flexible structural members of the building. Unfortunately it is associated with early damage in the masonry as well. Ultimate drift and energy dissipation capacity of confined masonry have been found to improve with horizontal reinforcement (Aguilar et al., 1996) or other more sophisticated techniques (Colombo et al., 2000). However, as commented above, it does not seem to have a significant effect in delaying the emergence of the first crack in the panel. Hence early damage in the panel is not avoided with this technique.

Table 2-8 Ratio V_u/V_{cr} reported from different ciclic tests (reported by Crisafulli, 1997)

Reference quoted by Crisafulli	*No of specimens*	*Type of Loading*	V_u/V_{cr}
Govindan et al.	1	cyclic	2.09
Klinger and Bertero	2	cyclic	1.27 to 1.95
Leuchars and Scrivener	1	cyclic	1.26
Liaw and Kwan	1	dynamic	1.62
Meli	10	cyclic	1.00 to 1.69
Sanchez et al.	3	cyclic	1.00 to 1.41
Sanchez et al.	3	cyclic	1.00 to 1.68
Yamin and Garcia	8	cyclic	1.01 to 1.29

Table 2-9 Statistical Evaluation of TestsResults on Masonry Infilled Frames reported by CEB, (1994)

Type of Infilled Frame		*Shear Strength Ratio**		*Residual Strength Ratio***		*Storey Drift corresponding to Max. Shear*		*Displacement Ductility Ratio****	
		Average	*CV*	*Average*	*CV*	*Average*	*CV*	*Average*	*CV*
No local damage in frame	Integral infill	3.34	0.43	3.92	0.21	1.14%	1.25	5.80	0.52
	Non-Intg. Infill	3.80	0.40	2.01	0.15	3.66%	0.59	4.88	0.35
Local damage in frame	Integral infill	1.44	0.10	1.44	0.10	2.55%	0.55	4.66	0.27
	Non-Intg. Infill	1.79	0.26	1.49	0.05	0.88%	0.98	7.07	0.71

* *Ratio of the strength of the MIF to the strength of the bare frame*
** *Ratio of the residual strength of the MIF at 2-3% to the residual strength of the bare frame*
*** *Displacement ductility ratio defined at* $V = 0.85V_u$

The literature review shows that there have been attempts to formulate a comprehensive description of the cyclic behaviour of masonry infilled frames. Most make use of a diagonal strut model to represent the masonry infills, and then, complete sets of hysteretic rules have been defined for the strut (Klinger and Bertero, 1976; Crisafulli, 1997). The diagonal strut model is explored in detail in section 2.3.3.2. Later in this thesis, one of these models, developed by Crisafulli (1997), will be used in the numerical modelling of the proposed system.

2.3.2 Types of Failure of Masonry Infilled Frames

As commented above, it has been observed that any of the two main elements, masonry infills or frames, may be the cause of failure. It also has been observed that these two failure scenarios themselves may develop different features depending on the load conditions and the relative values of their mechanical characteristics. They are discussed next.

2.3.2.1 Failure of the Masonry Panel

The failure of masonry infills features debonding of the mortar-brick interfaces, cracking and crashing of the bricks, etc. In most cases, however, it does not present a unique pattern but rather a combination of several patterns. Crisafulli summarised roughly, as presented in Figure 2-1, the patterns that may present each of the failure modes. In the following sections, each type of failure will be studied and defined in terms of the concepts described earlier in this chapter.

- ***Shear Cracking of the masonry infill.*** This is the most common pattern found either experimentally or in actual structures subjected to moderate to strong earthquakes. The failure may feature any of the patterns presented in Figure 2-1: cracking along mortar joints and cracking due to diagonal tension in the bricks. These patterns are similar to the first two described in section 2.2.2.6. The parameters that govern the strength vary depending on the ratio of the normal stress to the shear stress (f_n/τ).

- ***Compressive Failure of the masonry infill.*** As summarised in Figure 2-1, two mechanisms are observed in this type of failure: crushing of the corners of the infill and compressive failure of diagonal struts formed in the infill due to diagonal cracking. This last pattern follows one of the patterns discussed in the previous section. Crushing of the corners may occur for relatively flexible frames, which yield a small contact surface in the corners after the infill has split from the frame. Crisafulli (1997) reports that, apart from some specimens tested by Brokken and Bertero (1981), this failure mode has rarely been observed in masonry infilled reinforced concrete frames.

- ***Flexural Cracking of the masonry infill.*** This type of failure may be observed in infilled frames where flexure prevails over shear and the framing columns are weak. It may be the case in multistorey buildings. In this failure type, cracks appear in the tensile side of the infill. Flexural cracking, however, is rarely observed because separation of the panel-frame interface usually occurs first, preventing the tension columns from transmitting the tension to the infill.

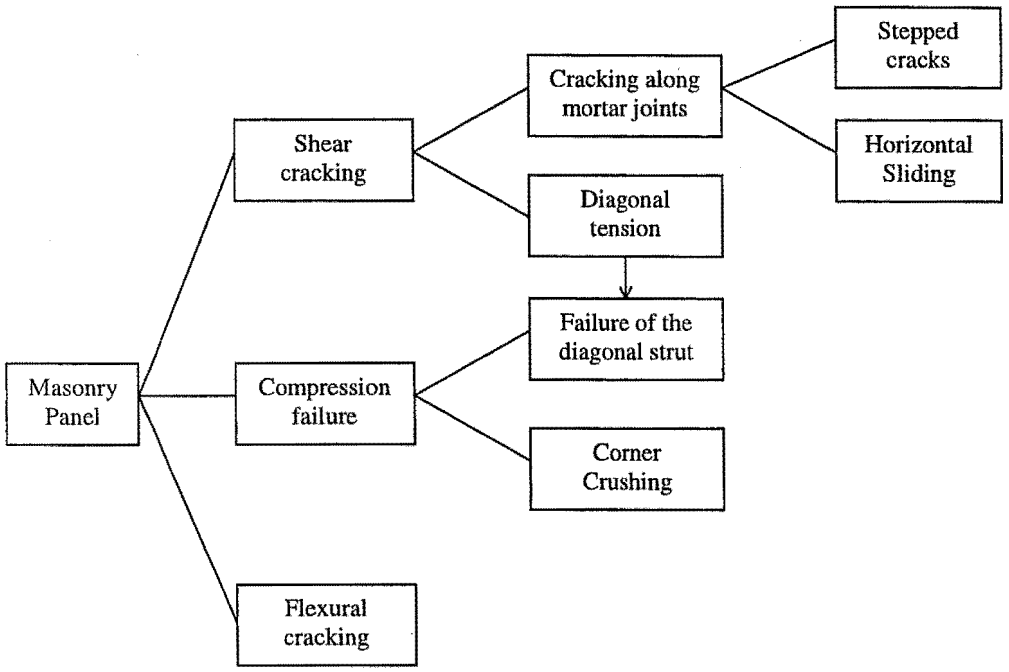

Figure 2-1 Modes of failure observed in Masonry Infills (after Crisafulli, 1997)

2.3.2.2 Failure of the Reinforced Concrete Boundary Frame

The failure of the frames depends on the mechanical characteristics of the frame and its interaction with the masonry infills. Crisafulli classifies the types of failure according to the summary presented in Figure 2-2. The four types proposed by him are reviewed briefly next.

- ***Flexural Collapse Mechanism in the frame.*** After the separation of the masonry infill from the frame, significant flexural actions may develop in the frame due to the lateral loading. Plastic hinges are frequently observed in both ends of the framing columns. The beams, on the other hand, rarely develop plastic hinges. The development of the hinges in the columns is not regarded as a collapse mechanism if the masonry panel is still able to transmit diagonal compression. The system would be acting as a braced pinned truss, rather than a braced frame. The failure of the infill through horizontal sliding may induce the development of hinges at

the middle height of the columns. The inelastic deformation demand in this case is larger than in the previous case (Crisafulli, 1997).

- ***Failure due to Axial Loads in the frame.*** The bracing action of the masonry infill induces axial forces in the boundary frame. Tension and compression axial loads are developed as a consequence of this mechanism. Compressive failure of the columns is rarely detected, although failure due to buckling of the longitudinal reinforcement may be observed for severe cyclic loading. Tensile failure of columns, on the other hand, is frequently observed. The failure may feature either yielding of the longitudinal reinforcement or slipping of the bars at their anchorage.

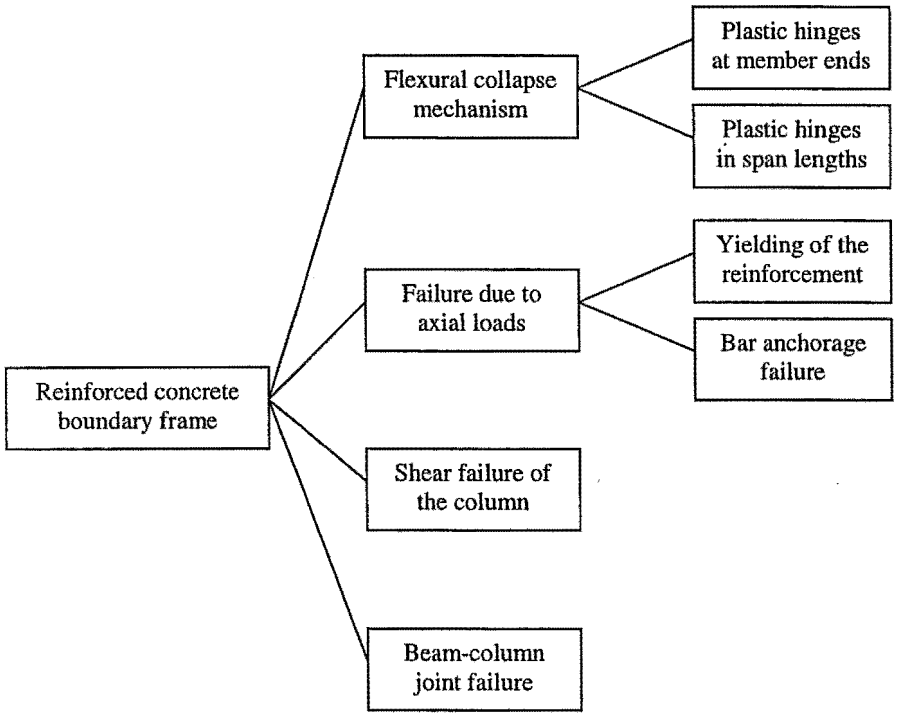

Figure 2-2 Modes of failure observed in Reinforced Concrete Boundary Frames (after Crisafulli, 1997)

- ***Shear Failure of the Columns.*** Significant shear actions are mainly found at the end of the framing columns, in the loaded corners. The failure features one or more diagonal cracks crossing the column section (Crisafulli, 1997). A conservative approach is usually used to prevent this mode of failure. In this approach, the lateral reinforcement of the columns is designed to be able to carry the expected shear in the entire wall.

- ***Beam-Column Joint Failure.*** Failure at the beam-column joints may be caused by the concentrations of high normal and tangential stresses at the end of the corners, transmitted by the beam and columns. Diagonal cracking of the joints is observed in this type of failure. The development of this mode of failure decreases the capacity of the beams to transmit the lateral forces to the columns, transferring a higher proportion to the infills. The problem is worsened due to the reduction of the contact length of the infill with the frame, causing even larger stress concentrations in the infill.

2.3.3 Models for the Representation of Masonry Infills

Models that represent the behaviour of masonry infills have been set up to undertake the analysis of any structure with masonry infills. These are different from frame members, in which the models could be formulated almost intuitively. The formulation of models for masonry infills required a significant amount of previous research. The difficulty of the incorporation of infills in the analysis and design reflected in apathy of engineers to take them into account in the analysis and design process, and even now in some countries it is not difficult to find analysis and design procedures ignoring the masonry infills (Kappos et al., 1998; Madan et al., 1997).

A number of models have been developed since the late 1950's, varying in definition and complexity. The first ones attempted to model only the seemingly elastic behaviour corresponding to the initial response. Later, the models were improved to represent the non-linear response of the infills under monotonic load. Finally, researchers collected enough information to attempt to develop a model able to represent the non-linear behaviour of the infills and the deterioration of its properties due to cyclic loading. A detailed and referenced evolution of this process can be found somewhere else (Madan et al., 1997; Crisafulli, 1997). Two approaches were followed for the development of analytical models of masonry infilled frames: the use of micromodels and the use of macromodels. Both are reviewed next, along with the Crisafulli's diagonal strut model, which will be used later in this work.

2.3.3.1 Micromodels

Micromodels are mainly developed using finite elements. They take into account characteristics such as the strength and stiffness of the masonry units, strength and stiffness of the mortar, the bonding between these elements and between the infill and the frame, the non-linear behaviour of the frame, etc. In order to make the analysis possible, the most suitable tool is a non-linear finite element analysis. Most of the models that researchers use to make a close analytical modelling of the actual structure are of this type. However, it requires a considerable amount of calculation and can be considered as unsuitable for the everyday analysis and design of buildings. A comprehensive reference of available models can be found somewhere else (Chiou et al., 1999)

2.3.3.2 Macromodels

Macromodels are devised to summarise all the relevant properties of the infilled frame in a simpler equivalent model with a small number of sub-elements. These models are the ones preferred by designers because they may be incorporated relatively cheaply in the design of structures with infills. Although there is large variety of formulations, most of the models developed are based on simple diagonal struts. Other macromodels have also made use of column analogies, entire storey mechanisms and other formulations (Crisafulli, 1997), but none of them have the flexibility and popularity of the strut model. Because of its importance, a further discussion on the diagonal strut model is undertaken in the next paragraphs.

In the ***diagonal strut model***, the infill is represented by diagonal bracing struts, which act mainly in compression. The struts are deactivated when the lateral load causes an axial tensile load greater than their equivalent tensile strength, which is rather small compared to the compressive strength. Ultimately, the diagonal strut model defines an axial force R_c, which is the result of the product of the transversal area of the strut, A_{ms}, times its axial stress, $f_{m\theta}$, which is assumed uniform in the section:

$$R_c = f_{m\theta} A_{ms} \qquad \text{(Eq. 2.1)}$$

The axial uniform stress, $f_{m\theta}$ is drawn from the strain-stress curve of masonry. Initial values of E_m equal to those of masonry under compression orthogonal to the bed joints, may be acceptable for the diagonal strut (see section 2.2.2.4). The cross section of the diagonal strut, A_{ms}, is constant along the length of the strut and usually defined as a rectangle with one side equal to the actual thickness of the masonry infill and an equivalent width which is usually related to the total diagonal length. The simplest models use only one strut for each diagonal. Several definitions of the equivalent width, w, have been proposed. The simplest ones define the width as a fraction of the diagonal length of the infill, d_m. Stafford Smith (1962) found values of w/d_m varying from 0.10 to 0.25. Paulay and Priestley (1992) recommend that a conservative value may be $w/d_m = 0.25$ for a lateral force level only up to 50% of the ultimate capacity of the masonry. More complex definitions of the equivalent width take into account the relative stiffness of the panel to the frame and the aspect ratio of the panel (Crisafulli, 1997). The ratio w/d has also been found to vary with the level of damage of the infill. According to Crisafulli (1997), ratios $w_{cracked}/w_{uncracked}$ ranging from 0.50 to 0.85 have been reported.

Some variations of the strut model use more than one strut for each side and others incorporate friction elements to represent failure patterns such as horizontal shear sliding. It was found, however, that the single strut model gives a good estimation of the stiffness of the masonry infilled frame and of the axial loads in the framing elements (Crisafulli, 1997), although the moments in the framing members from such a model may be rather different from the actual ones in the masonry infilled frame.

2.3.3.3 Crisafulli's Diagonal Strut Model

Crisafulli represents the behaviour of the infills with the combined action of a single diagonal strut in both diagonals of the frame. The strut model tries to incorporate the three stages discussed in section 2.3.1 and the possible collapse mechanisms discussed in section 2.3.2.1 all together. The model also accounts for the stiffness degradation of the infill due to cyclic loading, making it able to be used in a non-linear dynamic analysis. Crisafulli's model uses Eq. 2.1 to cover all the range of situations described here. For the definition of $f_{m\theta}$, the model uses a set of hysteretic rules defined for masonry in compression. The compressive strength of the diagonal strut is redefined as described below.

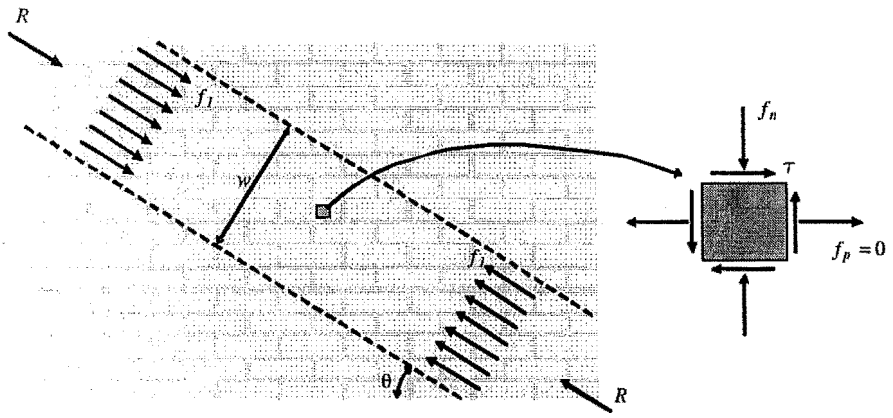

Figure 2-3 Stress-state in masonry within the Equivalent Diagonal Strut region

The compressive strength of the diagonal strut, $f'_{m\theta}$, should take into account all the different types of failure expected in the infills. Crisafulli defines the shear strength of masonry, τ_o, for a given value of the compressive load, f_n, considering the three different failure types described in section 2.2.2.6. Crisafulli assumes that the tension stresses, f_p, in the lateral direction are small compared to the compressive stresses, f_n (Figure 2-3). It allows him to use the equations 2.2 and 2.3 to relate the shear stress τ and the vertical compressive stresses f_n. Clearly, the stress f_1 is equivalent to the diagonal compressive stress $f_{m\theta}$. The compressive strength of the diagonal strut, $f'_{m\theta}$, is equal to the stress f_1 that induces the masonry to reach its shear capacity.

$$f_n = f_1 \sin^2 \theta \qquad \text{(Eq. 2.2)}$$

$$\tau = f_1 \sin\theta \cos\theta \qquad \text{(Eq. 2.3)}$$

Crisafulli's model is built into the software RUAUMOKO (Carr, 2000), where two options are available: the complete model or a simplified one that behaves only elastically. The parameters required by RUAUMOKO for the definition of the hysteretic model are shown in Table 2-10 and Table 2-11. A visual reference for the definition of the parameters is provided in Figure 2-4.

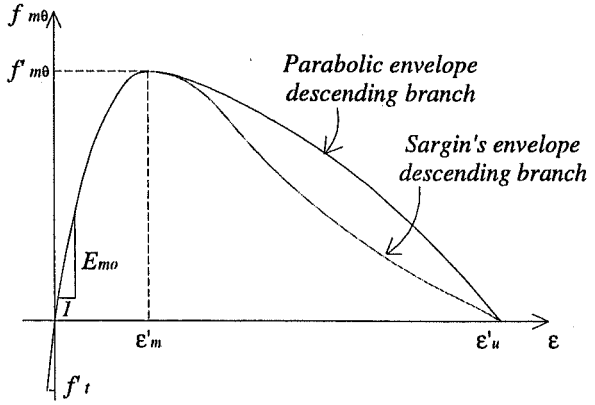

Figure 2-4 Crisafulli's masonry strut strength envelope

Table 2-10 Parameters required for the definition of the strain-stress relationship of Crisafulli's Strut Model in the software RUAUMOKO (Carr, 2000)

Parameter	*Description*	*Admissible Range of Values*	*Commentaries*
FC	Compressive Strength ($f'_{m\theta}$)	FC < 0.0	It has to be calculated accounting for all possible failure type
FT	Tensile Strength (f'_t)	FT > 0.0	In the lack of reliable information, it may be taken as zero
UC	Strain at $f'_{m\theta}$ (ε'_m)	UC < 0.0	Crisafulli reports that this parameter varies between –0.002 and –0.005
UUL	Ultimate Strain (ε'_u)	UUL < 0.0 UUL ≤ 1.5 UC	It is usually defined as a multiple of ε'_m. Crisafulli comments that values of the order of 20 ε'_m may be regarded as large, smaller values, therefore, are recommended.
UCL	Closing Strain	--	Defines the limit strain at which the cracks partially close and compressive stresses can be resisted. Crisafulli recommends values between 0 and 0.003
EMO	Initial Elastic Modulus of Masonry (E_{mo})	EMO ≥ 2FC/UC	A value greater than $2f'_{m\theta}/\varepsilon'_m$ is recommended because it yields an adequate ascending branch of the curve
GUN	Stiffness Unloading Factor	GUN ≥ 1.0	It controls the slope of the unloading branch. Crisafulli reports that usual values range between 1.5 and 2.5
ARE	Strain Reloading Factor	ARE > 0.0	It defines the point where the reloading curve meets the strength envelope. Although values between 0.2 and 0.4 were found for masonry under compression, Crisafulli comments that larger values are required to account for the other sources of non-linearity in the infills. He uses ARE = 1.5

Table 2-11 Parameters required for the definition of the Geometry of Crisafulli's Strut Model in the software RUAUMOKO (Carr, 2000)

Parameter	*Description*	*Admissible Range of Values*	*Commentaries*
AREA1	Initial strut cross-sectional area	AREA1 > 0.0	The area of the strut is defined by its equivalent width. In section 2.3.3.2 it was found that w may vary between 0.10 and 0.25. In the case that 2 areas are used, the initial area AREA1 may be defined slightly larger.
AREA2	Final strut cross-sectional area	AREA2 ≤ AREA1	The final area AREA2 may be taken as 70% to 90% of the initial area AREA1
R1	Displacement at 1	R1 < 0.0	This is the displacement at which the initial area begins to reduce. It may be taken as $\varepsilon'_m d_m/5$
R2	Displacement at 2	R2 ≤ R1	This is the displacement at which the area reaches the final area AREA2. Crisafulli recommends to take $\varepsilon'_m d_m$
IENV	Envelope Index	1 or 0	It defines the descending branch of the envelope curve: IENV = 1 Sargin strain-stress envelope descending branch (Crisafulli, 1997) IENV = 0 Parabolic strain-stress envelope descending branch

2.4 Conventional MIF and CM Buildings

2.4.1 Conventional Seismic Design and Construction Practices

Customarily, MIF and CM are used to resist lateral loads trying to take advantage of their high initial lateral stiffness. In some cases the masonry is isolated to prevent undesired or uncontrolled modes of failure. Customary design techniques, however, are not intended to meet a Performance Based Scheme. They were devised to meet, at best, a two level approach. The difficulties that it has caused are discussed later in section 2.4.2. Next, these conventional systems are discussed in more detail.

2.4.1.1 Masonry Infilled Frames acting as Shear Walls

This is perhaps the most common pattern in which MIF and especially CM are used. When the shear walls are properly engineered, they may be regarded as reliable in a two level approach. For low intensity events, the masonry infills dominate the dynamic response of the structure due to the panels' high initial stiffness, preventing any large drifts. For moderate to large earthquakes, the friction developed in the cracked surfaces as well as in the frame-infill interfaces dissipate large amounts of the input energy, protecting the rest of the structure.

Regarding the ***analysis*** of these elements, the current practice goes from no analysis at all in non-engineering structures to a full tri-dimensional analysis of the structure (Bariola, 1994). For masonry structures, where regularity and simplicity have been set in the conceptual design stage, a simple equivalent static analysis appears to be reliable enough for a seismic design (Tomasevic, 1999).

The simplest model for the structure, and one of the most popular ones, considers the structure as a group of uncoupled shear walls connected by the floors, which are regarded as rigid in their own plans (Bariola, 1994). Ignoring of the coupling action results in conservative actions for the walls, but it may result in overstressing of the coupling beams. The coupling action is sometimes addressed modelling the walls as single vertical elements (like a column), with rigid ends along a fraction or all of its total width. Then, the rigid ends are connected to the beam elements. Unfortunately, the column-analogy approach cannot be used to model realistically multi-bay walls, or infills of non-regular patterns.

In the last few years the use of equivalent diagonal strut models (see section 2.3.3.2) is increasing, and some regulations are introducing some standard practices for their use (FEMA, 1997). The advantage of the use of diagonal struts is that they permit the coupling of the walls and allows representing any pattern of the distribution of infills within the structure. To model the equivalent diagonal struts, however, at least compression-only elements are required (or other more complex purposely made type of elements), which are not common in general structural-analysis software and, therefore, only monotonic loading can be performed in most cases.

In customary practice, the seismic loads are usually defined with an equivalent elastic static analysis, where the forces have been determined from a design spectrum provided by the design regulations. In this case, most of the design regulations also provide the designers with simple equations to find the fundamental period of the structure (IAAE, 1996). The calculation of the fundamental period is followed by the definition of a seismic coefficient, drawn from an acceleration design spectrum based, in most of the cases, on the seismic response of a linear-elastic single-degree-of-freedom (SDOF) oscillator. The total base shear is calculated as a fraction of the total weight of the structure. This fraction is defined by the seismic coefficient, and other parameters that depend on the seismicity of the zone, the type of soil of the site, the importance of the building, and the ability of the building to sustain plastic deformations. This last parameter is sometimes referred as the performance factor, R.

In conventional seismic design procedures, the basic design base-shear, is intended to represent the demand of an earthquake of a return period of around 475 years, or 10% of probability of exceedance in 50 years, which, in most cases, is also defined as the seismic demand for an ultimate state level of the structure. The seismic demands at the serviceability level, if addressed, are usually taken as a fraction of this base shear. Also it can be found that in most seismic codes (IAAE, 1996), low values

of the so called "performance-factor" are set for masonry structures. This means that, according to the codes, structures with masonry do not perform well during plastic excursions, and therefore, plastic deformations have to be avoided.

The seismic demands are not applied alone. They are combined with other types of loads that affect the structure. The combination of loads depends on the type of design approach that is being used. The Working Stress approach and the Ultimate Strength approach are the two approaches used, in practice, for the design of masonry structures. In the Working Stress approach the elements have to be proportioned so that when the working-stress load-combinations are applied, the stresses in the structure are below specified allowable stresses (or working stresses). In the Ultimate Strength approach the actions generated in the structure by factored-load-combinations have to be below the design strength (reduced nominal strength) of the elements.

The ***design*** and ***construction*** practice, in a way similar to the analysis practice, ranges from non-engineered structures to the use of sophisticated techniques to control and improve the behaviour of the infills. As expected, after a damaging earthquake, most of the total damage in the masonry building stock is found in the first group. The non-engineered structures are built following empirical rules, many times without technical criteria, material specifications are non-existent and no supervision of construction practice is observed.

Due to the alarming number of non-engineered masonry-buildings, simplified methods for low buildings have been developed in some countries. They establish minimum horizontal areas (or lengths in some cases) of masonry walls per unit of area of the building. The Colombian code, for example, incorporates a method of this type as an alternative to a more elaborated one, also presented in the code (Yamin and Garcia, 1994). The Colombian alternative simplified method requires, in 1 or 2 storey buildings, a minimum horizontal area of confined masonry, which depends on the thickness of the walls and the seismic zone. The requirements are presented in Table 2-12. Apart from requiring basic details to confine the masonry, no additional design is demanded in this case.

Table 2-12 Minimum horizontal confined wall area in each main direction for the empirical design of one- and two-storey houses according to the Colombian Code (Yamin and Garcia, 1994)

Wall thickness (cm)	*Min. Percentage* of Confined Masonry Walls for the different Seismic Risk Zones*		
	High	*Intermediate*	*Low*
14	1.7 %	1.1 %	0.7 %
12	2.2 %	1.4 %	1.0 %
10	2.4 %	1.6 %	1.2 %
* *The percentage relates the total cross section of walls to the total area of the building plan*			

With respect to conventional engineered structures, most of the building codes demand the verification of two states, the serviceability limit-state and the ultimate limit-state. The serviceability limit-state is set to prevent any excessive damage in the building for service loads (including earthquakes regarded as frequent), and the ultimate limit-state must prevent the occurrence of catastrophic collapse of the structure and protect human life. The serviceability limit-state, however, is rather relaxed in the seismic aspect compared with the ultimate limit-state and, in general, seismic behaviour is not addressed explicitly.

The ***serviceability-limit-state*** is controlled by codes through permissible inter-storey drifts, which vary depending on the type of the structure. Strictly speaking, no actual design procedure is required for this level of design. It is rather a verification of the behaviour of the structure, once it has already been designed to meet the ultimate limit state. Furthermore, very few codes explicitly address the control of the seismic behaviour of the structure at the serviceability limit state. Most of the codes only limit the inter-storey drifts at the ultimate state level. This is because in customary two-level design schemes, if the building meets the ultimate limit-state seismic requirements (including drift control), it is expected that it will perform well under serviceability seismic loads.

In customary practice, for the ***ultimate-limit-state***, the design aims to provide enough strength to the structural elements to make them meet the amplified seismic loads described earlier, expecting to produce, ultimately, a life-safe structure. Maximum inter-storey drifts are also set up to prevent the damage in the structure reaching an extent that can jeopardise human life.

With respect to the design of the individual structural elements, customary design-practice differentiates between masonry infills and confined masonry. In confined masonry, from the actions obtained in the analysis, the masonry is expected to carry the compressive and shear stresses whereas the framing elements are expected to carry the tensile and bending actions (Bariola, 1994). In masonry infilled frames, the masonry infills are not expected to carry vertical loads, as it is difficult to get good bond at the top of the infill. The rest of the actions are distributed as in confined masonry. The way in which the elements are proportioned depends on the approach that is used. Conventional approaches are the Working-Stress and the Ultimate-Strength approach.

In a ***Working-Stress*** approach the demand has to be equal to or below the allowable-stresses. The design loads for this approach are not increased and the seismic load is actually reduced. It is expected that under these load combinations the elements will behave elastically, and a reserve strength is left in the structure to allow it meet larger eventual demands. The allowable stresses, therefore, are well below the actual strength of the elements (ICBO, 1997).

For the ***Ultimate-Strength*** approach, the strength of the elements is designed to meet amplified combined loads. Since the design is set at the limit of the capacity of the structure, the theoretical strength (or nominal strength) has to be reduced to take into account the uncertainties that may affect it. In masonry, however, the Strength-Design approach is not as common as the Working-Stress approach. The release of the NEHRP Provisions (FEMA, 1997) in the United States, however, seems to indicate that the Strength approach will ultimately be the standard one for masonry. Although the NEHRP Provisions are not mandatory, they represent the basis for future codes in the United Sates. The reduction-factors and the nominal-strength factors proposed in the NEHRP Provisions are presented in Table 2-13.

Table 2-13 Reduction Factors proposed by NEHRP Provisions (FEMA, 1997)

Type of Action	*Type of Masonry*	*Reduction Factor*
Axial Load, Flexure, and Combination of Axial Load and Flexure	Reinforced Masonry	0.85
	Plain Masonry	0.60
Shear	Both	0.80
Bearing	Both	0.60

The NEHRP Provisions, however, do not consider the benefit of the confining frame, since confined masonry is rather unusual in the United States. Other codes, on the other hand, does differentiate between plain masonry and confined masonry (Meli, 1994). Their Strength-Design approach is therefore more realistic in that regard.

Control of the damage is addressed marginally at the ultimate state, since it is more intended to protect human life rather than prevent excessive economic loses. Permissible inter-storey drifts are set to that end. The calculation of inter-storey drifts is based on deformations drawn from an elastic analysis of the structure. These elastic deformations are amplified by a parameter related to the ductility given to the structure. Some typical permissible inter-storey drifts are presented in Table 2-14.

The codes also limit the thickness of the masonry as well as the longitudinal and transversal reinforcement in framing columns and beams. In order to prevent the sliding shear failure mode the aspect ratio of the confined panels is also limited. New designs are incorporating horizontal reinforcement in the masonry panels, enough to carry all the horizontal shear action. The technique is expected to prevent an early soft storey mechanism and to diffuse the potential diagonal cracking in the infill (Gallegos 1994).

Table 2-14 Inter-storey Drift Limits according to different Codes (adapted from Bariola, 1994 and UBC, 1997)

Country	*Displacement amplified to take into account plastic deformation YES/NO*	*Amplification Factor*	*Drift Limit %*
Canada	YES	*PF*	1 to 2
USA (UBC, 1997)	YES	0.7 *PF*	2.0 to 2.5 *
Mexico	YES	*PF*	0.6 to 1.2
Colombia	YES	*PF*	1
Peru	YES	0.75 *PF*	1 to 1.5
Chile	NO	Not applicable	0.2
Where *PF*: Performance Factor			
** The UBC, 1997 states that the inter-storey drifts may be exceeded when it is demonstrated that structural and non-structural elements can tolerate larger drifts without jeopardise life safety.*			

2.4.1.2 Isolation of the Masonry Infills

The extensive damage in masonry infills during moderate earthquakes has led to more rigorous schemes when they are designed as shear walls (Aguilar, 1996). They are limited to small ductility values or no ductility at all. In practice, this is reflected in larger design forces in the masonry walls th

at led designers to look for alternative systems. In some cases, especially when the density of the walls is limited for architectural reasons, it was found that designing the building using only the bare frames was cheaper than making the masonry walls participate of the lateral load resisting system. Larger amounts of ductility were permissible for this type of structure and the "performance factor" in this case yielded lower static equivalent lateral forces. The infills only needed to be isolated properly from the frame and designed to sustain the locally generated forces. Certainly, this practice is better than analysing and designing the structure as bare frames and then infilling the frames with masonry. However, as is discussed below, there are some considerations that are not taken into account in current practice and that the codes have not addressed.

Effective isolation of the infills is very difficult to achieve. Complete isolation of the elements seems almost impossible with current practices, due to the lack of well engineered isolating devices, inadequate maintenance or even plain structural behaviour. Paulay and Priestley (1992) state that even when we have a well maintained gap isolating the walls at the top and on both sides, it still will be in contact with the beam beneath the panel, affecting the beam's stiffness and probably jeopardising a weak beam-strong column scheme. The practice of neglecting the "isolated" masonry elements, therefore, has to be replaced by accepting their interaction with the main structure.

The customary ***analysis*** of a structure with isolated masonry infills is not different from the analysis of the bare frames. The frame elements are modelled as if the building was just a skeleton shaped by the beams and columns. No consideration of the potential stiffening effect of the infills is taken into account.

An important issue is the identification of the maximum storey drift in storeys where masonry panels have been placed. The storey drift is used as a reference for the design of the infill-frame gap. The usual procedure is to calculate the drift from a static-elastic analysis and then amplify it by the ductility factor used in the definition of the equivalent lateral forces for the structure.

Codes also define the total forces that the isolated panels have to sustain. Although not always stated in the codes, the forces are derived from the inertial forces that the maximum total accelerations will cause in the panel. The calculated forces have to be distributed in proportion to the mass distribution of the element. Explicit equations are presented in some codes such as the one proposed in the 1997 Uniform Building Code (ICBO, 1997). Some codes also state that the infills (and any other element) must be able to sustain the interaction forces drawn from a study of deformation compatibility between the main structure and its elements.

The ***design*** of isolated masonry panels is done independently from the rest of the structure. Larger consideration is given to the out of plane behaviour since isolated infills lack the supporting effect provided by the surrounding frames. The design of isolated infills is usually done using a working-stress approach. When the forces generated by the interaction of the infill and the main structure are addressed (ICBO, 1997), they are regarded as ultimate-state ones, and a strength-design approach for the infills is permitted.

2.4.2 Observed Seismic Performance of MIF and CM Buildings

If the seismic performance of engineered MIF and CM buildings is assessed within the conventional life-safety context, one would find it satisfactory. The literature review shows that in the last major events there have been minimum loss of lives in these kinds of buildings and the complete collapse of well designed MIF or CM buildings has been exceptionally rare (Schultz, 1994; Bruneau, 1995; Langenbach, 1994). But if the seismic performance is assessed in terms of the observed damage, then the outcome would not be that positive. In this context, one had to say that poor seismic performance has been observed in masonry infilled frames, with the damage mainly concentrated in the masonry infills (Duzuke and Dawe, 1995). The assessment in this context is rather alarming. There are extreme cases in which it has been advised to avoid the use of masonry as a structural component when seismic loads are expected (Langenbach, 1994).

The fact that the buildings do not collapse and loss of lives are almost inexistent, means that MIF and CM are capable of achieving the seismic performance that most of them were designed for: life safety. The poor seismic performance, therefore, should not be completely attributed to the system but to the ill definition of the expected seismic performance. What is clear is that seismic design based chiefly in achieving life-safety of structures appears to be insufficient today.

Another important factor in this conflicting judgement of masonry buildings is that the expectations of society have changed in the last decades, and designers and code-makers have not been able to identify these changes in time. Langenbach (1994), for example, comments on what was observed following the 1989 Loma Prieta Earthquake. He states that, historically, if the kind of cracking in the masonry infills which was observed in many of these buildings had been observed following a major earthquake, people would have considered the damage as minor, and the buildings would have continued in use after minor repairs. He points out that at the Ferry Building in San Francisco, the evidence of shifted masonry and cracked arches from the 1906 Earthquake is still visible. However, following the 1989 earthquake the expectations were significantly different. Cracks were no longer acceptable. Four years later, by the time Langenbach's paper was written, most of these buildings were unoccupied and continued to deteriorate, with their owners often in bankruptcy, and with no hazard mitigation of any kind in place.

In developing countries, the trend of assessing seismic performance in terms of damage and functionality is gaining momentum. Peru, for example, suffered two strong earthquakes in less than ten years: the Nasca Earthquake in 1996 (Bariola and Kuroiwa, 1997, Quiun et al. 1997) and the Arequipa Earthquake in 2001 (Fierro, 2001, Bariola, 2001), and Peruvians have experienced at great cost the necessity for an improvement in the seismic performance of their building stock. In each event many confined masonry buildings intended for classrooms in schools or universities were damaged to an extent that classes were suspended for weeks or even months while repairs were being made. Although no one was killed in these buildings, the economic losses were huge for a poor economy as in Peru and, even worse, the education of the students was badly affected in those regions. It was encouraging to see that new buildings, built according with the new more stringent Peruvian seismic standards, only were damaged when they had a low density of masonry shear walls, as in other cases they were undamaged.

The practice of isolating the masonry from the rest of the structure was also tested in past earthquakes. In the referred earthquakes in Peru, in buildings where joints large enough to avoid interaction with the frames were provided, no damage was observed in the masonry. Unfortunately, there were many cases when interaction occurred, inducing significant damage, not only to the masonry panel but also

to the RC frame (Muñoz et al. 1997). The most common pattern of damage was the short column mechanism in the adjacent columns.

In the events in Peru, it was also observed that, when possible, the owners decided to replace the confined masonry walls by reinforced concrete ones. Although this meant a larger initial investment, it was expected that the extent of the damage in a future similar event would be reduced. What it means is that the owners themselves decided to set more demanding seismic-performance-objectives for their properties, and realised that conventional confined masonry was not able to provide this. The same trend has been observed in Mexico, reinforced by the fact that more stringent seismic codes have developed after the occurrence of damaging earthquakes in that country (Aguilar et al., 1996)

2.5 MIF and CM Buildings in a Performance Based (PB) Environment

The last part of the previous section discloses the fact that rather than blaming masonry for the poor seismic performance of some buildings in the past, owners and designers should be more careful about the expected seismic performance of the building. The prescriptive codes that we have today have shifted the attention of designers and builders from seismic performance to fulfilment of the prescriptions established by the codes. In the Peruvian earthquakes commented above, even the officials that checked the compliment of the standards were surprised by the extent of the damage in some buildings.

The new trend of seismic design based on performance, needs to be implemented for masonry buildings as well. The implementation of performance-based design will probably limit the range of structures for which confined masonry is suitable. This, however, is less detrimental than the generalisation and total disapproval of masonry as a structural material in seismic regions.

Before proceeding with the analysis, it is necessary to review what performance-based design is, and how it is being implemented. One has to be aware, however, that the existing guidelines (SEAOC, 1995, FEMA, 1997) are mainly intended for the control of conventional structural systems. A short discussion on the basis of PB philosophy is conducted next. This discussion will help the handling of the alternative system proposed later in this thesis.

2.5.1 Performance Based Seismic Design

Due to the relative poor seismic performance of some traditional systems, the necessity of a performance-based seismic-design approach for new structures was identified some years ago (SEAOC, 1995). Prescriptive-only codes have been shown to be unable to ensure a satisfactory seismic performance of buildings.

In a performance-based (PB) scheme, a series of design ***performance-objectives*** has to be defined. There can be several performance-objectives for a single structure. Each *performance-objective* (PO) is a statement that relates a ***performance-level*** (PL) in a structure to an ***earthquake-design-level*** (EDL). Every structural and non-structural system and material is expected to meet these performance-objectives.

Having more than one design performance-objectives changes our concept of failure. In this context, "failure" does not necessarily mean the collapse of the structure. Failure means that a performance-objective has not been reached. As the performance objectives are defined before the design, it is unlikely that a structure can exactly meet each of them. Hence, the designer must learn to be flexible with the "failure" of the structure. It is clear that some of the objectives such as the life-safety one are a must, but some of the others are just based in economic grounds. On the same grounds, the option of relaxing some of the levels and allowing for the probability of doing some future repairs in the building should not be ruled out. The total cost can be calculated adding to the initial cost the expected losses at every failure level. The losses should be weighted by the probability of occurrence of the same level earthquake. This way of calculating the cost of a structure gives one the opportunity to minimise the cost in a rational way, integrating seismic reliability and socio-economic facts.

Perhaps the most significant documents available to date on the issue are the SEAOC Vision 2000 (SEAOC, 1995), ATC 40 (ATC, 1996) and FEMA 273 (FEMA, 1997). ATC 40 and FEMA 273 are guidelines prepared for the evaluation and retrofit of concrete buildings and of existing buildings respectively. SEAOC Vision 2000, on the other hand, has almost no limit in its application and expands the concept of PB design to a more comprehensive PB Earthquake Engineering. But these are not the only existing sources on PB design, many other organisations and researchers are involved in the process, developing PB procedures according to their own agenda. Extensive bibliographical references on the issue can be found somewhere else (Ghobarah, 2001).

For the purposes of setting this study in context, a summary of the basic definitions of performance levels, earthquake design levels, and finally performance objectives for different buildings, proposed by SEAOC (1995), are presented in Table 2-15. The SEAOC (1995) complemented Table 2-15 with a detailed list of the expected damage for every performance level in all the significant systems and elements in the building. From the design viewpoint, it has an important practical value because it shows how the performance levels are reflected in the entire building. However, one has to bear in mind that, ultimately, the performance levels are controlled by the statements in Table 2-15. It means that, ultimately, the specifications commented above can be relaxed if that doesn't affect the performance objectives; or that they may have to be tightened if that is necessary to meet the addressed level.

Table 2-15 Performance Levels adopted for this study (after SEAOC, 1995).

Performance Level	*Extent of Damage*	*Description of the Damage in the Overall Building*
Fully Operational	Negligible	*Lower Limit*: No damage, continuos service *Higher Limit*: Continuous service, facility operates and functions after earthquake
Operational	Light	*Lower Limit*: Most operations and functions can resume immediately. Repair is required to restore some essential services. Damage is light *Higher Limit*: Structure is safe for occupancy immediately after earthquake. Essential operations are protected, non essential operations are disrupted.
Life Safe	Moderate	*Lower Limit*: Damage is moderate. Selected building systems, features or contents may be protected from damage *Higher Limit*: Life safety is generally protected. Structure is damaged but remains stable. Falling hazards remain secure.
Near Collapse	Severe	*Lower Limit*: structural Collapse Prevented. Non-structural elements may fall *Higher Limit*: Structural damage is severe but collapse is prevented. Non-structural elements fall.
Collapse	Complete	*Lower Limit*: Portions of primary structural system collapse *Higher Limit*: complete structural collapse

Earthquake-design-levels (EDL) are the demand levels associated with every performance-objective set for the building. Seismic hazard analyses are the basis for the determination of EDLs. A set of EDLs suggested by SEAOC (1995) is presented in Table 2-16, where the probability of exceedance, however, has been shifted to match a common 50 years design life in all the levels.

Table 2-16 Earthquake Design Levels

Earthquake Design Level	*Return Interval*	*Probability of Exceedance*
Frequent	43 years	69% in 50 years
Occasional	72 years	50% in 50 years
Rare	475 years	10% in 50 years
Very Rare	970 years	5% in 50 years
In low seismicity regions, the "Very Rare Earthquake" should be based on a calculated Maximum Capable Earthquake in the region		

Finally, for the definition of each of the design performance-objectives one needs to combine one of the performance-levels with one of the earthquake-design-levels. The selection of the performance objectives defines the whole seismic performance of the structure during its design life. The selection, therefore, is rather a socio-economic issue, mainly guided by the importance of the edification or the expectations of the owner. SEAOC (1995) established three sets of performance objectives for three types of facilities: Safety Critical facilities, Essential Hazardous facilities and Basic facilities (Table 2-17).

Table 2-17 Performance Objectives for three types of Edifications (After SEAOC, 1995)

Safety Critical Facilities		*Essential-Hazardous Facilities*		*Basic Facilities*	
Earthquake Design Level	*Minimum Perf. Level*	*Earthquake Design Level*	*Minimum Perf. Level*	*Earthquake Design Level*	*Minimum Perf. Level*
Frequent	Fully Operat.	Frequent	Fully Operat.	Frequent	Fully Operat.
Occasional	Fully Operat.	Occasional	Fully Operat.	Occasional	Operational
Rare	Fully Operat.	Rare	Operational	Rare	Life-Safe
Very Rare	Operational	Very Rare	Life-Safe	Very Rare	Near Collapse

Figure 2-5 shows, in matrix fashion, the performance-objectives described in Table 2-17. For the purposes of this study, the basic-facility-objectives will be used. Nevertheless, the procedure may be adapted to meet the other objectives.

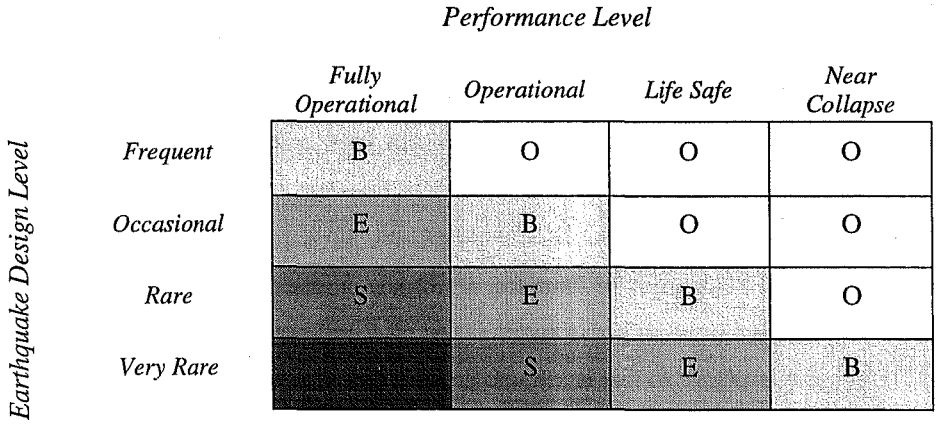

***B**: Basic Objective; **E**: Essential/Hazardous Objective; **S**: Safety Critical Objective*

***O**: Unacceptable Performance (for New Construction)*

Figure 2-5 Performance Objectives in Matrix Form (After SEAOC, 1995)

2.5.2 Available Methodologies to Reach the Performance Objectives at the Design Stage

Whatever method is chosen for design, it has to depart from a proper definition of performance objectives, which are to be set by the client according to his/her expectations. At the analysis/design stage the methodology should have the means to identify properly the earthquake design levels and the performance (or damage) levels. The levels must be settled using parameters able to be defined quantitatively to allow an objective assessment of the performance. Then, the methodology adopted has to be able to deal explicitly with the selected parameters. It will permit the design checking its outputs directly against the limits set up for the damage-related parameters.

Unfortunately, ***current code approaches*** are not particularly suited for the procedure described above. Most of the current seismic codes defined, at their best, a two-level serviceability/life-safety seismic design approach, with emphasis in life-safety (IAEE, 1997). Secondly, the earthquake design levels are not treated probabilistically, and even the fact that the life-safety level earthquake is set, in most of the cases, for a return period of 475 years, this information is hardly found in the seismic codes (IAEE, 1997). Thirdly, current codes address the seismic design in terms of equivalent seismic forces (IAEE, 1997), and consequently, the design is mainly based in providing the structure with enough strength to sustain those forces. The main design parameter induced by code schemes is, therefore, the strength of the structure, which is rather uncorrelated to damage. Even though code makers are aware of the necessity of the control of damage, they keep on using a force-based scheme because they have been trying to upgrade a scheme that wasn't intended for this purpose.

Alternative design methodologies more suitable for performance-based design are being developed (SEAOC, 1995). The alternative methodologies deal directly with parameters closely related to the level of damage in the structure. One example of this alternative approaches is *Displacement-Based Design*. It is intended to design a structure to not to exceed deformation limits for a given design earthquake level. It is known that displacements (that are set from target storey drifts) are closely correlated to levels of damage. In this approach, no equivalent forces are used. Displacement spectrums for different levels of damping are required instead of the acceleration spectrums used in the force-based scheme. Another example is the *Energy-Based Design* approach. This procedure aims at designing the structure so that it can handle and dissipate as much or more energy than the expected input energy in the design earthquake. Theoretically, in an extreme, one can design a structure to handle the input energy storing most of it in form of kinetic and elastic energy (although it ultimately will be dissipated by the natural damping of the structure). One can also design the structure to dissipate most of the input energy in the very event, either through hysteretic behaviour or through natural or added damping. The amount of energy dissipated and how it is dissipated is strongly correlated to the level of damage and, therefore, this approach can be efficiently used in a

performance-based scheme. Unfortunately, these alternative approaches still lack of general reliable methodologies, and, therefore their application is still limited.

2.5.3 Conventional MIF and CM Buildings in a Performance Based Environment

As discussed in section 2.4.2, extensive damage has been observed in unreinforced masonry structures in recent destructive earthquakes. It is even claimed that the most expensive damage in these events was derived from cracking of masonry partitions or infills (Duzuke and Dawe, 1995). As a consequence of this, masonry is widely thought to be unsuitable in complying with performance-based requirements in seismically prone regions (SEAOC, 1995). This may be a reasonable conclusion when dealing with conventional systems. Although there are studies that claim that masonry structures can meet acceptable performance-based objectives, these studies refer to modern U.S. masonry construction, i.e. hollow concrete or clay masonry units reinforced horizontally and vertically and filled with grout (Klinger, 1997). The same studies make it clear that unreinforced masonry (URM) is definitely not suitable for a performance environment. It is unfortunate to see that the masonry infills in MIF are usually placed in the same category of plain URM (Bruneau, 1995), which is harmful for the already deteriorated public perception of masonry as a structural material.

Another critical point of masonry buildings in a performance-based environment is the large number of factors that can influence their performance, not to mention the variability of those factors. That has been observed over and over earlier in this chapter. This complicates the realization of a basic principle of performance-based seismic design: the production of predictable dependable structures.

It is not surprising therefore the difficulty to find in the literature proposals for the performance-based seismic design of MIF and CM buildings. Rodriguez and Rodriguez (2000) dealt with the performance based design of confined masonry buildings but they limited the scope of the performance objectives to only one: collapse prevention. Rodriguez and Rodriguez base their proposed methodology on the fact that the deformation capacity of confined masonry appears to have much less variability than the strength capacity (see section 2.3.1). It is actually suggested that 0.40% would be a reasonably conservative estimation of drift at the collapse level. But again, this level of permissible drift for a collapse state is clearly restrictive for confined masonry structures, and would demand a large density of masonry shear walls to keep the drift below that prescribed level.

The obvious solution to make MIF and CM buildings meet performance-based demands has already been proposed indirectly by current performance-based guidelines: to limit the use of masonry close to its elastic range (SEAOC, 1995). Less restrictive alternatives however may exist. It can be demonstrated that it is possible to reach an acceptable and dependable seismic performance in a

confined masonry building choosing an appropriate structural system. This aspect is addressed in the next section.

2.5.4 Alternatives to Upgrade the Seismic Performance of MIF and CM Buildings

There are at least three ways to improve the seismic performance of CM buildings: ***a)*** more demanding performance levels, ***b)*** the improvement of the capacity of the masonry and ***c)*** search of more efficient structural systems.

More demanding performance levels will probably lead to the use of a different construction material. It is clear that the emphasis should be on limiting the lateral displacement to the point where the masonry does not exceed the first-crack stage for the basic design earthquake (rare earthquake).

Improvement of the capacity of the masonry is also limited. In a seismic context, the capacity refers not only to the strength but also to energy dissipation and flexibility of the masonry. The brittle nature of the masonry does not allow increasing its flexibility without damaging it and, although improvements are expected in its energy dissipation capacity with, for example, the incorporation of horizontal reinforcement, this does not prevent the damage in the masonry either. A careful control could lead to an improvement of the strength, and that would be the only aspect of the capacity that can be expected to enhance without damaging the masonry.

Search of more efficient structural systems is maybe the most promising option if one decides to keep masonry as a structural material. The most attractive technical solution would be the base isolation of these buildings. The large stiffness of masonry buildings make them get the most benefits from base isolation. Significant research is being conducted at the moment and the results are promising. (Moroni et al., 2000). Other innovative systems can also be options here. In the last few years there has been interesting research in rocking systems as part of aseismic buildings (Priestley et al., 1999; Restrepo et al., 2001). Rocking systems as aseismic structures have been known for a while (Houssner, 1956) and although they have inspired other philosophies in seismic design the system as such has not been much used.

2.6 Conclusions

- Masonry is governed by a large number of parameters that demand intensive supervision to get a good quality final product. The most critical factors are the mechanical characteristics of the masonry-unit and the competence of the mason. For the mortar, it is up to the mason to produce an adequate mortar that, not only matches standard specifications, but also is suitable for the environmental conditions and the type of masonry-unit that is being used. Information

about the basic mechanical characteristics of the masonry-units should be demanded from the manufacturers.

- The large number of significant parameters also makes very difficult the definition of reliable theoretical models for masonry. There is large variation in the values of the mechanical characteristics as well, making unreliable the generalisation of empirical relationships. Empirical relationships should only be used in a local context, where the conditions of the tests that originated the relationships are expected to be fairly reproduced. Alternatively, if they are to be used more widely, empirical relationships should be accompanied by an extensive detailing of the conditions of the original tests and other characteristics of the specimens and their components. Regular testing of masonry should be encouraged as there is not a completely dependable "recipe" to meet mechanical characteristics of masonry.

- The first-crack drift in MIF and CM is a characteristic that apparently cannot be improved with conventional techniques. Ultimate drift, however, can be improved with additional reinforcement or other more sophisticated techniques. As expected, the energy dissipation capacity of MIF and CM is also improved. These techniques, however, do not help delaying the emergence of the first crack in the masonry.

- Because of the difficulty in the modelling of masonry, masonry infills are many times ignored in the analytical modelling of masonry infilled frames. The diagonal-masonry-strut model seems to be the most suitable one to model masonry infills, and its use is already being encouraged by some seismic codes through appropriate guidelines.

- Conventional MIF and CM buildings are capable of achieving a life-safety goal. Their seismic performance, however, has been regarded as poor when damage is considered in the assessment. As a consequence of that, the public perception towards masonry as a structural material in seismic regions is negative. It does not help the fact that, some times, masonry infills in MIF are placed in the same category as plain URM.

- Masonry structures are punished by seismic codes with low performance-factors, assuming that MIF and CM buildings do not have the ability to sustain significant plastic deformations. The implementation of performance-based standards is likely to further restrict the scope of application of conventional MIF and CM.

- There exist alternative structural systems that should be explored to improve the seismic performance of MIF and CM buildings, particularly in the more demanding environment set by performance-based design.

Chapter 3 Concept Development of Confined Masonry Buildings using Rocking Walls

3.1 Introduction

In the previous chapter it was observed that a performance-based scheme would restrict the use of MIF and CM structures as they are conventionally designed and built. It was also observed there that a less restrictive option would be the use of appropriate alternative structural systems. This chapter discusses the option of using rocking walls as a structural system capable of providing a desired seismic performance. It is proposed that rocking systems be used in MIF or CM buildings with a low density of lateral-force-resisting-elements, where the demand expected in conventionally built MIF or CM walls (or even reinforced concrete walls) might result in damage during earthquakes.

The ability of rocking to protect structures from earthquakes has been noted as early as the 1950's (Houssner, 1956). Yet, rocking has not been developed as much as other alternative structural systems and applications of rocking systems in aseismic structures are scarce (Cormack, 1988; Sharpe and Skinner, 1983). The renewed focus on the seismic performance of buildings has meant that rocking is being considered as an attractive alternative structural solution. Applications in precast walls have been explored (Priestley et al., 1999; Rahman and Restrepo, 2000), and even comprehensive seismic design procedures have been proposed for prestressed rocking bridge piers (Mander and Cheng, 1997). In this chapter, the most relevant features of rocking walls are reviewed, and the aspects discussed here, will be the basis for the formulation of a seismic design methodology, developed in Chapter 4.

3.2 Mechanics of a Rocking Wall

The simplest rocking scheme is the one that assumes that the rocking wall is rigid. That assumption is taken for most of the derived equations here on. A rocking rigid wall may be defined as an oscillating system, though it is different from the common harmonic-type oscillating system, as it presents a rather bilinear stiffness. In this section, a major emphasis is given to the study of its free vibration, trying to address, in this state, most of the dynamic characteristics of the system. Housner (1963) was among the first interested in the rocking system as a structural type and, certainly, the first in publishing some of the kinematic equations presented in this section.

3.2.1 Free Vibration of a Rocking Rigid Wall

Fig. 3-1 shows a rigid wall rocking about its edge *O*. The system has horizontal, vertical and rotational components of acceleration that generate inertial forces, which are counteracted by the reaction at the base and the weight of the body.

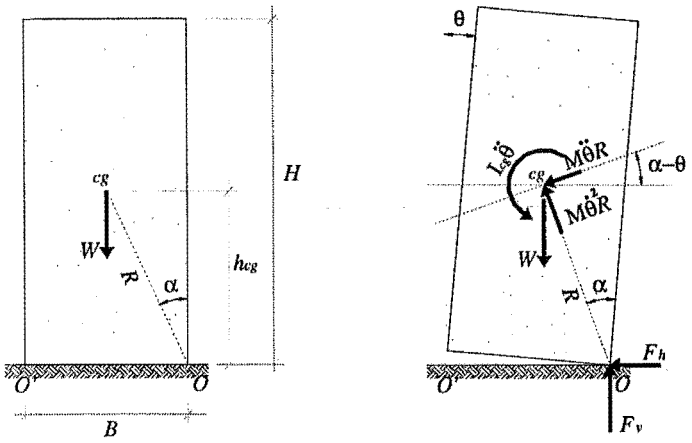

Fig. 3-1 Dimmensions and actions in a rocking rigid wall

In general, apart from rotation of the wall about the edges, it may be expected that bouncing and sliding will occur at impact. When constraints, such as no sliding and no bouncing are imposed on the system, it is possible to describe the movement with the rotation θ. In this case, one only needs to define the dynamic equilibrium of moments about the point *O*. From Fig. 3-1 one gets:

$$\left(I_{cg} + MR^2\right)\ddot{\theta} + WR\sin(\alpha-\theta) = 0 \qquad \text{(Eq. 3.1-a)}$$

or

$$I_o\ddot{\theta} + WR\sin(\alpha-\theta) = 0 \qquad \text{(Eq. 3.1-b)}$$

In the equation above, $WR\sin(\alpha-\theta)$ is the restoring moment due to the self-weight of the wall. In cases in which $(\alpha-\theta)$ is small, $\sin(\alpha-\theta)$ may be reliably approximated by $(\alpha-\theta)$. This is the case for slender walls with ratios h_{cg} to $B/2$ greater than three, where the angle α is about 18° and the difference between the sine and the angle is less than 2%. It is important to note though that even in cases where the ratio $(h_{cg})/(B/2)$ is around 1, the difference is less than 10%. For practical purposes, therefore, one may assume that the free vibration of the system may be evaluated by the following linear differential equation:

$$I_o\ddot{\theta} - WR\theta = -WR\alpha \qquad \text{(Eq. 3.2)}$$

Note that the differential equation above is not constrained to a rectangular rocking wall but rather to any single rocking mechanism with mass M, weight W and moment of inertia I_{cg}.

If the rocking element is released from rest with an initial displacement $\theta = \theta_o$, the initial conditions for the system are $\theta = \theta_o$ and $d\theta/dt = 0$, when $t = 0$. It leads to the solution presented in Eq 3.3 (Housner, 1963), which is valid between two successive impacts:

$$\theta = \alpha - (\alpha - \theta_o)\cosh\left(\sqrt{\frac{WR}{I_o}}\, t\right) \qquad \text{(Eq. 3.3)}$$

And from there:

$$\dot{\theta} = -(\alpha - \theta_o)\sqrt{\frac{WR}{I_o}}\sinh\left(\sqrt{\frac{WR}{I_o}}\, t\right) \qquad \text{(Eq. 3.4)}$$

$$\ddot{\theta} = -(\alpha - \theta_o)\frac{WR}{I_o}\cosh\left(\sqrt{\frac{WR}{I_o}}\, t\right) \qquad \text{(Eq. 3.5)}$$

Note that the solution above is evaluated for the case when the rocking wall is coming down from $\theta = \theta_o$. The preceding stage, when the wall is rotating upwards, can be derived with negative values of time. Therefore, the total time range covered by this equation is $-T/4 \leq t \leq T/4$. It is important to observe that the rotational acceleration is always negative.

Assuming that at impact, no bounce occurs and the friction forces are large enough to prevent sliding at the base, the wall will rock about the opposite end of the base O'. If there are no loses of energy during the impact, the wall will end up in a similar position that when it was released, this time, however, rotating about the point O'. No bouncing of the wall at impact, however, implies that some kinetic energy is lost whether in plastic deformation or radiated vibration energy at the base and, therefore, the amplitude in the following half cycle will diminish. However, for the purposes of defining a period in the conventional way only, it will be assumed here that the oscillation is symmetric. This assumption allows one to state that the time taken by the wall from the rest position ($t = 0$) until it impacts at its base is equal to ¼ of the total period of the oscillation. When $\theta = 0$, therefore, $t = T/4$, where T is the "period" of the oscillation. Replacing these values in the above equation, shows that the "period" of the system can be calculated as:

$$T = 4\sqrt{\frac{I_o}{WR}}\cosh^{-1}\left(\frac{1}{1 - \theta_o/\alpha}\right) \qquad \text{(Eq. 3.6)}$$

Figure 3-2 shows that T is strongly dependent of the ratio θ_o/α tending to infinity as the ratio approaches to 1. It means that, within that range, the larger the displacement, the longer the "period". Priestley et al. (1978) report excellent experimental agreement with this equation for a large range of

amplitudes in a model with different base conditions, provided the period was larger than the non-rocking period of the system.

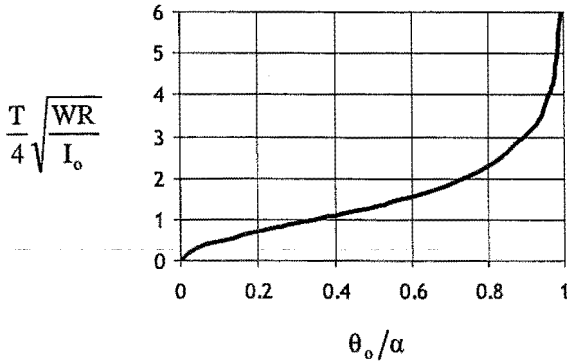

Figure 3-2 Period against amplitude in a rocking wall

Before proceeding, it is important to observe how the restoring moment depends on the angle θ. The rigid wall offers an infinite stiffness to any external load that is below the one required to trigger rocking. After rocking is triggered, the stiffness is negative, which means that the restoring moment decreases with increasing θ (Fig. 3-3). Once θ equals α (when the centre of gravity of the wall is vertically over the supporting edge) the restoring moment equals zero. Beyond this point, in a static context, overturning follows.

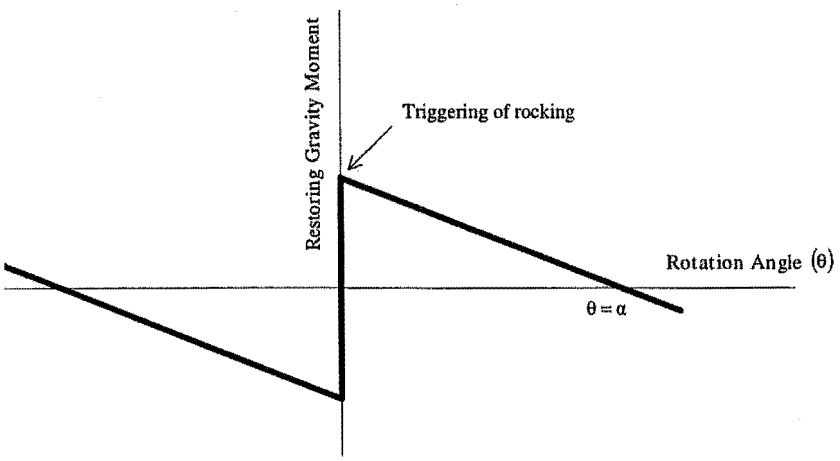

Fig. 3-3 Moment – Rotation in rocking walls

The systems that are to be dealt with in this thesis are not expected to get close to the unstable condition, where $\theta = \alpha$, and therefore, this condition will not be considered further.

3.2.2 Forces in a Rocking System

It is necessary to identify the forces in the system for design purposes. They are defined here. The second part of this section deals with the definition of the forces at impact.

a) Forces in the System before Impact

The scheme in Fig. 3-1 allows for the definition of the forces F_h and F_v in terms of the rotation θ. They would be:

$$F_v = W + M\ddot{\theta}R\sin(\alpha-\theta) - M\dot{\theta}^2 R\cos(\alpha-\theta) \qquad \text{(Eq. 3.7-a)}$$

or (for small angles):

$$F_v = W + M\ddot{\theta}R(\alpha-\theta) - M\dot{\theta}^2 R \qquad \text{(Eq. 3.7-b)}$$

$$F_h = -M\ddot{\theta}R\cos(\alpha-\theta) - M\dot{\theta}^2 R\sin(\alpha-\theta) \qquad \text{(Eq. 3.8-a)}$$

or (for small angles):

$$F_h = -M\ddot{\theta}R - M\dot{\theta}^2 R(\alpha-\theta) \qquad \text{(Eq. 3.8-b)}$$

In the definition of F_v above, the inertial forces due to the radial and tangential acceleration of the mass are always going to be negative (see equation 3.5) and therefore the static solution $F_v = W$ is going to be an upper limit for the dynamic solution. Since the equations above relate the forces to the time through a hyperbolic function, the maximum and minimum values for these expressions will be found in the extremes when $t = 0$ and $t = \pm T/4$. It can be demonstrated that with the contribution of the inertial forces, F_v will be between the extremes presented below:

$t = 0, \quad \theta = \theta_o$

$$F_{v(t=0)} = W\left(1 - \frac{MR^2}{I_o}\alpha^2\left(1 - \frac{\theta_o}{\alpha}\right)^2\right) \qquad \text{(Eq. 3.9)}$$

$t = \pm T/4, \quad \theta = 0$

$$F_{v(t=T/4)} = W\left(1 - \frac{MR^2}{I_o}\alpha^2\left(1 + 2\left(\frac{\theta_o}{\alpha}\right) - \left(\frac{\theta_o}{\alpha}\right)^2\right)\right) \qquad \text{(Eq. 3.10)}$$

The ratio MR^2/I_o can at its largest value be equal to 1.00 (single lumped mass), the most common values being equal or less than 0.75 ($MR^2/I_o = 0.75$ for a rectangular wall). Combining this ratio with practical values of α and θ_o, (ratio $H/B > 1$ and drift < 5%) one can see that the inertial forces might account for forces in the order of $0.05W$, which will be always opposing the load W. Therefore, it is proposed to use, for practical purposes, the static solution of F_v:

$$F_v = W \qquad \text{(Eq. 3.11)}$$

The definition of the horizontal force F_h can be dealt with in a similar way. The maximum and minimum values of F_h will be found when $t = 0$ and $t = \pm T/4$:

$t = 0, \quad \theta = \theta_o$ $$F_{h(t=0)} = W\left(\frac{MR^2}{I_o}\alpha\left(1-\frac{\theta_o}{\alpha}\right)\right)$$ (Eq. 3.12)

$t = \pm T/4, \quad \theta = 0$ $$F_{h(t=T/4)} = W\left(\frac{MR^2}{I_o}\alpha\left(1-2\left(\frac{\theta_o}{\alpha}\right)+3\left(\frac{\theta_o}{\alpha}\right)^2-\left(\frac{\theta_o}{\alpha}\right)^3\right)\right)$$ (Eq. 3.13)

As it can be observed, the difference between these two extreme values depends on the ratio θ_o/α. The difference can be significant large for values of θ_o/α above 0.50. The upper limit of both extreme values though is the same, and can be used for design purposes:

$$F_h = W\left(\frac{MR^2}{I_o}(\alpha)\right)$$ (Eq. 3.14)

This is not only an upper limit for F_h but also will differ from the actual analytical solution by less than 10% for practical values of α and θ_o. One can then rewrite this expression in the following way:

$$F_h = W\alpha_{eff}$$ (Eq. 3.15)

where $$\alpha_{eff} = \left(\frac{MR^2}{I_o}\right)\alpha$$ (Eq. 3.16)

The reason for this change is that now one can define α_{eff} in terms of the geometry of the wall and find that it is possible to use an effective radius, R_{eff}, with a definition very close to that commonly used to represent a multi-storey building by a SDOF oscillator.

$$\alpha_{eff} \approx \sin\alpha_{eff} = \frac{B/2}{R_{eff}}$$ (Eq. 3.17)

where $$R_{eff} = \left(\frac{I_o}{MR^2}\right)R = \left(\frac{I_o}{MR}\right)$$ (Eq. 3.18)

or $$R_{eff} = \left(\frac{\int_M r^2 dM}{\int_M r dM}\right)$$ (Eq. 3.19)

In summary, the reacting forces F_v and F_h can be represented by an equivalent static solution where the static lateral load is applied at a height, R_{eff}, as defined above:

$$F_v = W$$ (Eq. 3.11)

$$F_h = W\alpha_{eff}$$ (Eq. 3.15)

As it will be observed later, there is also the necessity of defining a simple relationship between the two forces, F_h and F_v. The fact that the equivalent static solution is an upper bound to the dynamic problem, does not guarantee that one can use equations 3.11 and 3.15 to relate F_h to F_v. However, a different approach leads to a solution equivalent to the use of the static one. Taking moments about the centre of gravity of the rocking wall, *c.g.*, one gets:

$$F_h = -F_v \tan(\alpha-\theta) + \frac{I_{cg}\ddot{\theta}}{R\cos(\alpha-\theta)} \qquad \text{(Eq. 3.20-a)}$$

or (for small angles):

$$F_h = -F_v(\alpha-\theta) + \frac{I_{cg}\ddot{\theta}}{R} \qquad \text{(Eq. 3.20-b)}$$

Again, the maximum and minimum values of these expressions will be when $t = 0$ and $t = \pm T/4$:

$t = 0, \quad \theta = \theta_o$

$$F_{h(t=0)} = F_{v(t=0)}\alpha\left(1-\frac{\theta_o}{\alpha}\right)\left(\frac{I_o - MR^2\alpha^2\left(1-\frac{\theta_o}{\alpha}\right)^2 - I_{cg}}{I_o - MR^2\alpha^2\left(1-\frac{\theta_o}{\alpha}\right)^2}\right) \qquad \text{(Eq. 3.21)}$$

$t = \pm T/4, \quad \theta = 0$

$$F_{h(t=0)} = F_{v(t=0)}\alpha\left(\frac{I_o - MR^2\alpha^2\left(1+2\frac{\theta_o}{\alpha}-\left(\frac{\theta_o}{\alpha}\right)^2\right) - I_{cg}}{I_o - MR^2\alpha^2\left(1+2\frac{\theta_o}{\alpha}-\left(\frac{\theta_o}{\alpha}\right)^2\right)}\right) \qquad \text{(Eq. 3.22)}$$

In the equations above, for small values of α and knowing that MR^2 is of the same order of I_o and I_{cg}, and that θ_o/α is always in the range from 0 to 1, one can say simplify the equations above into:

$t = \pm T/4, \quad \theta = 0$

$$F_{h(t=0)} = F_{v(t=0)}\alpha\left(1-\frac{\theta_o}{\alpha}\right)\left(\frac{I_o - I_{cg}}{I_o}\right) \qquad \text{(Eq. 3.23-a)}$$

or

$$F_{h(t=0)} = F_{v(t=0)}\alpha_{eff}\left(1-\frac{\theta_o}{\alpha}\right) \qquad \text{(Eq. 3.23-b)}$$

$t = \pm T/4, \quad \theta = 0$

$$F_{h(t=0)} = F_{v(t=0)}\alpha\left(\frac{I_o - I_{cg}}{I_o}\right) = F_{v(t=0)}\alpha\left(\frac{MR^2}{I_o}\right) \qquad \text{(Eq. 3.24-a)}$$

or $$F_{h(t=0)} = F_{v(t=0)}\alpha_{eff} \qquad \text{(Eq. 3.24-b)}$$

From these results, the relationship between F_h and F_v, derived from the equivalent static solution, is only a good approximation of the actual forces when the ratio θ_o/α is small or when the rotation is close to $\theta = 0$. For these cases, therefore, one can say that:

$$F_h = F_v\alpha_{eff} \qquad \text{(Eq. 3.25)}$$

This relationship is needed to define in a practical manner the base shear developed at impact in the rocking wall. This is addressed in the next section.

b) Forces in the System at Impact

The forces developed at impact are expected to be the largest forces during the rocking process. For design purposes it is important, therefore, to define a close equation for the expected impact load at the base of the wall. The impact load will be defined using an impact amplification factor f_{imp}, applied to the approximate equivalent static solution for F_h and F_v defined in equations 3.11 and 3.15. The impact problem in deformable bodies is rather complex as it involves the analysis of travelling shock waves through the deformable body. However, for the purposes of this analysis, simplified energy considerations will be used. All the flexibility of the system will be constrained to the contact elements, which in the case of a rigid wall will represent the stiffness of the foundation. In the case of a non-perfectly rigid wall, it will be defined as two springs in series, combining the stiffness of the foundation and the stiffness of the wall. Figure 3-4 defines the stages to be used for the evaluation of the process. Figure 3-4 also shows the horizontal and vertical contact springs at the base of the rocking wall, with stiffness k_x and k_y respectively.

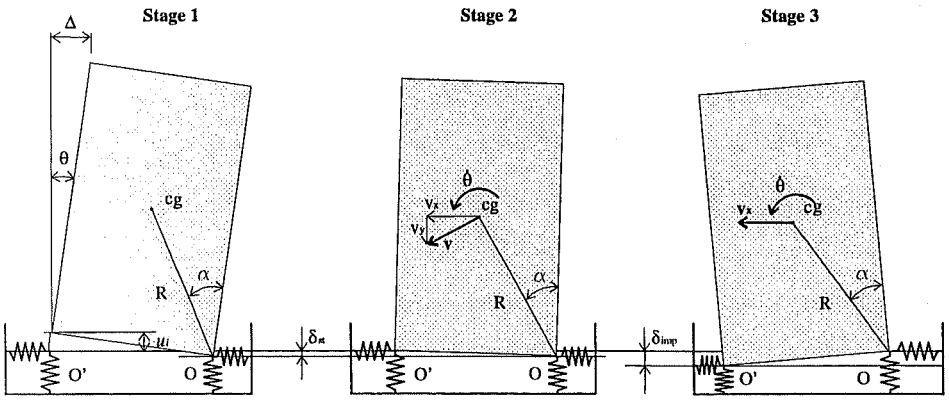

Figure 3-4 Stages of the impact process

The initial conditions of the system are defined by the uplifting of one end of the wall up to a height u_i. Then, the wall is released. Three stages will be defined, on which the energy is to be compared. The initial conditions of the system, where the wall presents it maximum uplift, define stage 1. Stage 2 is defined immediately before impact, and stage 3 is defined at the maximum deformation of the contact elements.

Only potential and strain energy is present in stage 1. The potential energy is defined by the initial uplifting of one end and the depression due to the static deformation of the vertical springs, $\delta_{st} = W/k_y$ (see Fig 3-4). The strain energy is given by the deformation of the springs due to the initial value of the forces F_h and F_v. The static approximate solution (equations 3.11 and 3.15) is used to define the forces F_h and F_v.

$$E_{p1} = W\left(\frac{1}{2}(u_i - \delta_{st})\right) \qquad \text{(Eq. 3.26)}$$

$$E_{s1} = \frac{W^2}{2k_y}\left(\frac{k_y}{k_x}\tan^2\alpha_{eff} + 1\right) \qquad \text{(Eq. 3.27)}$$

$$E_{k1} = 0 \qquad \text{(Eq. 3.28)}$$

In stage 2, most of the potential energy has been transformed in kinetic energy. The uplifting u_i has been reduced to zero and only the depression due to the deformation of the vertical springs defines the potential energy of the system. The strain energy will be taken as the same as it was in stage 1, as it was found in the previous section that the reaction forces remain fairly constant for practical values. In the definition of the kinetic energy, the angular velocity will be set in terms of the tangential velocity v: $\dot{\theta} = v/R$.

$$E_{p2} = W\left(-\frac{1}{2}\delta_{st}\right) \qquad \text{(Eq. 3.29)}$$

$$E_{s2} = E_{s1} \qquad \text{(Eq. 3.30)}$$

$$E_{k2} = \frac{Mv^2}{2} + \frac{I_{cg}\dot{\theta}^2}{2} \qquad \text{(Eq. 3.31-a)}$$

or:

$$E_{k2} = \frac{Mv^2}{2}\left(1 + \frac{I_{cg}}{MR^2}\right) = \frac{Mv^2}{2}\left(\frac{I_o}{MR^2}\right) \qquad \text{(Eq. 3.31-b)}$$

Finally, stage 3 defines the maximum deformation in the springs that are impacted upon by the rocking wall. It will be assumed that at this stage, the springs at the other end have been unloaded and, therefore, all the strain energy is due to the deformation in the impact springs. The potential energy is also defined only by the depression δ_{imp}. It also will be assumed that impact only affects the vertical velocity of the *c.g.* of the masses, which is zero when the impact springs reach the maximum deformation. The horizontal and the angular velocity of the system will be regarded as the same as they were immediately before impact occurred. That was observed in preliminary numerical models. Note that the horizontal velocity v_x is related to the total velocity by $v_x = v\cos\alpha$.

$$E_{p3} = W\left(-\frac{1}{2}\delta_{imp}\right) \qquad \text{(Eq. 3.32)}$$

$$E_{s3} = \frac{\delta_{imp}^2 k_y}{2}\left(\frac{k_y}{k_x}\tan^2\alpha_{eff} + 1\right) \qquad \text{(Eq. 3.33)}$$

$$E_{k3} = \frac{Mv^2\cos^2\alpha}{2} + \frac{I_{cg}\dot{\theta}^2}{2} \qquad \text{(Eq. 3.34)}$$

The evaluation of the different expressions for the energy in the system at any stage leads to some simplifications, as some of the energies are found to be much smaller than the total energy in the system. It can be observed that the initial strain energy E_{s1} is very small compared to the initial potential energy E_{p1}. After operating one can find that the ratio E_{s1}/E_{p1} is:

$$\frac{E_{s1}}{E_{p1}} = \frac{\left(\frac{k_y}{k_x}\tan^2\alpha + 1\right)}{\left(\frac{u_i}{\delta_{st}} - 1\right)} \qquad \text{(Eq. 3.35)}$$

In the numerator, k_y and k_x are of the same order in a rocking wall, which means that after its ratio is multiplied by $\tan^2\alpha$, the value in the numerator will be close to 1. In the denominator, the values of u_i that one may have at the design stage are much greater than the initial static deformation δ_{st} and, therefore, one expects to get a large number in the denominator. One can find that when practical values are placed in the above equation, the ratio E_{s1}/E_{p1} is less than 0.02. For practical purposes, therefore, E_{s1} (and consequently E_{s2}) can be neglected. As the design value u_i is much larger than δ_{st} one also can ignore this last term in the definition of the potential energy of the system. Neglecting the contribution of δ_{st} is conservative as δ_{st} is always going to reduce the total height that defines the initial potential energy of the system.

With these simplifications, the total energy at every stage would be:

stage 1 $$E_1 = \frac{Wu_i}{2} \quad \text{(Eq. 3.36)}$$

stage 2 $$E_2 = \frac{Mv^2}{2} + \frac{I_{cg}\dot{\theta}^2}{2} \quad \text{(Eq. 3.37-a)}$$

or $$E_2 = \frac{Mv^2}{2}\left(\frac{I_o}{MR^2}\right) \quad \text{(Eq. 3.37-b)}$$

stage 3 $$E_{k3} = -\frac{W\delta_{imp}}{2} + \frac{\delta_{imp}^2 k_y}{2}\left(\frac{k_y}{k_x}\tan^2\alpha_{eff} + 1\right) + \frac{Mv^2\cos^2\alpha}{2} + \frac{I_{cg}\dot{\theta}^2}{2} \quad \text{(Eq. 3.38)}$$

Comparing the energy of stages 1 and 2 one can obtain the velocity immediately before impact occurs:

$$v^2 = \frac{Wu_i}{M}\left(\frac{MR^2}{I_o}\right) = gu_i\left(\frac{MR^2}{I_o}\right) \quad \text{(Eq. 3.39)}$$

And equating the total energy in stage 2 to the total energy in stage 3 one gets the following second order equation for δ_{imp}:

$$\delta_{imp}^2\left(k_y\left(\frac{k_y}{k_x}\tan^2\alpha_{eff} + 1\right)\right) - \delta_{imp}(W) - (Mv^2\sin^2\alpha) = 0 \quad \text{(Eq. 3.40)}$$

The solution of this second-degree equation is:

$$\delta_{imp} = \frac{W}{k_y}\frac{\left(1 + \sqrt{1 + 4\left(\frac{k_y}{k_x}\tan^2\alpha_{eff} + 1\right)\left(\frac{Mv^2}{W^2/k_y}\sin^2\alpha\right)}\right)}{2\left(\frac{k_y}{k_x}\tan^2\alpha_{eff} + 1\right)} \quad \text{(Eq. 3.41)}$$

Finally, the factor of amplification due to impact will be:

$$f_{imp} = \frac{k_y}{W}\delta_{imp} \quad \text{(Eq. 3.42)}$$

The amplified forces $F_{v\,imp}$ and $F_{h\,imp}$ can now be calculated with:

$$F_{v\,imp} = f_{imp}F_v \quad \text{(Eq. 3.43)}$$

$$F_{h\,imp} = F_{v\,imp}\alpha_{eff} = f_{imp}F_v\alpha_{eff} = f_{imp}F_h \quad \text{(Eq. 3.44)}$$

Even a greater simplification may be achieved if the angle α_{eff} is small enough to make $(k_y/k_x)\tan^2\alpha_{eff}$ << 1. If this is the case the impact factor f_{imp} may be taken as:

$$f_{imp} = \frac{\left(1+\sqrt{1+4\left(\frac{Mv^2\sin^2\alpha}{W^2/k_y}\right)}\right)}{2} \qquad \text{(Eq. 3.45)}$$

Notice that, in the previous and following analysis, the excitation at the base was not taken into account. This means that, in the event of an earthquake, the work done by the base shear at the foundation is not taken into account. This affects the balance of energy as developed above. It is expected that, as rocking will significantly uncouple the first mode of vibration from the oscillation at the base, the equations above will still be valid.

3.2.3 Energy Dissipation Capacity of a Rocking Rigid-Wall

Different from other oscillating systems, the model abruptly dissipates energy at the point of discontinuity according to the impact conditions. Immediately before and immediately after the impact, only kinetic energy is present in the system (assuming that the zero value of potential energy is defined at the rest position of the wall). Hence, the reduction in the energy of the system at impact, may be defined by the reduction of kinetic energy at that stage:

$$r = \left(\frac{1}{2}I_o\dot{\theta}_2^{\,2}\right)\Big/\left(\frac{1}{2}I_o\dot{\theta}_1^{\,2}\right) = \left(\frac{\dot{\theta}_2}{\dot{\theta}_1}\right)^2 \qquad \text{(Eq. 3.46)}$$

Applying the principle of conservation of the angular momentum, it can be demonstrated that the reduction factor, r, is equal to (Housner, 1963):

$$r = \left(1-\frac{MR^2}{I_o}(1-\cos 2\alpha)\right)^2 \qquad \text{(Eq. 3.47)}$$

In classical analytical dynamics, loses of kinetic energy at impact are usually expressed in terms of a coefficient of restitution, e, (Goldsmith, 1960) which is equal to the ratio of the velocities after and before impact. In a strict sense, the coefficient of restitution for this ideal case is $e = 0$ since it is assumed that no bounce occurs at impact. The velocities that are compared in Eq. 3.44 are not the result of bouncing but rather velocities required to meet the principle of conservation of the angular momentum. For convenience, however, the same name, the coefficient of restitution e, has been given to this ratio.

$$e = \frac{\dot{\theta}_2}{\dot{\theta}_1} = 1 - \frac{W}{g}\frac{R^2}{I_o}(1 - \cos 2\alpha) \qquad \text{(Eq. 3.48)}$$

It is important to note that both terms, r and e, only depend of the shape of the wall, which may be defined by either the angle α or the slenderness ratio H/B. In Figure 3-5 it can be observed the variation of these parameters with respect to the slenderness ratio of the wall. The fact that the restitution factor is negative for H/B < $1/\sqrt{2}$ means that, at this range, the wall does not rock but bounces back and rotates about the same end. Again, the bounce at this stage is not related to any elastic behaviour at contact but just a requirement of the idealised system to meet the principle of conservation of angular momentum.

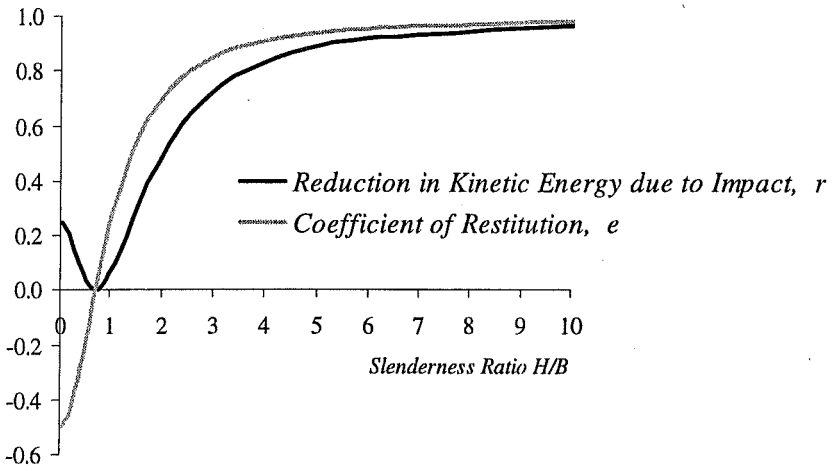

Figure 3-5 Reduction factor and coefficient of restitution vs slenderness ratio

The coefficient of restitution, e, allows one to calculate the velocity immediately after impact from the velocity immediately before impact. With the velocity immediately after impact, the amplitude of the half cycle after impact can be found. It can be demonstrated that the amplitude at any n half-period is given by Eq. 3.49 (Housner, 1963). The implication of this equation is shown in Fig. 3-6, where it can be observed that the coefficient of restitution strongly affects large amplitude oscillations, whereas at low amplitudes its effect is less dramatic. The number of impacts required to get negligible amplitudes is also strongly dependent of the coefficient of restitution of the system.

$$\frac{\theta_n}{\alpha} = 1 - \sqrt{1 - r^n\left(1 - \left(1 - \frac{\theta_o}{\alpha}\right)^2\right)} \qquad \text{(Eq. 3.49)}$$

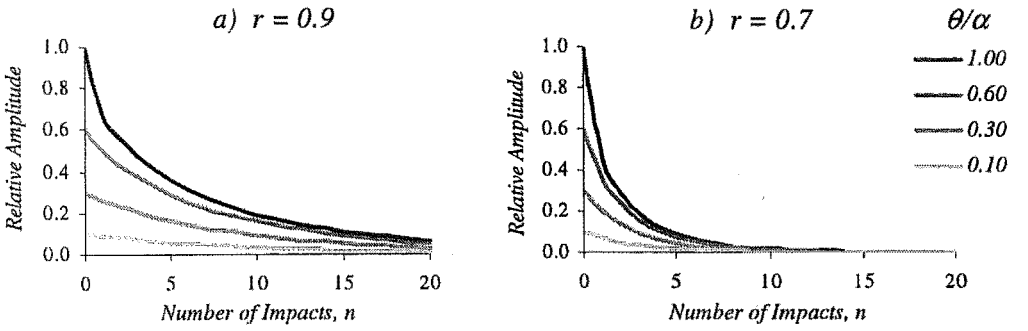

Figure 3-6 Decaying of amplitude in a rocking wall

Priestley et al. (1978) proposed that the process of energy dissipation in the rocking system might be represented by equivalent viscous damping. To that end, they used the equation that relates the fraction of critical damping to the decaying amplitude of the oscillation:

$$\lambda = \frac{1}{2m\pi} \ln\left(\frac{\Delta_o}{\Delta_m}\right) \qquad \text{(Eq. 3.50)}$$

Where m is the number of complete cycles and Δ_o and Δ_m are the initial amplitude and the amplitude at the m^{th} cycle respectively. Using the angular amplitude after the n^{th} half cycle, and realising that $n = 2m$, one finds that the relation between the energy reduction factor, r, and the equivalent percentage of critical viscous damping, λ, is given by the following equation:

$$\lambda = \frac{1}{n\pi} \ln\left(\frac{\theta_o/\alpha}{1-\sqrt{1-r^n\left(1-\left(1-\theta_o/\alpha\right)^2\right)}}\right) \qquad \text{(Eq. 3.49)}$$

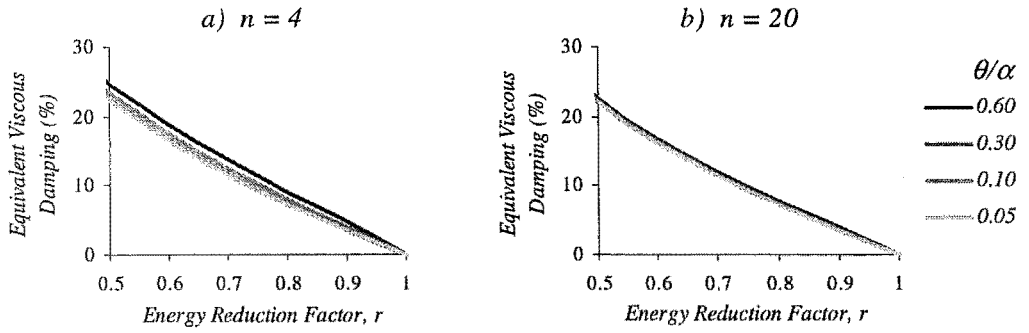

Figure 3-7 Equivalent viscous damping of a rocking system as a funtion of "r"

It is interesting to note (Figure 3-7) that the influence of the ratio θ_0/α is negligible for practical values of the range of r. It is also worth noting that the equivalence is consistent for any number of cycles as observed in the two charts in Figure 3-7, which compare the results when n is taken as 4 and 20.

A perfectly plastic impact process is only ideal as some energy is actually stored by the system and recovered after impact. It has been found, however, that the rocking process may be reliably represented by the derived equations considering a higher value of the energy reduction factor, r. Priestley et al. (1978) tested a model which, according to Eq. 3.44 should have a value of $r = 0.72$. The measured amplitude-decay of the wall matched the decay predicted by Eq. 3.49 when a value of $r = 0.87$ was used though, or an equivalent viscous damping (EVD) of about 4%. Kariotis et al. (1985) report an EVD of 4% in an unreinforced-masonry rocking-wall, which corresponds to $r = 0.87$. The dimensions of the specimen are not stated in their report and, therefore, no comparison can be made with the theoretical value proposed by Housner. Kariotis et al. (1985) also report that the same EVD was found for low and large initial displacements, showing that the initial displacement has little influence in the energy dissipation capacity of the system. This is predicted by Eq. 3.49. Aslam et al. (1980) calculated a best-fit coefficient-of-restitution, e, for a number of rocking concrete walls. They found a value $e = 0.925$, which leads to $r = e^2 = 0.86$. The ratios H/B of Aslam's specimens are stated in Table 3-1, where all the results reported above are compared.

Table 3-1 Experimental values of the reduction factor, r, for rocking walls

Case	*H/B*	*R (m)*	*Theoretical r*	*Best-fit r*	*Material of the Wall*
Priestley et al. (1978)	3.5	1.03	0.72	0.87	--
Kariotis et al. (1985)	--	--	--	0.87	unreinf. masonry
Aslam et al. (1980)	4.3	0.50	0.85	0.86	concrete
	5.0	0.38	0.90	0.86	concrete
No damage was reported in any case.					

Priestley et al. (1978) also report that the experimental value $r = 0.87$ was independent of the foundation-conditions of the system. They tested the wall on a rigid base, on a rubber pad and on a soil base and in the three cases, the same value of r was observed. Note that, even though a "best fit" r can be found to represent the observed behaviour, there is not clear trend on how to get this value from the theoretical reduction factor, r. Actually, the EVD seems to be limited to rather low levels. In Priestley et al's walls, for example, the EVD should have been of above 10% (Figure 3-7) for that value of the reduction factor, r, instead of the observed 4%. Furthermore, the reported experimental results are actually drawn from deformable walls, and another energy-dissipation mechanisms, therefore, should be expected to have contributed to the total EVD of the system.

3.3 Mechanics of a Rocking Wall dragging additional Mass

As commented in section 3.2.1, equation Eq 3.1 can be applied to any single rocking mechanism with mass M, weight W and moment of inertia I_{cg}. This generalisation, however, is not enough, as our interest is not only in single rocking walls but rocking walls as part of a major structure. Only some minor modifications of the solution for the isolated rocking wall, are required to define all parameters of interest in this combined system. This is dealt with in the next section.

3.3.1 Free Vibration of a Rocking Rigid Wall dragging additional Mass

A rocking wall dragging an extra mass supported in a pinned-base column can represent a structure in which the rocking walls are expected to be the only lateral resistant element. When the structure has more than one storey, the additional mass can be represented with an effective mass M_{eff2}, at an effective height h_{eff2} (similarly to what will be done in section 4.2.1 with Eqs. 4.1 and 4.2). This system is schematically shown in the next figure.

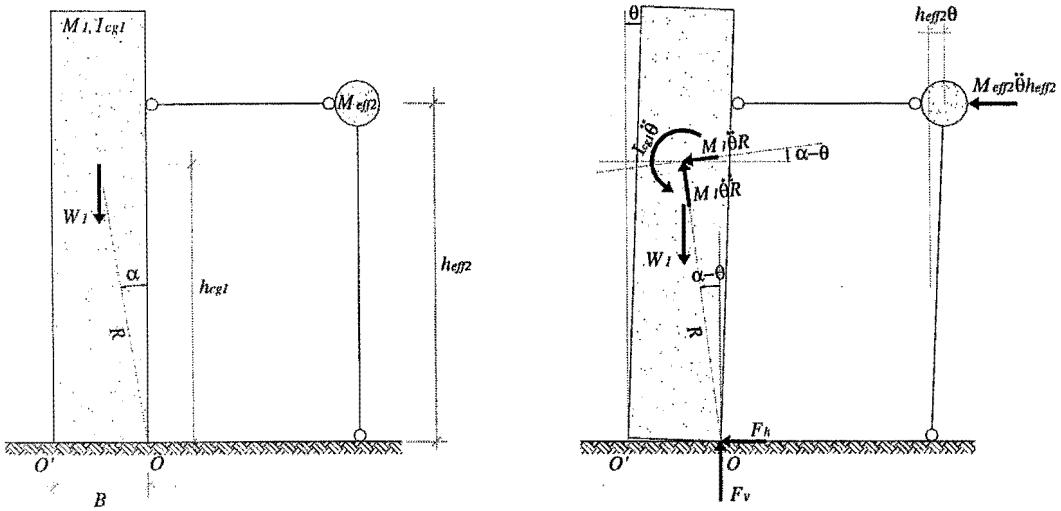

Figure 3-8 Rocking wall dragging additional mass

Taking equilibrium of moments about O, leads to the following equation:

$$\left(I_{cg1} + M_1 R^2 + M_{eff\,2} h_{eff\,2}^2\right)\ddot{\theta} + W_1 R \sin(\alpha\text{-}\theta) = 0 \qquad \text{(Eq. 3.51-a)}$$

or:

$$I_{o\,comb}\ddot{\theta} + W_1 R \sin(\alpha\text{-}\theta) = 0 \qquad \text{(Eq. 3.51-b)}$$

or for small angles:

$$I_{o\,comb}\ddot{\theta} + W_1 R(\alpha\text{-}\theta) = 0 \qquad \text{(Eq. 3.52)}$$

where

$$I_{o\,comb} = I_{cg1} + M_1 R^2 + M_{eff\,2} h_{eff\,2}^2 = I_{o1} + M_{eff\,2} h_{eff\,2}^2 \qquad \text{(Eq. 3.53)}$$

This is the same differential equation as that for the single rocking wall (Eq. 3.2). Therefore, the solution for the rotation θ, as well as for the angular velocity and acceleration, is the same as for that case. This time however, the moment of inertia about the pivoting corner, I_o, includes the additional mass M_2, and the definition of the weight is limited to the weight of the rocking element, W_1. With these modifications, the solution for the "period" of the free vibration of the system is also applicable.

3.3.2 Forces in a Rocking System dragging additional Mass

a) Forces in the System before Impact

The vertical reaction, F_v, has the same form as that for the isolated rocking wall. Using the same reasoning it can be proved that for this case, the static solution of the system is an upper bound to the dynamic one. For design purposes therefore, one can say:

$$F_v = W_1 \qquad \text{(Eq. 3.54)}$$

However, the solution for the horizontal reaction, F_h, has to include the extra inertial force due to the additional dragged mass, M_{eff2}.

$$F_h = -M_1\ddot{\theta}R\cos(\alpha-\theta) - M_{eff2}\ddot{\theta}h_{eff2} - M_1\dot{\theta}^2 R\sin(\alpha-\theta) \qquad \text{(Eq. 3.55)}$$

or (for small angles): $$F_h = -M_1\ddot{\theta}R - M_{eff2}\ddot{\theta}h_{eff2} - M_1\dot{\theta}^2 R(\alpha-\theta) \qquad \text{(Eq. 3.56)}$$

Again, it is possible to define the range of variation of this force by evaluating the extreme cases (when $t = 0$ and $t = \pm T/4$).

$t = 0, \quad \theta = \theta_o \quad$ $$F_{h(t=0)} = W\left(\frac{M_1R^2 + M_{eff2}h_{eff2}R}{I_{o\,comb}}\alpha\left(1-\frac{\theta_o}{\alpha}\right)\right) \qquad \text{(Eq. 3.57)}$$

$t = \pm T/4, \ \theta = 0$

$$F_{h(t=T/4)} = W\left(\frac{M_1R^2 + M_{eff2}h_{eff2}R}{I_{o\,comb}}\alpha\left(1-2\left(\frac{\theta_o}{\alpha}\right)+3\left(\frac{\theta_o}{\alpha}\right)^2-\left(\frac{\theta_o}{\alpha}\right)^3\right)\right) \qquad \text{(Eq. 3.58)}$$

As in the case of the isolated wall, the upper bound for the horizontal reaction F_h, is:

$$F_h = W\left(\frac{M_1R^2 + M_{eff2}h_{eff2}R}{I_{o\,comb}}(\alpha)\right) \qquad \text{(Eq. 3.59)}$$

Again, this solution for F_h can be given in terms of and effective angle α_{eff}:

$$F_v = W\alpha_{eff\ comb} \qquad \text{(Eq. 3.60)}$$

where $$\alpha_{eff\ comb} = \left(\frac{M_1R^2 + M_{eff\,2}h_{eff\,2}R}{I_{o\,comb}}\right)\alpha \qquad \text{(Eq. 3.61)}$$

As it was done before with the isolated rocking wall, one can define this angle in terms of an effective radius $R_{eff\ comb}$:

$$\alpha_{eff\ comb} \approx \sin\alpha_{eff\ comb} = \frac{B/2}{R_{eff\ comb}} \qquad \text{(Eq. 3.62)}$$

where $$R_{eff\ comb} = \left(\frac{I_{o\,comb}}{I_{o\,comb}M_1R^2 + M_{eff\,2}h_{eff\,2}R}\right)R$$

$$\Rightarrow R_{eff\ comb} = \left(\frac{I_{o\,comb}}{M_1R + M_{eff\,2}h_{eff\,2}}\right) \qquad \text{(Eq. 3.63)}$$

Again, this expression can be described in a more fundamental way using the earlier definition for the effective heights:

$$R_{eff\ comb} = \left(\frac{\int_M r^2 dM}{\int_M r dM}\right) \qquad \text{(Eq. 3.19)}$$

b) Forces in the System at Impact

Following the same approach as for the isolated rocking wall, the expected total energy of the system can be defined at every significant stage. In this case the contribution of the mass M_{eff2}, has to be accounted for. The velocity of the dragged mass can also be defined in terms of the velocity of the *c.g.* of the rocking wall, v, using the equation $v_{eff2} = (h_{eff2}/R)v$. With these modifications, the total energy of the system would be:

stage 1 $$E_1 = \frac{W_1u_i}{2} \qquad \text{(Eq. 3.64)}$$

stage 2 $$E_2 = \frac{M_1v^2}{2} + \frac{I_{cg1}\dot{\theta}^2}{2} + \frac{M_{eff\,2}v_{eff\,2}^{\ 2}}{2} \qquad \text{(Eq. 3.65-a)}$$

or $$E_2 = \frac{Mv^2}{2}\left(\frac{I_{o\,comb}}{MR^2}\right) \qquad \text{(Eq. 3.65-b)}$$

stage 3

$$E_{k3} = -\frac{W_1 \delta_{imp}}{2} + \frac{\delta_{imp}^2 k_y}{2}\left(\frac{k_y}{k_x}\tan^2 \alpha_{eff\ comb} + 1\right) + \frac{M_1 v^2 \cos^2 \alpha}{2} + \frac{I_{cg1}\dot{\theta}^2}{2} + \frac{M_{eff\,2} v_{eff\,2}^2}{2} \qquad \text{(Eq. 3.66)}$$

Comparing the energy in stages 2 and 1 one gets the velocity at the *c.g.* of the rocking wall:

$$v^2 = \frac{W_1 u_i}{M_1}\left(\frac{M_1 R^2}{I_{o\,comb}}\right) = g h_i \left(\frac{M_1 R^2}{I_{o\,comb}}\right) \qquad \text{(Eq. 3.67)}$$

And comparing the second and third stages one gets:

$$\delta_{imp}^2 \left(k_y\left(\frac{k_y}{k_x}\tan^2 \alpha_{eff\ comb} + 1\right)\right) - \delta_{imp}(W_1) - (M_1 v^2 \sin^2 \alpha) = 0 \qquad \text{(Eq. 3.68)}$$

The solution in this case would be:

$$\delta_{imp} = \frac{W_1}{k_y}\frac{\left(1 + \sqrt{1 + 4\left(\frac{k_y}{k_x}\tan^2 \alpha_{eff\ comb} + 1\right)\left(\frac{M_1 v^2}{W_1^2/k_y}\sin^2 \alpha\right)}\right)}{2\left(\frac{k_y}{k_x}\tan^2 \alpha_{eff\ comb} + 1\right)} \qquad \text{(Eq. 3.69)}$$

Although the structure of the solutions for v^2 and δ_{imp} is the same as those in the case of the isolated rocking wall, it was necessary to conduct this brief analysis to identify which parts of the combined structure (masses and weights) are "active" at every stage of the impact process. Now that the solutions for v^2 and δ_{imp} are realised, the impact factor, f_{imp}, and the alternative simplified solutions for the system can be found as in the case of the isolated rocking wall.

3.3.3 Energy Dissipation Capacity of the Rocking Rigid-Wall dragging additional Mass

The equations that were developed for the isolated rocking wall can be used here to identify the reduction of energy of the system due to impact. In this case, however, one needs to identify the "active" parts of the structure that are contributing at every stage. After comparing angular momentums before and after the impact one gets the following equations, in which the sub-indexes identify the "active" part for each case. These equations can be used to define the equivalent viscous damping of the system in the same way as in the case of the isolated rocking wall.

$$r = \left(1 - \frac{M_1 R^2}{I_{o\,comb}}(1 - \cos 2\alpha)\right)^2 \qquad \text{(Eq. 3.70)}$$

$$e = 1 - \frac{M_1 R^2}{I_{o\,comb}}(1 - \cos 2\alpha) \qquad \text{(Eq. 3.71)}$$

3.4 Rocking Masonry Walls as an Aseismic System

3.4.1 Positive Aseismic Features of a Rocking Wall

The bilinear-elastic behaviour observed when the rocking wall is statically laterally loaded (Figure 3-9) implies some positive aspects from a seismic-design point of view. They are listed and discussed below.

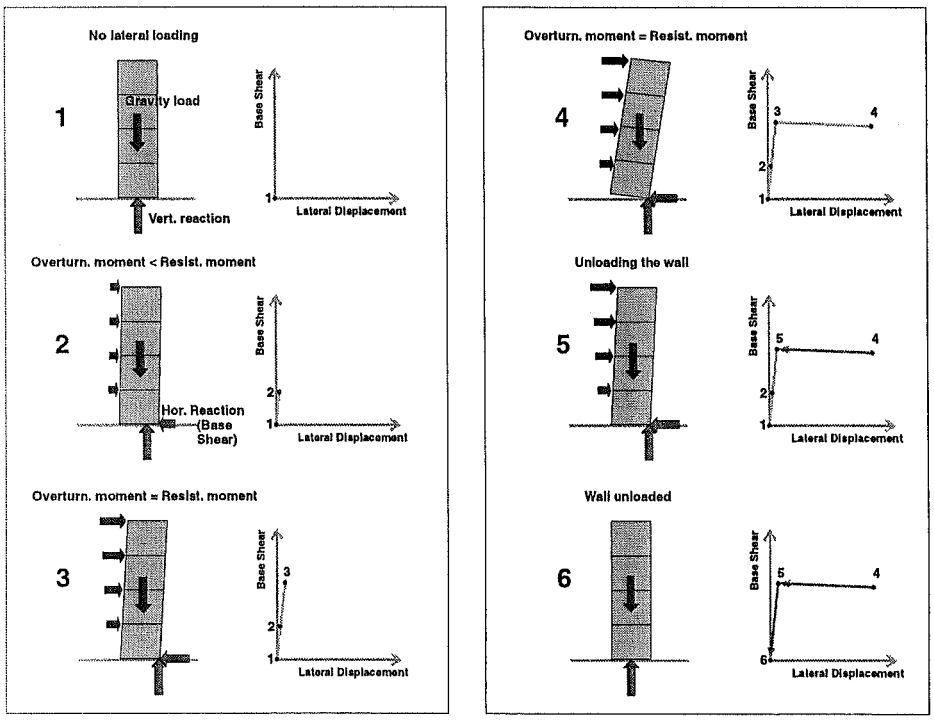

Figure 3-9 Static lateral loading of a rocking wall

- *The base shear is almost independent of displacement.* This means that there is a limit for the strength-demand on the wall. Unfortunately this is only true in a static context. In a dynamic context one has to account for the impact forces, which may significantly increase the demand.

- *The rocking wall can sustain large lateral displacements without damage.* The designer can set the triggering of rocking at a level where no damage is expected in the wall. If this is done, the wall will rotate as a rigid body without further deformation. This fact, accompanied by the

independence of the base shear from the lateral displacement, means that the structure is softened but without being damaged. The effective period therefore will get larger and will move the response of the structure usually into a less demanding region of the acceleration spectra. To achieve this in conventional structures one expects the structure to undergo plastic deformation and therefore get damaged. This is not so in this case.

- *Re-centring mechanism.* The intrinsic re-centring mechanism of the system avoids residual displacements after the structure is displaced laterally. For this to be true, the rocking threshold should be defined before any plastic deformation is induced to the wall.

- *Linear pattern of lateral displacement.* After rocking is triggered the wall moves as a rigid body, maintaining an almost linear displacement profile. If it is stiff enough, it will force the same linear profile to the rest of the structure. The benefit is twofold. First, the deformation is evenly distributed along the height of the structure and not concentrated in a particular level (usually ground level). Secondly, the modelling of the structure, as a SDOF system, is more reliable as the displacement profile is more certain (the benefit in this case is due to the certainty of the pattern rather than in the pattern per se).

- *Dual (stiff / flexible) behaviour of the system.* Rocking is not triggered if the demand does not exceed the passive restoring moment. It implies that there is a range of lateral forces where the wall will behave like a fixed-base wall. There is the possibility, therefore, to take advantage of the high initial stiffness of the wall to face the seismic demands at the serviceability level. Rocking, hence, may be triggered at a greater seismic demand, where larger displacements are preferred to the alternative of damage in the masonry infills. There is not such a possibility in fixed walls, where the infill is expected to increase its level of damage as the severity of the seismic demand increases.

3.4.2 Negative Aseismic Features of a Rocking Wall

Although the list above looks promising from a seismic-design perspective, there are also negative aspects in the behaviour of rocking walls:

- *Low energy dissipation capacity.* The main mechanism of dissipation of energy is through radiation of energy to the ground through impact. It can be demonstrated that for practical dimensions of the walls this only amounts to about 4% of equivalent viscous damping for large displacements and about 2% in smaller displacements.

- *Impact actions can be large.* The impact of the wall against the foundation may cause large impact forces to the wall. This can crush the concrete in the impacting region. Impact, however, is not only a problem for the impacting region. Impact also induces high vertical and

horizontal floor accelerations to the rest of the structure. These accelerations induce inertial forces in the reactive elements increasing the demand in the structure. Also, as it was discussed before, large floor accelerations are not desirable for the performance of the structure as they also may induce damage to the contents of the building.

- *Lateral displacements can be large.* This has to do with the low energy dissipation capacity of the system. Even though during large lateral displacements the walls may still be free of damage, it will be complicated to detail the rest of the structure to be able to accommodate such displacements and rotations. In an extreme, even overturning of the wall could be expected.

- *Seismic response is difficult to predict.* Large variability has been observed in the response of rocking walls to seismic-type oscillations at the base (Chik-Sing et al, 1980) and in the best cases only overturning can be reasonably predicted (Makris and Roussos, 1998). Evaluation of response spectra show that, again, this is mainly due to the lack of an efficient energy-dissipation mechanism of the system: the variability of spectral curves is larger in systems with low energy dissipation capacity than in systems with larger energy dissipation capacity.

- There is a need for *kinematic compatibility* of the whole building with the rocking pattern of the walls. The building needs to be able to allow the rocking walls to rock in any loading condition and proper detailing needs to be developed to avoid damage in other structural and non-structural components of the building.

3.5 Adapting Rocking Walls to meet a Target Performance

Research conducted on RC rocking walls has shown that the presence of hysteretic energy dissipators may improve the seismic response of a rocking system. Rahman and Restrepo, (2000) and Holden et al. (2002) have used pieces of mild steel connecting the base of the rocking wall with the foundation expecting them to yield axially during the uplift of the wall. The cyclic static tests conducted by these researchers confirmed the contribution of the dissipators towards creating flag-shaped hysteresis-loops in their force-displacement response. Rahman and Restrepo, (2000) reported that the observed histeresis-loops represented up to 14% of equivalent viscous damping. The effect of the yielding pieces of steel at the base of the wall is shown schematically in Figure 3-10. Using dissipators in the rocking wall does not undermine the positive aseismic features of rocking walls listed in section 3.4.1. They rather diminish the impact actions and provide a controlled source of dissipation of energy without damaging the rest of the structure. By having a controlled source of energy dissipation one can use some of the design methodologies suitable for a proper performance-based design.

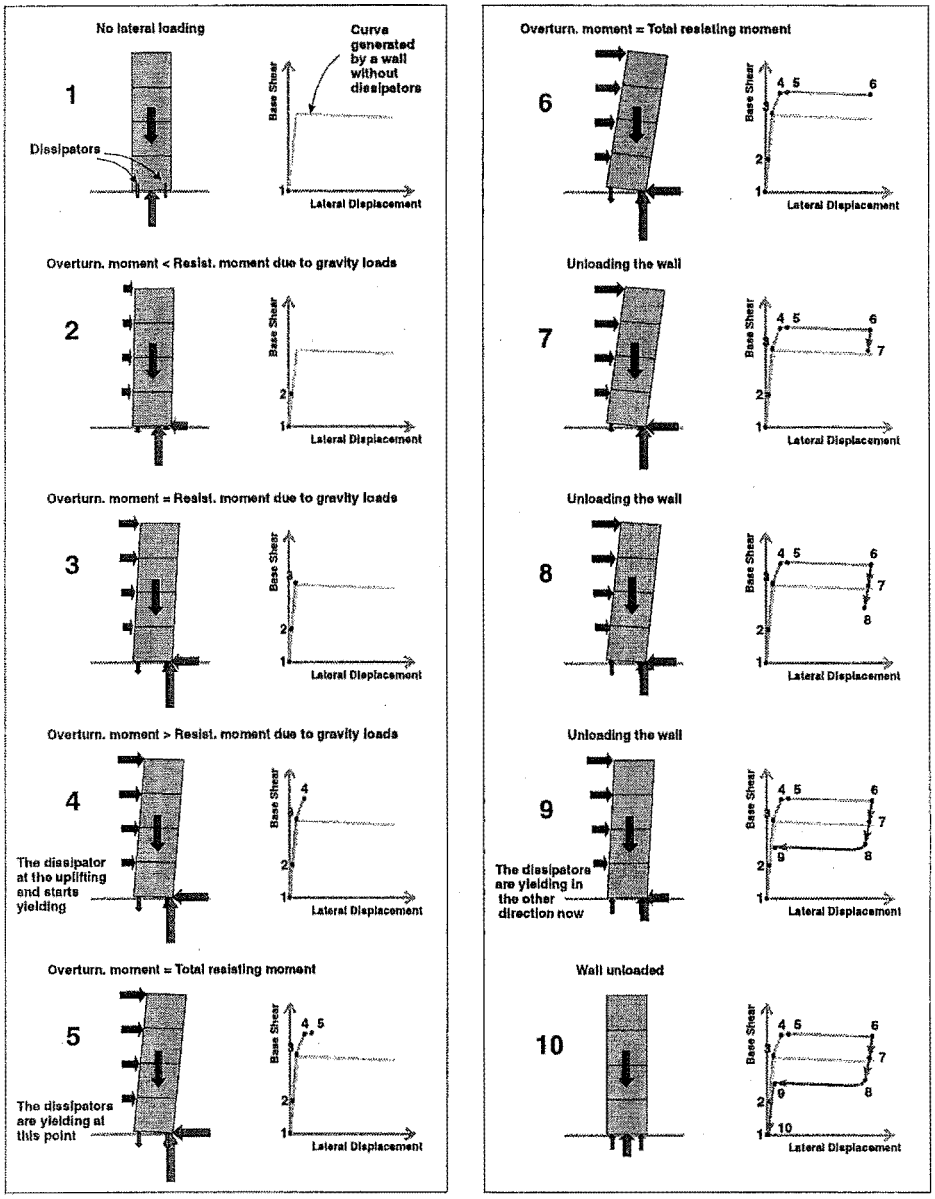

Figure 3-10 Static lateral loading of a rocking wall with dissipators

3.5.1 Forces in a Rocking System with Hysteretic Energy Dissipators at the Base

a) Forces in the System before Impact

Again, the static solution provides an upper bound to the definition of the forces F_h and F_v. For this case, they will be defined as:

$$F_{\mathrm{h}} = \left(W + 2F_y\right)\alpha_{eff} \qquad \text{(Eq. 3.72)}$$

$$F_{\mathrm{v}} = W + 2F_y \qquad \text{(Eq. 3.73)}$$

Where F_y is the yielding force of the dissipators.

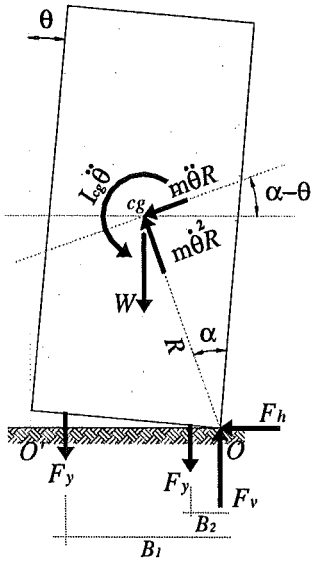

Figure 3-11 Rocking wall with hysteretic energy dissipators

b) Forces in the System at Impact

The same approach that was used for rocking walls without dissipators in section 3.2.2 will be used here. Apart from the energy at the three defined stages, however, one must account for the work done by the hysteretic energy dissipators as they yield all the way until the impact process finishes. The depression due to the initial deformation of the springs, δ_{st}, will not be accounted for in this case. However, one does have to account for the elastic energy stored in the dissipators. It will be assumed that in all three stages the steel dissipators are yielding. The elastic energy stored in the dissipators will be the same in any case and, therefore, will be cancelled out when comparing the cases.

Work done from stage 1 to 2 $$W_{1-2} = -2F_y\left(\frac{u_i}{2} - 2\frac{F_y}{k_d}\right) = -F_y u_i - 4\frac{F_y^2}{k_d} \qquad \text{(Eq. 3.74)}$$

Work done from stage 2 to 3 $$W_{2-3} = -2F_y\frac{\delta_{imp}}{2} = -F_y\delta_{imp} \qquad \text{(Eq. 3.75)}$$

Where k_d is the stiffness of the dissipators and $2F_y/k_d$ is the elastic deformation that the dissipators undergo before yielding in the opposite direction. Note that for Eq. 3.74 to be valid, $u_i/2 > 2F_y/k_d$.

Comparing stages 1 and 2, and accounting for the work done by the dissipators, $W_{1\text{-}2}$, one can define the velocity immediately before impact:

$$v^2 = g u_i \frac{\left(1 - \frac{2F_y}{W} + \frac{8F_y^2/k_d}{Wh_i}\right)}{\left(\frac{I_o}{MR^2}\right)} \qquad \text{(Eq. 3.76)}$$

Comparing stages 2 and 3, and accounting for the negative work done by the dissipators, one gets a second order equation that leads to the following definition of δ_{imp}:

$$\delta_{imp} = \frac{(W - 2F_y) + \sqrt{(W - 2F_y)^2 + 4k_y\left(\frac{k_y}{k_x}\tan^2\alpha_{eff} + 1\right)Mv^2\sin^2\alpha}}{2k_y\left(\frac{k_y}{k_x}\tan^2\alpha_{eff} + 1\right)} \qquad \text{(Eq. 3.77)}$$

In the equation above, k_y and k_x are usually of a similar order, therefore, if α is rather small ($\alpha < 10^o$) then $\tan^2\alpha$ will be a very small number and the expression ($k_y/k_x \tan^2\alpha + 1$) can be replaced by 1. In that case, δ_{imp} can be calculated with:

$$\delta_{imp} = \frac{(W - 2F_y) + \sqrt{(W - 2F_y)^2 + 4k_y Mv^2\sin^2\alpha}}{2k_y} \qquad \text{(Eq. 3.78)}$$

However, this is not the maximum deformation that the springs at the base can sustain. Towards the end of the impact process, the forces in the dissipators can change direction due to the uplifting of the other end of the rocking wall. In that case, equilibrium conditions would require an increase in the reaction at the base of the wall of a magnitude equal to the absolute change in the actions in the dissipators. The maximum change one could expect would be $4F_y$ (from $-2F_y$ to $+2F_y$). If the dissipators are very stiff, this change could occur very quickly, and the increase in the reaction at the impacting corner may be fully developed by the time the impact deformation reaches its peak. The maximum expected impact deformation would occur in that case and it would be:

$$\delta^*_{imp} = \delta_{imp} + 4\frac{F_y}{k_y} \qquad \text{(Eq. 3.79)}$$

The actual impact deformation would be between these two extremes and would depend on the flexibility of the dissipator. A soft dissipator will lead to impact actions close to δ_{imp}, while a stiff dissipator would lead to impact deformations close to δ^*_{imp}. Conservatively, until experimental information is found, the design impact amplification factor can be defined as:

$$f_{imp} = \frac{\delta^*_{imp} k_y}{W + 2F_y} \qquad \text{(Eq. 3.80)}$$

3.5.2 Total Accelerations in the System

Total accelerations are an important parameter within a performance-base scheme, and the following analysis is intended to predict them. As the rocking system uncouples, at some extent, the oscillation of the wall from the shaking at the base, one can attempt to predict the total accelerations that might occur in the system during an earthquake from those expected in the simple rocking model. The acceleration can be obtained from Eq. 3.5 or derived from the expected inertial forces in the system. The second option is more appealing as simple close equations have been derived to define the expected forces in the centre of gravity of the system (they are the same as the reactions at the base). Following this approach, the expected total horizontal acceleration, a_{hi}, at any height of the wall, h_i, can be derived from the next equation. Noise must be expected from the higher modes of free vibration in the structure, as they are not uncoupled at all.

$$a_{hi} = \frac{h_i}{h_{eff}} \frac{F_h}{m} \qquad \text{(Eq. 3.81)}$$

The impact amplification factor, f_{imp}, has to be used to define the peak accelerations when impact occurs. The same approach might be used to define vertical accelerations, although in this case there is no uncoupling from the vertical base shaking.

3.5.3 Energy Dissipation Capacity of the Rocking Rigid-Wall with Hysteretic Energy Dissipators

In large levels of seismic demand, the energy dissipators alone provide most of the hysteretic damping in the system. Figure 3-12 represents the cyclic lateral loading of a rocking wall with perfectly rigid-plastic dissipators. The enclosed areas can be used to calculate the equivalent viscous damping (EVD) of the system using the following equation (Kramer, 1996):

$$\xi_h = \frac{2}{\pi} \frac{A_{hl}}{A_{ext}} 100\% \qquad \text{(Eq. 3.82)}$$

Where A_{hl} is the area enclosed by the hysteretic loops and A_{ext} is the total rectangular area defined by the coordinates of the maximum force-deformation point. Figure 3-12 also allows determining the magnitude of the areas in terms of other already known parameters.

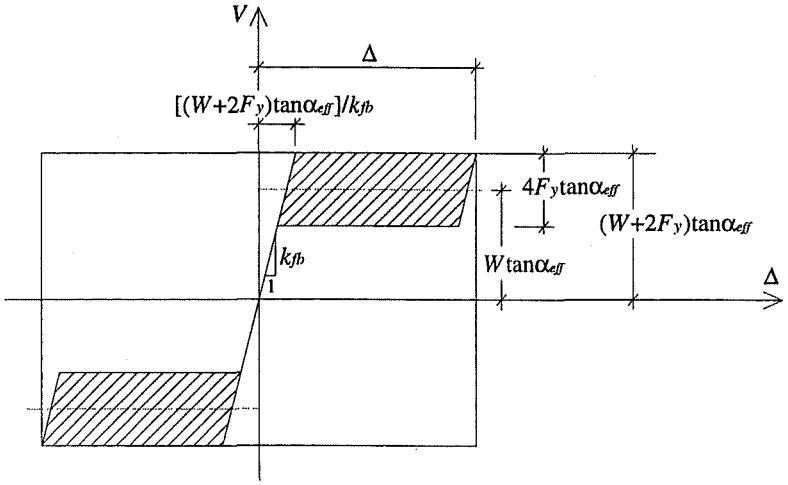

Figure 3-12 Areas for the calculation of equivalent viscous damping due to dissipators

After operating, Eq. 3.82 becomes:

$$\xi_{h-ideal} = \frac{2}{\pi}\frac{\beta}{(1+\beta)}\left(1-\frac{W(1-\beta)\tan\alpha_{eff}/K_{fb}}{\Delta}\right)(100\%) \qquad \text{(Eq. 3.83)}$$

where $$\beta = \frac{2F_y}{W} \qquad \text{(Eq. 3.84)}$$

In most cases, the deformation of the rocking wall before rocking is much smaller than the total deformation of the system, Δ. If that is expected, Eq. 3.83 may be reduced to:

$$\xi_{h-ideal} = \frac{2}{\pi}\frac{\beta}{(1+\beta)}100\% \qquad \text{(Eq. 3.85)}$$

For large lateral displacements, this ideal equivalent viscous damping could reach values of the order of 15% to 25%. This value, however, has been defined assuming a perfect rigid-plastic dissipator. Since it is not possible to find such a dissipator in a real structure, correction factors need to be defined to account mainly for the smaller hysteretic loops that one should expect when using a real imperfect dissipator.

Since the wall is behaving elastically, the hysteretic loops depicted in Figure 3-12 have the same area as the total area of the hysteretic loops produced by the dissipators, $\sum A_{1i}$ (Figure 3-13). The correction of the dissipated energy, therefore, can be made in the areas depicted in Figure 3-13. Three factors were used to that end. Factor C_1 accounts for the non-perfect rigidity of the dissipators; C_2 accounts for the curved shape of the hysteretic loops; and factor C_3 accounts for corrections that the

experimental evidence would require one to do (a value of $C_3 = 0.85$ is recommended later in Chapter 6). With these corrections, the design hysteretic equivalent viscous damping ξ_h is:

$$\xi_h = C_1 C_2 C_3 \xi_{h-ideal} \qquad \text{(Eq. 3.86)}$$

The definition of the three factors takes into account possible different locations of the dissipators in the base of the wall (Figure 3-11). The initial stiffness k_d and the yielding load F_y, are recommended to be constant to maintain symmetry in the dynamic response of the rocking wall and, therefore, will be treated as such in the following analysis. Factor C_1 can be defined as the sum of the ratios between the areas A_{2i} and A_{1i} (Figure 3-13):

$$C_1 = \sum \frac{A_{2i}}{A_{1i}} = \sum \left(1 - \frac{2F_y}{\Delta_{di} k_d}\right) \quad where \left(1 - \frac{2F_y}{\Delta_{di} k_d}\right) \geq 0 \qquad \text{(Eq. 3.87)}$$

Where Δ_{di} is the vertical deformation and stiffness of each dissipator. For certain combinations of F_y, Δ_d and k_d, the equation above might produce negative values, this only means that the dissipator is still within the elastic region and is not dissipating any energy. In that case the ratio should be taken as zero. C_1 can also be defined in terms of the lateral displacement of the structure, Δ. Assuming that the deformation of the wall is small compared to the total lateral displacement after rocking has occurred one can define C_1 as:

$$C_1 = \sum \left(1 - \frac{2F_y h_{eff}}{\Delta B_i k_d}\right) \quad where \left(1 - \frac{2F_y h_{eff}}{\Delta B_i k_d}\right) \geq 0 \qquad \text{(Eq. 3.88)}$$

The definition of C_2 requires the testing of the dissipators as the shape of the loops depends on properties of the material and the type and dimensions of the dissipator. Values between 0.80 and 0.90 were found in the experimental work described later in Chapter 5.

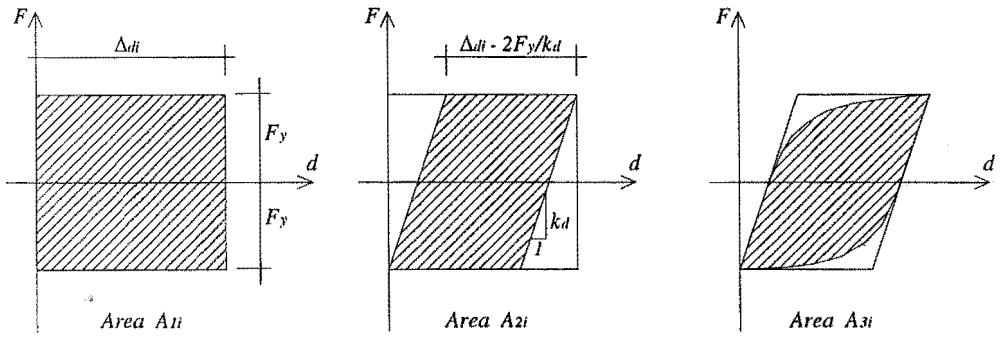

Figure 3-13 Correction of the hysteretic loop of a dissipators

The hysteretic damping due to the dissipators is not the only source of energy dissipation in the structure. Equivalent viscous damping (EVD) due to impact and other mechanisms intrinsic to the structure need to be added to get the total EVD of the system. The EVD intrinsic to the structure, ξ_o, has been found to be very small when a structure is behaving elastically, usually below 2% (Early, 1989). The EVD due to impact, ξ_i, has been defined in a previous section in this chapter. Mander and Cheng (1997) have pointed out that the definition of the EVD due to impact, following Houssner's approach is not compatible with the EVDs calculated following an energy approach, and therefore they can not be added up. Mander and Cheng, however, found that the results are close enough when the lateral displacement is less than 0.25 the width of the rocking wall.

When dissipators are used, the contribution of the impact to the total energy dissipation capacity of the system is small. In the design stage, acknowledging that one is getting at least 10% of equivalent viscous damping from the hysteretic dissipators, one could either define the EVD from the impact process simply as 2% or, conservatively, neglect it. This is reinforced by the experimental evidence exposed in section 3.2.3 that showed the unreliability of the impact energy dissipation mechanism.

As the EVDs described above represent parallel energy dissipation mechanisms, and acknowledging the limitation pointed out by Mander and Cheng in the definition of the EVD due to impact, the expressions can be added up to produce the total EVD of the system. The total equivalent viscous damping of the system is therefore:

$$\xi = \xi_o + \xi_i + \xi_h \qquad \text{(Eq. 3.89)}$$

3.6 Conclusions

- For practical dimensions (ratio $H/B > 1$) and initial rotations (drift < 5%) of rocking walls, the total average forces observed in a rocking wall can be reliably approximated to the forces obtained with a static analysis. The forces due to the impact of the rocking wall against the foundation, however, need to be calculated. The impact forces can be calculated with an impact factor f_{imp}, for which an equation has been proposed in this chapter.

- Rocking walls have many positive features from a seismic point of view, namely: the base shear is almost independent of displacement; the rocking wall can sustain large lateral displacements without damage; rocking walls have a re-centring mechanism; a well defined linear pattern of lateral displacement; and the dual (stiff/flexible) behaviour of the system.

- Rocking systems have also negative aspects that need to be addressed if they are to be used to provide the aseismic capacity in a building. They are: low energy dissipation capacity; impact

actions can be large; lateral displacements can be large; and seismic response is difficult to predict. It was found that most of these negative issues have their origin in the lack of a reliable source of energy dissipation in rocking walls.

- Hysteretic energy dissipators placed at the base of rocking walls can provide a reliable source of energy dissipation to the system as well as reduce the impact actions expected in this system. An equation has been provided to calculate the energy-dissipation-capacity of the system in terms of equivalent-viscous-damping (EVD).

Chapter 4 Seismic Design of a Structure with Rocking Walls as the Main Lateral Resistance Elements

4.1 Introduction

The reliable definition of a rocking system as a single degree of freedom elastic oscillator, along with the predictability of the energy dissipation capacity of the system, allows the use of seismic design methodologies suitable for a PB scheme. Mander and Cheng (1997) have proposed a design procedure for post-tensioned rocking bridge piers based on the Capacity Spectrum method. Their method, however, relied in energy dissipation of the system due to the impact of the rocking piers against the foundation. In this chapter, the Direct Displacement-Based method (Priestley and Kowalsky, 2000) was adapted for the seismic design of buildings with rocking walls incorporating hysteretic dissipators. Mander and Cheng's, however, can also be readily adapted to allow for hysteretic dissipators. This chapter also includes the comprehensive seismic design of a prototype building, which is to be modelled and tested as described in following chapters.

4.2 Proposed procedure for the seismic design of the structure

4.2.1 Displacement Based Seismic Design of the System

A main goal of this research is to see whether this system can be designed to meet PB demands or not, and whether it is possible to reliably predict the seismic performance of the structure for different levels of demand. It was found that the Direct Displacement-Based design method (Priestley and Kowalsky, 2000) could be tailored for this purpose. A helpful flowchart showing the method can be found somewhere else (Nakaki et al., 1999). The procedure, adapted for our system, is described next.

a) Definition of the System as a SDOF Oscillator

A proper definition of the effective height should account for the rotation of the rocking parts of the system. As observed in the previous chapter, however, in practical cases the contribution of these actions is negligible, and always conservative. This contribution is even less important in the case when extra mass is being dragged with the wall. Therefore, an inverse-triangular pattern of the lateral displacement, neglecting the rotational component, can be reliably used to model of the structure as a SDOF system. It can be demonstrated that for such a profile, a structure with masses at different

heights can be represented by an effective mass, M_{eff}, and an effective height, h_{eff}, as defined in the following Eqs:

$$M_{eff} = \frac{\left(\sum_{i=1}^{i=n} m_i h_i\right)^2}{\sum_{i=1}^{i=n} m_i h_i^2} \quad \text{(Eq. 4.1)}$$

$$h_{eff} = \frac{\sum_{i=1}^{i=n} m_i h_i^2}{\sum_{i=1}^{i=n} m_i h_i} \quad \text{(Eq. 4.2)}$$

b) Definition of the Maximum Displacement

The maximum displacement is defined by the permissible drift at every earthquake level. As the wall is expected to behave like a rigid body, the maximum displacement is taken as:

$$\Delta = h_{eff}\, drift_{permissible} \quad \text{(Eq. 4.3)}$$

c) Definition of the Equivalent Viscous Damping (EVD) of the system (ξ)

At this stage, one needs to assume a level of damping that has to be verified later in the process. A good initial guess is in the order of 12% to 20% of EVD.

d) Definition of the Effective Period (T_{eff})

The effective period is taken from the corresponding displacement spectra. Seismic standards usually present only spectra for 5% of viscous damping. The displacement spectra for viscous damping different than 5% can be derived using the equation proposed in the EC8, as reported and suggested by Priestley and Kowalsky (2000) for this purpose. In this equation, ξ is expressed in percentage of the critical damping.

$$\Delta_{(T,\xi)} = \Delta_{(T,5)}\left(\frac{7}{2+\xi}\right)^{1/2} \quad \text{(Eq. 4.4)}$$

e) Definition of the Effective Stiffness (K_{eff})

This is derived treating the system as a SDOF system. The effective stiffness is therefore calculated with the equation:

$$K_{eff} = \frac{4\pi^2}{T_{eff}^2} M_{eff} \quad \text{(Eq. 4.5)}$$

f) Definition of the Base Shear (V)

As the system is treated as elastic with viscous damping, the base shear is calculated with:

$$V = K_{eff}\Delta \qquad \text{(Eq. 4.6)}$$

g) Definition of the Required Capacity of the Energy Dissipators (F_y)

The capacity of the energy dissipators is defined through their yielding point and deformation demand. The deformation demand can be calculated from the expected drift, whereas the yielding point can be calculated using Eq. 3.72. Rearranging this equation one gets:

$$F_y = \frac{1}{2}\left(\frac{V}{\alpha_{eff}} - W\right) \qquad \text{(Eq. 4.7)}$$

The resultant force in the dissipators, $2F_y$, needs to be checked against the gravity load W. The minimum expected value for W has always to be able to yield the dissipators back to their original position. Failing to do so will lead to residual displacements in the structure since the dissipators will maintain the plastic deformations that they had when the seismic event finished. If this is the case, the EVD, assumed in step **c)**, should to be reduced leading to a lower required value of F_y.

h) Checking of the Actual Equivalent Viscous Damping (EVD) of the System (ξ)

The EVD in the system can be calculated as explained in Chapter 3. The total EVD, now has to be compared with the initially assumed value. If the difference is too large, the cycle has to be repeated from step **c)** in this sequence.

4.2.2 Assessment of the Overall Performance

The previous procedure will yield a structure that meets a target displacement for that level of demand. This alone, however, is not enough to assess the seismic performance of the system. The expected drift at every level of seismic demand as well as the absolute floor accelerations also need to be checked. The following issues should be evaluated at this stage:

a) Verification of the Likelihood of Rocking during Frequent and Occasional Earthquakes

As discussed in Chapter 3, in order to prevent excessive lateral displacements during frequent and occasional earthquakes, the dual behaviour of the system, can be exploited. Rocking may be controlled to be triggered at demands larger than frequent earthquakes and if possible larger than occasional earthquakes. The equivalent static lateral load for these levels of seismic demand (F_{demand}) can be compared with the threshold of rocking ($F_{threshold}$). Having ratios (F_{demand})/($F_{threshold}$) smaller than 1 does not necessarily mean that the wall will not rock at these levels. Rocking may be triggered due to the

contribution of the higher modes of the wall that may modify the expected moment at the base of the wall. Unexpected peaks in the ground motion may also trigger the rocking process. However, the likelihood of the rocking will be larger for ratios $(F_{demand})/(F_{threshold})$ larger than 1.00.

b) Expected Lateral Displacement at Other Earthquake Excitation Levels

Assuming that the deformation before rocking begins is smaller than the total maximum deformation, the EVD of the system will be the same. It can be observed that, up to periods of around 4 seconds, typical displacement spectra follow a fairly straight line. When this is the case, it can be demonstrated that the maximum displacement for an earthquake level different than the design one is as stated in Eq. 4.8 (see appendix A), where *RF* is the risk factor as the type proposed by the NZS4203.

$$\Delta_{RP\neq 475\,years} = (RF)^2 \Delta_{RP=475\,years} \qquad \text{(Eq. 4.8)}$$

The assumption of equal EVD is not conservative for the lower levels of the seismic demand. For these lower levels, the efficiency of the dissipators can be significantly less than the expected in the more demanding levels. This would be the case if the dissipators are too flexible. It will be reflected in a reduction of the correction factor C_1, which could actually be equal to zero if by the time the wall has reached its maximum uplifting the dissipator has not yet yielded. It is advisable, therefore, to account for the reduction in the efficiency of the dissipators when dealing with the lower levels of seismic demand (frequent and occasional earthquakes). The definition of C_1, however, depends on the lateral drift and therefore one would have to go through an iterative procedure to define the drift that produces the initially assumed damping or find other relationships to work out a closed form equation for the solution. The iterative procedure can be summarised as follows:

- Assume the expected drift. This value allows calculating the lateral displacement first and the uplifting of the wall next.
- Calculate EVD of the system. One can use the values assumed for the lateral displacement of the system and the uplifting of the wall.
- Calculate the spectral displacement for this level of EVD and seismic demand and compare it with the initially assumed lateral displacement. If the displacement spectrum can be modelled with a straight line with slope, m_d, it can be shown that the lateral displacement, Δ, will be:

$$\Delta = M_{eff} \frac{4\pi^2}{V} (m_d)^2 \qquad \text{(Eq. 4.9)}$$

In Appendix A, it is demonstrated that a closed form equation for Δ can be produced for this case. The slope, m_d, of the displacement spectrum for any level of damping and seismic demand was defined as a function of the slope, $m_{d\text{-}475\text{-}5\%}$, and the risk factor, *RF*.

$$\Delta = \frac{Q_1 B_d k_d + 2F_y h_{eff} C_2 C_3 \xi_{h-ideal}}{(2+\xi_o+\xi_i+C_2 C_3 \xi_{h-ideal})B_d k_d} \quad \text{(Eq. 4.10)}$$

and

$$Q_1 = \frac{28\pi^2}{V} M_{eff} (RF)^2 (m_{d-475,5\%})^2 \quad \text{(Eq. 4.11)}$$

c) Maximum Expected Absolute Acceleration

Due to the rigid-body type motion of the structure, the maximum total acceleration is expected to occur at the top of the building. The basic value established in Eq. 3.81, however, would need to be amplified by the impact factor, f_{imp}, to get the maximum expected acceleration.

d) Risk of Sliding

Considering only the static gravity actions and friction, the sole requirement to allow rocking before sliding is a geometric consideration. It can be shown that the ratio between the width of the wall and the height of the application of the equivalent lateral load need to be smaller than two times the coefficient of friction between the base of the wall and the foundation, μ.

$$B/h_{eff} < 2\mu \quad \text{(Eq. 4.12)}$$

Or, when α is small:

$$\alpha_{eff} < \mu \quad \text{(Eq. 4.13)}$$

Based in this equation one may decide to discard the system or detail elements that prevent the sliding of the wall. Dynamic considerations like vertical accelerations, however, may make this relationship unreliable. Later, in the next chapter, it will be shown that the risk of sliding can be overcome by designing the dissipators to prevent sliding as well. This would prevent sliding in any case.

4.2.3 Modifying the Response of Rocking Walls

If the resulting system is not completely satisfactory, there is still the possibility of modifying the response of the system through the actions described below. These will affect the threshold of rocking and the impact actions:

- *Modifying the base length of the wall.* The base length of the wall is directly proportional to the threshold of rocking as well as to the effects of impact. An increase in the length will delay the triggering of rocking but amplify the effects of impact. A reduction on the length will reduce the effects of impact but lower the rocking threshold. A reduction of the base length also leads to a reduction of the vertical displacements caused by the uplifting of the wall.
- *Modifying the tributary load of the wall.* This action will also affect the features discussed above in a similar way. An increase in the tributary load would also increase the restoring moment of the wall allowing the use of larger dissipators.

- *Post-tensioning the wall with vertical un-bonded cables.* This action will delay the triggering of rocking and increase marginally the initial stiffness of the wall. Post-tensioning, however, may affect the system, as the stiffness of the post-tensioning cables remains unchanged during rocking and therefore would increase the strength demand with increased displacement.

Once the viability of the rocking system has been verified or the required modifications have been done, the design can proceed.

4.3 Seismic Design of a Prototype Masonry Building with Masonry Walls

4.3.1 Description of the Prototype Building and Definition of its Mass and Weight

The prototype building that is defined here is the same building that will be modelled and tested as described later in Chapter five. It is not intended to represent a particular building but to recreate a seismic demand equivalent to the one expected in the kind of buildings that this research is targeting. The benefit of the approach is that it will simplify the modelling and testing process. Figure 4-1 shows the principal characteristics of the structure.

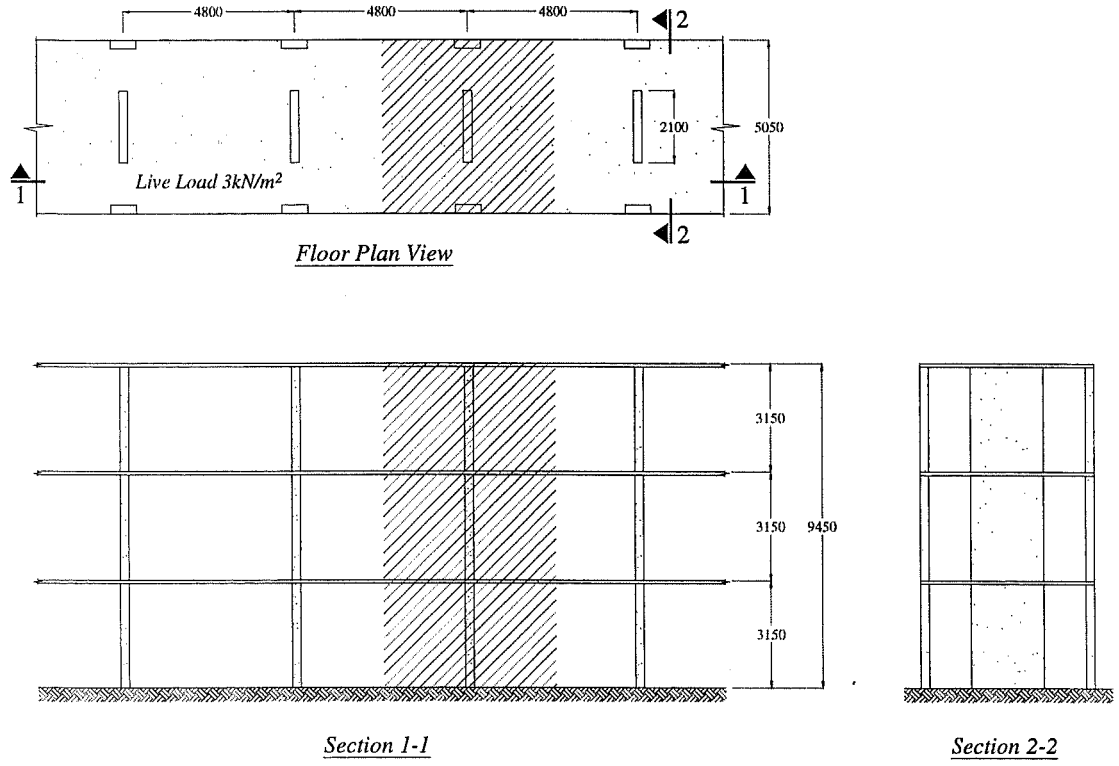

Figure 4-1 Prototype building showing typical section to be designed (hatched section)

Only the short span of the building, that has the walls, is analysed here. In this direction, it will be assumed that the rocking walls with hysteretic dissipators are the only structural elements that provide the lateral capacity of the structure. The section to design is the hatched region of the structure in Figure 4-1, which is typical. Because of the regular pattern of the structure, the seismic demand in the hatched-section, in this direction, can be defined as the inertial forces induced by the mass of the same hatched-section during an earthquake.

The thickness of the slab will be taken as 80mm, the section of the external columns as 250mm x 300mm, and the section of the wall as 2100mm x 270mm. The slab will contain 4 stiffening beams in the direction normal to the wall system, with sections 200mm x 280mm. Two of these beams are connected with the external columns to form the frame that will provide the lateral capacity of the system in the longer direction. The density of reinforced concrete will be assumed as 2400kg/m3 and the density for the masonry 1800kg/m3. The basic live load is taken as 3.00kPa. For the seismic design at the most demanding levels, the seismic live load will be taken as 25% of the basic one, that is 0.75kPa. At the roof level, an overload of 0.40kPa is added. The tributary areas for the wall and columns are (4.80m x 3.33m) 16.6m2 and (4.80m x 0.86m) 4.3m2 per floor respectively.

With this information, the masses of the different components of the building can be calculated. Table 4-1 lists the masses of each element. The elements are defined individually per floor. In the case of the slabs and beams, the tributary area that corresponds to the section to be analysed defines their length. The equivalent total weights corresponding to the live load per floor and the additional dead load in the roof are also calculated in Table 4-2.

Table 4-1 Masses of the elements of the prototype building

Element	*Material*	*Dimensions (m x m x m)*	*Mass (kg)*
Single external column p/floor	concrete	0.25 x 0.30 x 3.07	553
Single confining column p/floor	concrete	0.27 x 0.30 x 3.07	597
Masonry panel p/floor	masonry	0.27 x 1.50 x 3.07	2238
Tributary section of slab	concrete	0.08 x 4.80 x 5.05	4654
Tributary section of longitudinal beam	concrete	0.20 x 0.20 x 4.50	432

Table 4-2 Live load and additional dead load in roof

Element	*Load per m^2 (N/m^2)*	*Area (m x m)*	*Total weight (kN)*
Live load per floor	750	4.50 x 5.00	16.8
Additional dead load in roof*	400	4.80 x 5.00	9.6
*In South America sloping concrete is usually poured in the roof to drain off rain water.			

To proceed with the seismic design, it is necessary to define the dynamic masses at each level. With the results presented in the previous tables it is possible to define these masses as follows:

Table 4-3 Dynamic masses at each level

Element	*Top floor*		*2nd and 1st floor*		*Ground floor*	
	Quant.	*Mass (kg)*	*Quant.*	*Mass (kg)*	*Quant.*	*Mass (kg)*
Slab	1	4654	1	4654	0	0
Beams	4	1728	4	1728	0	0
Masonry panel	½	1119	1	2238	½	1119
Confining columns	2 x ½	597	2 x 1	1194	2 x ½	597
Exterior columns	2 x ½	553	2 x 1	1105	2 x ½	553
Load on roof	1	960	1	0	0	0
Live load	1	1688	1	1688	0	0
Total mass		*11298*		*12606*		*2268*

The next parameter to define is the gravity load that is transferred through the rocking wall. This is defined in the procedure as *W*. As it is observed in this definition of *W*, it is not necessarily the same as dynamic masses associated to the wall. The calculation is presented in the following table.

Table 4-4 Vertical load (W) transferred by the rocking wall

Element	*Quant.*	*Mass (kg)*	*Weight (kN)*
Slab	3 x 0.71	9913	97.1
Beams	6	864	8.5
Masonry panel	3	6714	65.8
Confining columns	6	3581	35.1
Exterior columns	0	0	0.0
Load on roof	1 x 0.71	688	6.7
Live load	3 x 0.71	3594	35.2
Total vertical load (W)			*248.5*

4.3.2 Definition of the Seismic Performance-Objectives for the Prototype

4.3.2.1 Definition of the Performance Levels

The scheme proposed by SEAOC (1995) described in Chapter 2 was followed. The performance levels are described quantitatively in Table 2-27. As mentioned in that chapter, SEAOC (1995) also proposed a list of limits for some measurable parameters to specify these performance levels. The drift related ones are presented in the next table.

Table 4-5 Permissible drifts according to SEAOC (1995)

Performance Level	*Max. Instant Drift*	*Max. Residual Drift*
Fully Operational	< 0.20% +/-	Negligible
Operational	< 0.50% +/-	Negligible
Life Safe	< 1.50% +/-	< 0.50% +/-
Near Collapse	< 2.50% +/-	< 2.50% +/-

4.3.2.2 Definition of the Earthquake Design Levels

The earthquake design levels are taken here as defined in Chapter 2. New Zealand is one of the few countries where the local seismic code provides information for design earthquakes of different return periods. To put this analysis in context, therefore, the guidelines in the NZS4203 (1992) will be adopted. The next table shows the risk factors, *RF*, provided by the NZS4203 (1992) for different demand levels respect to the standard 475 years return period earthquake. The recurrence intervals do not match exactly the ones proposed by SEAOC. Given the nature of seismic hazard studies, these slight alterations will not affect the validity of the results.

Table 4-6 Risk Factors for different return periods according to the 4203NZS

Earthquake Design Level	*Recurrence Interval*	*Risk Factor (RF) according to NZS4203*
Frequent	43 years	0.45
Occasional	72 years	0.60
Rare	475 years	1.00
Very Rare	970 years	1.25

To define a complete picture of the demand, it will be assumed that the building is on intermediate soil in a zone of moderate seismicity. Figure 4-2 shows the displacement spectra derived from the NZS 4203 (1992) for three types of soils and various levels of damping in a moderate seismicity zone.

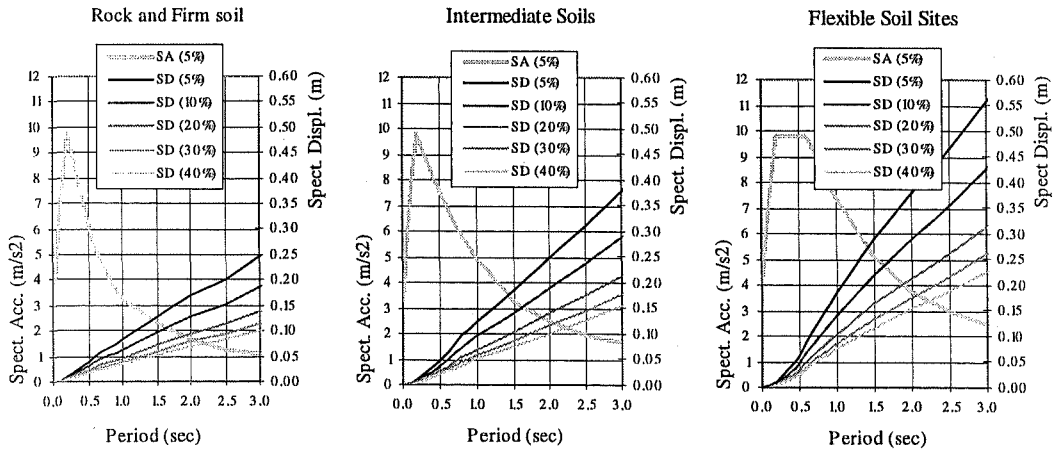

Figure 4-2 Spectral displacement for regions of moderate seismicity calculated from NZS 4203

4.3.3 Displacement Based Design of the Prototype

The sequence described in section 4.2.1 will be used to design the prototype building. Only the last iteration is presented in the chart. The design was conducted to meet the drift target for the "rare" level. This design was conducted based upon some premises that, later, the experimental work will show to need slight modifications. At this stage, experimental results relating to the performance of the dissipators were available. That information was used to define the correction factors *C1* and *C2*. The analysis was conducted using two types of dissipators, one yielding axially (dissipator *D1*) and the other yielding in flexure (dissipator *D3*). The design sequence using the iterative approach is presented in Table 4-7.

Table 4-7 Design sequence of prototype rocking wall

Parameter		*Equation*	*Prototype with dissip.D1*	*Prototype with dissip. D3*	*Units*
Effective Mass of the structure	m_{eff}	Eq. 4.1	31163	31163	kg
Effective Height of the structure	h_{eff}	Eq. 4.2	7.20	7.20	m
Max. Drift expected for a Rare EQ	$drift_{perm}$	-	1.50	1.50	%
Max. Displacement	Δ	Eq. 4.3	0.108	0.108	m
EVD assumed for the system	ξ	-	21.0	17.5	%
Effective Period (interm. soil assumed)	T_{eff}	Fig. 4-2	1.57	1.48	s
Effective Stiffness	K_{eff}	Eq. 4.5	499.1	561.7	kN/m
Required Base Shear	V	Eq. 4.6	53.9	60.7	kN
Required Capacity of Dissipators	F_y	Eq. 4.7	56.9	81.1	kN
EVD due to Dissipators (ideal)	$\xi_{h\text{-}ideal}$	Eq. 3.85	19.6	24.5	%
Dissipator stiffness	k_d	-	100000	12500	kN/m
Correction factor 1	C_1	Eq. 3.88	0.96	0.60	-
Correction factor 2	C_2	-	0.85	0.85	-
Correction factor 3*	C_3	-	1.00	1.00	-
EVD due to dissipators (corrected)	ξ_h	Eq. 3.86	16.1	12.4	%
EVD due to Impact	ξ_i	-	2	2	%
EVD intrinsic of the structure	ξ_o	-	3	3	%
Total EVD in the System ($\xi_{hc} + \xi_i + \xi_o$)	ξ	-	21.1	17.4	%
**This value would probably need to be corrected after the experimental data has been produced*					

It is clear that dissipator *D1* produces a more efficient system. It was not possible, however, to design and build a proper model of dissipator *D1* in the time that we had available for that purpose. The model of dissipator *D1* that was built presented local buckling problems as it is discussed in Chapter 5. The less efficient but more reliable dissipator 3 was finally used for the model.

Although the structure is expected to sustain large displacements, it was decided to set a low value for the intrinsic damping (ξ_o) for 2 reasons: Firstly, to allow for the fact that the model representing the prototype will not have the elements that would provide a good deal of the intrinsic damping of the

building. Secondly, it will be intended to avoid significant deformations in any components of the building but the dissipators. As it is observed in the analysis, this seems to be a valid strategy as the dissipators are able to provide most of the required energy dissipation capacity for the structure.

After completing this stage of the design, the performance objectives have to be evaluated. Table 4-8 presents a summary of the results of the expected performance of the structure. Some comments about each of the parameters are presented below.

The ratio $W/(2F_y)$ is a measure of the capacity of the building to yield the dissipators back to the original position, preventing any residual drift in the system. The value in the table shows that, in both cases, the system has enough reserves to prevent any residual displacement after plastic deformations have been induced in the dissipators.

For the definition of the equivalent static lateral load in the frequent and occasional levels, the New Zealand Standard 4203 (NZS, 1992) defines a constant design spectral acceleration for periods from 0 to 0.45 seconds. This spectral acceleration is 0.8g (in elastically responding structures) for an earthquake with a recurrence interval of 475 years. This design spectral acceleration was multiplied by the risk factors defined in Table 4-6 to get the seismic demand for frequent and occasional events for ductility 1.00. In Table 4-8, this demand is compared with the force that triggers rocking in the system. The table shows that, for this particular case, one should expect rocking in all performance levels. Therefore, this system has to be treated as a rocking one when calculating the expected drift for these levels. The results are again presented for the prototype structure using dissipators *D1* and *D3*.

Table 4-8 Summary of the expected seismic performance of prototype structure

Parameter	*Eq.*	*Prototype with Dissip.D1*	*Prototype with Dissip.D3*	*Units*
Ratio $W/(2F_y)$	-	2.25	1.60	-
Triggering of Rocking ($F_{threshold} = V$)	-	53.9	60.7	kN
Design Spectral Acc. Frequent EQ (0.45 x 0.80g)	-	0.36	0.36	g
Static Equiv. Lat. Seismic Force Frequent EQ ($F_{frequent}$)	-	109.9	109.9	kN
Ratio $F_{frequent}/F_{threshold}$	-	2.04	1.81	-
Design Spectral Acc. Occasional EQ (0.60 x 0.80g)	-	0.48	0.48	g
Static Equiv. Lat. Seismic Force Occas. EQ ($F_{occasional}$)	-	146.6	146.6	kN
Ratio $F_{occassional}/F_{threshold}$	-	2.72	2.42	-
Max. Drift expected for a Frequent EQ (RF=0.45)	Eq. 4.12	0.33	0.68	%
Max. Drift expected for an Occasional EQ (RF=0.67)	Eq. 4.12	0.57	0.86	%
Max. Drift expected for a Rare EQ (RF=1.00)	Eq. 4.12	1.50	1.56	%
Max. Drift expected for a Very Rare EQ (RF=1.25)	Eq. 4.12	2.26	2.22	%
Max. Acc. expected at roof (non-amplified by f_{imp})*	Eq. 3.81	0.23	0.26	g
**This value needs to be amplified by f_{imp} which varies with different drifts*				

The expected drifts exceed the limits set for them in the lower levels of demand. In the prototype with dissipators *D1* they are slightly above the limits but in the prototype with dissipators *D3* they are exceeded by a greater amount. The drifts expected for the prototype with dissipators *D1* are reasonably close to the limits to regard the performance as satisfactory. In the prototype with dissipators *D3*, however, one has to decide whether to repeat the procedure, starting this time with the seismic demand corresponding to the "fully operational" level, or assess if the drift limits can be relaxed and then detail the building to be able to sustain the drifts presented in the table above without exceeding the corresponding limit levels of damage.

4.3.3.1 Definition of the Design Base Shear

The design base shear can reach two extreme values. Firstly, preliminary numerical analysis of a rocking system showed that the inverse-triangular lateral displacement profile is not well defined before rocking starts. The effective height, h_{eff}, therefore may be at a height different to the defined by Eq. 4.2; and the force required to trigger rocking may be different to the basic one, V. To account for this fact it is proposed to assume that the shape of the lateral displacements of the structure could be following a rectangular profile when rocking is triggered. This will lead to a shorter effective height, equal to the height of the centre of gravity of the masses. As a result of this shift in the height, the base shear could increase to:

$$V_1^* = \frac{h_{eff}}{h_{cg}} V \qquad \text{(Eq. 4.14)}$$

The second extreme value is related with the impact actions. The magnitude of the design base shear is calculated by applying the impact amplification factor, f_{imp}, to the basic shear force V, as calculated with a linear horizontal displacement profile pivoting at a corner of the wall, as presented in the next equation. The largest of the values in Eqs. 4.14 and 4.15 should be taken as the design shear force.

$$V_2^* = f_{imp} V \qquad \text{(Eq. 4.15)}$$

Before calculating f_{imp}, it is necessary to define the numerical values of the parameters required in equations 3.76 through 3.80. A summary of some of the required parameters is presented in Table 4-9.

Table 4-9 Parameters for the calculation of f_{imp} - First list

Parameter	*Value*	*Unit*
$I_{o\,comb}$	1615 x 10^3	kg.m2
R	6.49	m
$M_1 R^2$	1311 x 10^3	kg.m2
$I_{o\,comb} / M_1 R^2$	1.23	-

Regarding the stiffnesses k_y and k_x, it will be assumed that the segment of the foundation which the wall impacts against can be represented by a concrete strut of 0.15m^2 of area and 0.60m length. Taking E = 20GPa, this concrete strut yields a stiffness $k_{cs} = EA/L$ = 5000kN/m. This definition was made arbitrarily but it is expected that will not have a great consequence because the resultant stiffness, k_y, is a series of two springs, one being k_{cs} and the second to be defined k_{wy}, which is much more flexible than k_{cs}, and therefore will govern the resultant combined stiffness. The second spring represents the impacting corner of the wall. The axial stiffness of the column and masonry strut plus the flexural stiffness of the base beam have to be combined. The next figure shows schematically how the springs representing the stiffness of the impacting corner are to be defined.

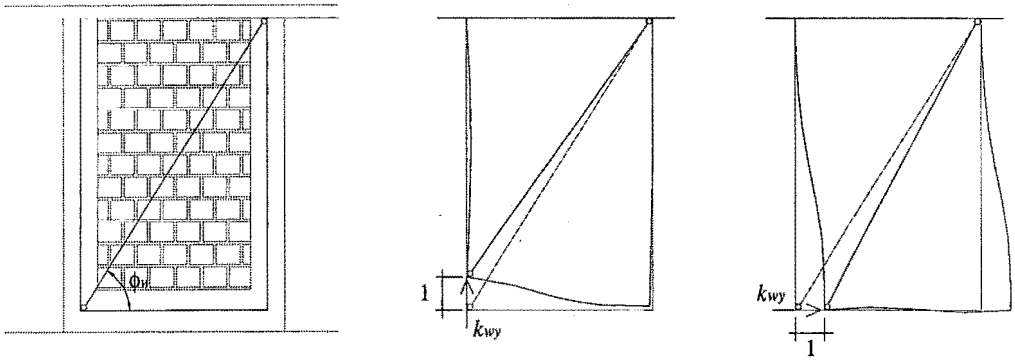

Figure 4-3 Definition of spring stiffness at the impacting corner of the wall

A simplified definition of the stiffness k_{wx} and k_{wy} is presented here. The columns and beams are treated independently assuming no rotation of the joints. This assumption leads to a stiffer structure and therefore, the resulting f_{imp} will be conservative. The next equation gives the vertical stiffness of the impacting corner of the wall:

$$k_{wy} = k_{col-axial} + k_{beam-flexure} + k_{ms}\sin^2(\phi_w) \qquad \text{(Eq. 4.16)}$$

or more explicitly:

$$k_{wy} = \frac{E_{col}A_{col}}{L_{col}} + \frac{12E_{beam}I_{beam}}{L_{beam}^3} + \frac{E_{ms}A_{ms}}{L_{ms}}\sin^2(\phi_w) \qquad \text{(Eq. 4.17)}$$

And for the horizontal spring at the same corner:

$$k_{wx} = 2k_{col-flexure} + k_{ms}\cos^2(\phi_w) \qquad \text{(Eq. 4.18)}$$

or more explicitly:

$$k_{wx} = 2\left(\frac{12E_{col}I_{col}}{L_{col}^3}\right) + \frac{E_{ms}A_{ms}}{L_{ms}}\cos^2(\phi_w) \qquad \text{(Eq. 4.19)}$$

The cross section of the columns is 0.27m x 0.30m (A_{col} = 0.072m^2, I_{col} = 0.0006m^4). And their length is 3.00m. The masonry struts have a cross area defined by its thickness (0.27m) and a width equal to

0.35 times the diagonal of the panel (0.35 x 3.18 = 1.11m). The width was defined conservatively large to produce a stiff infill. The length of the masonry strut is equal to the length of the diagonal of the panel (3.18m). Finally, the beam will have a section of 0.27m x 0.50m (I_{beam} = 0.0028m^4), and a length of 1.80m. Table 4-10 shows a summary of the parameters required to complete the calculation of f_{imp}.

Table 4-10 Parameters for the calculation of f_{imp} – Second list

Parameter	*Value*	*Unit*
$k_{col\text{-}flexion}$	5400	kN/m
$k_{col\text{-}axial}$	540000	kN/m
$k_{beam\text{-}flexion}$	56300	kN/m
k_{ms}	709000	kN/m
k_{wy}	1150000	kN/m
k_{cs}	5000000	kN/m
k_y	933000	kN/m
k_{wx}	169000	kN/m
k_x	169000	kN/m

The values on this table, together with those in Table 4-9 complete the information required to calculate f_{imp}. However, the impact factor f_{imp} is also a function of the drift and therefore, will yield different values for the different performance levels. A summary of the results for the prototype structure with the two different kinds of dissipator is presented in Table 4-11.

Table 4-11 Impact factors, f_{imp}, for different levels of demand

	Prototype with dissipator D1			*Prototype with dissipator D3*		
Event	*Expected Drift (%)*	f_{imp}	f_{imp} *simplified**	*Expected Drift (%)*	f_{imp}	f_{imp} *simplified**
Frequent	0.33	1.20	1.25	0.68	1.57	1.62
Occasional	0.57	1.28	1.34	0.86	1.59	1.65
Rare	1.50	1.54	1.61	1.50	1.67	1.74
Very Rare	2.26	1.70	1.77	2.22	1.75	1.82
**f_{imp} was calculated using the simplified equation 3.78 for δ_{imp}*						

Returning to the definition of the design base shear, V^*, from equations 4.14 and 4.15, it is clear that there will be a single value for Eq. 4.14 but a set of four values for Eq. 4.15. It is up to the designer to define the capacity of the structure to sustain that force demand within the performance levels wanted for the structure.

*Table 4-12 Design shear force V**

Parameter	*Prototype with dissipator D1*	*Prototype with dissipator D3*	*Unit*
Basic Shear Design Force, V	53.9	61.5	kN
Ratio h_{eff}/h_{cg}	1.17	1.17	-
Design shear force V_1*	63.2	71.1	kN
Design shear force V_2* for a frequent event	64.7	95.9	kN
Design shear force V_2* for an occasional event	69.7	97.1	kN
Design shear force V_2* for a rare event	83.6	101.9	kN
Design shear force V_2* for a very rare event	91.7	106.8	kN

Finally, the definition of f_{imp}, also allows for the calculation of the expected maximum absolute accelerations in the building. The basic absolute roof acceleration was defined in Table 4-8. In Table 4-13, the basic absolute acceleration is combined with f_{imp} to produce the maximum absolute accelerations expected at each level of demand.

Table 4-13 Maximum absolute roof accelerations

Parameter	*Prototype with dissipator D1*	*Prototype with dissipator D3*	*Unit*
Basic absolute roof acceleration	0.23	0.26	g
Absolute roof acceleration for a frequent event	0.28	0.41	g
Absolute roof acceleration for an occasional event	0.30	0.42	g
Absolute roof acceleration for a rare event	0.36	0.44	g
Absolute roof acceleration for a very rare event	0.39	0.46	g

4.4 Conclusions

- The Direct Displacement Method can be successfully adapted for the seismic design of a system with rocking walls. A design procedure has been developed in this chapter. In theory, it is also possible to establish a number of other details that would give a good picture of the expected seismic performance of the structure for any performance level.

- The analysis of a prototype model has shown that the initial stiffness of the dissipators may have a significant impact on the expected drift of a system with rocking walls, particularly in weak to moderate events. In large events the difference of having a flexible or a stiff dissipator seems to be less significant.

Chapter 5 Experimental Work: Preliminaries

5.1 Introduction

Guidelines to get a comprehensive picture of the seismic performance of a building with rocking walls have been given in the previous chapter. The analytical model used to that end, incorporated the main features of a real structure. There were some aspects that appeared marginal and therefore were not included. It is expected that the neglected features do not have a significant effect in the seismic performance of the building. This assumption, however, needs to be backed by experimental verification.

Potential conflicts would be most likely to come from the ideal dynamic behaviour of the model. Therefore, it was decided that dynamic tests needed to be conducted. The model to be tested represents the prototype that was analysed at the end of the previous chapter.

The preliminary aspects of the experimental work are described in this chapter, addressing the objectives, the formulation of the reduced scale model, the design and detailing of its components, the materials that were used and finally its construction and instrumentation. This chapter also describes the experimental work conducted on the properties of the energy-dissipators, a process that led to the selection of the dissipators that were finally used in the model. Some of the results presented here were used in the design of the prototype described in the previous chapter.

5.2 Objectives of the Experimental Work

The main objective of the experimental work is the verification of the seismic performance of the new proposed structural system. A comprehensive set of performance parameters has been worked out with the theory developed in the previous chapter for a prototype structure. The values found there will be contrasted with the ones observed in the experiments. It is expected that the dynamic tests would provide information about the following aspects:

- Actual seismic performance of the system;
- Actual energy dissipation capacity of energy dissipators;

- Degree of predictability of the system and
- Experimental reference for the numerical modelling of the system.

Complementary testing is also conducted to define some of the required design parameters. In doing so, it is expected to get experimental information about the next points:

- Verification of structurally relevant characteristics of the construction materials and,
- Verification of the main characteristics of the energy dissipators, particularly their cyclic behaviour.

5.3 Description of the Tests

As described in the introduction of this chapter, most of the uncertainties of the theory developed for this new system are in the dynamic aspects of the behaviour. Hence, it was decided to conduct dynamic tests on a model at different levels of seismic demand. One of the main characteristics of this system is that it has the potential to avoid damage in the structure. It is expected, therefore, to be able to conduct a large number of dynamic tests with the same model.

Logistic limitations (specially the capacity of the shaking table) forced the use of a reduced-scale model rather than a full-scale prototype. The prototype to be modelled is the same that was analysed in the preceding chapter. Even though reduced-scale models are discouraged for use when testing masonry infilled frames (Harris and Sabnis, 1999), the expected low demand in the masonry panels allows the formulation of a reliable model. It is acknowledged that the conflicts in reduced-scale masonry models are triggered at large deformations in the masonry, which are not expected in this structural system.

A number of recorded time-history ground-motions will be used to reproduce the seismic demand at different levels. These time-histories were scaled, up or down, to match the design spectra from a particular site. Of course, the site is the same as that used for the design of the prototype that is being modelled. The records were also modified in the time-dimension to meet the dimensional criteria discussed in the following section.

5.4 Definition of the Reduced Scale Model

The three basic dimensions chosen for the dimensional analysis were length (L), modulus of elasticity (E) and mass (M). These three dimensions can be defined independently of each other and all other dimensions of interest can be defined as a combination of these basic three. The similitude ratio for the

length (S_L) was defined as 0.4. This will result in the maximum possible height of the model to fit on top of the shaking table (4.180 m). The similitude ratio for the modulus of elasticity (S_E) was defined as 1. As E has the same dimensions as stress, the capacity of the actual prototype is properly represented by the model if the same material is used, which was the case here. Finally, the similitude ratio for the mass (S_M) was chosen to yield a similitude ratio for the acceleration (S_A) equal to 1, so that the similitude ratios of mass (S_M) and weight (S_W) are the same. The convenience of this choice is discussed later in this section. The similitude ratios for all the dimensions of interest are presented in Table 5-1.

Table 5-1 Similitude ratios for the model structure

Dimension	*Symbol*	*Definition*	*Similitude Ratio*
Geometry and Materials			
Length	S_L	S_L	0.400
Area	S_{area}	$(S_L)^2$	0.160
Volume	S_{volume}	$(S_L)^3$	0.064
Mass	S_M	S_M	0.160
Weight	S_F	$S_E S_L^2$	0.160
Density	$S_{density}$	$S_M /(S_L)^3$	2.500
Modulus of Elasticity	S_E	S_E	1.000
Natural Period of the Structure	S_T	$(S_M /S_L S_E)^{1/2}$	0.632
Loading			
Force	S_F	$S_E S_L^2$	0.160
Moment	S_{moment}	$S_E S_L^3$	0.064
Time	S_T	$(S_M /S_L S_E)^{1/2}$	0.632
Frequency Content of Excitation	$S_{frequency}$	$(S_E S_L/S_M)^{1/2}$	1.581
Output			
Drift	S_{drift}	-	1.000
Displacement	S_L	S_L	0.400
Velocity	S_V	$(S_E S_L^3 /S_M)^{1/2}$	0.632
Acceleration	S_A	$S_E S_L^2 /S_M$	1.000
Stress	S_E	S_E	1.000

Having defined the similitude ratio for the length (S_L = 0.40), it is possible to show how the model-structure would look. The general characteristics of the reduced-scale-model are exposed in Figure 5-1. Defining the structure to meet the similitude-ratio for the length, however, does not imply that the other dimensions will be modified in their corresponding similitude ratios. However, the general characteristics of the model as presented in Figure 5-1 were maintained, and were the starting point in the process of meeting the similitude ratios for the other dimensions.

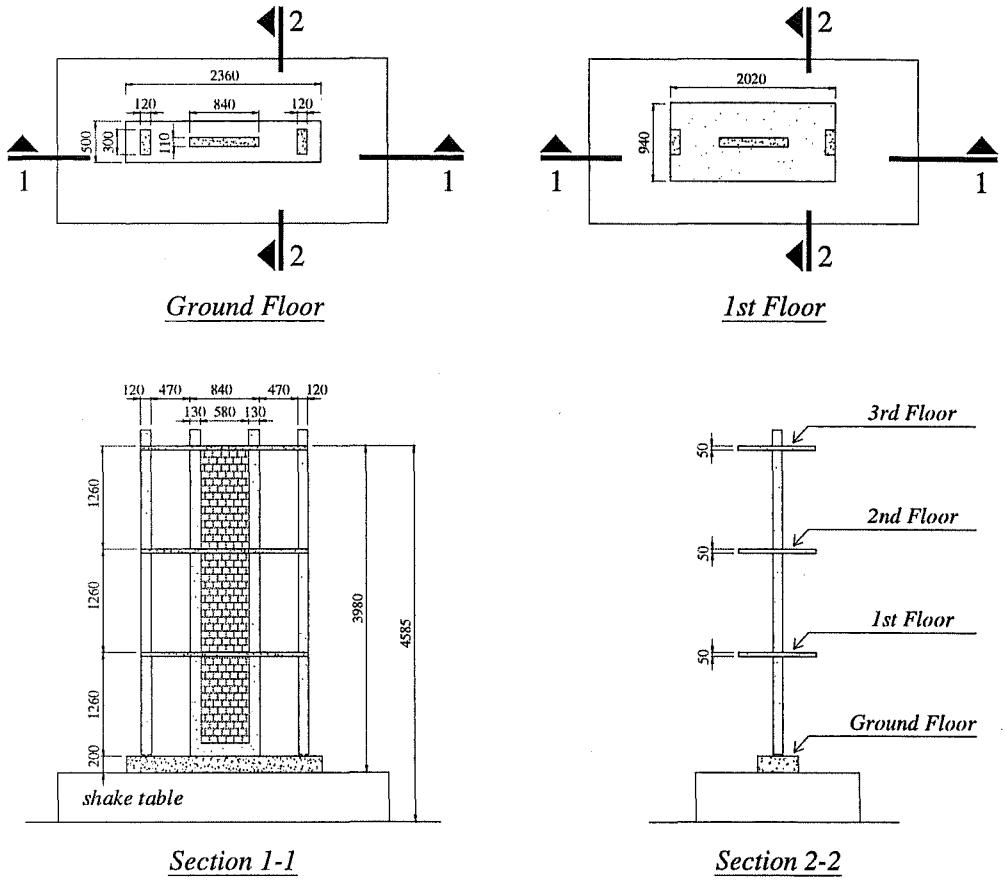

Figure 5-1 General description of model

Since it was decided to use in the model the same materials of the prototype, it was not possible to match the required similitude ratio for the density ($S_{density}$ = 2.50). Additional mass had to be attached to the model to compensate for the larger density required for the model. Having defined S_A = 1.00, the gravity is the same for the prototype and the model and, therefore, the extra-mass attached will exactly compensate for the necessary extra-weight. All the extra-mass is to be attached to the slabs, in a region where only elastic behaviour is expected. In this way, it is expected to recreate the actual demand without modifying the structural characteristics of the components of the model. To get the required extra-mass, the masses of the dimensionally correct model and the actual model were compared. The extra-mass is the mass necessary to compensate the difference. Lead ingots were used for this purpose. A summary of this process is presented in the next table.

Table 5-2 Mass and extra-mass in the model-structure

Floor	*Dimensionally correct mass of model-structure (kg)*	*Actual mass of reduced-scale structure (kg)*	*Extra mass attached (lead ingots) (kg)*	*Total mass of model: structure+ ingots (kg)*
Ground Floor	363	200	0	200
First Floor	2017	611	1400	2011
Second Floor	2017	611	1400	2011
Third Floor	1808	411	1400	1811

Due to reasons discussed below, the final characteristics of the model could not match exactly the result from the dimensional analysis. The slab had to be built slightly thicker because of the lack of reinforcement fine enough to be used in the required detailing. Since the slabs were expected to behave elastically, with low levels of demand, it is unlikely that the outcome of the experiment would be significantly affected. There was also a major problem in the size of the bricks, as it was not possible to acquire or produce bricks of the required reduced-dimensions. Considering that the aim was to produce masonry of conventional structural characteristics, it was decided to use prototype-size bricks reducing only their length by 40% to match the required thickness of the masonry panel. The resultant strength and stiffness of the masonry in the model was of magnitudes expected for conventional masonry.

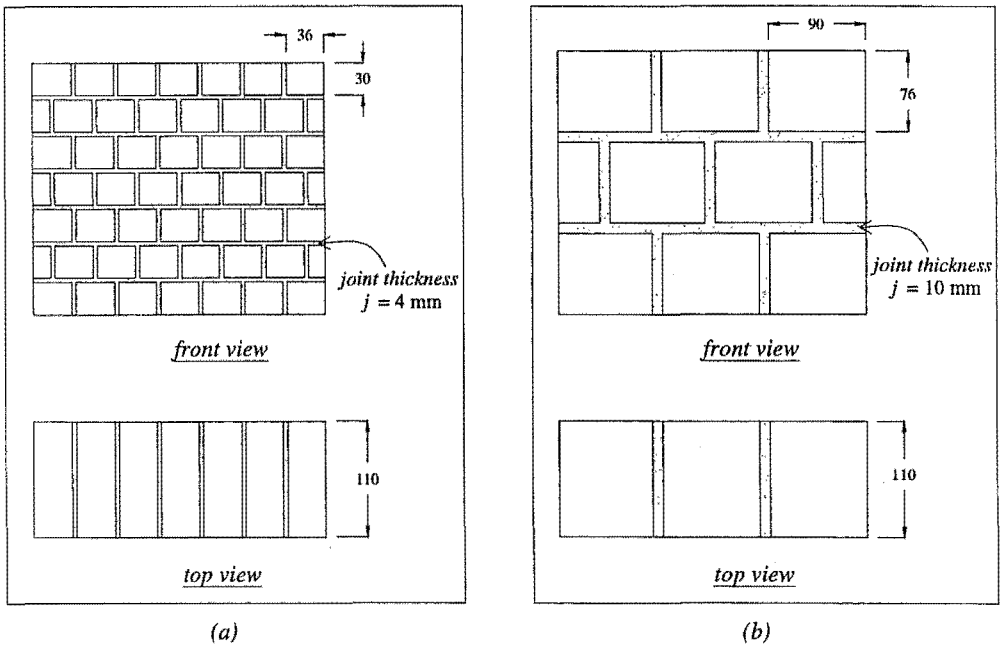

Figure 5-2 Masonry built with reduced bricks (a) and masonry as it was built (b)

Finally, the dimensional analysis also indicates that the time-histories to be used need to be scaled down by 0.632 in the time dimension and the amplitudes scaled up by S_L, S_V or S_A, for displacement, velocity or acceleration time-histories respectively.

5.5 Design and Testing of the Hysteretic Dissipators

5.5.1 Framework for the design of the Hysteretic Dissipators

The most efficient dissipator for this structure is a rigid-perfectly-plastic dissipator, on which one is able to define a plastic plateau. This ideal hysteretic-dissipator would produce the fattest hysteretic loops although, in theory, an ideal friction-device could also perform the same work. The use of friction-devices is an alternative that also should be studied; here, however, it was decided to go for mild-steel hysteretic-dissipators for their easier availability. Previous models of rocking walls with hysteretic dissipators at the base had used mild steel bars, expected to yield axially (Rahman and Restrepo 2000; Holden et al., 2002). Once the drift and yielding point of the dissipator has been defined, the required section and length can be defined. The most appealing feature of a dissipator yielding axially is its large initial stiffness, which leads to fat hysteretic loops with a resulting large energy dissipation in each cycle. The problem with the steel bars is that they might buckle under a compressive load before yielding in compression. To prevent the buckling Rahman and Restrepo (2000) and Holden et al. (2002) embedded the dissipators in the concrete-body of the rocking wall. During some of these tests, however, failure in the connections prevented the full development of the capacity of the dissipators. A shortcoming of this approach is that one cannot say if the dissipator is still satisfactory or needs to be replaced after an earthquake. Further, if the dissipators do need to be replaced, it would be very difficult to do so.

To avoid the problems mentioned above, it was decided to attach the dissipators externally to the wall. This would ease the inspection or the eventual replacement at any time. To prevent buckling, the dissipators were embedded in grout in a surrounding case. Testing of the dissipators showed that the prevention of buckling was not an easy task. Later, this problem required looking for an alternative solution. Dissipators yielding in flexure, although less efficient, proved to be more reliable than the ones yielding axially as their behaviour was more stable. Three types of dissipators were designed and tested. This process is described next.

5.5.2 Design and Testing of dissipator D1

The two parameters that need to be defined are the section and length of the dissipator. The section is defined as that required to provide a yielding force equal to the one required by the design. As large deformations are expected, the ultimate stress is taken to calculate the section of the dissipator. The length is defined so that the maximum expected uplift of the wall does not exceed a fraction of the

deformation at the ultimate strain of the steel. This fraction was taken as 50% for the maximum credible earthquake ("Very Rare" EQ) and 25% for the "Rare" earthquake, typically defined with a return period of 475 years for a 50-years-life structure.

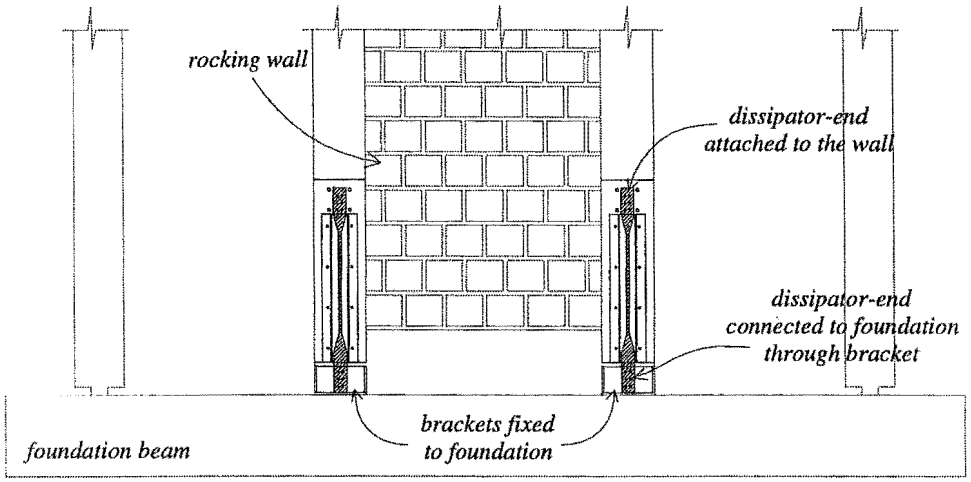

Figure 5-3 Set-up of axial histeretic dissipators D1

Three specimens from a 3 mm thickness, mild steel sheet, intended for the manufacturing of the dissipators, were preliminarily tested. The experimental average results were: yield stress 191 MPa; ultimate stress 253 MPa; and strain at ultimate stress 0.23 mm/mm. The expected demand for the dissipators is derived from the expected demand for the prototype structure modifying the parameters by the corresponding similitude ratio. Therefore, the required F_y for the model will be 0.16 times the required F_y for the prototype; and the expected uplift of the rocking-wall-model is 0.40 times the uplift in the prototype. With these values, the required dimensions of the dissipator were calculated as follows:

Table 5-3 Design sequence for dissipatorsD1

Description	*Units*	*"Rare" event*	*"Very rare" event*
Required F_y	kN	9.11	9.11
Ultimate strength f_u of material	MPa	253	253
Required cross section of dissipator	mm^2	36.0	36.0
Maximum expected drift	%	1.50	2.26
Base of wall	mm	840	840
Expected elongation (maximum uplift)	mm	12.6	19.0
Maximum strain of steel	mm/mm	0.230	0.230
Maximum permissible strain of steel	mm/mm	0.25x0.230	0.50x230
Minimum required length	mm	219	165

The characteristics of the dissipator are presented in the next figure. It was intended to use four dissipators of this type in the rocking wall: two sets of two dissipators at each side of the wall. That is the reason why the section was made around half the required one. The final effective cross-section of each dissipator was 21 mm^2 and a combined section of 42 mm^2 for the set of two dissipators, resulting in a nominal capacity of $F_y \doteq 10.6$ kN.

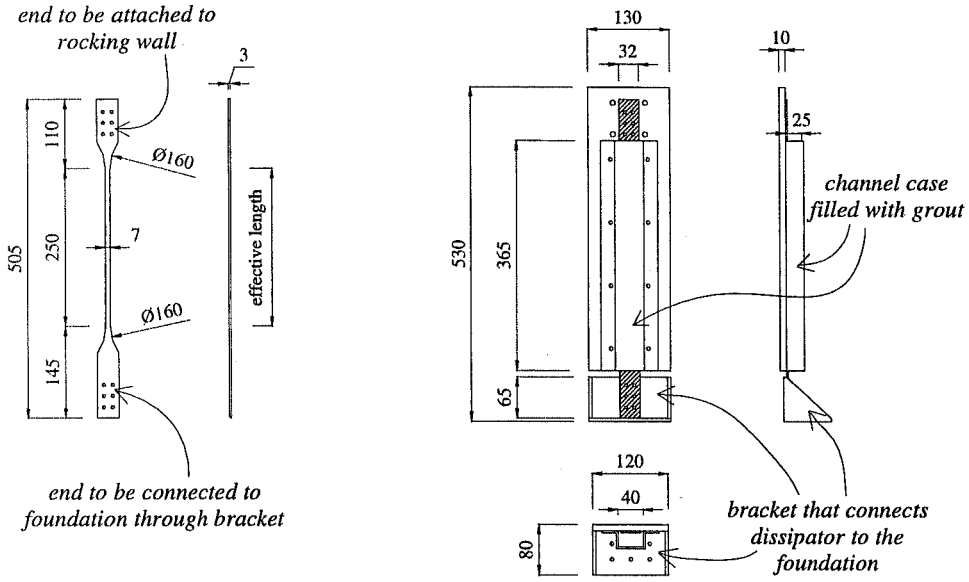

(a) Dissipator (D1) -front and side view-

(b) Dissipator (D1) in case -front, side and top view-

Figure 5-4 Dissipator D1

This model was tested in pairs (as they were expected to work in the wall. In general, the main purpose of the tests of the dissipators was to observe their hysteretic behaviour and their consistency at deformations of the order of the ones predicted by the seismic design. The displacement-history and load-displacement plot is presented in Figure 5-5.

The tests showed that the dissipator *D1* could not sustain the design deformations without buckling. Local buckling of the region of the dissipator inside the case caused the formation of "waves" that led to large friction forces between the body of the dissipator and the grout in the case. This appeared to occur at an early stage but became inadmissibly large for deformations above 5 mm (only 30% of the maximum required by design). In the load-displacement plot depicted in Figure 5-5, a flat region at – 32 kN can be observed. At this point, the load exceeded the limit for which the load-cell was calibrated. The load-cell had to be recalibrated after those cycles to record the larger than expected loads.

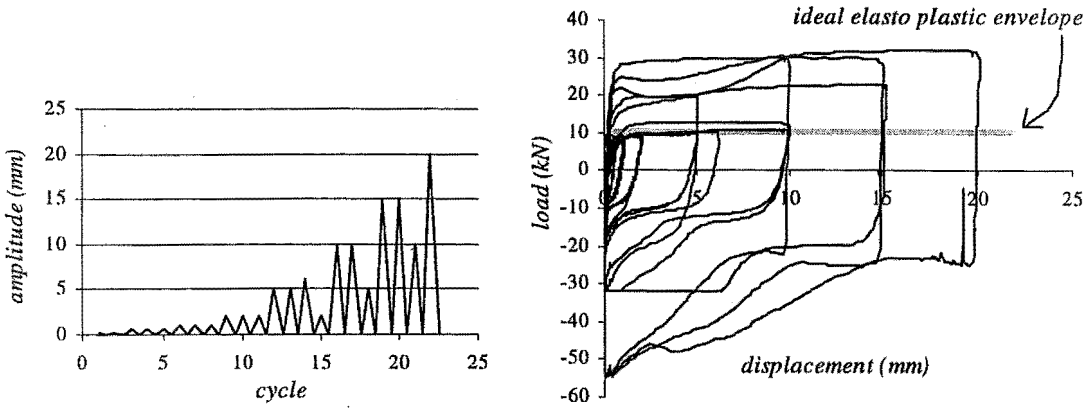

(a) Displ. history (dissipator D1) *(b) Load-displ. response (dissipator D1)*

Figure 5-5 Cyclic testing of dissipator D1 (see comments in this section)

5.5.3 Design and Testing of dissipator D2

In this case, the vertical force transferred by the dissipator to the rocking wall is the force required to yield the dissipator in flexure. Although the hysteretic loops of these dissipators are smaller than the ones obtained with a dissipator yielding axially, dissipators designed in this way proved to be more reliable and stable than the first model. The set-up for this kind of dissipators is shown in Figure 5-6.

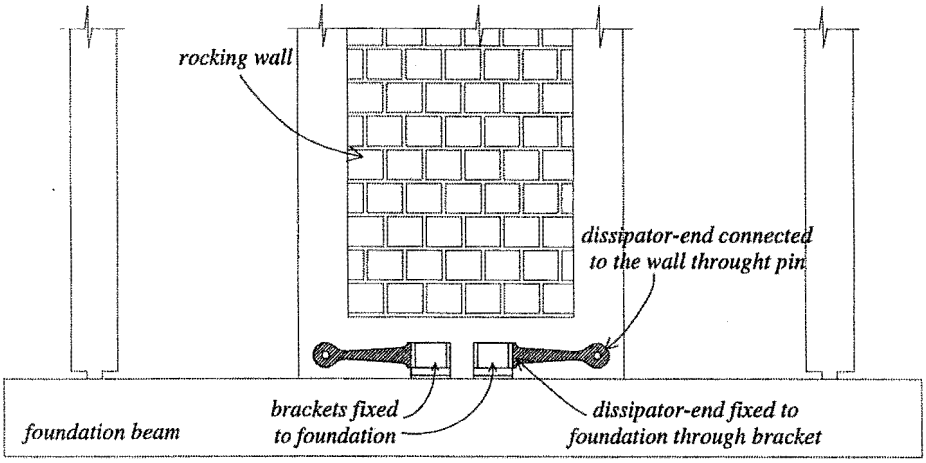

Figure 5-6 Set-up for flexural hysteretic dissipator D2

The flexural dissipators act as cantilever beams with their internal-ends fixed to the foundation through a bracket. The pin connection of the other end transfers only the shear load F_d to the corner of the wall. The intended behaviour is presented in Figure 5-7. In the same figure, it is also shown how the dissipators can prevent sliding of the wall, giving more flexibility for the definition of the geometry of the wall.

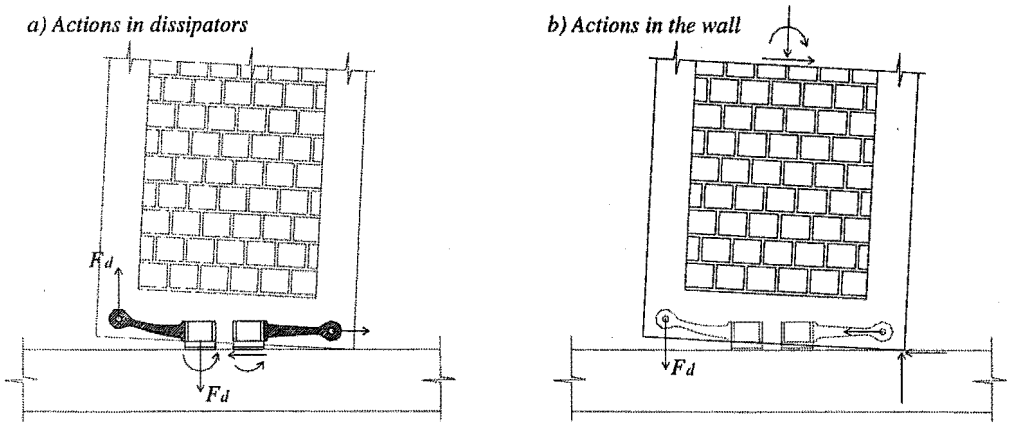

Figure 5-7 Actions in flexural dissipators and wall when the rocking wall uplifts

The arm of the dissipator can be designed to yield uniformly along its length. This avoids the occurrence of regions with excessive plastic deformation. To induce even triggering and development of plastic deformations in the dissipator a parabolic shape of the active region, or "arm", is required. It was observed, however, that in the region of the parabola that corresponds to the "arm" of the dissipator, a straight line could closely represent the parabolic curve. In the design of the dissipator, therefore, the "arm" was modelled with straight lines. This eased the manufacturing process. Mild steel was used in these dissipators. It had an average yield stress of 280 MPa, an ultimate stress of 342 MPa and an ultimate strain of 0.22 mm/mm.

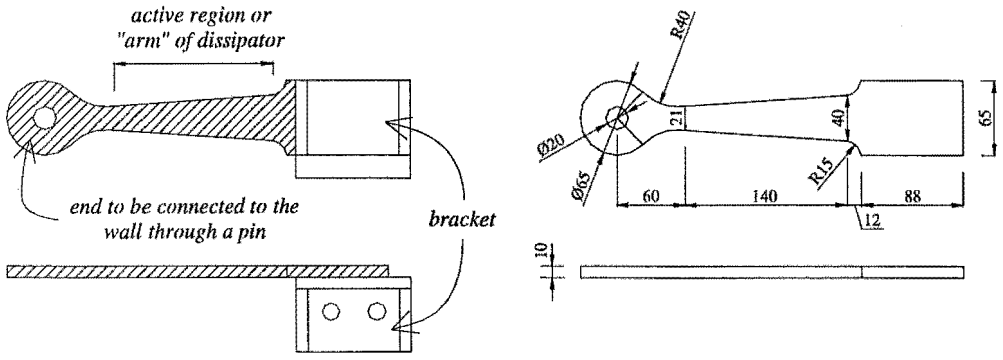

Figure 5-8 Dissipator D2 with and without bracket (side and top view)

The design of this dissipator was conservative. The aim was to avoid excessive plastic deformations so as to prevent local buckling in the active region or "arm". The dissipator showed a consistent response during the test, even for deformations four times larger than the design values (Figure 5-9). The length of the arm also was made conservatively long to avoid any significant contribution of the axial forces, induced in the dissipator, to the nominal design capacity of the dissipator, F_y. The increasing contribution of the axial forces can be observed in the increasing slope of the envelope of the load-

displacement diagram for dissipator *D2* at large vertical deformations. In the load-displacement plot in Figure 5-9, the two incomplete cycles observed at 32mm and 42mm were made to recalibrate the linear potentiometer.

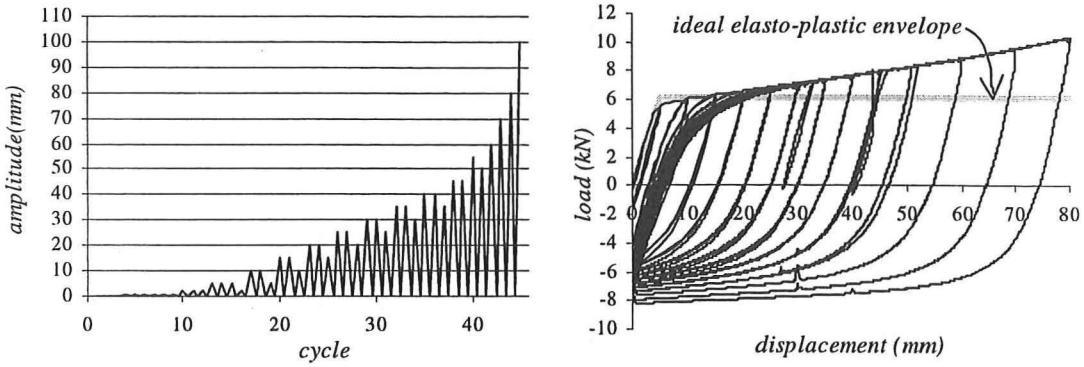

(a)Displacement history (dissipator D2) *(b) Load-displ. response (dissipator D2)*

Figure 5-9 Cyclic testing of dissipator D2 (see comments in this section)

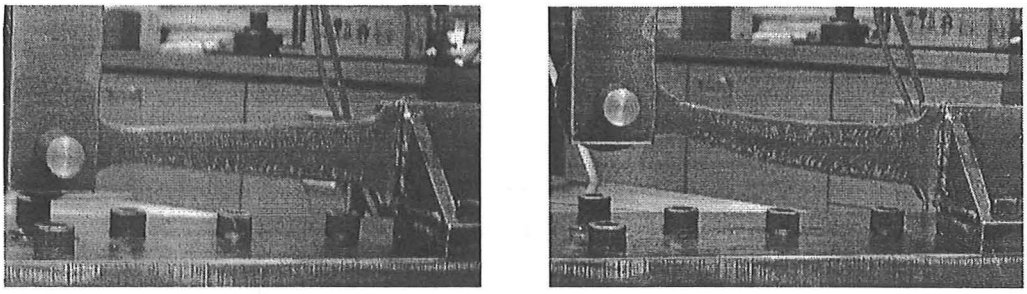

(a) vertical displacement = 0 mm *(b) vertical displacement = 80 mm*

Figure 5-10 Two views of dissipator D2 during static-cyclic testing

There was no sign of local buckling anywhere in the active region or "arm" of the dissipator. The test demonstrated that it was possible to make the design less conservative, especially with respect to the initial stiffness. A larger initial stiffness would imply fatter hysteretic loops and improved energy-dissipation-capacity.

5.5.4 Design and Testing of dissipator D3

This is an improved version of the dissipator *D2*. After the testing of the previous model it was found that buckling in the compression region of the arm was unlikely. This allowed a reduction in the length of the arm to give a larger initial stiffness and a more compact set-up of the dissipators at the base of the rocking wall (Figure 5-11).

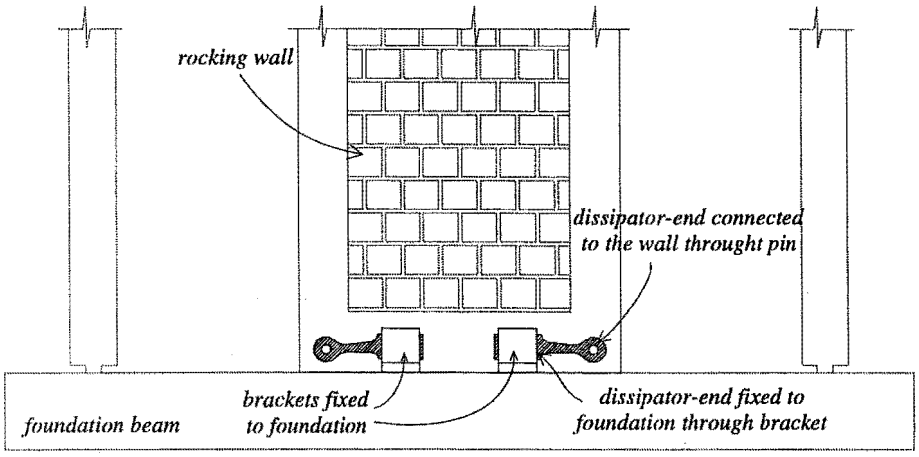

Figure 5-11 Set-up for flexural hysteretic dissipator D3

Making the dissipator shorter, however, could induce significant axial strain in the dissipator that would disturb the design vertical force transferred to the wall. The shape of the dissipator was modified to alleviate this problem (Figure 5-12). Since the extent of the unwanted disturbance directly depends on the angle of the dissipator with the horizontal, an initial offset (downwards) of 8 mm was given to the arm. It would increase the range of vertical deformation over which the axial forces induced in the dissipator do not contribute significantly to the vertical force transferred to the wall. Also, the hole for the pin was slotted towards the centre of the wall to prevent the dissipator transferring any tension to the base beam of the rocking wall when travelling upwards. These modifications give a range of around 16mm of mostly undisturbed vertical displacement. The vertical displacement expected in a "very rare" earthquake according to the design is 17mm and, therefore, it is mostly covered in that range. Finally, as it was done with the dissipator *D2*, it was also possible to model the parabolic shape of the dissipator-arm with two straight lines. The mild steel used in the manufacturing of the dissipaters had an average yield stress of 283 MPa, ultimate stress 340 MPa, and ultimate strain of 0.24 mm/mm.

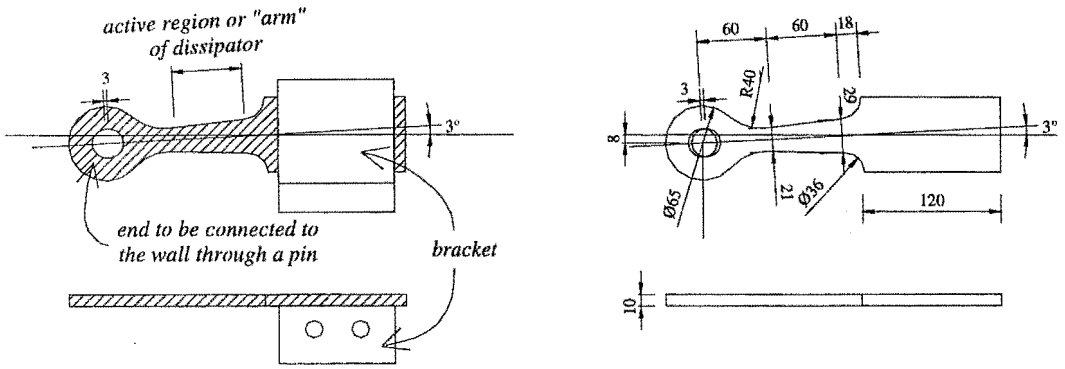

Figure 5-12 Dissipator D3 with and without bracket (side and top view)

A set of two dissipators was tested in a static-cyclic test. The target design force (F_y = 12.8 kN) is consistently reached at about 15mm of vertical displacement. Beyond this point, the measured vertical force begins to increase due to the influence of the axial forces induced in the dissipator. The results showed a good agreement with what was expected in the design.

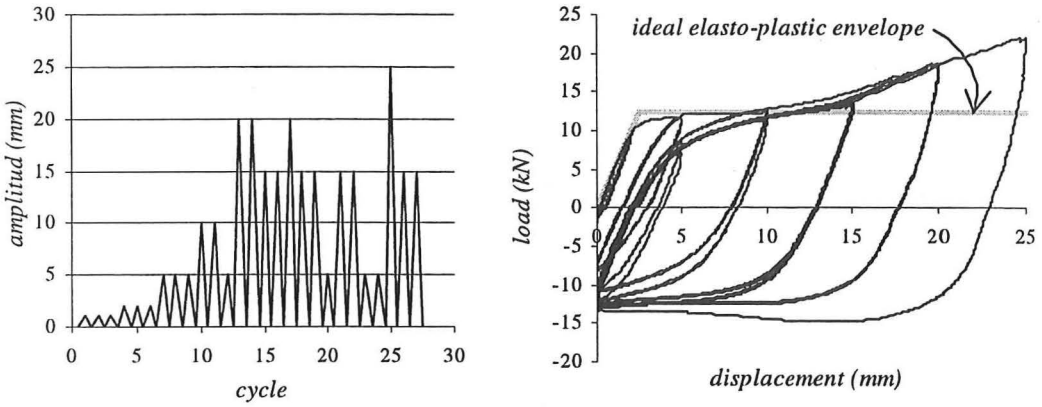

(a) Displ. history (dissipator D3) *(b) Load-displ.response (disipator D3)*

Figure 5-13 Cyclic testing of dissipator D3

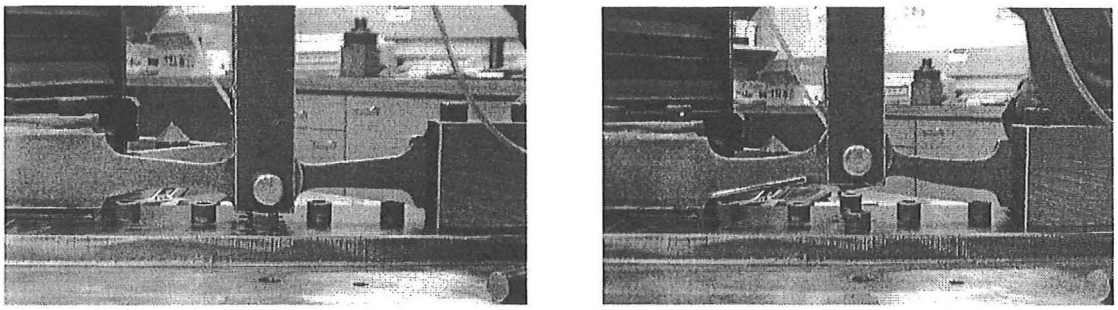

(a) vertical displacement = 0 mm *(b) vertical displacement = 25 mm*

Figure 5-14 Two views views of dissipator D3 during static-cyclic testing

5.5.5 Comparing the Observed Behaviour of Dissipators

The load-displacement responses for dissipators *D1*, *D2* and *D3* displayed above are compared here to have a complete picture of their advantages and disadvantages. In Figure 5-15 and Figure 5-16, cycles with the same amplitude are put side by side. To make the results comparable, the measured-load from dissipator *D2* was doubled as a single dissipator was tested in that case (sets of two dissipators were tested in the other cases).

The small-amplitude cycles show how the stiffer dissipator *D1* is already dissipating energy at that early stage while the others remain elastic. On the other hand it is clear that for medium to large amplitude cycles, the friction forces developing in the axial dissipator make its response unreliable. This contrasts with the consistency of the hysteretic loops in the flexural dissipators. The loops in the flexural dissipators also show good agreement with the assumed shape in the previous chapter, validating that model. The cycles with the largest displacements in dissipator *D3* show how quickly the vertical forces can grow passing the design-vertical-displacement due to the contribution of the axial forces induced in the dissipator. This is not observed in the more conservative dissipator *D2*.

It was decided that the dissipator *D3* was the best choice for the model-structure. It has a reliable behaviour in the required deformation-range and is stiff enough to provide an acceptable energy dissipation capacity to the structure.

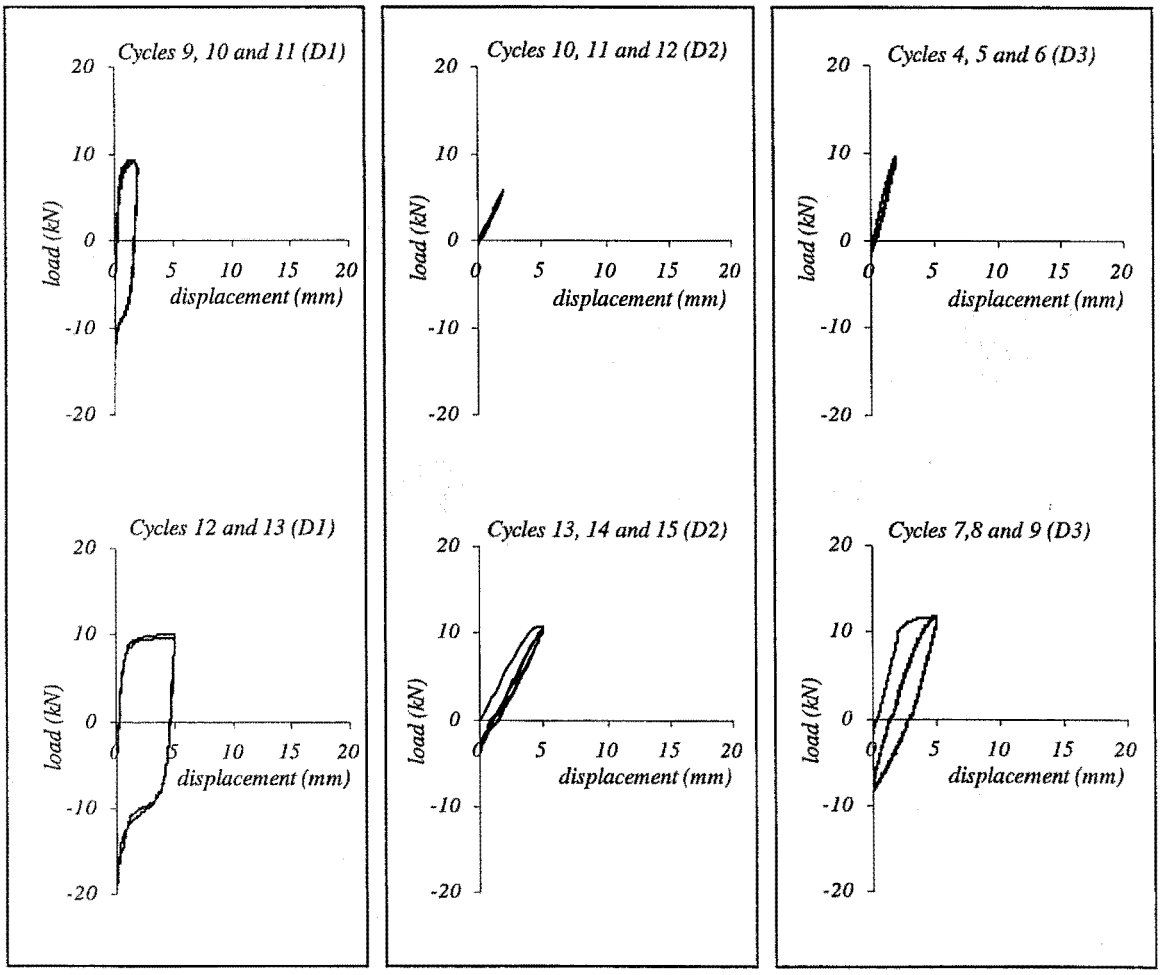

Figure 5-15 Comparisson of hysteretic loops of dissipators D1, D2 and D3 for small displacements

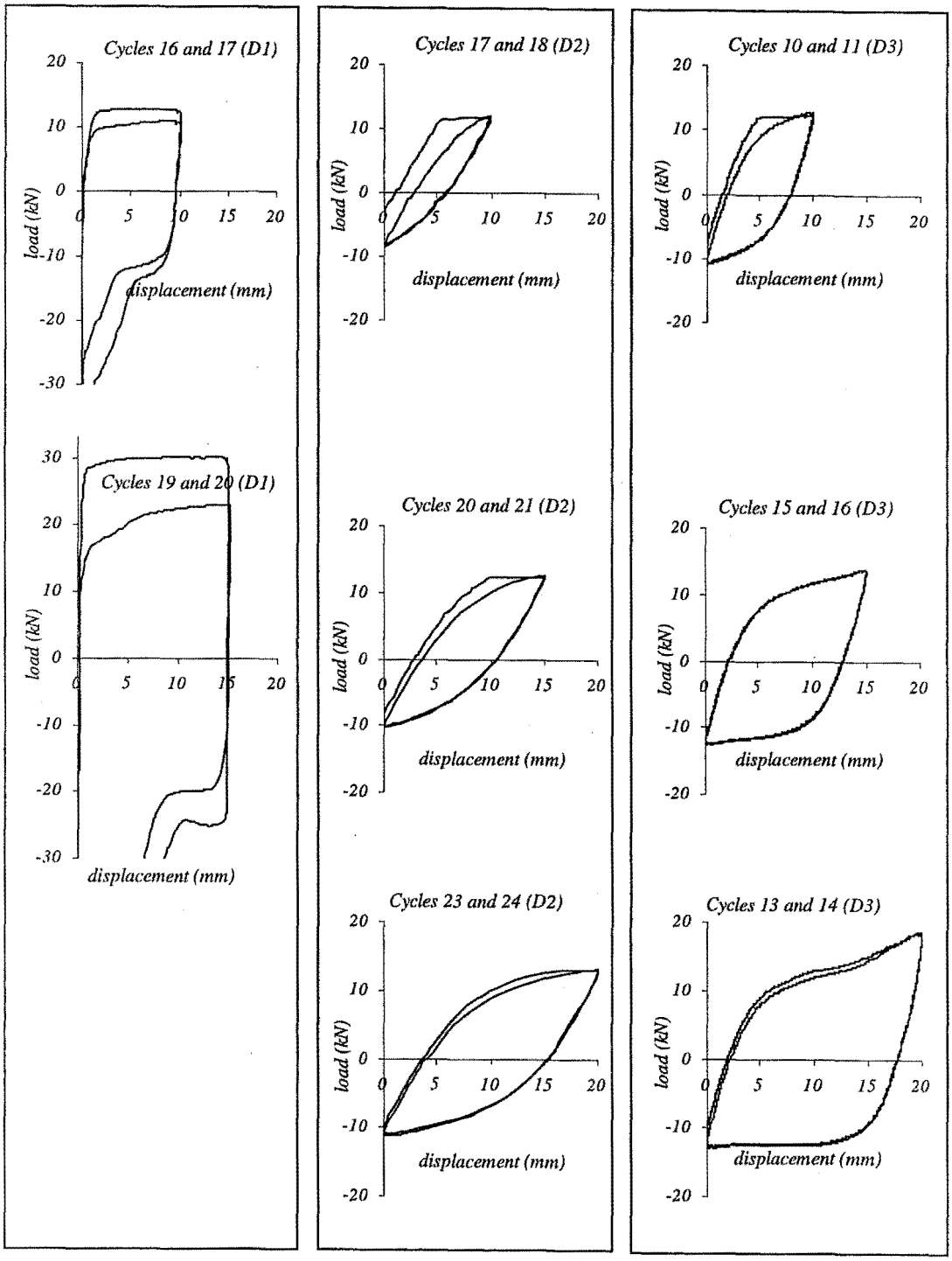

Figure 5-16 Comparisson of hysteretic loops of dissipators D1, D2 and D3 for large displacements

5.6 Design of Structural Members and Detailing of the Specimen

As it was done with the dissipators, the demand expected in the specimen was derived from the demand for the prototype. However, unlike the dissipators, all other structural elements will be designed to behave elastically. As discussed earlier in Chapter 4, the rocking wall with hysteretic dissipators is the only element required to provide the necessary lateral stiffness and energy dissipation capacity of the system. To avoid damage in any region in the structure, the slabs and exterior columns are detailed to have purposely-built hinges that would accommodate the deformation induced by the lateral oscillation of the system. These hinges were located in the regions immediately next to the wall and exterior columns as depicted in Figure 5-17. The strength demand of the slabs and exterior columns, therefore, is defined only by gravity loads.

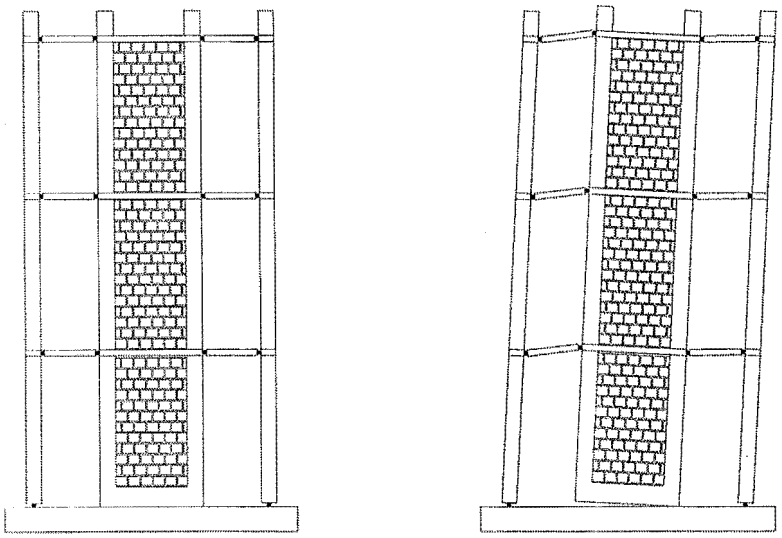

Figure 5-17 Drawing of specimen showing intended built-in hinges in exterior columns and slabs

This section also will address the detailing of some regions in the structure that are expected to sustain exceptionally large stresses or perform some particular tasks.

5.6.1 Rocking Wall

The masonry wall is the element that will provide the seismic capacity to the structure, and as discussed in the previous chapter, it is expected to behave elastically. The actions that the wall will need to withstand are described in the next table. Since it was decided to protect the wall from damage at all levels, the design force would be the one corresponding to the more severe ("very rare") event. The table, however, presents all other levels to show that they do not differ significantly. The basic vertical and horizontal forces (F_v and F_h) have been derived from the values corresponding to the prototype multiplying those forces by the similitude ratio $S_F = 0.16$. $F_{m\theta}$ is the force expected for the

masonry diagonal-strut assuming that this strut alone is transferring all the lateral actions to the foundation. The angle φ_w is the angle of the diagonal of the masonry panel with a horizontal line (Figure 3.16), which in this case is 61° or 1.07 radians. Finally, F_{cc} is the force expected in the confining column that is impacting the foundation.

Table 5-4 Maximum forces expected during impact in the rocking-wall at ground level

Earthquake level	*Total horizontal force*	*Force in the masonry strut*	*Total vertical force*	*Force in the confining column*
	$F_h = V$ *(kN)*	$F_{m\theta} = V/\cos\varphi_w$ *(kN)*	$F_v = (f_{imp})(W)$ *(kN)*	$F_{cc} = F_v - (F_{m\theta})\sin\varphi_w$ *(kN)*
Basic forces (no amplif.)	9.7	20.1	41.0	23.4
Frequent	15.2	31.5	64.3	36.7
Occasional	15.4	31.9	65.1	37.2
Rare	16.2	33.5	68.4	39.1
Very Rare	17.0	35.1	71.7	40.9

With the above information it is possible to define the required strength of the masonry and columns using any of the methods discussed in Chapter 2. A diagonal strut however, seem to be the best choice to model the response of the confined masonry at impact. An amplification factor of 1.25, conventionally used for seismic loads, is used here to get the design forces for the masonry strut and the confining columns. The design forces are therefore

$$F_{m\theta}^* = 1.25 \times 35.1 \text{ kN} = 43.9 \text{ kN}$$

and

$$F_{cc}^* = 1.25 \times 40.9 \text{ kN} = 51.2 \text{ kN}$$

Assuming that the width of the equivalent diagonal strut is 0.25 times the length of the diagonal (Crisafulli, 1997, Paulay and Priestley, 1995), the section of the strut would be 110mm x (0.25x1200mm) = 33,000 mm^2. For the column, the section is 110mm x 130mm = 14,300mm^2. Therefore, the design stress for the diagonal strut and confining column would be:

$$f_{m\theta}^* = F_{m\theta}^*/A_{m\theta} = 43900\text{N} / 33000\text{mm}^2 = 1.33 \text{ MPa}$$
$$f_{cc}^* = F_{cc}^*/A_{cc} = 51200\text{N} / 14300\text{mm}^2 = 3.58 \text{ MPa}$$

The design-stress in the masonry can be compared with the strength-capacity of the masonry strut for that given angle ($\varphi_w = 61°$). Crisafulli's model, described in Chapter 2, was used to get the strength of the masonry strut. Details of this are described later in this chapter in section 5.7.1. Note that it is not expected to be any significant flexural demand on the confining columns as the masonry panel is expected to sustain negligible distortions.

With respect to the reinforcement in the confining columns, it was decided to define the longitudinal steel so that it can transfer the force in the dissipator without subjecting the masonry to significant tensile strain. The chosen design-strain for the bars was 10% of the typical design strain of masonry under compression: 0.0020 x 10% = 0.0002. The required reinforcement is therefore:

$$A = \frac{P}{E\varepsilon} = \frac{12800N}{200\times10^3 MPa \times 0.0002} = 320mm^2$$

Four steel bars ϕ10 (A = 314 mm^2) were used as reinforcement. Of course, the stress in the reinforcing bars needs to be within the elastic region. The stress in the bars is P/A = 12600N / 314mm^2 = 40MPa, which is well within the elastic range of the steel.

5.6.2 Exterior Columns

In the prototype, the exterior columns are the structural elements that provide the lateral resisting capacity of the system in the direction orthogonal to the rocking wall. In the plane of the rocking wall, however, the exterior columns are not expected to contribute to the seismic capacity of the system. The dominant point in the design was the detailing of the base of the column so that it can behave as a pin connection (Figure 5-17). A single layer of four steel bars ϕ10 (A = 315mm^2) connects the base of each exterior column to the foundation. The load that is to be transferred is a compressive load of 10kN, which results in a stress of 31.7MPa in the bars. This single layer is overlapped above the intended pin connection by a steel cage made up of two layers of 4ϕ10 bars each that are the reinforcement of the column all the way through to the top floor.

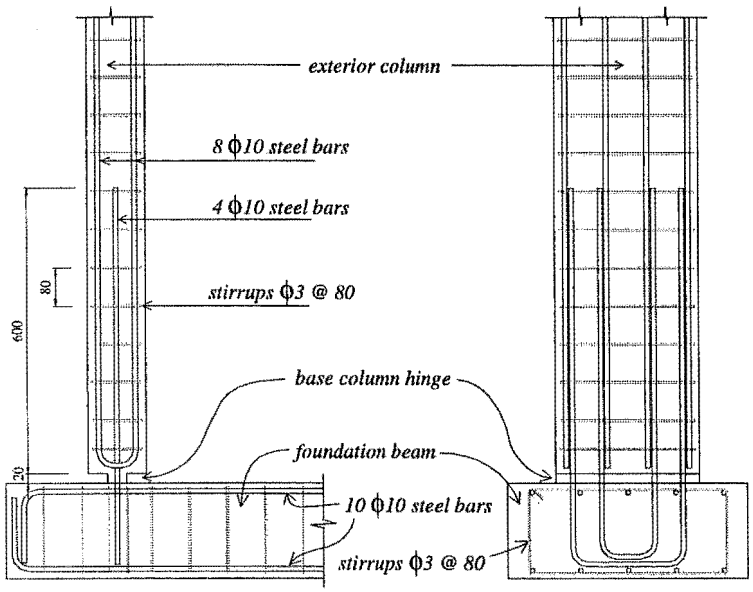

Figure 5-18 Detailing of exterior column (side and front views)

5.6.3 Slabs

The design of the slabs was dominated by the detailing of the intended hinges as depicted in Figure 5-17. The hinges would prevent the lateral oscillation of the structure inducing any significant demand in the main body of the slabs. The slabs were designed to act as cantilevers transferring the load to the wall and exterior columns. The section of the slab between the exterior column and wall was designed to transfer its load to the middle section of the slab and from there to the exterior column and the wall as a simply supported beam. Figure 5-19 shows the transference-of-load flow intended for the slabs

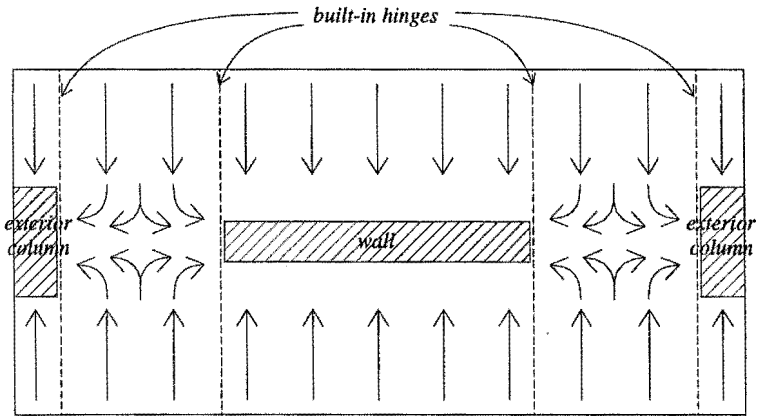

Figure 5-19 Plan view of model-slab showing intended transference of loads

A steel mesh made of $\phi = 5.3$ mm wire, with a spacing of 75mm, was enough to provide the required "negative" reinforcement for the cantilevering sides of the slab (Figure 5-20). Additional reinforcement was necessary to transfer shear from the section of the slabs spanning between the wall and the exterior columns. This reinforcement, however, was arranged to provide a minimum of flexural stiffness to the slab in the hinge region (Figure 5-21). A groove was built in the slabs along the intended hinge to avoid unnecessary damage in the concrete. There were two types of grooves, one with a depth of 10mm and a width of 20mm, the second with a depth of 20mm and a width of 10mm. Two regions in the slab were left without grooving to observe the extent of the damage in the concrete for that case. The additional reinforcement was also used to stiffen the central region of the suspended section of the slab to try to transfer the load mostly through this area of the slab to the wall and exterior column.

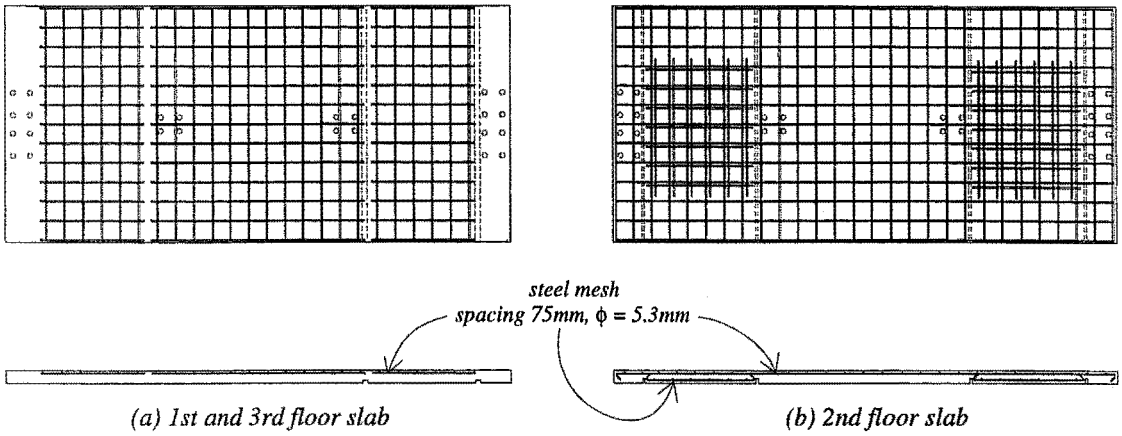

Figure 5-20 Plan and front view of slab showing reinforcing mesh

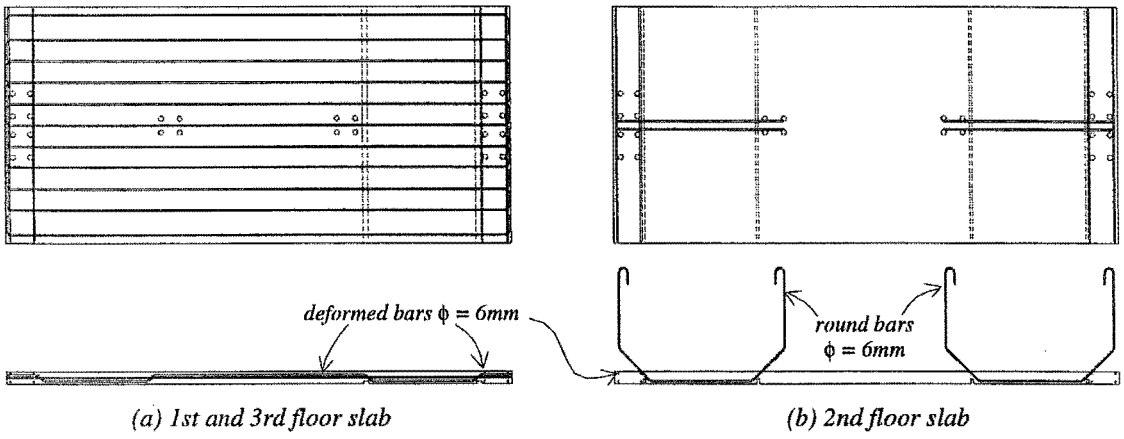

Figure 5-21 Plan and front view of slab showing additional reinforcement

5.6.4 Other Structural Details

5.6.4.1 Impacting region in the wall and foundation

The impacting regions in the wall and foundation were to be subjected to large stresses, as the impacting areas are rather small. For the foundation, a steel plate was placed on the impacting region with an area large enough to transfer the actions to the concrete with stresses well below the capacity of the concrete. Similarly, for the impacting corners of the rocking wall, a steel case was used to increase the area of concrete that received the impact actions. The final design is shown in Figure 5-22.

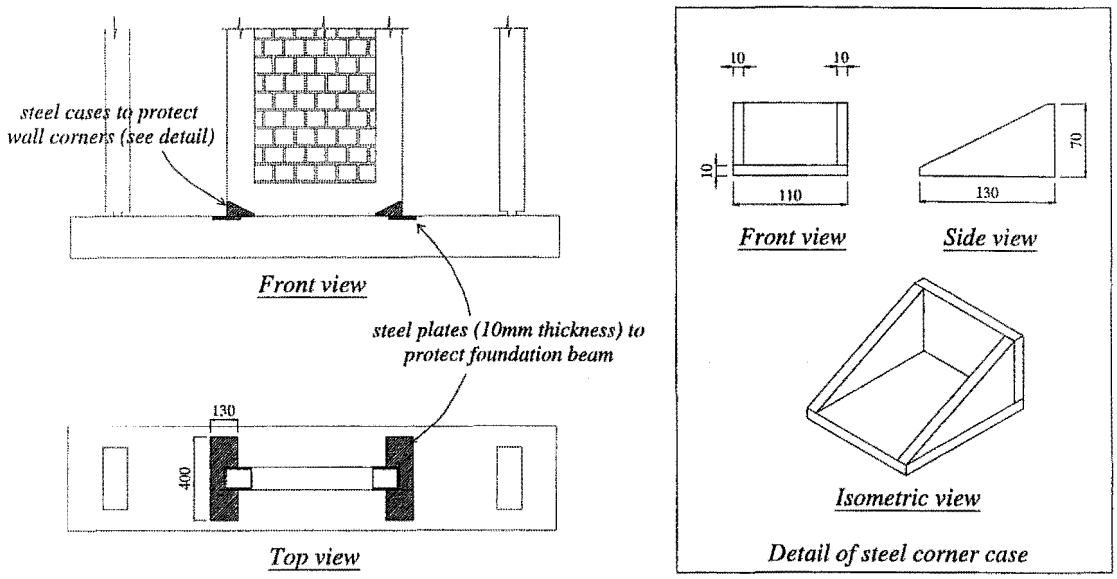

Figure 5-22 Protection of the regions subject to impact

5.6.4.2 Connections for the dissipators

The dissipators transfer their action to the lower corners of the rocking wall. The corner, therefore, needed to be detailed to properly transfer these forces. Steel tubes were placed at the base of the columns to receive the force from the dissipators via pins. The tubes in turn were surrounded by the longitudinal reinforcement of the vertical columns and the base beam allowing a direct transference of the loads to the longitudinal reinforcement of these elements.

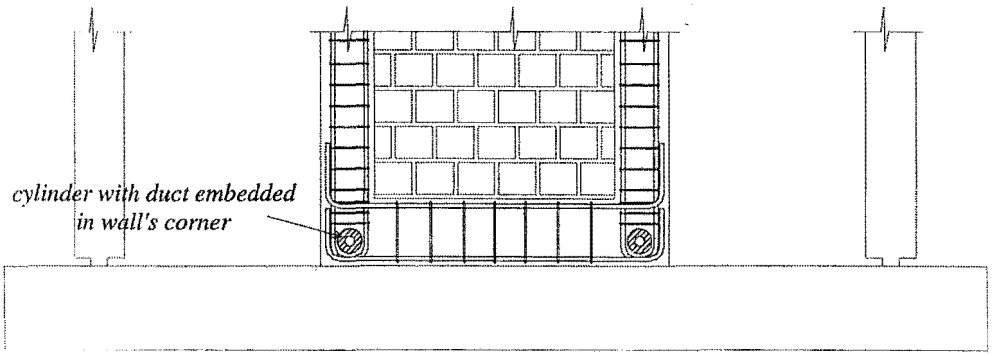

Figure 5-23 Steel tubes and reinforcement at the base-corners of the rocking-wall

To keep the cylinders in position during the casting, they were welded to the corner cases. The corner cases, therefore, where slightly modified to hold the cylinders, as it is observed in the next figure. Attaching the cylinders to the corner cases also served to avoid possible debonding of the cases from the corner.

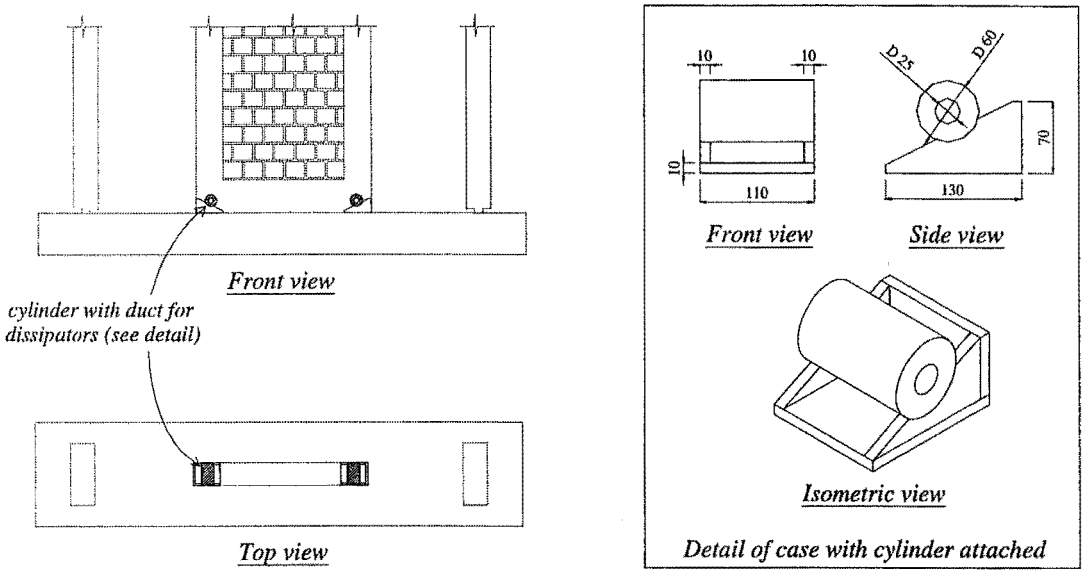

Figure 5-24 Steel tubes attached to corner cases

The other end of the dissipators also needed to be connected to the foundation. It had to be a fully-fixed type of connection to allow the dissipators to behave like cantilevers. A bracket was attached to the back end of the dissipators and the brackets were bolted to a steel plate that was anchored to the foundation. Four dissipators were connected to the base of the wall, two at each side. The detail of the connection of the first set of two dissipators is shown in Figure 5-25.

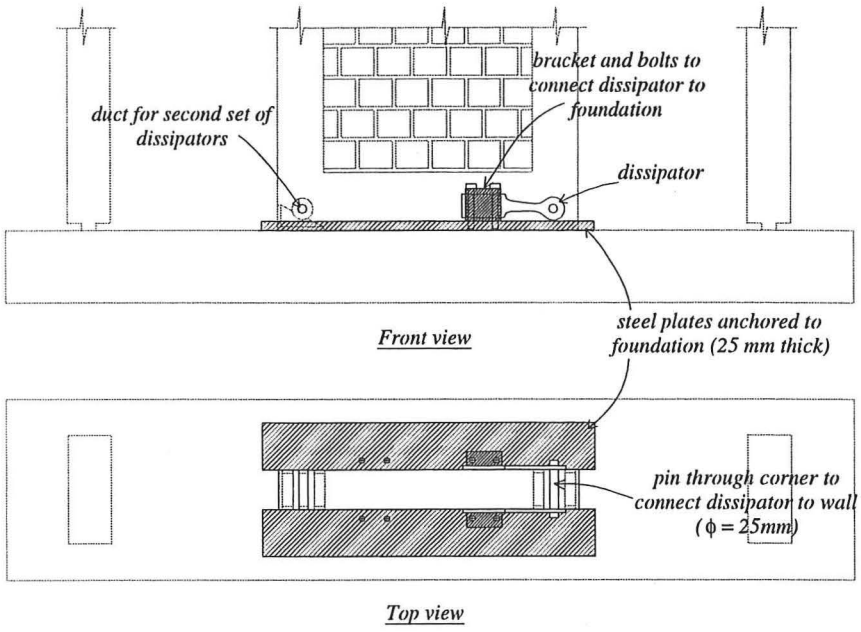

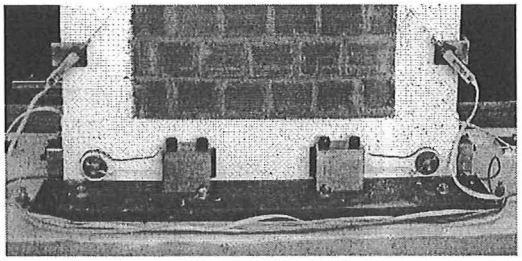

Figure 5-25 Connection of dissipators to foundation and rocking wall

5.7 Construction of the Specimen

5.7.1 Materials

5.7.1.1 Concrete

Two types of concrete were used. Premixed concrete was used for the slabs and foundation beam. It was specified to f'_c = 25MPa at 28 days, and 75mm slump. The rest of the concrete was prepared on site with an intended f'_c = 25MPa at 28 days, and a slump of 75mm. In both cases the maximum aggregate was 6mm. The slabs and foundation beam were precast almost two months earlier, the other elements were cast in place. Standard compressive tests were conducted in the concrete with the results shown in Table 5-5.

Table 5-5 Average compressive strength of concrete from standard tests

Description	*7 days (MPa)*	*14 days (MPa)*	*28 days (MPa)*	*Age at the time of testing the model (days)*
Premixed concrete	17.4	20.8	23.6	61
Concrete at first level	12.3	16.5	19.2	41
Concrete at second level	13.1	--	22.7	32
Concrete at third level	13.9	--	22.3	26
**Three samples were tested in all cases*				

5.7.1.2 Steel

Different types of reinforcement were used according to the necessities and availability in the local steel market. Apart from the reinforcement across the intended hinges in the slabs, any other steel reinforcement in the structure was expected to behave elastically. A description of the nominal characteristics is presented in Table 5-6.

Table 5-6 Nominal characteristics of steel reinforcement used in model

Location in model	*Diameter (mm)*	*Type of bar*	*Grade (MPa)*
Long. reinforcement in beams and columns	10	deformed	430
Stirrups in beams and columns	4	round	300
Reinforcing mesh in slab	5.3	round	430
Additional reinforcement in slabs	6	deformed	300
Additional reinforcement in slabs	6	round	300

5.7.1.3 Masonry

Local (New Zealand) clay bricks and ready mixed mortar were used to build the masonry panels. Laying of the bricks was made carefully but the labour was not specialised. Not much structural information was known from the bricks because in New Zealand they are produced only for veneers and other non-structural elements. Shape-wise, the bricks can be regarded as solid with an effective area of 78%. The bricks have ten vertical holes aligned in two columns of five holes each. As mentioned in a previous section (section 5.4), the bricks were cut to produce the required thickness of the model-masonry-panel. The resultant unit is shown in Figure 5-26. A number of minor tests were conducted to learn more about the characteristics of the bricks, the summary is presented in Table 5-7.

Table 5-7 Results form tests on bricks and masonry

Property	*Units*	*Number samples*	*Average*	*SD*	*Ave-1(SD)*
Clay Bricks					
Compressive strength (⊥ to bed joint)	MPa	3	26.91	0.49	26.42
Tensile strength (parallel to bed-joint)	MPa	10	1.57	0.39	1.17
Masonry					
Brick-mortar shear bond strength (cohesion)	MPa	6	1.37	0.32	1.05
Brick-mortar coefficient of friction		6	0.57	0.02	0.55
Ultimate comp. strength (⊥ to bed-joint)	MPa	8	28.61	2.06	26.56
First crack comp. strength (⊥ to bed-joint)	MPa	8	15.79	2.36	13.43
Notes: All actions are uniaxial					

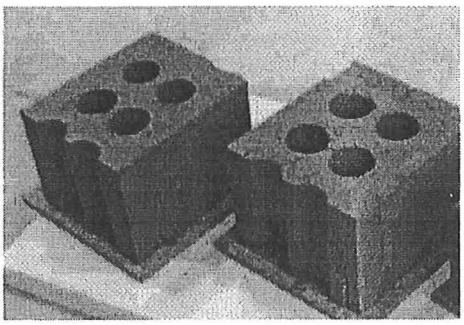

Figure 5-26 Bricks cut to a length of 110mm

The experimental data presented in the previous table was used to verify the capacity of the masonry and compare it to the demand as calculated in section 5.6.1. Crisafulli's model (Crisafulli, 1997) was used for that purpose. This model, defines the capacity of the masonry at any angle accounting for three possible failure modes as described in chapter 2. Conservatively, the values used to calculate the parameters in Table 5-8 were the observed averages minus one standard deviation. In the table, the resulting ratio demand/nominal-capacity = 0.73 would be equivalent to the conventional reduction factor used in conventional design.

Table 5-8 Calculation of the masonry-diagonal-strut's strength according to Crisafulli's model

Property	*Reference*	*Units*	*Value measured or calculated*
Factor Cs	Chapter 2	--	2.00
Factor Cn	Chapter 2	--	1.50
Reduced shear bond strength	Chapter 2	MPa	0.62
Reduced coefficient of friction	Chapter 2	rad	0.32
Thickness of the mortar joint	Chapter 2	mm	10
Height of the brick	Chapter 2	mm	76
Length of the brick	Chapter 2	mm	90
Diagonal's angle with horizontal line	Chapter 2	deg.	61
Diagonal compressive strength (sliding shear failure)	Chapter 2	MPa	3.52
Diagonal compressive strength (diagonal tension failure)	Chapter 2	MPa	1.82
Diagonal compressive strength* (diagonal's nominal capacity)		MPa	1.82
Seismic demand	Section 5.6.1	MPa	1.33
Ratio demand/nominal capacity		--	0.73
**This is the lowest of the values corresponding to any failure cases*			

5.7.2 The Construction Process

In the construction process it was attempted to reproduce the conditions under which a confined masonry wall would be built in South America (Casabonne, 1994). The masonry panel was built first and then the confining columns were cast at each side. For logistics reasons, however, the slabs were pre-cast and placed on top of the wall rather than cast in-situ. The construction process is schematically presented in twelve stages in Figure 5-27.

The process started with the casting of the foundation and precasting of concrete slabs (stage 1). It was followed by the precasting of the base beam of the rocking wall and the loading of the precast slabs with lead ingots (stage 2). The bricks were laid to complete the masonry panel (stage 3), then the confining and exterior columns were cast (stage 4) and the precast slab was placed on top of the wall and columns (stage 5). The procedure was repeated for the second (stages 6, 7 and 8) and third floor (stages 9, 10 and 11). Finally the dissipators were attached to the rocking wall (stage 12).

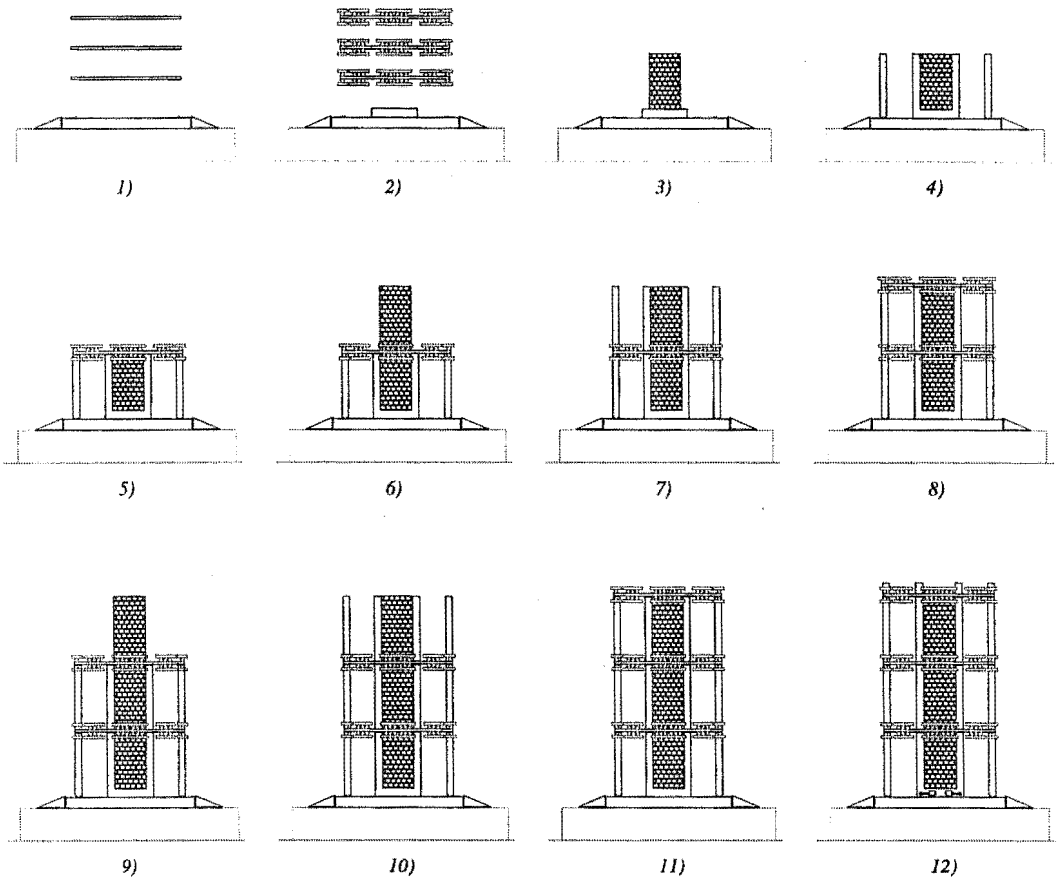

Figure 5-27 Construction stages of the specimen

5.8 Loading Apparatus and Instrumentation

5.8.1 Shaking Table

This facility is part of the Structures Laboratory of the Department of Civil Engineering at the University of Canterbury. The shaking table has a number of system-components that when combined result in a system capable of reproducing displacement time-histories. A detailed description of the system and each component can be found in Ang (1985). From the original set up of the shaking table, the control system, was upgraded. The Dartec M1000/A was replaced by a MTS Test Star II, which allows the reproduction of earthquake-like signals without the necessity of an external command, as it was necessary with the old controller. Figure 5-28 (drawn from that reference) shows an updated scheme of the main components and of the system and how they interact with each other.

The shake table has only one degree of freedom (East-West) and is displacement controlled. The actuators transfer an East-West force to the table thanks to the action of the pumping units. A feedback electric signal informs to the controller the displacement of the table and then the controller sets the servo-valves up to produce a displacement equal to the target displacement. Velocity and acceleration are not tracked and therefore cannot control efficiently high frequency accelerations since they produce very small displacements. This shortcoming caused problems during the tests. A summary of other significant characteristics of the table is presented in Table 5-9.

Table 5-9 Main characteristics of shaking table (after Ang, 1985)

Plan area	2.00 m x 4.00 m
Height above ground	700 mm
Material	Steel
Weight	24 kN
Natural frequency (unloaded)	20 Hz (approx.)
Table top	12 mm steel plate
Maximum travel	300 mm
Maximum velocity attainable	1 m/s
Static capacity	±250 kN
Dynamic capacity (nominal)	±200 kN

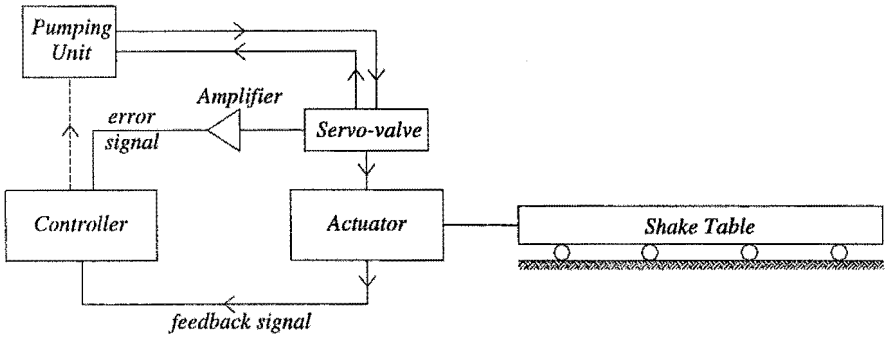

Figure 5-28 Sheme of the shaking table and its main components (updated form Ang, 1985)

5.8.2 Exterior Frame

An exterior frame was built to prevent a catastrophic collapse of the structure. More specifically, the purpose of this exterior frame was to set up a limit for the lateral displacement of the model and prevent any significant out of plane displacement. The exterior frame was made stiff enough so that it would not resonate with the model. The exterior frame allowed the model to have relative displacements of up to 300 mm. A schematic representation of this structure is presented in Figure 5-29.

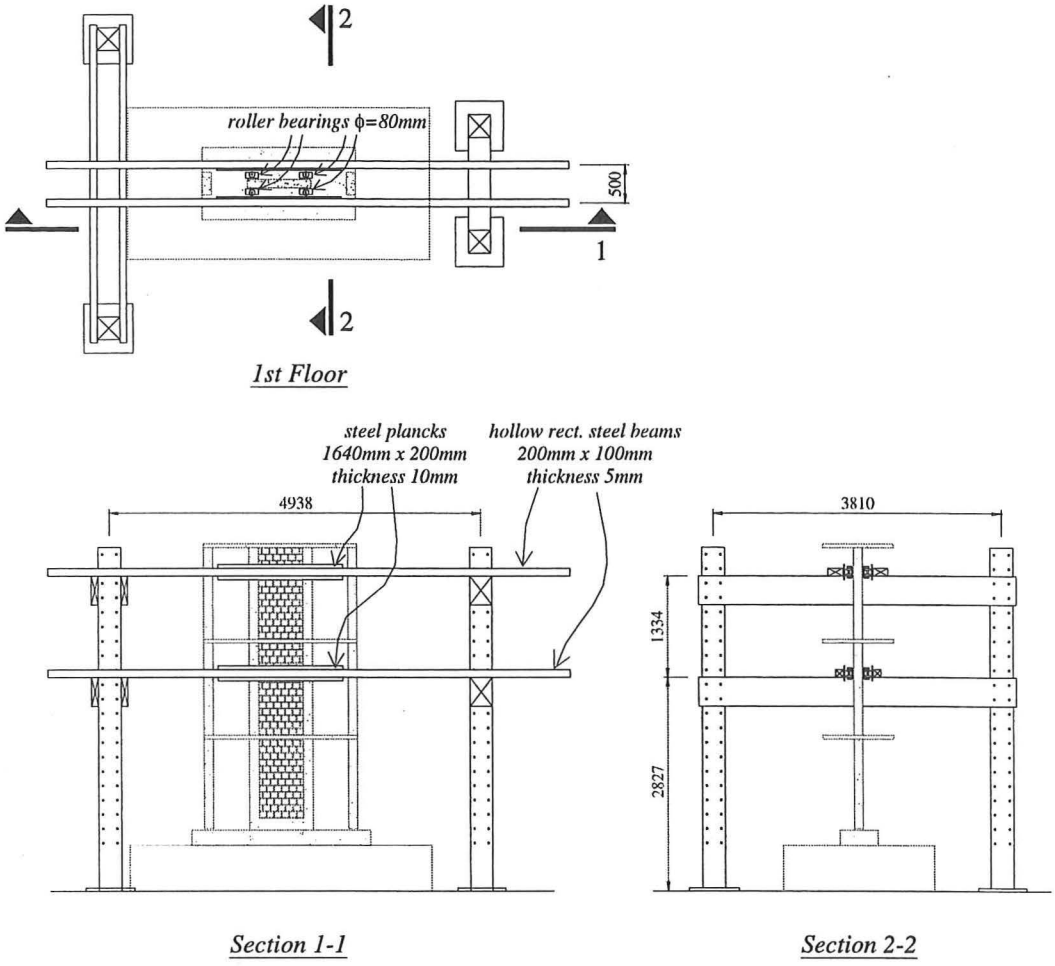

Figure 5-29 Exterior frame for specimen

With respect to the out-of-plane constrains, roller bearings were attached to the model so that minimum friction is created between the model and the exterior frame. Figure 5-30 shows this detail of the specimen.

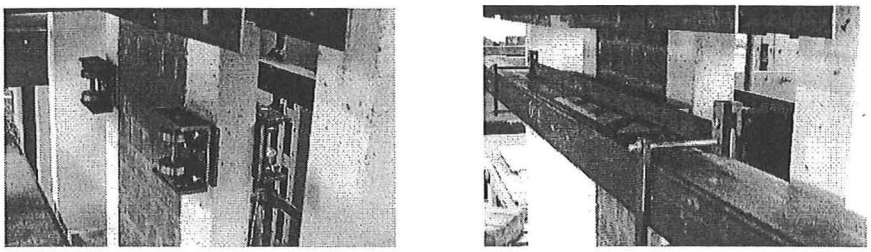

(a) *(b)*

Figure 5-30 Detail of roller bearings: (a) before and (b) after the exterior frame is in position

5.8.3 Instrumentation

The instrumentation consisted of an assemblage of accelerometers and linear potentiometers. Twelve accelerometers were used to get the absolute acceleration at different points of the system and the shaking table. The absolute accelerations will also be used to get the total inertial forces in the system. Eight of the accelerometers were set up to measure vertical accelerations in the rocking wall. The other four measured the horizontal acceleration at the first, second and third floor and at the top of the shake table. The final set up is shown in the figure below. Three linear potentiometers were connected to the first, second and third floors to get the absolute displacements of these floors. Another potentiometer (*P19*) provided the absolute displacement of the shake table that combined with the above-mentioned absolute displacements allowed to calculate the relative displacements of each floor. Six other linear potentiometers were set up to measure the diagonal deformation of the masonry panels. Two potentiometers were attached at each side of the rocking wall in the base to get the uplifting during the rocking. Finally, two potentiometers were placed at the foundation beam connected to the sides of the wall to observe any sliding at the base of the wall. A total of 26 channels were used to collect the data from the instruments. The numbering of the channels though went up to 27 because channel 15 was found to be faulty. In the definition of channels in Figure 5-31, the name of any instrument is defined by either an "*A*" for accelerometers or a "*P*" for potentiometers followed by the number of the channel that the instrument is using.

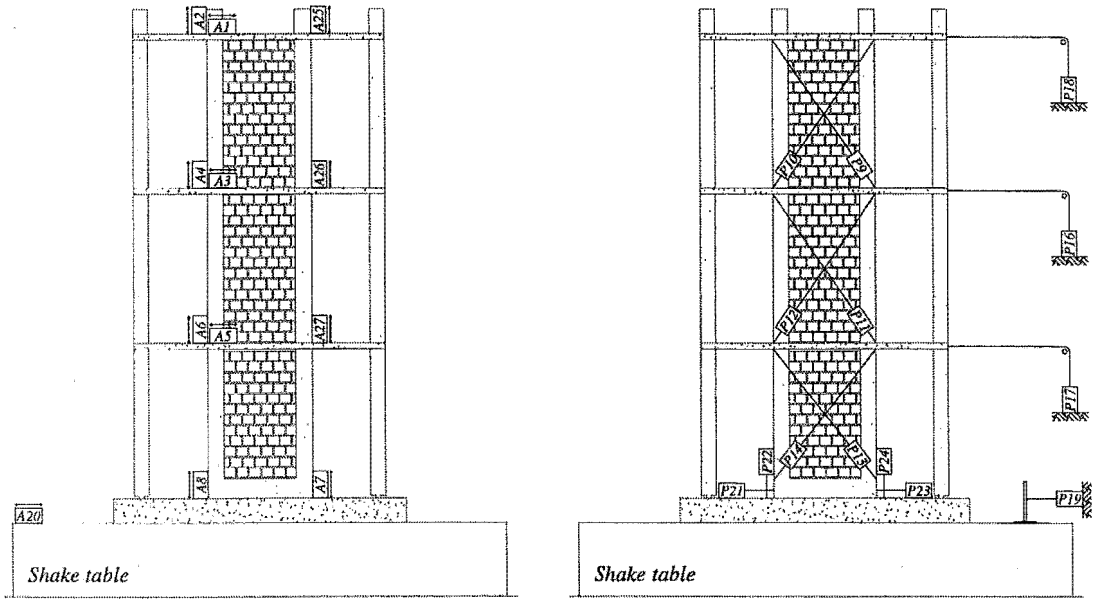

Figure 5-31 Location and direction of accelerometers and potentiometers in specimen

5.9 Conclusions

- It was decided that dynamic tests should be conducted if reliable experimental evidence was to be acquired for this system. Due to logistic limitations, especially the capacity of the shake table, it was necessary to define a reduced scale model to represent the prototype developed in Chapter 4. It is believed that the model that was so-produced can represent reliably the original prototype.

- Dissipators yielding axially provide large energy dissipation capacity through fat hysteretic loops, but their potential buckling made them unreliable. Dissipators yielding in flexure have a smaller energy dissipation capacity but their behaviour was found to be very reliable and stable.

- The testing of the flexural hysteretic dissipators validated the theoretical model developed in Chapter 3 to represent their energy dissipation capacity. The matching was only within the design deformation range of the dissipators though. Beyond this range the observed hysteretic cycles substantially diverged from the theoretical model.

- It is possible to develop adequate detailing to provide the structure with the characteristics required for this particular design system. In some of the details, however, the scale dimensions of the model had to be increased because of the lack of appropriate sized material, particularly deformed reinforcement steel of less than 6mm of diameter.

- In general, the construction of the specimen and its details did not require extreme expertise as the building process was conducted by people inexperienced in this kind of building. However, the detailing of the connections of the dissipators with the base corners of the rocking wall needed to be done carefully and could be difficult to produce in situ. It would be convenient if the detail element is made in a factory and brought to the site ready to be installed.

Chapter 6 Experimental Work: The Dynamic Tests

6.1 Introduction

The model designed in the previous chapter was subjected to a number of dynamic tests expected to assess the reliability of the design technique proposed in chapter 3. A larger than expected number of "runs" was conducted thanks to the efficient performance of the structure during large events. This chapter describes the details of the 60 "runs", analyses the results and compares them with the expected performance developed in Chapter 4.

6.2 Selection of Time-Histories and Schedule and List of the Dynamic Tests

6.2.1 Selection of the Ground-Motion Time-Histories

The most straightforward definition of the ground-motions required for the test would have been the generation of artificial time-histories whose response spectra match the prescribed spectra. However, ground-motions generated in that way might lead to unrealistic seismic demand (Naeim, and Lew, 1995). An alternative option is the use of records from real past earthquakes. These records could be chosen so that they impose a seismic demand equivalent to the design demand. To ease the process, it is possible to modify the amplitude of the original record to match a particular level of seismic demand. The criterion to define equivalent levels of seismic demand was the design spectra. The design spectra, however, are envelopes of different observed ground motions, rather than an expected typical response of a particular site and, therefore, it is unlikely to match the design spectra in all the range with a scaled version of a particular event. Hence the range should be covered with a suit of different records.

Five basic records were initially chosen and their amplitude modified to induce demand-levels equivalent to the design ones. There were four sets of design spectra that needed to be matched, one for each performance-objective. Different versions of the original ground-motions were created with different degrees of amplification in the amplitude. Kramer (1996), quoting other researchers, recommends that the scaling factor (the ratio of the target-amplitude to the amplitude of the record being scaled) should be kept close to 1, preferably between 0.5 and 2.0, and that analyses be conducted with several scaled records. It was the intention to keep the scaling-factors within that

range, but, as observed in Table 6-2, some versions were made with factors outside that range. The basic records that were used are described in Table 6-1.

As commented in the previous chapter, some distortion was expected from the shake table, especially in the high frequency region (section 4.8.1). For these reasons, it was decided that, the definition of the level of demand that a particular run was representing, was to be decided based on the response-spectra of the measured table-acceleration rather than the spectra of the original records.

Table 6-1 List of basic records used

Description	*M*	*Abbreviated Name*
1952 Kern County EQ, M7.5 Taft record N21E component	7.5	Taft-a
1952 Kern County EQ, M7.5 Taft record S69E component	7.5	Taft-b
1940 Imperial Valley EQ, M7.1, El Centro record 180 component	7.1	El Centro
1994 Northridge EQ, M6.8 Saticoy record S00E component	6.8	Saticoy
1994 Northridge EQ, M6.8 Sylmar record 000 component (channel 9)	6.8	Sylmar

The records, however, had to be filtered because of the limited displacement range of the shake-table (±150 mm). Once the ground-displacement time-histories were defined, all the frequency content below 0.1Hz (or oscillations of period above 10 seconds) was removed from the record. Apart from the Taft-b record, all other records were filtered in this fashion. Finally, amplitude and time were modified accordingly with the similitude ratios (S_L and S_T) worked out for the model. The amplitudes of the resultant ground-displacement time-histories were well within the displacement-boundaries of the table. Acceleration time-histories were derived from the modified ground-motions and compared with the original acceleration time-histories to be sure that no significant change was caused to the original record. They do not differ substantially from the original ones. The response spectra were also compared and once more, no significant difference was found.

Finally, apart from the earthquake records, the model was also excited in other ways. This is discussed in the next section.

6.2.2 Schedule of the Tests

A larger than expected number of test runs was conducted. Although the system was built to avoid significant damage, the seismic performance of the structure at large levels of demand was particularly efficient allowing more runs to be performed (Table 6-2).

Table 6-2 Summary of runs

Run Number	*Description*	*Scaling Factor*	*Expected Peak acceleration (g)*
Rocking wall with first set of dissipators			
Run 01	Impact at 3rd floor	--	--
Run 02	Impact at 2nd floor	--	--
Run 03	Impact at 1st floor	--	--
Run 04	translation +/-50mm	--	--
Run 05	White Noise 1	0.10	0.01
Run 06	White Noise 1	0.50	0.03
Run 07	White Noise 2	0.50	0.03
Run 08	White Noise 2	1.00	0.05
Run 09	Taft-a	0.50	0.09
Run 10	Impact at 1st floor	--	--
Run 11	Impact at 1st floor	--	--
Run 12	Taft-b	0.50	0.08
Run 13	Saticoy	0.10	0.05
Run 14	Saticoy	0.25	0.11
Run 15	Taft-a	0.10	0.02
Run 16	Taft-a	0.50	0.10
Run 17	Taft-b	0.10	0.02
Run 18	Taft-b	0.50	0.08
Run 19	Saticoy	0.25	0.11
Run 20	El Centro	0.10	0.04
Run 21	El Centro	0.56	0.20
Run 22	Taft-a	0.10	0.02
Run 23	Taft-a	1.13	0.20
Run 24	El Centro	0.84	0.30
Run 25	Taft-a	1.69	0.30
Run 26	El Centro	1.12	0.40
Run 27	Taft-a	2.26	0.40
Run 28	Sylmar	0.50	0.40
Run 29	El Centro	1.40	0.50
Run 30	Taft-a	2.83	0.50
Run 31	Sylmar	0.63	0.50
Run 32	Taft-a	0.10	0.02
Run 33	El Centro	0.10	0.04
Run 34	El Centro	0.56	0.20
Run 35	Taft-a	1.13	0.20
Rocking wall with second set of dissipators			
Run 36	El Centro	0.10	0.04
Run 37	Taft-a	0.10	0.02
Run 38	El Centro	0.56	0.20
Run 39	Taft-a	1.13	0.20
Run 40	El Centro	1.40	0.50
Run 41	Taft-a	2.83	0.50
Run 42	Sylmar	0.63	0.50
Run 43	Sylmar	1.00	0.80
Run 44	Sylmar	1.00	0.80
Run 45	Sylmar	1.25	1.00

Table 6-2 (contd.) Summary of runs

Run Number	*Description*	*Scaling Factor*	*Expected Peak acceleration (g)*
Rocking wall without dissipators			
Run 46	El Centro	0.10	0.04
Run 47	Taft-a	0.10	0.02
Run 48	El Centro	0.56	0.20
Run 49	El Centro	0.56	0.20
Run 50	Taft-a	1.13	0.20
Run 51	El Centro	1.40	0.50
Run 52	Taft-a	2.83	0.50
Run 53	Sylmar	0.63	0.50
Run 54	Sylmar	1.00	0.80
Run 55	Sine Pulse +/-2mm 2Hz	--	--
Run 56	Sine Pulse +/-10mm 2Hz	--	--
Run 57	Sine Pulse +/-10mm 2Hz	--	--
Run 58	Sine Pulse +/-40mm 5Hz	--	--
Rocking wall with second set of dissipators back in position			
Run 59	Sine Pulse +/-40mm 5Hz	--	--
Run 60	Sine Pulse +/-80mm 5Hz	--	--

Sixty dynamic tests were run. However, some of them are only marginally relevant, as they were used to observe the fidelity of the signal rather than to observe the seismic performance of the model. The first runs (1 to 3, 5 to 8 and 10 to 11) were mainly used to determine the natural periods of the structure. Runs 12 to 54 were intended to reproduce the seismic demand at the different design levels. Some runs in between, however, were only conducted as trials to check the instrumentation. These trial runs were scaled down to produce very low levels of demand. Thanks to the large number of dynamic tests it was possible to test the system under different conditions. Two sets of dissipators were built and were used at different stages. It was also possible to test the response of the structure without dissipators in runs 46 to 58. Finally, in runs 55 to 60, the structure was subjected to a sine-type impulse to observe its free-oscillation response with and without dissipators.

6.3 Recorded and Derived Time-Histories

6.3.1 Directly Recorded Time-Histories

As described in the previous chapter, accelerometers and potentiometers were set-up to measure directly a number of parameters. All data was recorded at a frequency of 400 Hz. In the next table, the recorded parameters are described and associated with the corresponding instrument. The name of the instrument also defines the number of its corresponding channel. Table 6-3 provides an abbreviated name that will be used in the next section to derive other parameters in terms of the ones described here. There, the abbreviate names will represent vectors containing the corresponding data.

Table 6-3 Time histories obtained directly from instruments

Time-histories description	*Location*	*Instrument*	*units*	*Abbreviated Name*
Absolute lateral displacement	3rd floor	P18	mm	D3
	2nd floor	P16	mm	D2
	1st floor	P17	mm	D1
	Table	P19	mm	D0
Base uplift	Wall base-left	P22	mm	BUL
	Wall base-right	P24	mm	BUR
Base slip	Wall base-left	P21	mm	BSL
	Wall base-right	P23	mm	BSR
Absolute horizontal acceleration	3rd floor	A1	g	AH3
	2nd floor	A3	g	AH2
	1st floor	A5	g	AH1
	Table	A20	g	AH0
Absolute vertical acceleration	3rd floor-left	A2	g	AV3L
	3rd floor-right	A25	g	AV3R
	2nd floor-left	A4	g	AV2L
	2nd floor-right	A26	g	AV2R
	1st floor-left	A6	g	AV1L
	1st floor-right	A27	g	AV1R
	Base wall-left	A8	g	AV0L
	Base wall-right	A7	g	AV0R
Masonry panel diag. Deformation	3rd floor (+)	P10	mm	M3A
	3rd floor (-)	P9	mm	M3B
	2nd floor (+)	P12	mm	M2A
	2nd floor (-)	P11	mm	M2B
	1st floor (+)	P14	mm	M1A
	1st floor (-)	P13	mm	M1B

6.3.2 Derived Time-Histories

The time-histories listed above were used to derive other time-histories described in Table 6-4. They have been calculated applying basic mechanical principles. The equations that define these derived quantities are also presented in the table. In the definition of these equations the abbreviate names associated with the directly-recorded-parameters are treated as vectors. All but one of the new time-histories could be defined in an automatic sequence of operations on those vectors. It was in the definition of the energy dissipated by the dissipators that some manual operations needed to be made. This time-history was calculated from the observed uplift of the base-corners in the rocking wall which defines the vertical deformations in the dissipators. Once the vertical deformation is known, the energy dissipated can be calculated for each half-cycle using the equations developed in Chapter 3 to calculate the area of the dissipator's hysteretic-loops. Organising those equations one ends up with:

Energy dissipated per half-cycle: $$A_3 = C_1 C_2 A_1 = C_2 \left(2F_y \Delta_d - \frac{(2F_y)^2}{k_d} \right) \geq 0 \qquad \text{(Eq. 6.1)}$$

Table 6-4 Time-histories obtained indirectly operating from direct readings

Time-histories description	*Location*	*Name*	*Equation*
Relative Lateral Displacement	3rd floor	RD3	D3 - D0
	2nd floor	RD2	D2 - D0
	1st floor	RD1	D1 - D0
Inter-storey Drift	3rd floor	ID3	(D3-D2) / 1260mm
	2nd floor	ID2	(D2-D1) / 1260mm
	1st floor	ID1	(D1-D0) / 1260mm
Average Drift	--	D	(D3-D0) / 3780mm
Lateral Inertial Load	3rd floor	LI3	1811kg × AH3
	2nd floor	LI2	2011kg × AH2
	1st floor	LI1	2011kg × AH1
Total Lateral Inertial Load Histories*	Base	BL	LI1 + LI2 + LI3
Increment in base displacement	--	IBD	IBD(i) = D0(i) - D0(i-1)
Incremental Work done on the system	--	IW	IW(i) = BL(i) × IBD(i)
Energy input in the system	--	IE	IE(i) = IE(i-1) + IW(i)
Energy dissipated by dissipators	--	DE	See notes in this section
*This load is assumed to be equal to the total base load neglecting the forces due to the intrinsic damping of the system			

6.4 Observed Properties of the Model

6.4.1 Main Non-Rocking Natural Period of Free Vibration

The evolution of the main non-rocking free-vibration period as the testing was conducted is observed in Figure 6-1. The main period was calculated from the recorded roof-acceleration time-history counting the cycles for a given length of time. The counting was made in the last part of the record, when the model is not excited anymore (in free oscillation) and it has stopped rocking.

As expected, the main non-rocking period became larger as the structure was softened by accumulated testing. The increase in the period however occurs mainly in jumps, whenever the structure sustains a drift larger than any other recorded earlier (Figure 6-1). If the structure does not undergo a significantly larger drift, its fundamental period will remain practically constant. However, the observed jumps after the model has exceeded a drift of 1% are very small. Since no damage was observed in the wall, it seems that the period is trying to reach a plateau defined by the main period of the wall alone (associated with the effective inertial mass).

The main non-rocking period seems to be affected by the yielding in the dissipators as well. The apparent reason is that the wall may be actually rocking very early thanks to the residual stresses in the dissipators (after they have yielded) that are pushing the wall up. In Run 36, where new dissipators were used, the period drops down again. As soon as they start yielding the period moves up to reach

the plateau observed immediately before the old dissipators were replaced. When the second set of dissipators (already with residual deformations) is removed, the period drops down again (Run 46). The opposite occurs when they are replaced (Run 59).

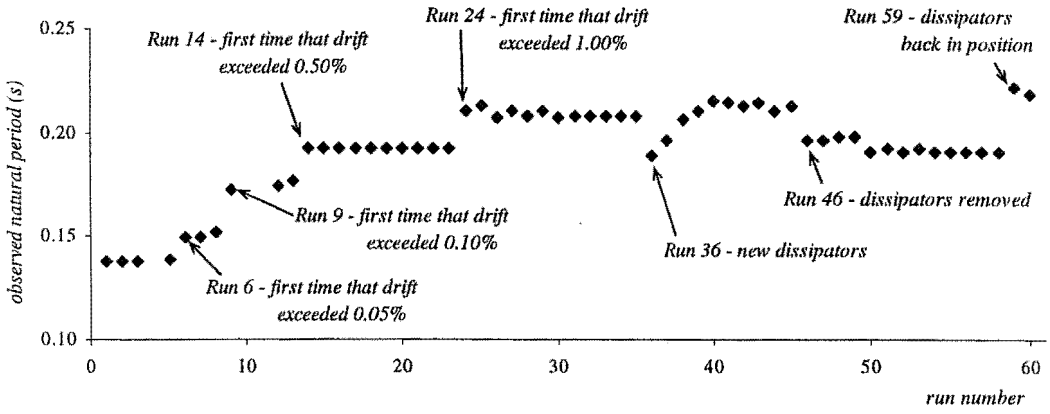

Figure 6-1 Observed first natural period in model-structure

6.4.2 Non-Rocking Stiffness of the System

The non-rocking stiffness of the system was derived from the measured non-rocking fundamental period. This stiffness can be regarded as the initial stiffness of the system in a lateral force-displacement plot. As expected, the stiffness degrades trying to reach the plateau corresponding to the stiffness of the wall alone. The evolution of the stiffness through the testing program responds to the same factors discussed above, in the section dealing with the observed main period of the model. The stiffness presented in the next figure was calculated from the observed main-period defined in that section. The mass that was used was the effective mass of the model, $M_{eff} = 4974$ kg.

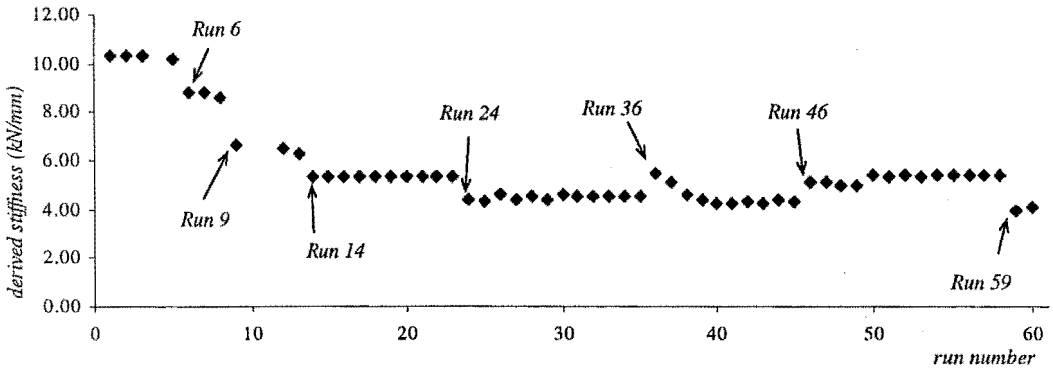

Figure 6-2 Observed lateral stiffness of the structure

6.4.3 Rocking Period of the System

The rocking period was calculated from the observed free oscillation of runs 57 through 60. The period was calculated for each cycle and plotted in Figure 6-3. The two plots there show the observed rocking period of the system with the rocking-wall with and without dissipators. The data for the wall without dissipators was compared with the theoretical equation derived in chapter 3. The combined rotational inertia of the system, $I_{o\ comb}$, was used to that end. The theoretical values matched well the observed rocking periods, validating the concept of a combined-rotational-inertia (Chapter 3). However, a divergence arises when the lateral drift of the system exceeds 1.5%. This is consistent with what was found later (section 6.6.6): for large drifts the system seems to be stiffened up.

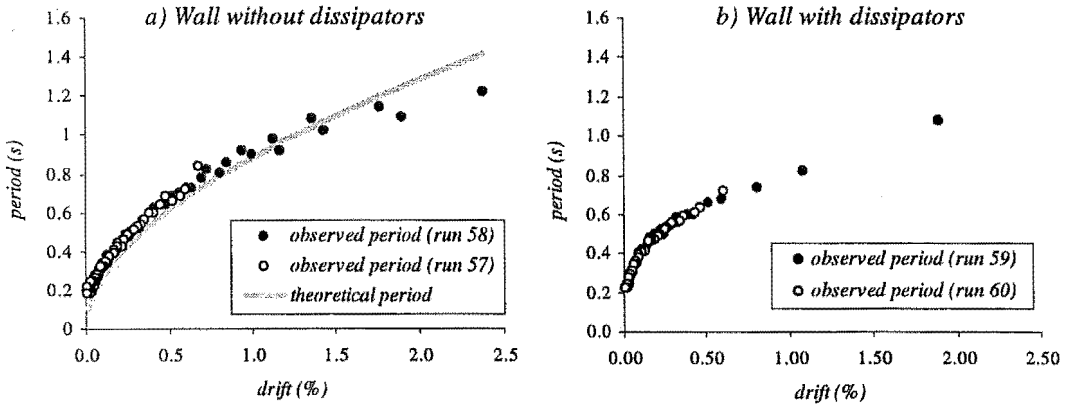

Figure 6-3 Observed and theoretical rocking period of the system

6.5 Actual "Seismic" Demand observed during the Dynamic Tests

6.5.1 Problems observed in the reproduction of the earthquake-records in the shake-table

As discussed in section 5.8.1, the shake table is displacement-driven and, therefore, cannot handle properly high frequency accelerations since they induce rather small displacements. Although the main frequency of the structure was away from the natural period of the table-structure system, it was found that the table was resonating with the higher modes of the structure. Although in a real scenario a similar phenomenon could be expected, (a phenomenon that some authors call double resonance, Kramer, 1996), the magnitude of some of the observed acceleration-peaks was unrealistically high. This problem, has been observed before, not only in this shake-table (Kao, 1998), but also in other experimental programs conducted on shake-tables (Lee and Woo, 2001). The problem, however, is particularly magnified in these tests because the rocking process is accompanied by impact actions of the rocking wall against the table, which feeds some high frequency energy back to the table. When analysed in the time domain, the results were worrying. The peak accelerations measured in the table largely exceeded the maximum accelerations of the input acceleration time-histories (Figure 6-4).

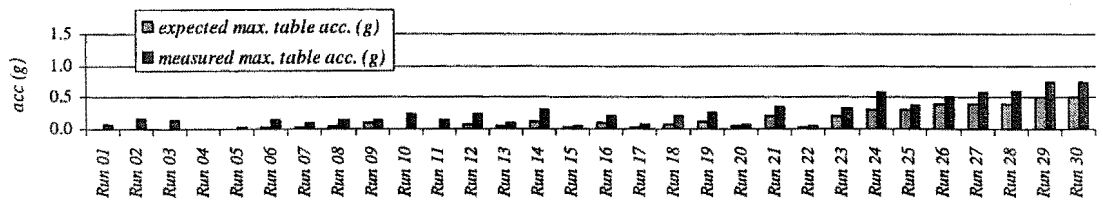

Figure 6-4-a Expected vs. measured peak table-acceleration (Runs 1 through 30)

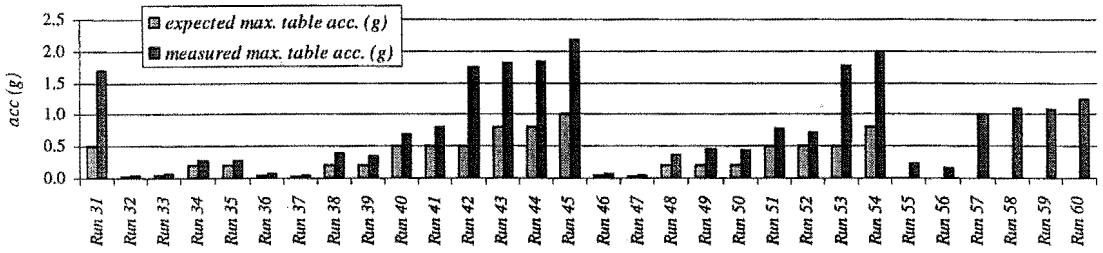

Figure 6-4-b Expected vs. measured peak table-acceleration (Runs 31 through 60)

The amount of noise was also worrying, causing the observed table-acceleration time-history to look very different from the original one. Figure 6-5 presents a typical case. Although the output in the time domain seems to show that the actual "seismic" demand imposed on the structure is greater than the intended one, it would be unrealistic to quantify the demand based only on the observed peak accelerations, especially noting that the peaks seem to be restricted to the high frequency domain.

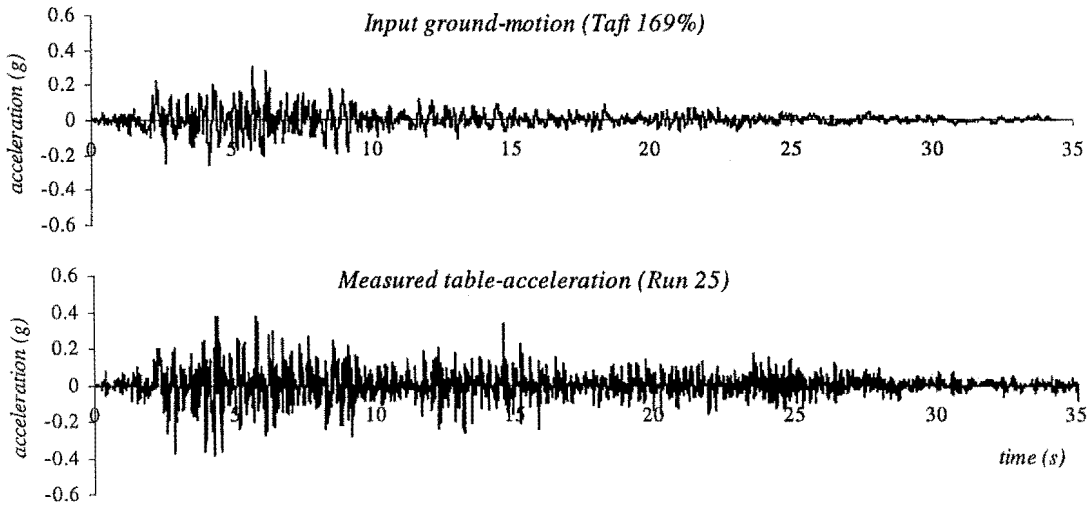

Figure 6-5 Comparison of original and observed table-acceleration time-histories

It was decided that a fairer assessment of the real "seismic" demand imposed to the model would be made in the frequency-domain. In the frequency-domain it was confirmed that the noise, and specially those peak-accelerations, were limited to the high frequency range. As expected, the acceleration response-spectra of the observed acceleration time-histories also showed large peaks only in the regions corresponding to high natural frequencies of the structure (particularly its second mode). These peaks did not exist in the spectra of the original input records. The actual inertial demand below the high frequency region is closely reproduced though. Figure 6-6 shows what was typically observed in almost every acceleration spectrum. In the same figure, the displacement spectrum corresponding to the same run is also presented. The displacement spectrum shows the small impact of the high frequency accelerations in the lateral deformations of the structure.

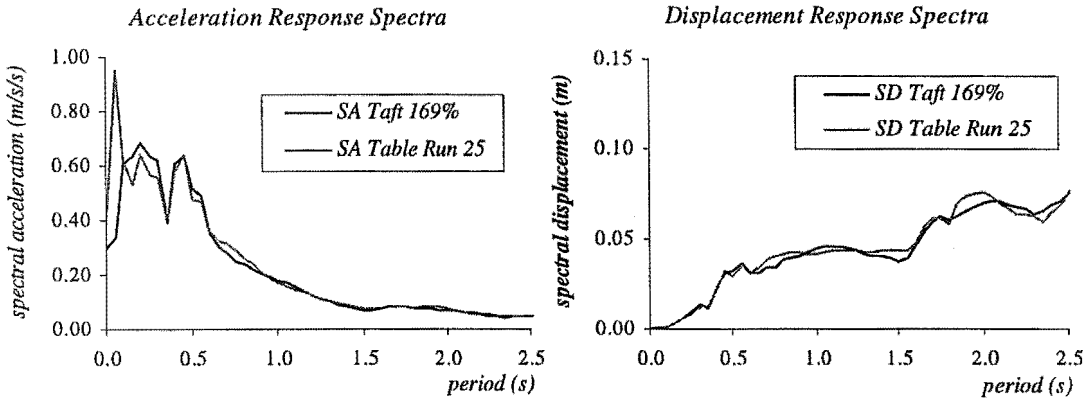

Figure 6-6 Comparison of response spectra of input and measured ground-motion time-histories (Equivalent Viscous Damping 5%)

Unfortunately, there were cases in which the shake-table just could not reproduce the records. It was particularly obvious with the Sylmar records. The main reason was a velocity capacity of the table (of the order of 250 mm/s), below the expected one (Figure 6-7b). The shake table was supposed to be able to deliver up to 1000 mm/s (section 5.8.1). Besides the lack of fidelity, in some of the tests the peak table accelerations were so large that, although they seemed to excite a higher mode of the model-structure, the induced total base-shear happened to be the largest measured in those runs. For these reasons, the runs derived from the original Sylmar record will be used only marginally.

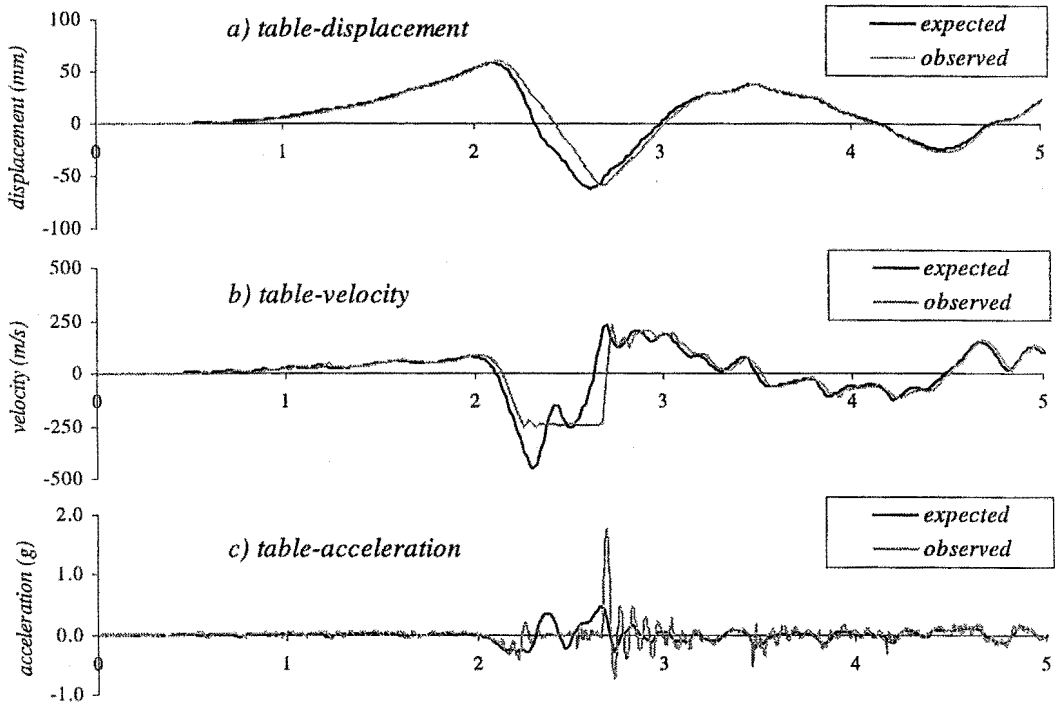

Figure 6-7 Expected and observed table time-histories in Run 42 (first 5 seconds)

6.5.2 Equivalent seismic-demand classification of the runs

In order to compare the observed performance with the expected one, it was necessary to define the "runs" that, after the distortion discussed above occurred, were able to reproduce a seismic-demand equivalent to the design one. To compare drifts, it was decided to choose "runs" whose displacement spectra matched the design spectra. In Figure 6-8, the displacement spectra of the "runs" selected to represent the demand for different levels is compared with the respective displacement design spectra.

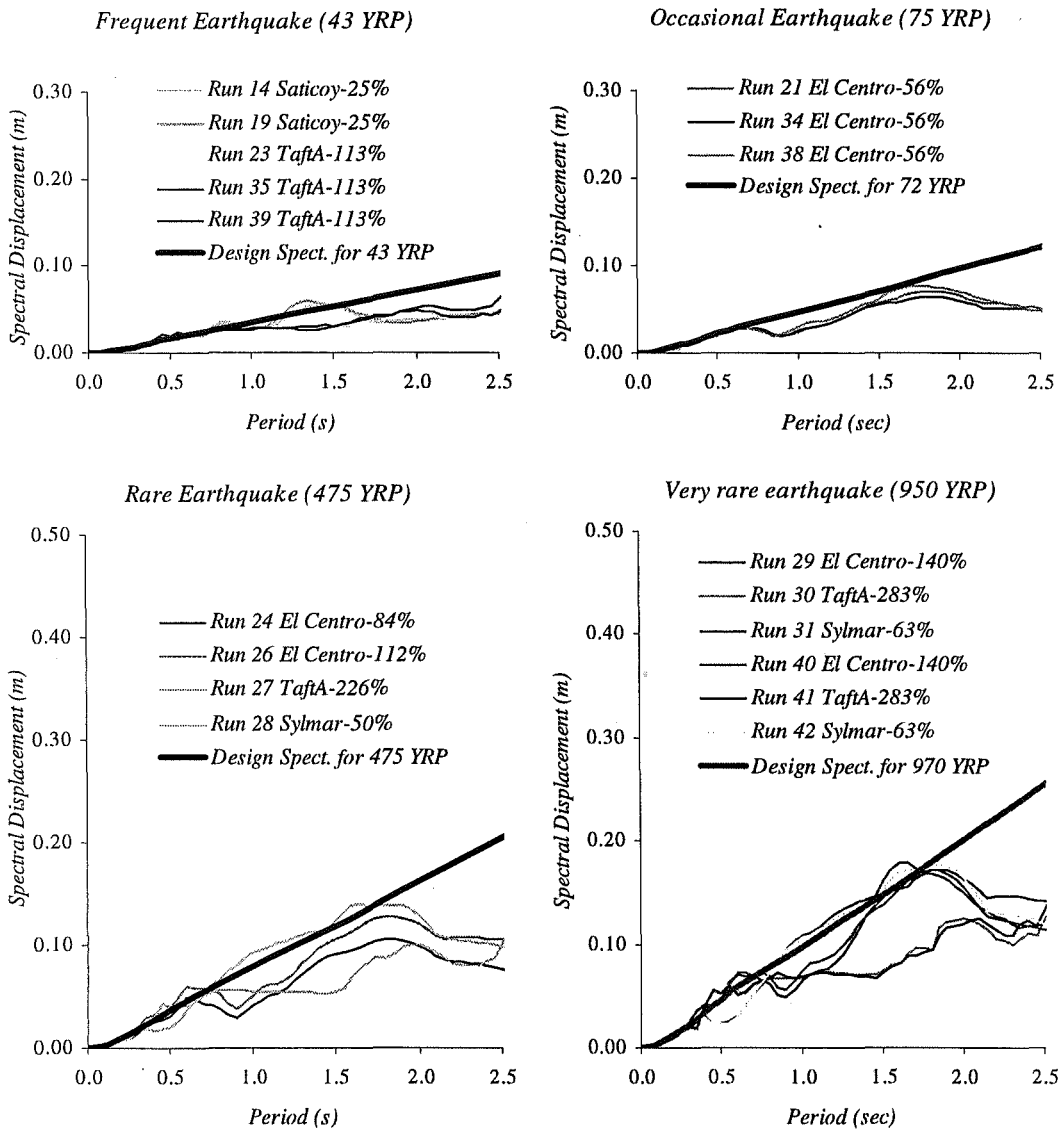

Figure 6-8 Displacement spectra of table-acelerations compared with design spectra (Equivalent Viscous Damping 5%)

The acceleration spectra of the same runs are presented in Figure 6-9. It is clear that some of those runs inflict unrealistically large inertial demands in the model. For the purposes of the assessment of inertial forces and absolutes accelerations runs 31 and 42 are taken off the list. These runs are the ones that present the large spectral-acceleration peaks in the very-rare-earthquake case. Their output, however, will be taken into account for the assessment of the observed drift of the model.

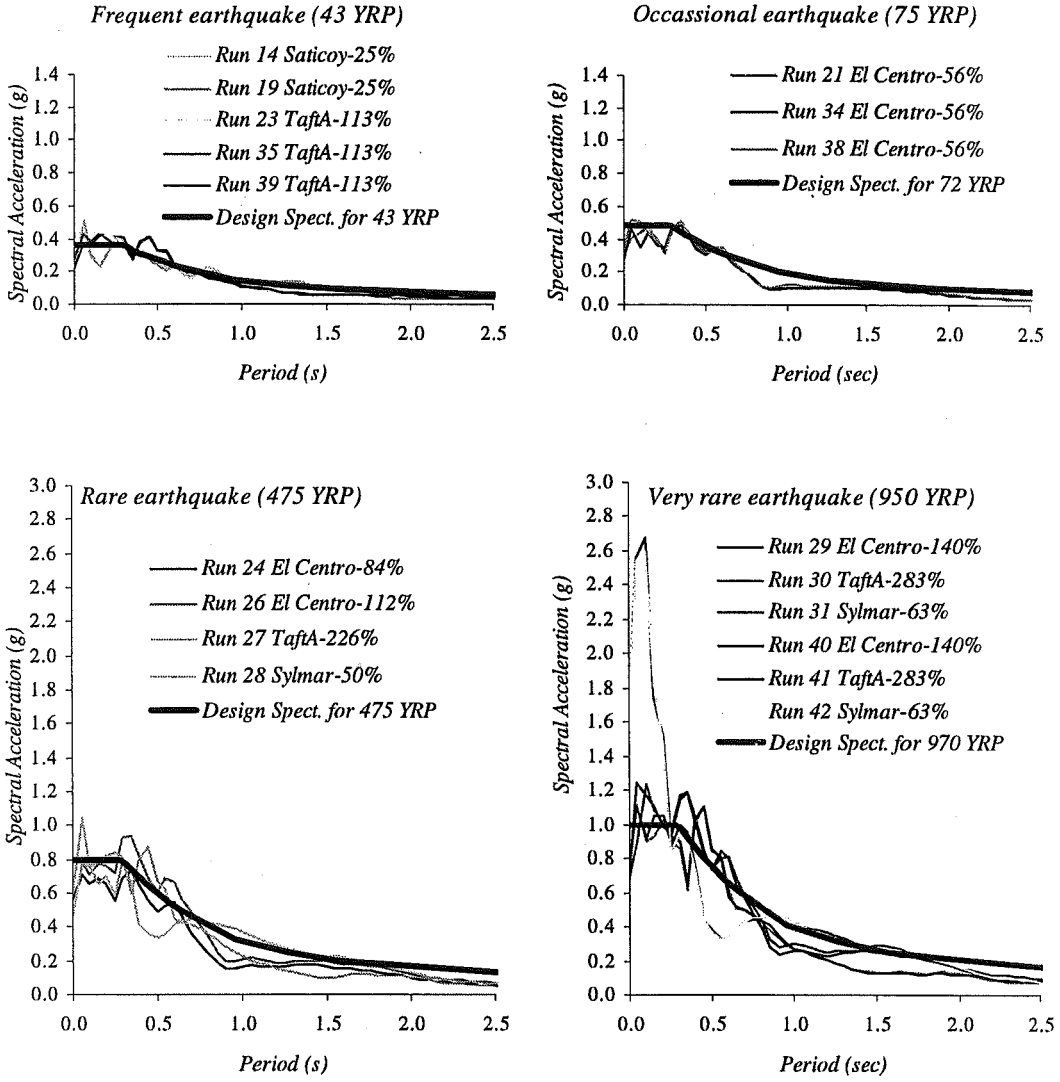

Figure 6-9 Acceleration spectra of table-acelerations compared with design spectra (Equivalent Viscous Damping 5%)

6.6 Assessment of the Seismic Performance of the Model

The seismic performance is assessed here through the evaluation of several parameters related to the performance of the system. Those parameters were qualitative and quantitatively defined in Chapters 3 and 4. The observed values are compared with the expected design values.

6.6.1 Transient Inter-Storey Lateral Displacements

The observed lateral displacement pattern, along the height of the specimen, was inverse-triangular. The inter-storey displacement demand was, therefore, evenly distributed along the height of the specimen. (Figure 6-10). Thanks to this shape, it is also possible to use the observed average drift to define the observed inter-storey drift at any level with enough accuracy.

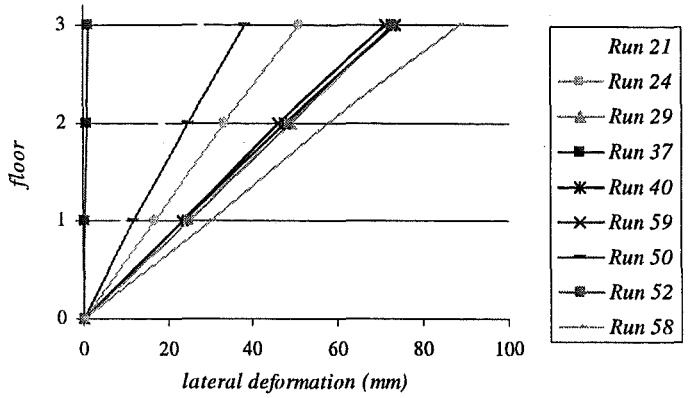

Figure 6-10 Observed lateral deformation pattern of 9 different runs

Maximum inter-storey drifts were found and compared with the expected drift. The observed drifts match reasonably well the expected ones. The cumulative distribution of the ratio between the Observed Peak Drift (OPD) and the Expected Peak Drift (EPF) shows that 78% of the observations were lower than the design drifts (Figure 6-11).

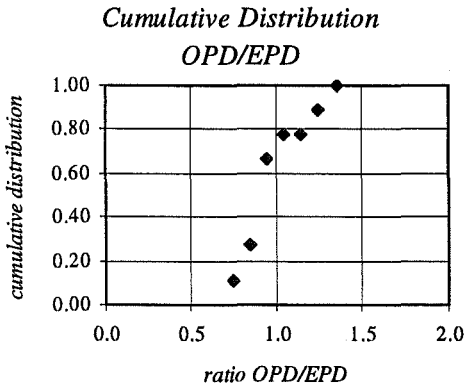

Figure 6-11 Cumulative Distribution of the ratio between the Observed Peak Drift (OPD) and the Expected Peak Drift (EPD)

The results are presented in more detail in Figure 6-12. In the lower levels of demand, the first observed drifts are below the expected ones but as the structure gets softer, the drift increases reaching a plateau. At the initial "runs" the stiffness of elements other than the wall and dissipators might be significant and, therefore, a larger than expected equivalent stiffness is developed by the model. One must remember that in the definition of the expected drift, at any level, the stiffness of any other element apart from the wall with dissipators was neglected (Chapter 3). This contrast could explain the smaller than expected drifts at the early runs (runs 14 and 19, and run 21).

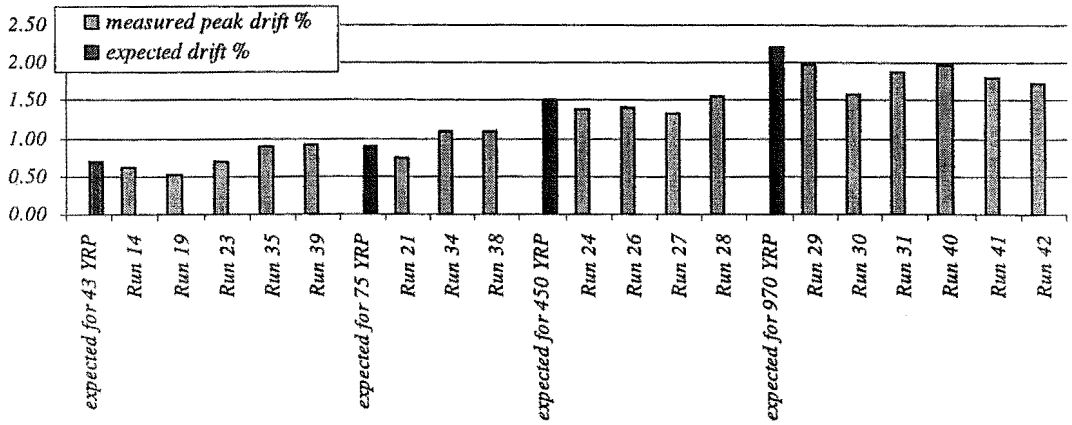

Figure 6-12 Observed peak drift compared with expected drift

In the final runs, the effective stiffness is closer to the expected effective stiffness. In the case of the final runs, however, the contribution of the intrinsic damping of the system probably reduced. That may explain the larger than expected drift in the later runs (runs 35 and 39, and runs 34 and 38). The most demanding regions are less sensitive to the variations of intrinsic damping and contribution of the initial stiffness of other members. However, at larger deformations there seemed to be a stiffening mechanism that increased the effective stiffness of the system, reducing the lateral drift of the system. The load-displacement pattern will later confirm this trend (section 6.6.6).

6.6.2 Permanent Drifts

The rocking wall was designed to avoid permanent drifts. To that end, the restoring moment, provided by the self-weight of the wall, was made greater than the maximum moment provided by the hysteretic dissipators. In Figure 6-13 the lateral roof displacement observed in Run-40 is shown along with the base uplift of the rocking wall. This was one of the most "seismically" demanding runs and even though the structure reached a peak inter-storey drift close to 2%, no permanent displacement was observed at the end of the run. That was the case in every single run.

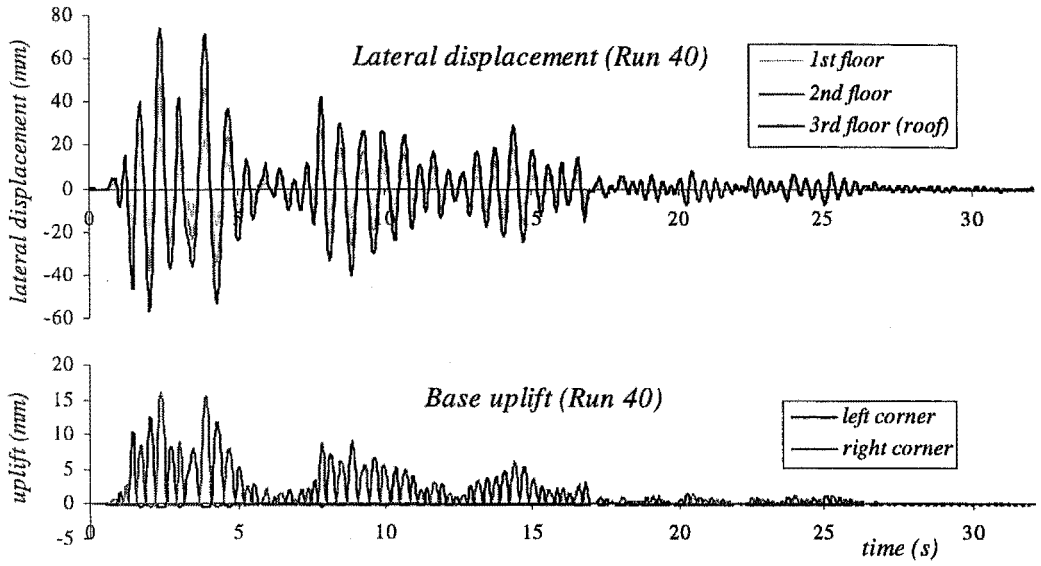

Figure 6-13 Observed lateral displacement and uplift

6.6.3 Base Uplift

At the design stage, the base-uplift was defined assuming that the rocking wall was rigid. It is necessary to assess this assumption because the energy dissipation capacity of the dissipators was defined based in the expected base-uplift of the rocking wall. The next equation would define the expected base-uplift if the rocking wall was perfectly rigid:

$$\Delta_{uplift} = AverageDrift \times BaseLength \qquad \text{(Eq. 5.2)}$$

The observed base-uplift is depicted in Figure 6-14. It is compared with the values predicted by equation 5.2. The good match in all the range of amplitudes confirms that the wall is stiff enough to be regarded as rigid in the definition of the base-uplift and therefore in the deformation induced on the energy dissipators.

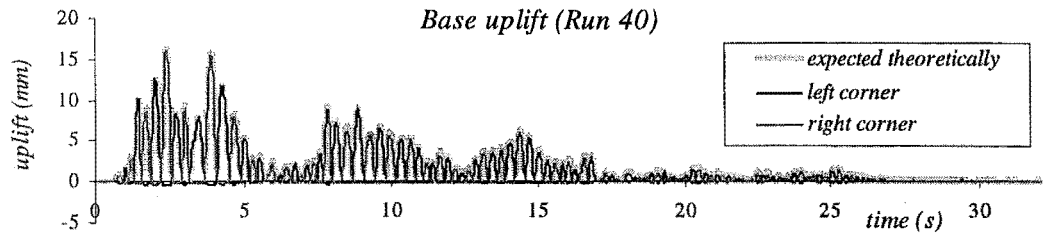

Figure 6-14 Obserfed base-uplift compared with base-uplift derived from observed drift

6.6.4 Base Shear Demand

The observed base-shear differed from the expected values because the theory developed in Chapter 3 did not model the stiffness provided by structural elements other than the rocking wall with dissipators. It is also possible that higher modes have affected the observed base shear. The statistical distribution of the ratio between the Observed Peak Base Shear (OPBS) and the Expected Peak Base Shear (EPBS) shows that only 25% of the results were within the expected design values (Figure 6-15). An amplification factor 1.5 times larger would have had to be applied to reach a level of reliability of 80%.

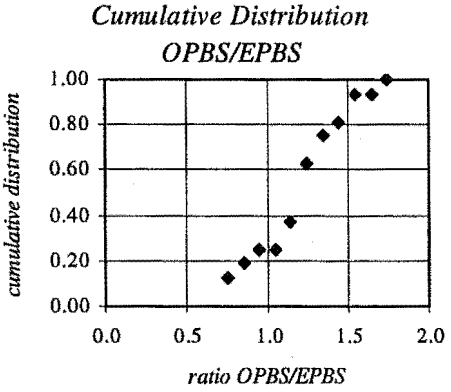

Figure 6-15 Cumulative Distribution of the ratio between the Observed Peak Base Shear (OPBS) and the Expected Peak Base Shear (EPBS)

In Figure 6-16, the results are shown in more detail. When the slabs developed the intended hinges the results were closer to the predicted ones (see runs above run 26). At large drifts, however, a new stiffening mechanism develops in the system, increasing the response. The influence of higher modes at these intensities was also more significant.

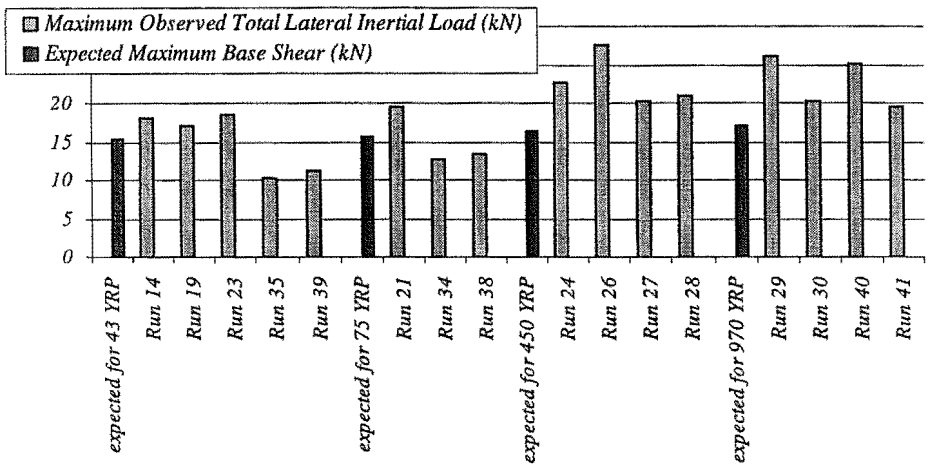

Figure 6-16 Observed peak total lateral inertial load compared with expected base-shear

The effects of the impact actions were obscured due to the presence of the stiffening mechanism. Most of the peaks observed in Figure 6-16 are due to this stiffening mechanism rather than to the impact of the wall against the foundation. The observed shear demand evolved as the structure softened. In Figure 6-17 three time-histories corresponding to the same ground motion are depicted. The first one, Run 21, presents larger peaks at the beginning due to the larger stiffness of the system. The hinges are not fully developed and it seems that the slab-beam still contributes with significant stiffness to the system. In runs 34 and 38, the hinges are largely softened and the base shear is limited by the basic intended capacity of the rocking wall.

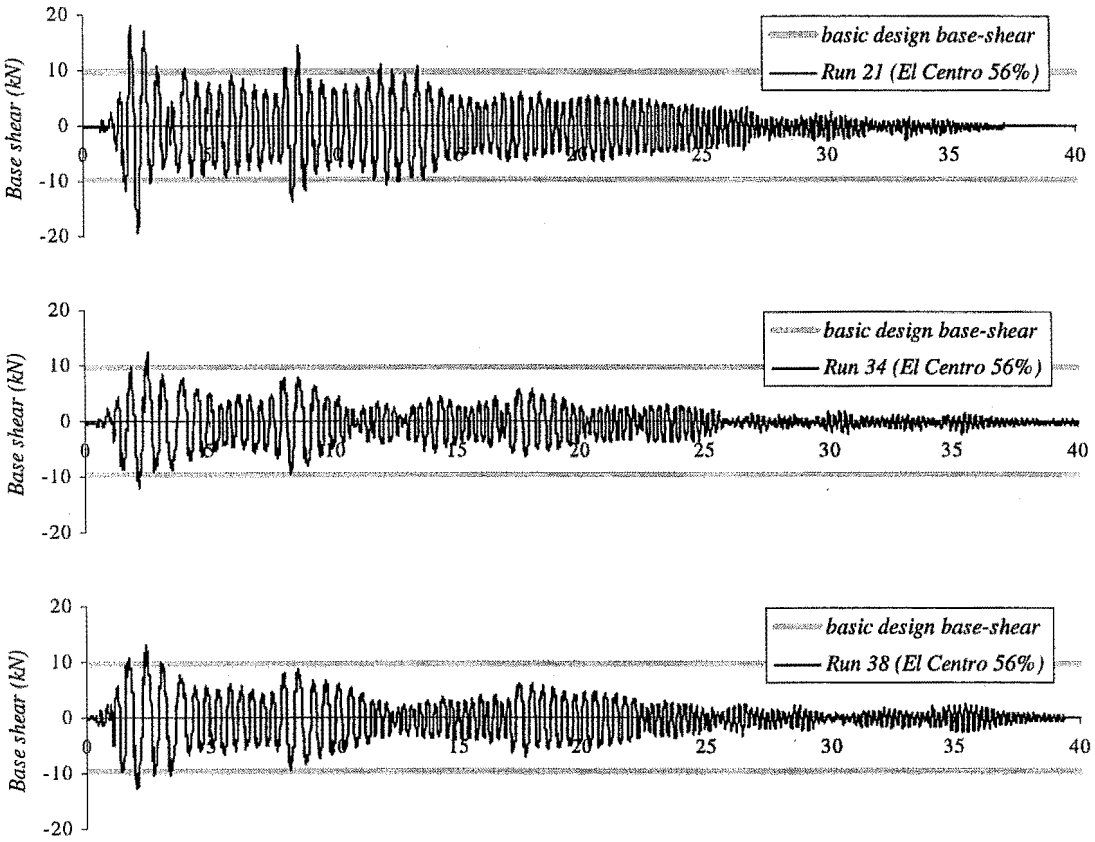

Figure 6-17 Base-shear time-histories for the same ground-motion at different runs

For a larger demand, and when the hinges are softened, again, unexpected peaks in the base-shear time-histories are observed. Figure 6-18 exposes that behaviour. When the base-uplift does not go further than 9mm (drift of 1.10%), the observed base shear is similar to the expected one. Otherwise, the observed base-shear goes beyond the expected limit. The records show consistently that the peaks occur when the drift exceeds 1.10%. This drift means 9mm base-uplift in the rocking wall. The dissipators, therefore, have not reached the point where their stiffness starts to escalate (found to be

around 16mm of vertical deformation in Chapter 5), and therefore, the peaks must be due to some stiffening action of other elements of the structure.

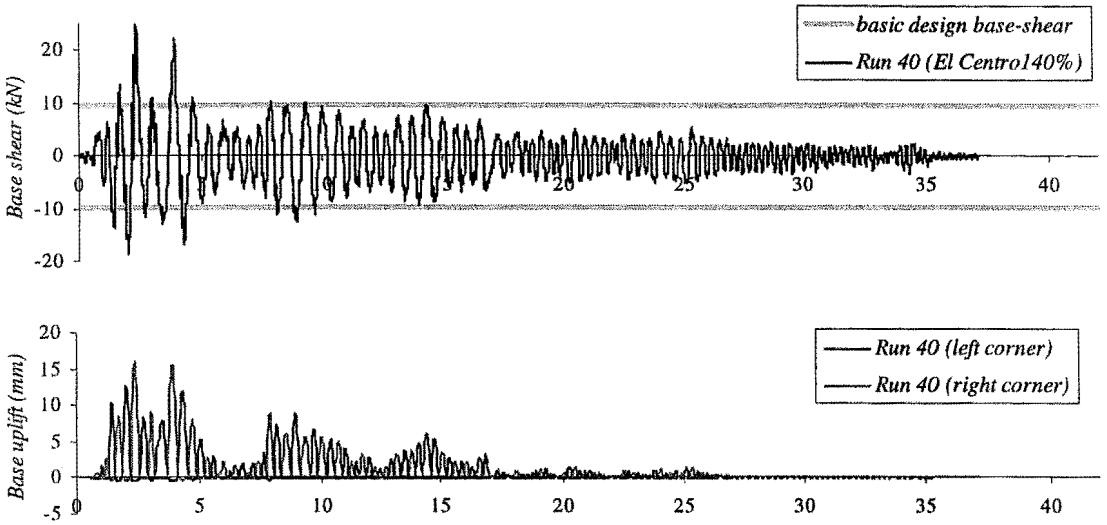

Figure 6-18-a Base-shear and base-uplift time-histories for Run-40

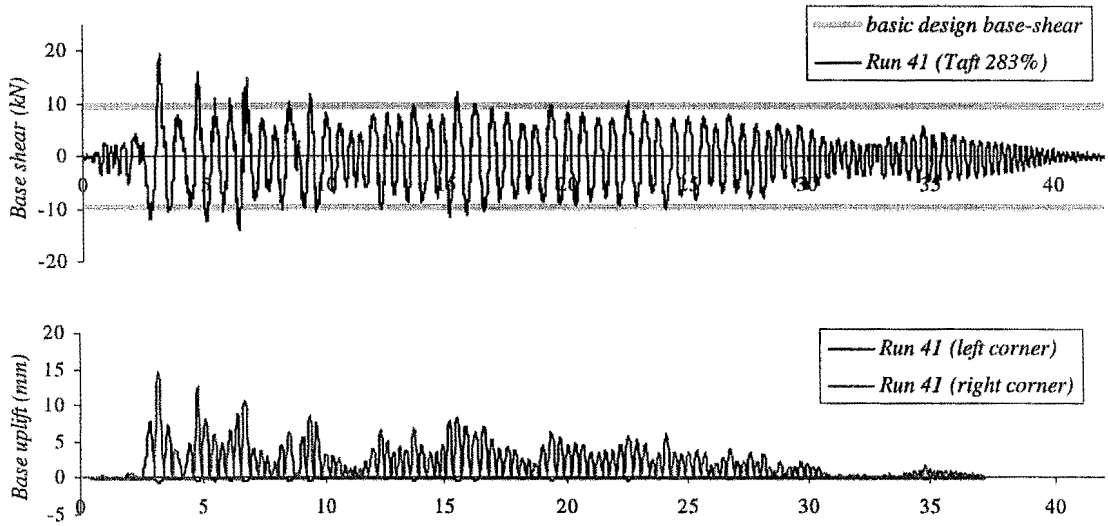

Figure 6-18-b Base-shear and base-uplift time-histories for Run-41

To complement the discussion in this section, two more runs are presented here. In this runs the rocking wall was without dissipators and, therefore, there is no influence of the dissipators at all in the response of the system. The peaks are observed again when the wall exceeds 1.10% drift (9mm base uplift). Note that in this case the expected basic base-shear has to be reduced because the dissipators are not contributing their design action, F_y.

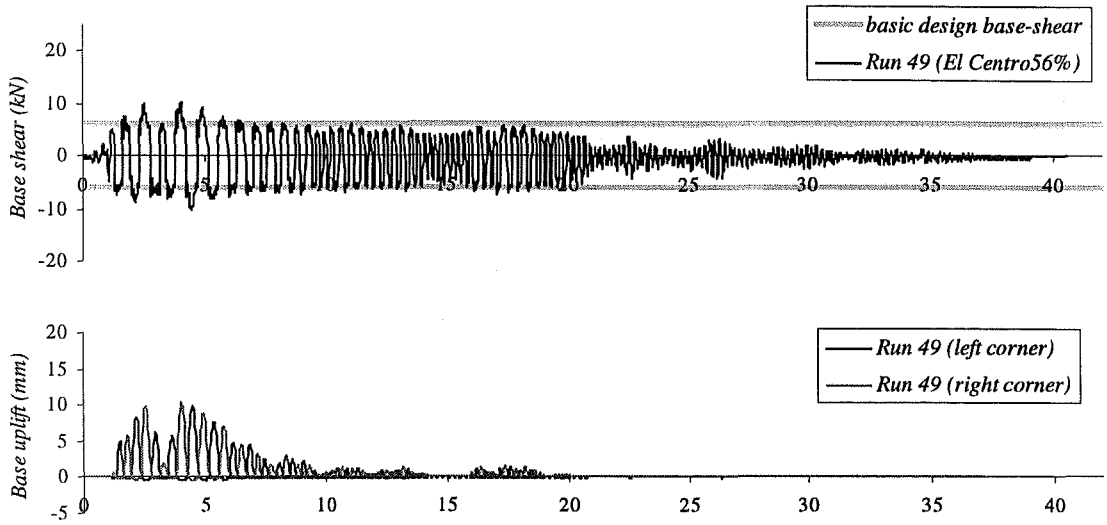

Figure 6-19-a Base-shear and base-uplift time-histories for Run-49

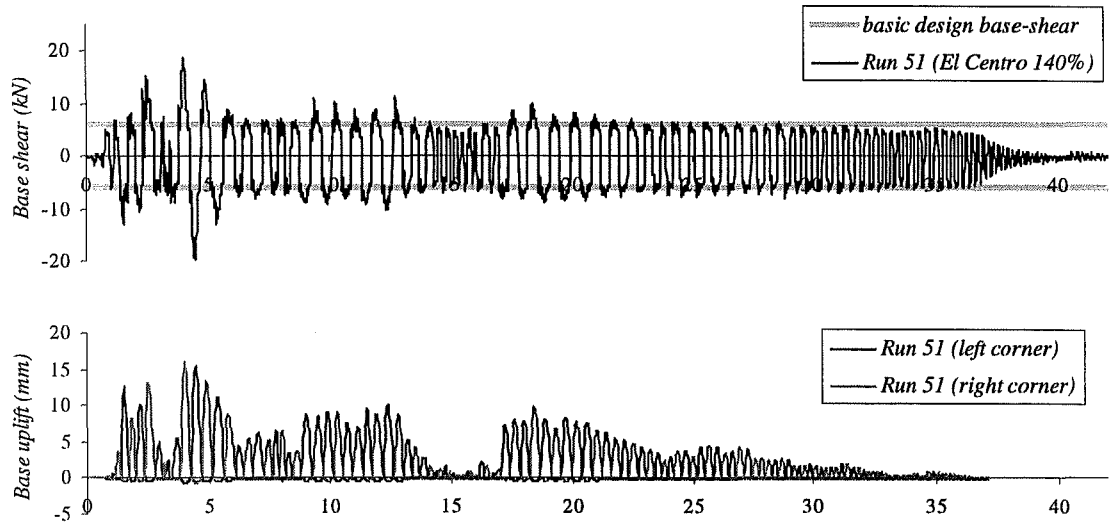

Figure 6-19-b Base-shear and base-uplift time-histories for Run-51

6.6.5 Inter-storey Shear Forces

The inter-storey shear-forces showed a response similar to the observed in the base-shear time-histories. The expected basic shear-forces matched reasonably well the observed time-histories; and the largest peaks were reached when the specimen is affected by the stiffening action of elements other than the rocking wall with dissipators. The effects of impact can be observed in Figure 6-20 and Figure 6-21, which present a closer look to two of the base-shear time-histories displayed in the previous section, as well as the shear-forces felt at higher levels. They are segments taken from the complete time-histories, and were selected from regions where the stiffening action of the other

structural elements was not observed. The only significant effect in the shear-forces of the higher-modes being excited is observed in the top floor. There, the inertial load of the top floor is not cancelled out by any other one load as it happens with the lower levels.

From the same figures, the dissipators also seem to soften the first-mode "wave" of the observed time-histories with beneficial effects in the total response. Unlike the rectangular-shape wave observed in the response of the system without dissipators (Figure 6-21), the system with dissipators presents a rather sine-like first-mode "wave", altered by the peaks due to impact (Figure 6-20). Thanks to this characteristic, the impact peaks do not coincide with the maximum amplitude of the main wave but rather take place when the main wave is close to the zero-line, leading to a diminished effect in the total response. The likely reasons of this characteristic shape are discussed later, in section 6.6.10.

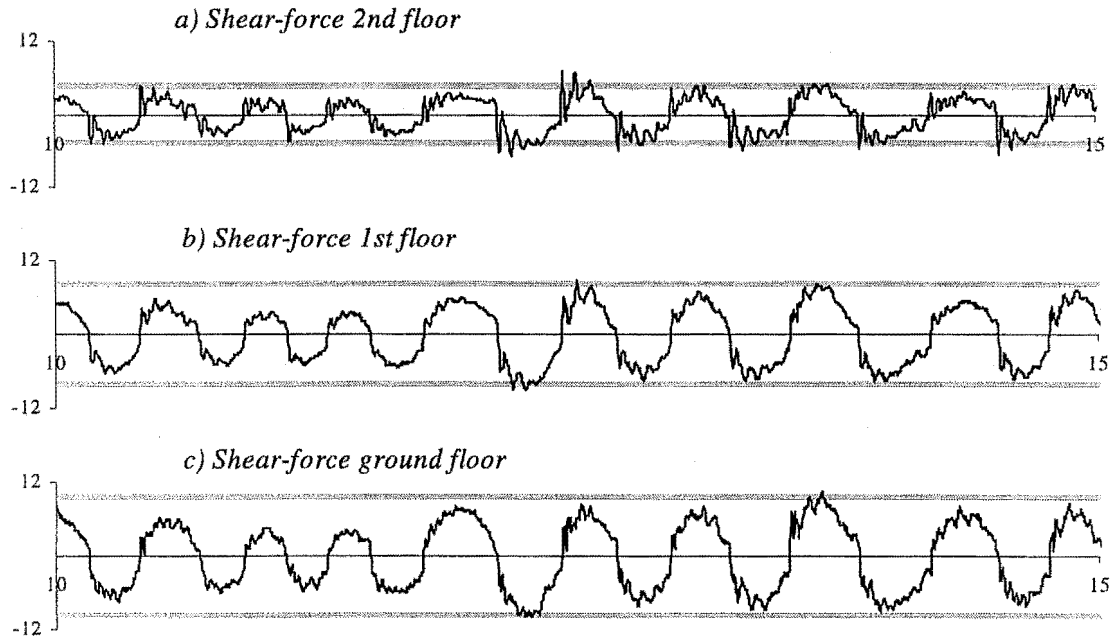

Figure 6-20 Effect of impact on interstorey shear forces in Run 41 (wall with dissipators)

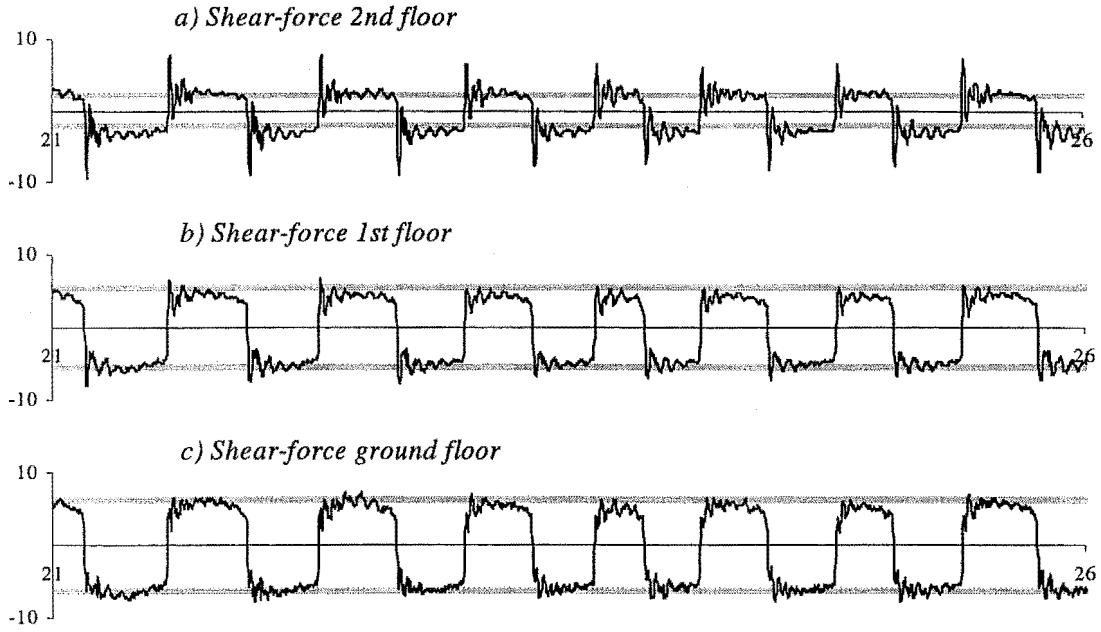

Figure 6-21 Effect of impact on interstorey shear forces in Run 51 (wall without dissipators)

6.6.6 Force-Displacement Pattern

Before evaluating the observed force-displacement pattern, a brief discussion about the expected pattern is made in this section. Assuming a perfect elasto-plastic dissipator, a perfectly rigid wall and ignoring the stiffness of the other structural elements, the expected force-displacement pattern can be obtained from the concepts developed in chapter 3. There are three cases that one can attempt to predict: 1) wall without disspators; 2) wall with new dissipators; and 3) wall with dissipators with residual deformation. The envelopes of the force-displacement plot for these cases would be:

Wall without dissipators:

$$V_{eff} = +\alpha_{eff} W \quad \text{when } \Delta_{eff} \geq 0$$
$$V_{eff} = -\alpha_{eff} W \quad \text{when } \Delta_{eff} \leq 0 \qquad \text{(Eq. 5.3)}$$

Wall with new dissipators

$$V_{eff} = \alpha_{eff}\left(W + 4k_d \alpha_{eff} \Delta_{eff}\right) \leq \alpha_{eff}\left(W + 2F_y\right) \quad \text{when } \Delta_{eff} \geq 0$$
$$V_{eff} = \alpha_{eff}\left(-W + 4k_d \alpha_{eff} \Delta_{eff}\right) \geq -\alpha_{eff}\left(W + 2F_y\right) \quad \text{when } \Delta_{eff} \leq 0 \qquad \text{(Eq. 5.4)}$$

Wall with dissipators with residual deformation

$$V_{eff} = \alpha_{eff}\left(W_{reduced} + 4k_d \alpha_{eff} \Delta_{eff}\right) \leq \alpha_{eff}\left(W + 2F_y\right) \quad \text{when } \Delta_{eff} \geq 0$$
$$V_{eff} = \alpha_{eff}\left(-W_{reduced} + 4k_d \alpha_{eff} \Delta_{eff}\right) \geq -\alpha_{eff}\left(W + 2F_y\right) \quad \text{when } \Delta_{eff} \leq 0 \qquad \text{(Eq. 5.5)}$$

where $W_{reduced} = W - 2F_y$

In the equations above, the term $\alpha_{eff}\left(4k_d\alpha_{eff}\right)$ can be regarded as the stiffness of the system due to the dissipators. Therefore, a cycle can be completed using this stiffness to model the travelling of the structure back to the origin. The definition of the stiffness however is only valid until the dissipators yield in the other direction. The range that is expected to be modelled is therefore $4F_y\alpha_{eff}$. The equations are displayed in Figure 6-22.

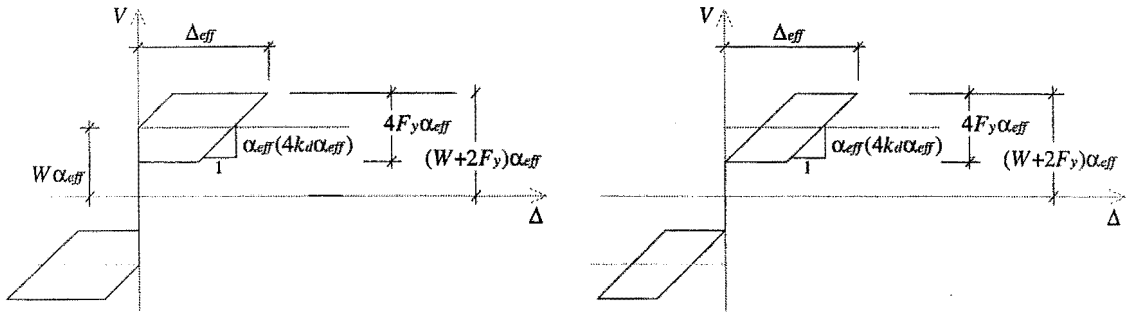

a) Wall with new dissipators *b) Wall with dissipators with residual deformation*

Figure 6-22 Force-displacement pattern expected in the system

The force-displacement pattern observed in the system is defined by the same circumstances described in the previous section dealing with the observed base shear. Figures representing the load-displacement pattern of the system for the same cases are presented here. The first plots (Figure 6-23) correspond to the runs when the dissipators underwent their first plastic deformation. Run 14 for the first set of dissipators and Run 38 for the second set of dissipators. As it was discussed in the previous section, in the initial runs, structural elements other than the rocking wall contributed significantly to the initial strength and stiffness of the system. That can be observed in Run 14 (Figure 6-23a). The dissipators were barely yielded and the structure offered a larger than expected strength and stiffness. On then other hand, by the time Run 38 was conducted, the hinges in the slab were well developed and therefore the base shear follows the plateau corresponding to the capacity of the system.

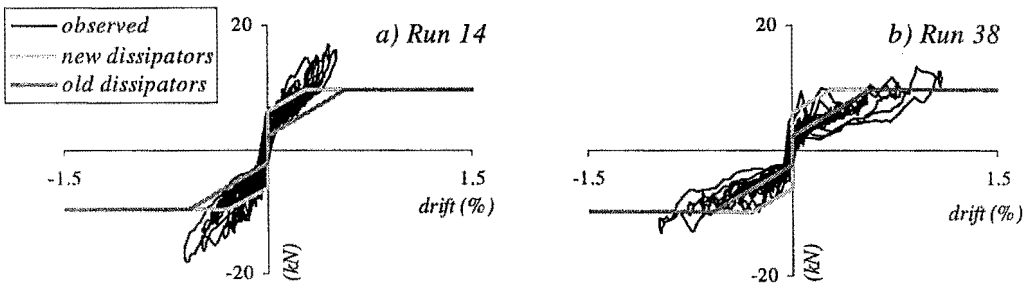

Figure 6-23 Observed and expected force-displacement pattern in model with new dissipators

In Figure 6-23, two envelopes are plotted because the envelope corresponding to the new dissipator (*new dissipators*) is expected to occur only once. Once the dissipator has undergone plastic deformation, the expected envelope would be the corresponding to dissipators with residual deformation (*old dissipators*). This is clear in Run 38 (Figure 6-23b). However, if one limits the plot only to the cycle when the dissipators first yielded, a good agreement is observed with the envelope expected for new dissipators (Figure 6-24).

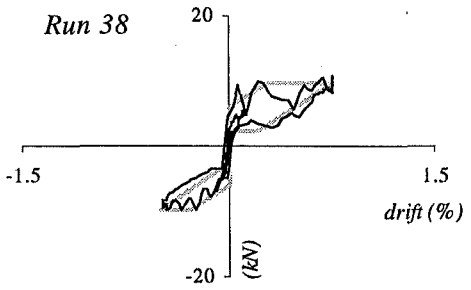

Figure 6-24 First yield cycle compared with expected one

Figure 6-25 shows the observed force-displacement for two cases in which the dissipators have already yielded. It compares very well with the expected envelope. However, as it was discussed in the previous section, large drifts seem to trigger a stiffening mechanism in the structure. The triggering of the stiffening mechanism was found to be around a drift of 1.10% as it can be observed again in Figure 6-25b.

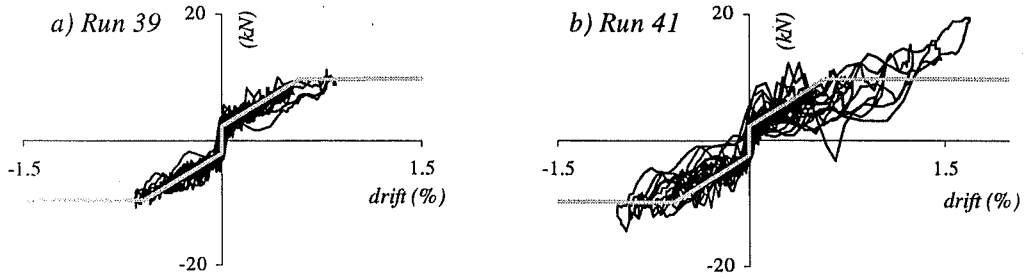

Figure 6-25 Observed and expected force-displacement pattern in model with old dissipators

Finally, Figure 6-26 shows the observed pattern when the wall was tested without dissipators. Again a good match is observed with the theoretical envelope until the structure reaches around 1.10% drift. Then the force starts to increase, confirming the existence of a stiffening mechanism in the system beyond that drift level.

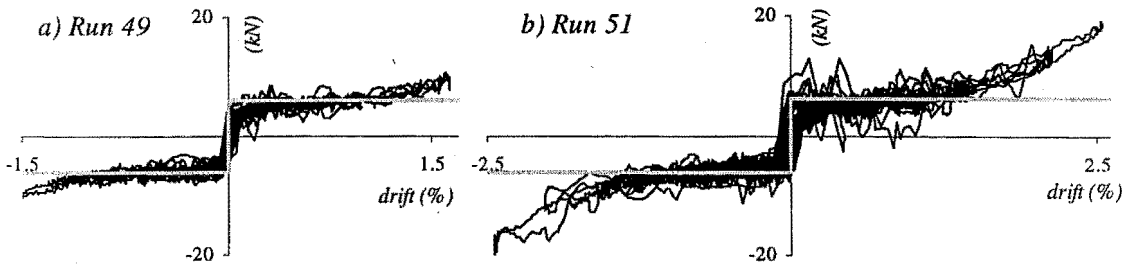

Figure 6-26 Observed and expected force-displacement pattern in model without dissipators

It was interesting to observed that in some runs there were large peaks in the base shear, that seem to be a combination of the large accelerations in the shake table and the contribution of higher modes of oscillation. It is significantly large in the Sylmar runs (near fault type ground motion). The response to this type of events should be carefully observed in future tests, in which the ground motions are reproduced properly. As commented earlier, in our case, the shake table produced very different ground motions (and therefore very different scenarios) for these cases.

6.6.7 Triggering of Rocking

The force-displacement plots in the previous section can also be used to observe at which level of demand rocking is triggered. In the system with dissipators, there were two conditions for which predictions were made. The wall with new dissipators would start rocking when V = 6.1kN and the wall with dissipators-with-residual-deformation would start rocking when V = 2.3kN. This coincides reasonably well with what is observed in previous sections (Figure 6-23, Figure 6-24 and Figure 6-25). When the dissipators are removed, the expected triggering of rocking also occurs when V = 6.1kN (Figure 6-26).

6.6.8 Horizontal Absolute Floor Accelerations

The basic absolute horizontal accelerations were calculated using the equations developed in chapter 3 and compared with the observed absolute floor-accelerations. Figure 6-27 shows the typical observed behaviour. First, note that the intended peak table-acceleration for run 41 was 0.5g, however, the distortion of the signal by the shake-table led to table-accelerations well above that value. In these conditions, it is difficult to draw a valid conclusion regarding the maximum absolute-acceleration that should be expected in the system. Nevertheless, it is clear that the absolute accelerations oscillate about the plateau defined by the basic expected acceleration, but reach its larger peaks due to the stiffening and strengthening action of the system, rather than to the impact of the wall against the foundation.

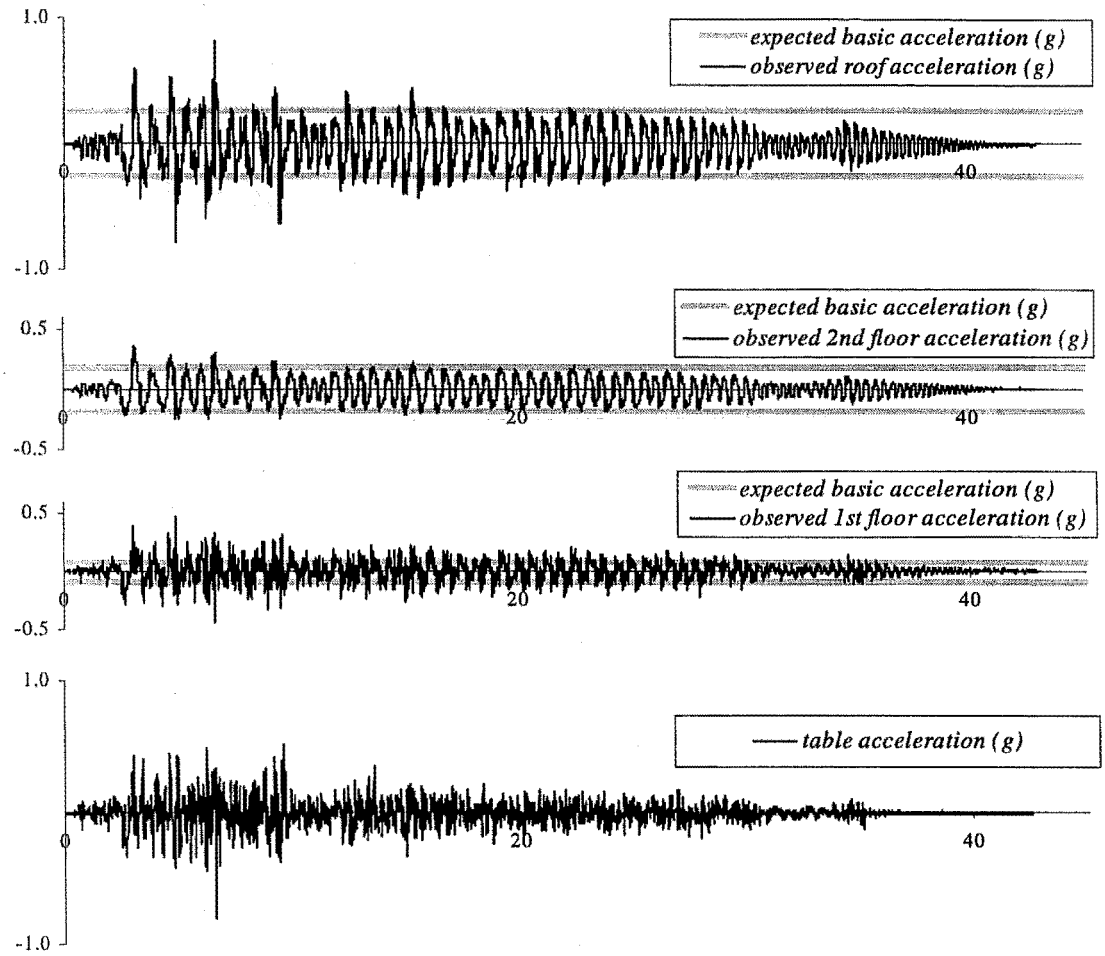

Figure 6-27 Observed absolute floor accelerations (Run 41)

To observe better the effects of impact in the absolute accelerations of the system, the response of the system at free oscillation was studied. Figure 6-28 compares the observed roof accelerations in the system *a*) without and *b*) with dissipators. In both cases the system was set into free oscillation by a single initial impulse. From those plots, it can be concluded that the dissipators reduce significantly the effect of the impact into the system. Secondly, the magnitude of the peak accelerations is directly proportional to the initial uplift in every cycle. And thirdly, unlike the wall without dissipators, the rocking in the system without dissipators occurs at different "levels", with lowered amplitudes as the drift diminishes.

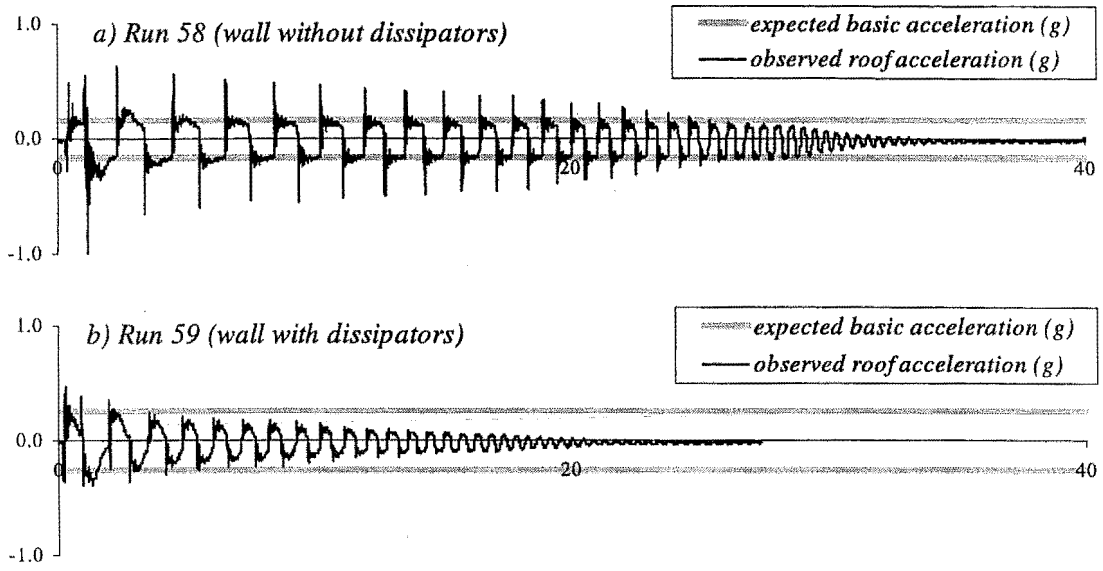

Figure 6-28 Acceleration peaks due to impact observed in free-oscillation runs

The effects of impact are also attenuated due to the softening effect of the dissipators in the main "wave" of the response. It was already discussed earlier in section 6.6.5 and can be appreciated in the details of the absolute acceleration time-histories depicted below in Figure 6-29.

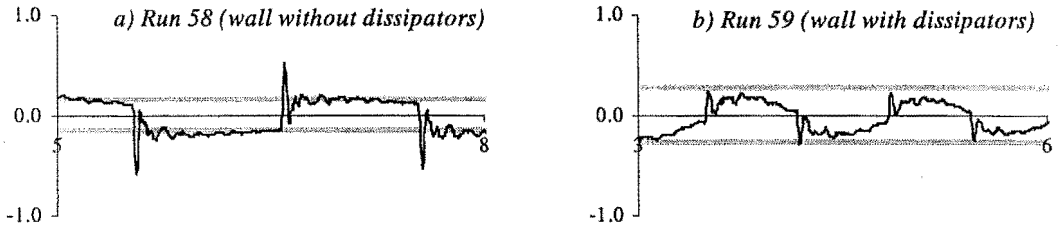

Figure 6-29 Detail of acceleration peaks due to impact in free-oscillation runs

6.6.9 Vertical Accelerations

Only the impact actions had a significant effect in the vertical accelerations, and they increased with increased drift. The dissipators did not seem to cause any reduction in the observed peak vertical accelerations. Furthermore, in general, for the same level of drift, the lower peak vertical accelerations were observed in the specimen when it did not have the dissipators.

The vertical accelerations were measured with accelerometers attached to the rocking wall and were observed to have a frequency of the order of 50 Hz. It is not possible to make any conclusions on the strength demand induced in the elements as the vertical acceleration measured in the wall is not

necessarily the vertical acceleration felt by the main mass, located in the slabs, especially with the relatively large flexibility of the slabs in the transverse direction.

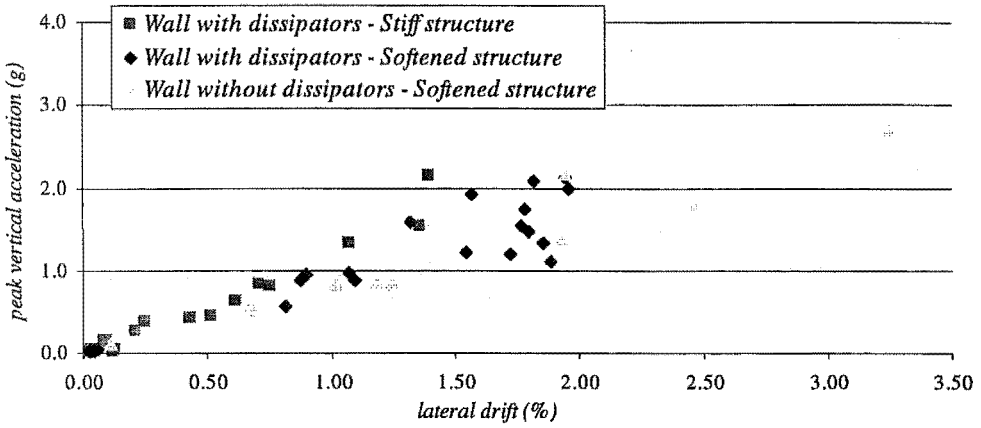

Figure 6-30 Observed peak vertical acceleration versus drift

6.6.10 Impact Effects

Through the previous sections of this chapter (sections 6.6.5 and 6.6.8), a number of comments have been made regarding the effects of impact in any particular performance parameter. The main finding was that impact does not seem to be a problem in terms of strength demand, especially if the rocking-wall has the dissipators attached, but it may be a problem in terms of the absolute accelerations generated in the wall.

In the earlier sections, it was found that, in general, the dissipators reduced the effects of impact in the response of the structure. It was mainly due to two reasons. First, the dissipators reduce the peak values (Figure 6-20 and Figure 6-21), and secondly the dissipators soften the shape of the first-mode "wave" in the response of the structure. The softening causes the impact-peaks to take place when the first-mode "wave" has a value rather close to zero (Figure 6-29). The reason of the "softening" is that the impact process starts before the dissipators in the opposite corner develop their full capacity. Actually, when rocking starts, the dissipators are pushing the wall upwards. Then, it takes a while until the dissipators are deformed far enough to develop their full design capacity, F_y, in the opposite direction and make the rocking wall reach the basic base shear, V. How long the dissipators take in this process depends on their initial stiffness. Very stiff dissipators probably would not produce a significant "softening" of the main wave. On the other hand, significant softening should be expected in "soft" dissipators such as the ones that were used in the dynamic tests.

The impact of the wall against the foundation excited higher modes of vibration in the structure, rather than the first mode, which was the assumption made for the definition of the impact factor, f_{imp}. For

this reason, impact does not have a significant effect in the total base shear observed in the structure. If the mode was able to be identified correctly, the impact energy, defined in Chapter 3, could have been equated to the strain energy stored in that mode. Then, the deformations and forces could have been derived. The problem is that it would be very difficult to identify, for sure, which mode would be the most excited, as it is not only dependant on the characteristics of the main structure but also on the characteristics of the impacting region.

It appears that since impact affects the higher modes of the structure defined in chapter 3, the impact factor, f_{imp}, would produce a conservative estimation of the total base-shear. The softening of the main wave also would help here. On the other hand, the impact factor, f_{imp}, could underestimate the peak absolute accelerations and the peak inter-storey shear-forces. This would need to be tested in the future. The author recommends the construction and testing of a rocking system which avoids the existence of the stiffening mechanism described in this chapter to observe the real effects of impact on the response.

6.6.11 Total Equivalent Viscous Damping

In order to calculate the equivalent viscous damping of the system the structure was set into free oscillation with an initial lateral impulse. Then, the decaying shape of the oscillation was observed. Figure 6-31 shows the roof displacement recorded for the wall with and without dissipators.

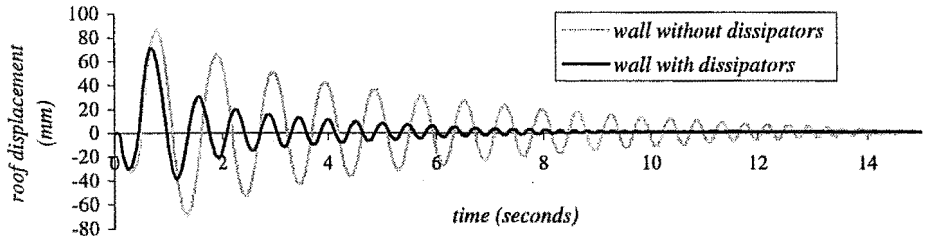

Figure 6-31 Observed free oscillation of the specimen with and without dissipators

As discussed in Chapter 3, the equivalent viscous damping (EVD) would depend on the extent of the lateral drift and, therefore, EVD values were calculated for every cycle of the decaying shape of the oscillation. The results are presented in Figure 6-32. First, the results show that equivalent viscous damping (EVD) due to impact (ξ_i) and other mechanisms intrinsic to the structure (ξ_o) were overestimated. They were taken as 2% and 3% respectively. In the tests, it was found that their joint value averages 2% to 3%, exceeding 4% only for large drifts (above 1.7% drift).

It seems that the EVD due to the dissipators, ξ_h, was also overestimated. Hindsight at the definition of ξ_h shows that the area enclosed in the hysteretic cycle was mirrored in the second half-cycle (Figure 3-12). In reality, the second half-cycle encloses a smaller area and therefore a diminution of the EVD should have been expected. The correction factor C_3, defined in section 3.5.3, will be used to account for this adjustment.

To get a better prediction of the expected total EVD of the system, some corrections need to be done. First, the term $(\xi_i + \xi_o)$ should be diminished and ξ_h should be reduced to account for the smaller hysteretic area. When $(\xi_i + \xi_o)$ is set to be 3% and ξ_h is reduced by the experimental correction factor $C_3 = 0.85$, the resultant EVD matches well the observed EVD values (Figure 6-32).

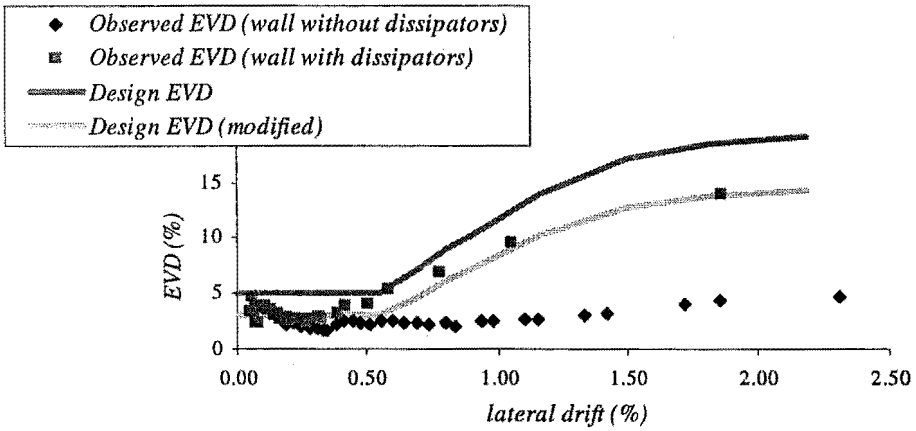

Figure 6-32 Equivalent viscous damping (EVD) of the system

The definition of the equivalent-viscous-damping though may be controversial when one has a system like this, where the total EVD changes rapidly with the drift. Different values of EVD can be derived depending on the number of cycles that one takes from the decaying shape of the free oscillation. Actually, in the case of this specimen, if one takes only half a cycle, the so-calculated maximum observed damping almost matches the predicted one. On the other hand, two or three cycles would lead to values even smaller than the observed in Figure 6-32. The author recommends further study in this subject.

6.6.12 Damage in Structural Elements

After 60 runs the only damage observed was in the slabs, mainly in the ones that had a shallow groove or did not have the groove along the hinge (Figure 6-33). The damage was limited to the concrete in the hinge regions, without affecting the loading capacity of the slab. The slabs were able to carry the loads without any problem over all runs, and the specimen is being kept for future testing. The rest of the structure, including the foundation beam did not show any sign of damage.

The largest deformation observed in the diagonal of any of the masonry panels was 0.67 mm, measured in the ground floor. This deformation amount only to a unit deformation $\varepsilon_m = 0.0005$, which is a fourth of the minimum value expected for ε'_m. In chapter 2, a range between 0.002 and 0.005 was found to be recommended for ε'_m. This value shows that the masonry was responding well within its elastic region.

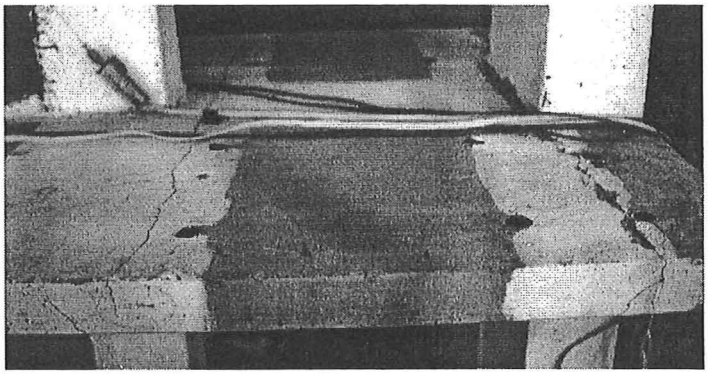

a) Slab without grooves

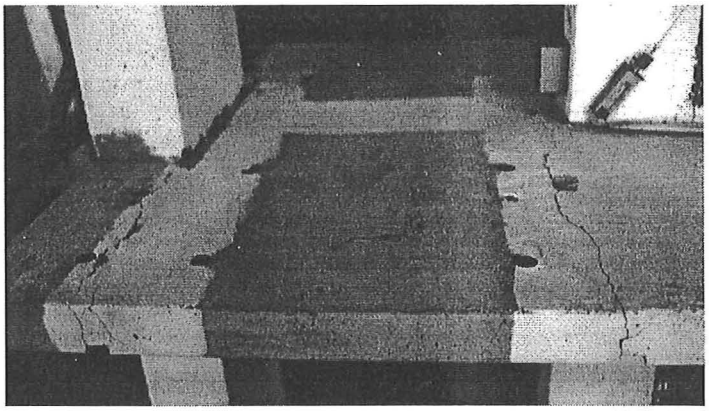

b) Slab with shallow grooves

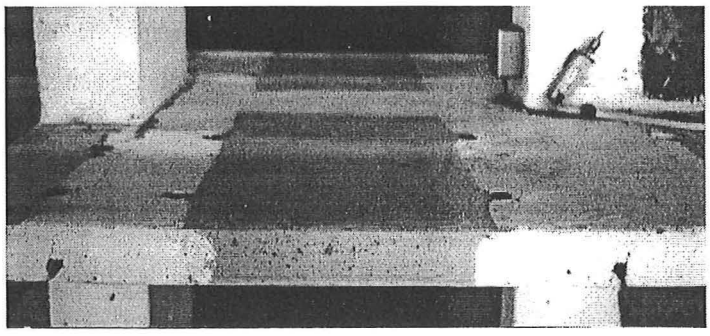

c) Slab with deep grooves

Figure 6-33 Damage observed in slabs

Apart from their expected residual stress, the dissipators were also in good condition and ready to be used again. The residual stress in the dissipators occurs after the dissipators yield for the first time, and then they are yielded back to its original position by the weight transferred by the rocking wall. This residual stress does not reflect in any permanent deformation in the system as a whole.

6.6.13 Aftershocks Performance

The specimen was subjected to 60 runs in the shake table, 31 of them exceeding 0.3g peak table acceleration. In three extreme cases the structure reached more than 2% drift and in one of them even reached 3.2% lateral drift. And after that, its design-capacity was not diminished. The structure did not have any permanent deformation. This result seems to prove that, if a system with rocking walls is designed with an adequate initial capacity, aftershocks should not be a problem.

6.7 Assessment of the Performance of the Dissipators

The two sets of dissipators that were used did not show any sign of degradation after the tests. The first set was later modified to serve as lateral stoppers when it was decided to observe the performance of the wall without dissipators.

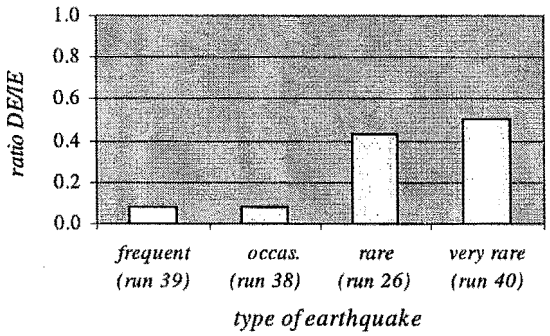

Figure 6-34 Typical ratio Dissipators-Hysteretic-Energy / Input-Energy (DE/IE)

The tests confirmed the energy dissipation capacity of the dissipators; and that it is reflected in the total EVD of the system. As expected, the energy dissipation capacity of the dissipators is more significant during large events because of their relative low initial stiffness (Figure 6-34).

The effects of the dissipators in the seismic performance were obscured at some extent by the existence of the stiffening effect of the slab-beams. Figure 6-35 *a*) and *b*) shows that, mainly thanks to this stiffening mechanism, the performance of the structure without dissipators is not too different to the performance of the system with dissipators. Although at first sight it may look like the stiffening mechanism helps to improve the performance of the structure, there are two problems with it. First, this mechanism is not predictable and second, even if it was predictable, it causes undesirably large

absolute-floor-accelerations (and therefore inertia-forces) that counter some of the features that made the rocking-system attractive in the first place (section 3.4.1). In the tests, it was clear, however, that as the hinges weakened in the beam-slabs, the performance of the specimen did not deteriorate and was able to match the expected drift. Later, in section 7.3.2, a numerical analysis will show that an ideal fully articulated model with dissipators would have matched the expected drifts.

The beneficial effects of the dissipators are clearly observed in other parameters. Figure 6-35 *c*) and *d*) shows the number of half-cycles that the structure undergoes with and without dissipators when subjected to similar ground motions. The number of cycles is a clear sign of the speed at which the system can dissipate the incoming energy.

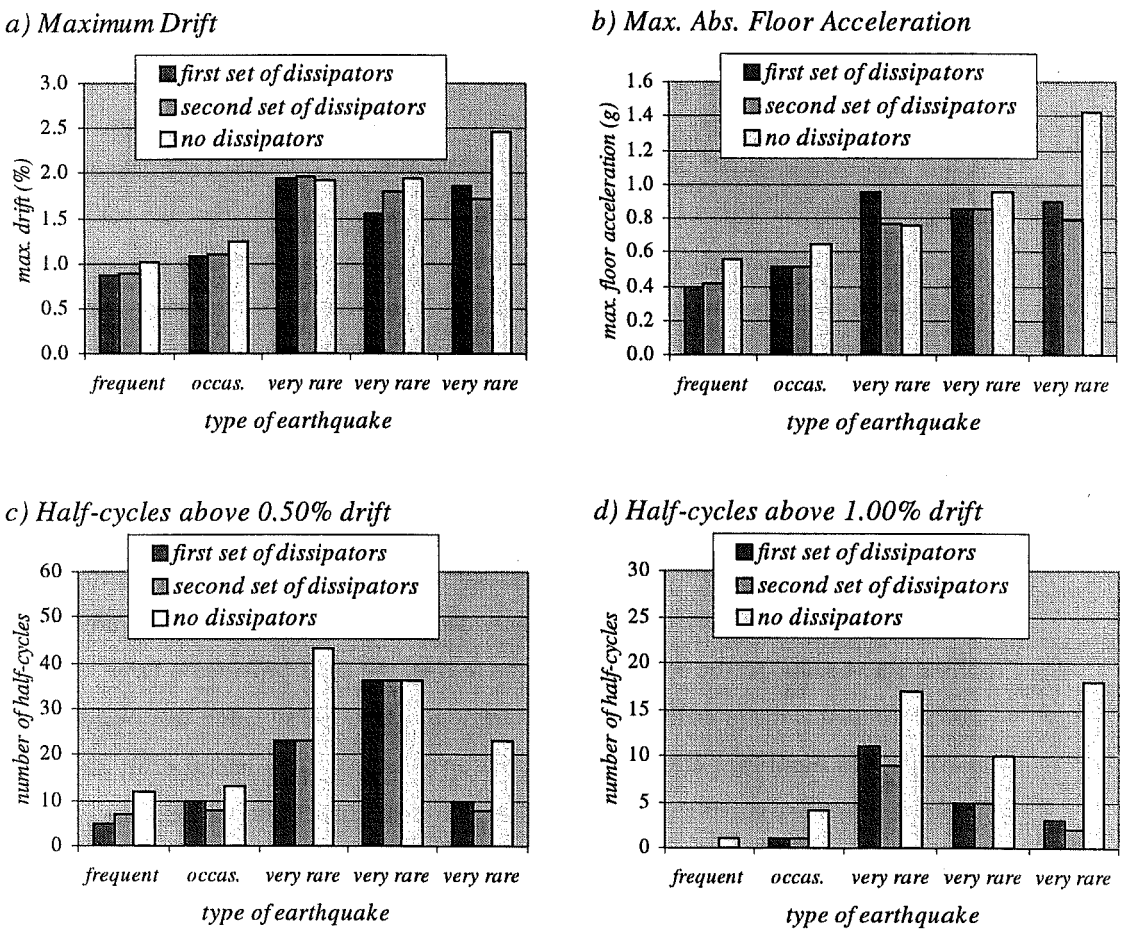

Figure 6-35 Comparison of performance of the system with and without dissipators

6.8 Conclusions

- The shake table needs to be upgraded. It cannot handle high frequencies properly and is not able to deliver its specified velocity capacity of 1000 mm/s. The improper handling of high frequencies led to very noisy signals that needed to be analysed in the frequency domain to confirm that the demand was reasonably equivalent to the intended one. The limited velocity capacity (around 250 mm/s) meant that some of the ground motions could not be reproduced in their most demanding segments, limiting the outcome of the tests.

- The definition of the combined rotational inertia, $I_{o\,comb}$, which extends the concept of a single-rocking-wall to a rocking-wall-dragging-additional-mass was validated by the dynamic tests.

- Dissipators with residual stress, i.e. dissipators that had already yielded, have a softening effect in the initial stiffness of the system. However, this does not seem to substantially affect the performance of the structure

- There was no significant damage in the structure after the 60 runs. The structure retained its design capacity throughout the test program. The only observable damage was in the hinge-regions in the slabs, especially in the ones that did not have the groove along the hinge. The hinges with the deep built-in hinge showed only minor cracks. Nevertheless, in all cases, the vertical load capacity of the slabs was preserved thanks to the detailing provided in the hinges.

- The system matched the expected performance only partially. Although damage was avoided and the observed drifts where within the expected range, larger than expected absolute accelerations (and therefore larger than expected inertial forces) were observed. It is believed that the main reason was that the model failed to exclude any significant effects of structural elements other than the rocking wall, mainly due to the lack of the built-in groove in 4 hinges of the slab-beams. At the early stage of the testing, the slabs provided a large initial strength and stiffness that distorted the expected behaviour. Later, this situation was overcome but only partially. No significant effect was observed up to around 1.1% lateral drift; however, as the drift increased beyond this value, the system was strengthened and stiffened again by the slab-beams, countering the expected behaviour. The influence of high modes in the response of the building also appears to grow with increased intensity.

- The tests proved the ability of the dissipators to provide the system with a prescribed energy dissipation capacity. The experimental reduction factor, C_3, was found to be of the order of 0.85. It is believed that this correction is mainly due to the lack of symmetry of the areas of the hysteretic loops in the definition of the EVD of the system due to the dissipators, as defined in Chapter 3.

Chapter 7 Computational Modelling and Investigation of Alternative Conditions of the System

7.1 Introduction

An inelastic dynamic numerical analysis of the proposed structure is undertaken here. The preceding experimental results are used to verify the reliability of the numerical model as well as to calibrate some parameters that were defined rather arbitrarily in the preliminary numerical modelling of the structure. Previous numerical models have been developed to model rocking walls of different sorts such as reinforced masonry shear walls with unbonded reinforcement (Madan et al., 1996) or prestressed concrete rocking walls (Priestley et al., 1999), and they have been compared successfully with experimental results. In neither case, however, the experimental results were from dynamic tests, forcing to make assumptions in aspects such as damping and impact of the structure against the foundation. The numerical model described in this chapter tries to model comprehensively what was observed in the dynamic tests, including damping and impact. First, an ideal structure is modelled. Then, after being compared with the experimental results, modifications are made to try to match the observed behaviour. Four basic numerical models were used, each of them representing different conditions of the specimen. The complete input files of these models can be found in Appendix B.

7.2 The Numerical Model

The software RUAUMOKO (Carr, 2000) was used to analyse numerically the structure. Various member types and hysteresis rules, built-in into the software, were used to model the different structural elements. RUAUMOKO also provides different options for the modelling of masses and damping of the structure, which were helpful in the definition of some particular characteristics of this system. There was not much trouble in the modelling of most of the superstructure as a rather elastic behaviour is expected there. Only the modelling of the strengthening-stiffening action due to the non-perfect hinges in the slab-beams demanded a painstaking calibration to be able to reasonably match the experimental results. More troublesome however was the modelling of the impact of the base of the wall against the foundation. A "contact" hysteretic rule was expected to model this part of the system. For the deformation-range that was observed in the dynamic tests, the hysteretic-dissipators can also be represented by a hysteretic-rule built-in in RUAUMOKO. All these and other parameters

chosen for the numerical model are discussed in deeper detail below. Figure 7-1 provides an overview of the main characteristics of the numerical model.

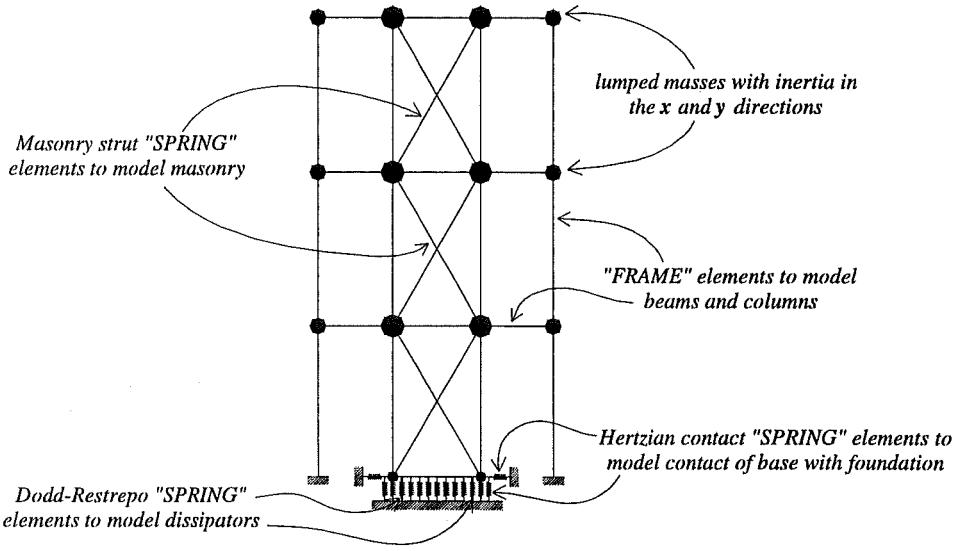

Figure 7-1 General characteristics of the numerical model to be used in the software RUAUMOKO

7.2.1 Columns and Beams

All concrete beams and columns were modelled as "FRAME" members (Carr, 2000). The beams that connect the rocking wall to the exterior columns were modelled as perfectly pinned at both ends. These elements were later combined with "beam-stiffeners" to reproduce their strengthening and stiffening action observed in the dynamic tests. The remaining frame elements, i.e. exterior columns and confining beams and columns, were modelled as built-in to the joints, but able to develop hinges at both ends. The plastic hinges were modelled using Takeda's Modified hysteretic rule (Carr, 2000). The parameters for the hysteresis rule were chosen close to the low limit suggested by Carr (2000). There was no need of a deep assessment in the definition of the parameters of these elements as they were expected to behave within their elastic range. This assumption was later confirmed when the results of the numerical modelling did not show any plastic hinge developed in these elements. The exterior columns of the first floor were initially modelled as pinned at the base but RUAUMOKO rendered a singular stiffness matrix. For that reason these columns were also modelled as built-in to the joints at both ends but, with its rather low strength capacity at the base, they effectively behaved as pinned at the base.

7.2.2 Beam-Stiffeners

Beam-stiffeners were used to reproduce the strengthening-stiffening action of the slab-beams observed in the dynamic tests. In the numerical model, the beam-stiffeners were placed in parallel with the beam-elements that connect the rocking wall with the exterior columns. The beam-stiffeners were used

after failing to reproduce the observed response with an ideal model that featured perfectly pinned beams connecting the rocking wall to the exterior columns. The type of model that was used was the Non-linear Elastic Power Rule (Carr, 2000). This rule features an exponential stiffness, allowing for the definition of a low stiffness for the initial segment of the deformation and larger stiffness when the deformation of the member increases. The definition of the parameters of the hysteresis rule had to be made calibrating the numerical results against the experimental data. This was perhaps the most laborious part of the numerical modelling. It was not possible to set a unique definition of these elements for all the runs, as the initial stiffness of the stiffeners had to be modified for every run to be able to match the observed results. This is discussed later in section 7.3.2.

7.2.3 Masonry Infills

The masonry infills were modelled using two diagonal struts per infill (Figure 7-1). "SPRING" members (Carr, 2000) following Crisafullli's hysteresis rule were used for that purpose (Crisafulli, 1997; Carr, 2000). In the definition of the parameters of the hysteresis rule, those parameters related to the strength of the masonry and the ones related to the infill geometry were drawn from the results in the preliminary testing of masonry (Chapter 5) and the geometrical characteristics of the masonry panel, respectively. The remaining values were within the range suggested by Crisafulli (1997). As with the frame elements, the masonry was expected to behave rather elastically and, therefore, the definition of the parameters that determine Crisafulli's hysteretic rule was not critical.

7.2.4 Dissipators

The dissipators were modelled using the Dodd-Restrepo steel hysteresis rule (Dodd and Restrepo, 1995; Carr, 2000). This hysteretic rule reproduces well the hysteretic response of the dissipators up to the maximum levels of deformation expected in the tests. In order to model the initial residual stress in the system a sine pulse, large enough to yield the dissipators, is to be run before every selected ground-motion time-history. Fifteen seconds of free oscillation are allowed after the pulse and before the selected time-history ground motion to allow the system to dissipate the initial energy.

7.2.5 Rocking at the Base

The modelling of the rocking at the base was made using a number of "SPRING" members (Figure 7-1) with a Hertzian Contact Spring hysteresis rule (Davis, 1992; Carr, 2000). This hysteresis rule is similar to the Non-linear Elastic Power rule described above (section 7.2.2) but features a gap that allows one to model compression only elements. The stiffness of the contact elements was defined approximately as the one expected for a concrete strut of $0.06m^2$ section and 0.60m length. The definition of the rest of the parameters was made contrasting the output impact actions with the observed ones in the dynamic tests.

7.2.6 Damping

The literature review showed that the decaying shape of the oscillation of rocking walls was experimentally found to be equivalent to the observed in a fixed-base SDOF oscillator with 4% of EVD (section 3.2.3). This can be misleading in the numerical modelling since the dissipation of the energy of the system is through mechanisms not necessarily related to the first mode of vibration of the wall (section 3.2.3). This is particularly critical if a damping matrix related to the initial stiffness of the structure is used. That is the type of damping matrix that was used here for the numerical modelling and that is one reason why it was decided to use a very low EVD for the first mode of oscillation. More details of the definition of the damping are described next.

RUAMOKO features an option in which the user can define the damping at every mode. This option was selected because of the interest in controlling the level of damping in the first mode and in the mode corresponding to the impact of the wall against the foundation. It was expected that the first mode in a rocking wall, once rocking is triggered, does not offer any significant damping and therefore it was defined as very low. Initially it was defined as 1% but later it was necessary to reduce it to 0% to match the observed results. It was expected that the higher modes, on the other hand, would still dissipate energy at a usual rate. Hence the damping for the higher modes was chosen as 3%. Note that this also affects the modes that account for the vertical vibration of the wall and the contact elements, which is expected to model at some extent the radiation of energy to the foundation at impact.

7.2.7 Time Step

The rocking on the base was very sensitive to the chosen time-step. The highest frequency that one may be interested in, is the one generated at the contact elements due to impact, which was expected to be in the order of 100 Hz (RUAUMOKO rendered a frequency of 40 Hz for this mode). In order to capture this frequency, time steps shorter than 0.0025 seconds were initially used for the time-history analysis. After the first runs it was observed that RUAUMOKO needed a smaller time-step to model the different hysteresis rules that where being used, particularly the ones whose stiffness is defined exponentially. It was necessary to reduce the time step to 0.000020 seconds to get the model work properly.

7.3 Numerical Simulations of the Dynamic Tests

In the preliminary modelling of the specimen an ideal numerical model was developed. This ideal model had the slabs pinned at both ends. As it was discussed earlier in Chapter 6, the specimen was actually built with different degrees of hinging in the slabs. The experiments demonstrated that the slab-beams have a significant effect in the response of the structure, inducing large absolute accelerations and causing larger inertial forces due to the unexpected larger stiffness of the system.

The other issue discussed in Chapter 6 was the difficulty in assessing the contribution of these elements in the response of the structure. The numerical model used in this chapter will try to model the response of the structure at the stage were the hinges have developed up to a relatively stable condition. Runs 38 and runs 40 and 51 are the main references. At this stage of the testing process the slabs have a strengthening and stiffening effect in the system only when it exceeds about 1.1% drift.

7.3.1 Comparing the ideal model with the observed results

In Figure 7-2, runs 38, 40 and 51 are compared with the output of the ideal numerical model, which had the ideal conditions described above. The ideal model is called ModelPH and, in the case when the dissipators are removed, the model is called ModelPHND.

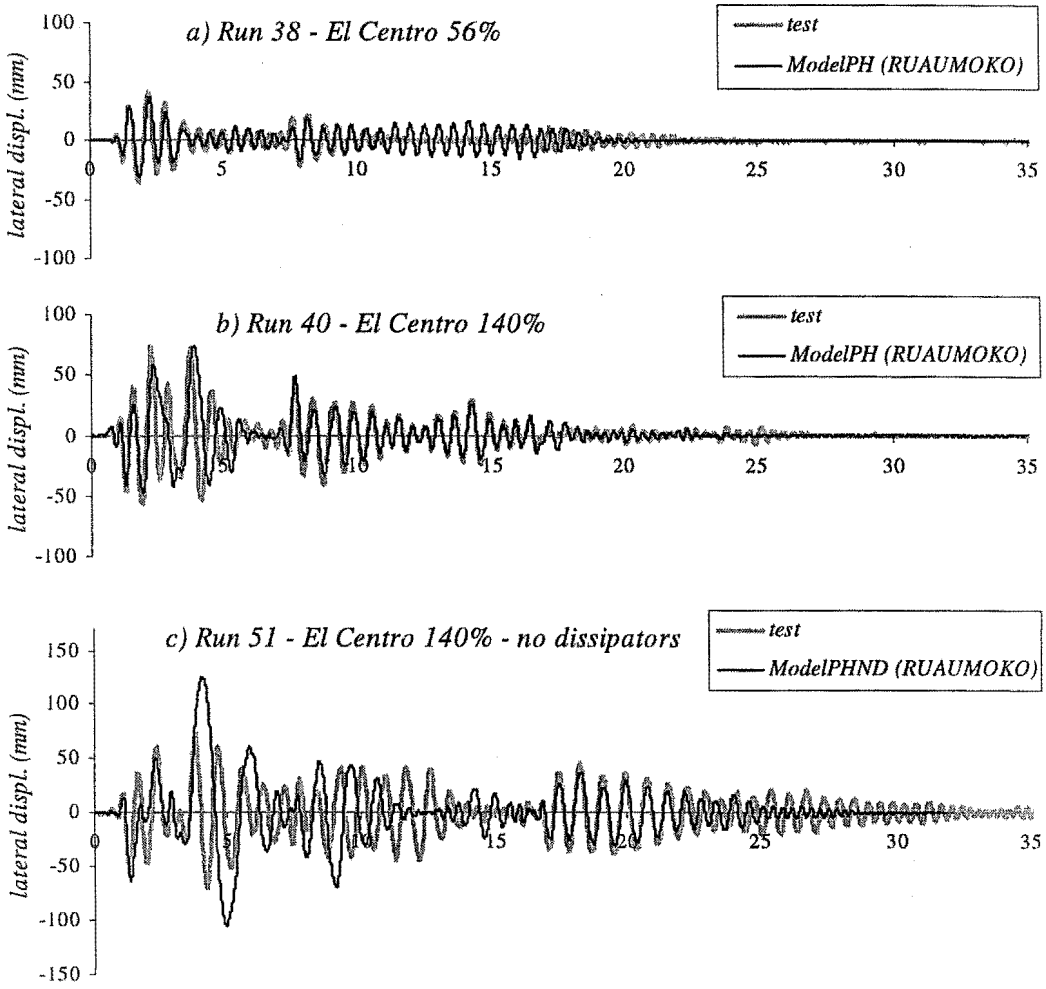

Figure 7-2 Calculated roof-displacement using numerical model with perfect hinges

In run 38, where the specimen was deformed only slightly above the critical drift of 1.1%, the numerical analysis is in good agreement with the observed roof-displacement. Even though there is

good agreement in the modelling of most of the time-length of Run 40, significant discrepancies are observed for large lateral displacements. That occurs in the time-segment from two to five seconds. The discrepancy arises because the ideal numerical model is more flexible than the real specimen at large deformations. The presence of a strengthening and stiffening mechanism is even more obvious when the output of the ideal numerical model is compared with the observed response in Run 50, where the specimen did not have dissipators.

The ideal model ModelPH can not reproduce the large peaks of the observed base-shear demand in the dynamic tests either. Figure 7-3 shows that the base-shear in the numerical model is rather limited by the expected basic design base-shear, with the peaks coinciding with the impact of the rocking wall against the foundation.

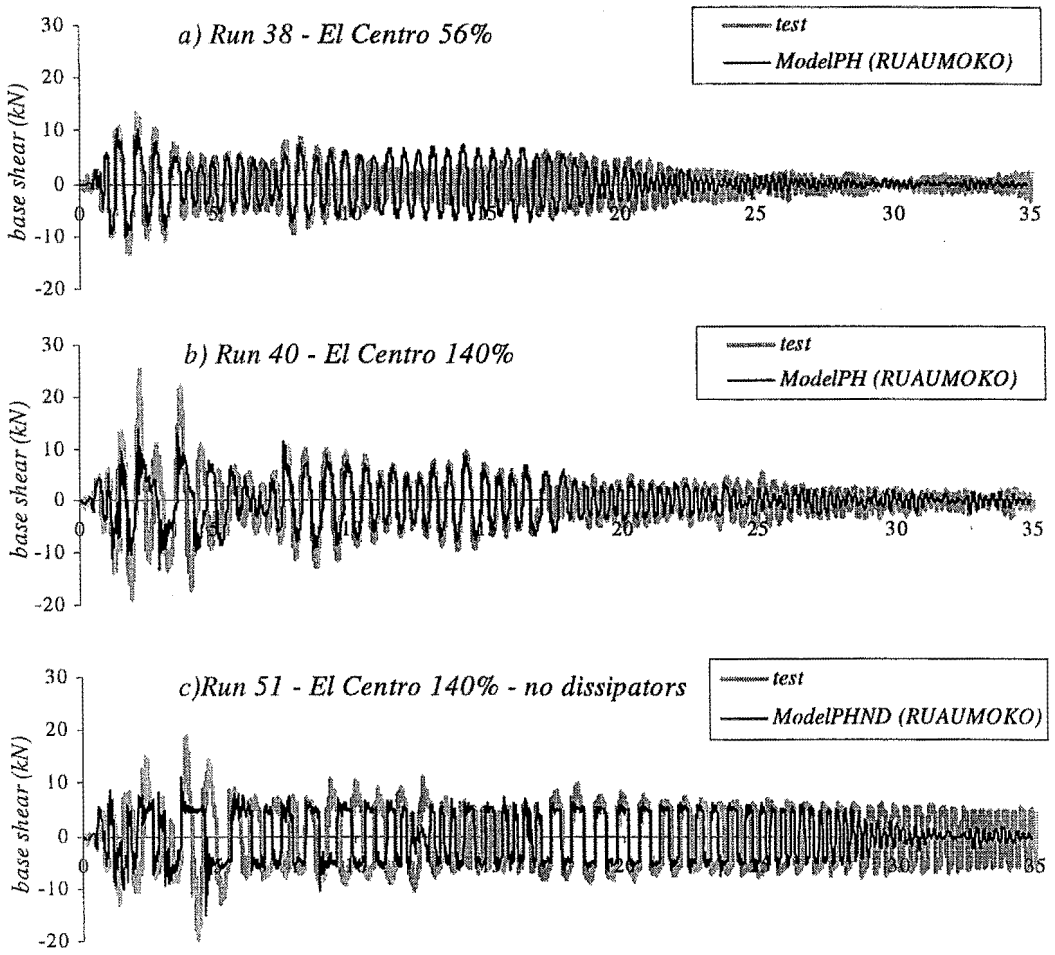

Figure 7-3 Calculated base-shear using numerical model with perfect hinges

7.3.2 Matching the observed results

In Chapter 6, it was mentioned that the strengthening-stiffening mechanism observed in the specimen was most likely caused by the slab-beams. In order to reproduce this effect, additional members were created in the numerical model. They were called beam-stiffeners (section 7.2.2). These stiffeners were placed in parallel with the perfectly pinned beams. The stiffeners were modelled to have a low stiffness for low levels of deformation, increasing exponentially until they reached significant stiffness for deformations corresponding to above 1.1% of lateral drift. The numerical models including these members are called ModelSH and ModelSHND, they represent the specimen with and without dissipators respectively.

In the definition of the stiffeners, however, the initial stiffness had to be changed at every run to have a good match with the observed behaviour. A constant initial stiffness was not able to reproduce the observed response of the specimen in all runs. After matching a run reasonably well, the initial stiffness had to be reduced for the next run. This is consistent with what was expected. Figure 7-4 shows that these modified numerical models can now reproduce the stiffer behaviour of the specimen under large deformations. The maximum moments observed in the stiffening elements in the numerical model were of the order of 2,000Nm. This value is lower than the potential flexural capacity of the slab-beams which, if calculated assuming the total depth of the slab, will be of the order of 10,000Nm.

Another aspect that had to be modified from the ideal model was the stiffness of the impacting regions. The value selected initially seemed to cause excessive high frequency noise in the response at impact, something unobserved in the actual testing. A reduction in the initial stiffness of the contact elements to around 20% of their original value (initially defined as described in section 7.2.5) resulted in acceleration and inertial forces closer to the observed ones. The softer contact elements, however, rendered a softer structure and larger lateral displacements. It was required to increase the damping in the vertical oscillation mode (mode 5 in the model) to be able to reproduce the observed response. The damping was increased from 3% to 4% of critical damping in the mode 5.

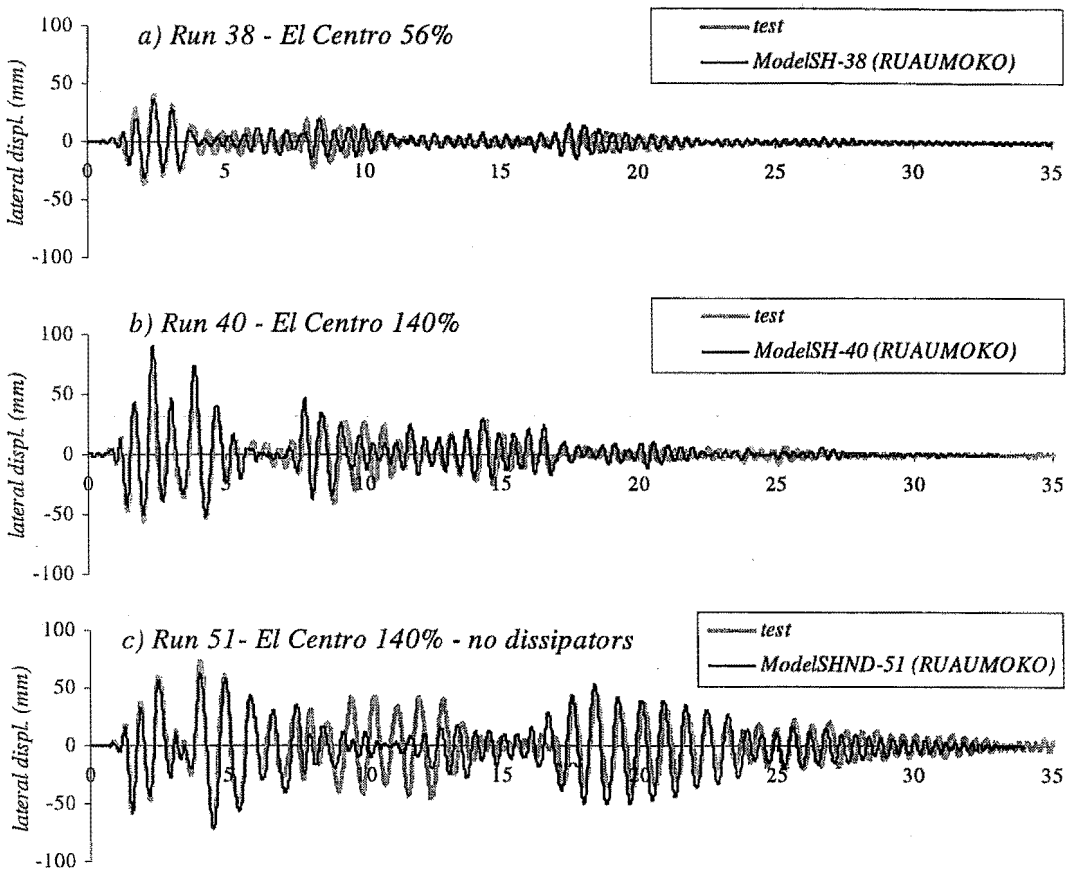

Figure 7-4 Calculated roof-displacement using numerical model with non-perfect hinges

The incorporation of the stiffeners also leads to a good agreement in the modelling of the base-shear. Figure 7-5 shows that the observed peaks are well reproduced by ModelSH and ModelSHND. These results confirm that the strengthening-stiffening action of the slab-beams has the potential to produce the effects observed in the dynamic tests.

Unfortunately, it was not possible to adjust the exponential curve of the stiffeners and the contact elements to reproduce the exact response along the entire time-length of the test. Overall though, the numerical model produced good agreement with the observed results and was able to match the maximum observed deformations and base shear.

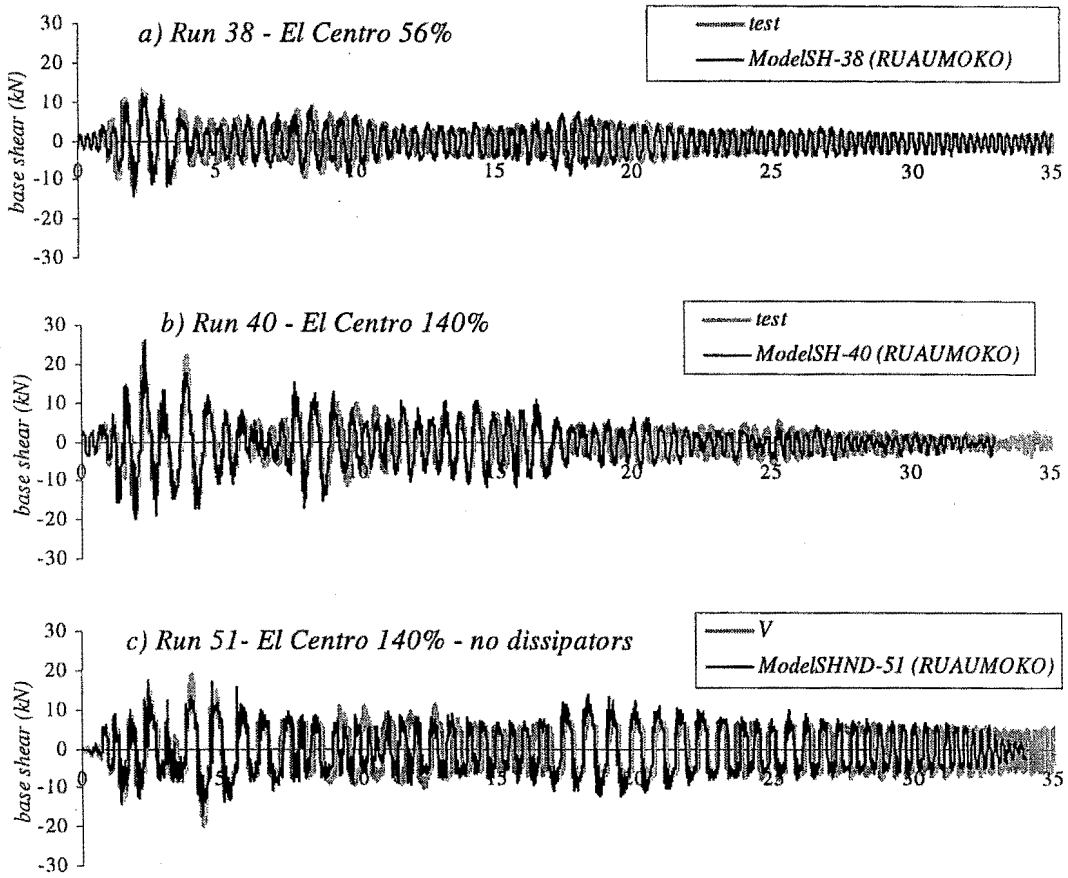

Figure 7-5 Calculated base-shear using numerical model with non-perfect hinges

The numerical model was also used to reproduce the free oscillation of the system (Runs 58 and 59). Figure 7-6 shows the excellent agreement with the observed response. To match the observed results, however, the initial stiffness of the beam "stiffeners" had to be further reduced to almost a fourth of the original initial value. This is reasonable as in the previous runs (Runs 51, 52, 53 and 54) the specimen sustained drifts of around 2% reaching in one case (Run 54) a drift of 3.28%. All the other parameters remained constant.

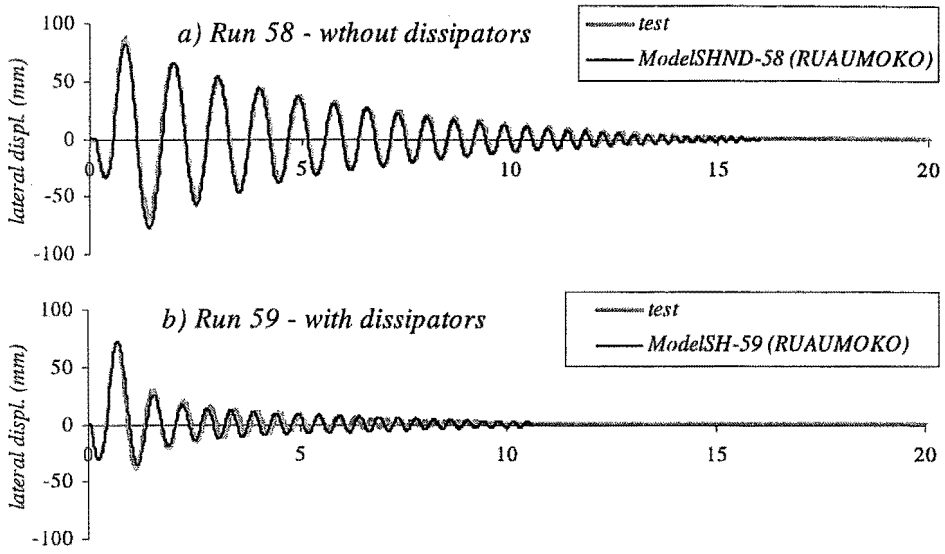

Figure 7-6 Reproduction of the observed free oscillation

Finally, the numerical analysis, using the ideal pinned slab-beams, shows that the lateral drift is also controlled without the presence of the "stiffeners". The cumulative distribution of the ratios between the Numerical Peak Drifts (NPD), obtained with the ideal numerical model, and the Expected Peak Drift (EPD) is shown in Figure 7-7. Although the reliability in the prediction of the peak drifts is only of 60%, this is consistent with the fact that the total damping of the system was overestimated (6.6.11).

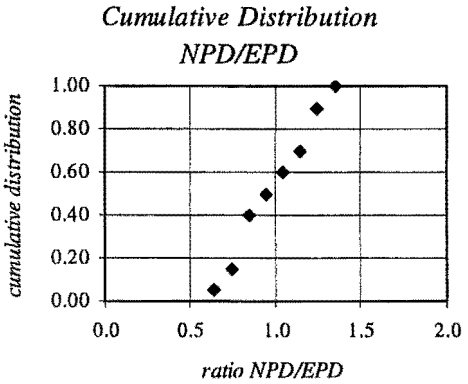

Figure 7-7 Cumulative Distribution of the ratio between the Numerical Peak Drift (NPD) and the Expected Peak Drift (EPD)

7.4 Investigation of the Effect of Variations in the System

Now that the response of the specimen can be numerically modelled, it is possible to investigate variations in the system. These are explored next. The numerical model to be used will be based on the final condition of the specimen (featuring weak stiffeners) and in the ideal model with perfect articulations. The time-history ground-motions used for the modelling were Taft-a, El Centro, and Sylmar. The characteristics of this ground motions are described in Table 6-1.

7.4.1 Effect of a Softer Impact Region

The softening of the impact region was thought to be able to reduce the impact effects in the system and protect the impacting regions of the structure. Priestley et al. (1978) used rubber in the base of rocking walls but the effect in the inertial forces was not measured. Mander and Cheng (1997) also used rubber pads to prevent the damage in the impacting regions of rocking columns with good results.

To assess this effect with the numerical model, the initial stiffness of the contact elements was made equal to 0.25, 0.50 1.00 and 2.00 times the apparent stiffness in the actual model. The results in the model with stiffeners are shown in Figure 7-8. A softer impact region seems to lead to smaller peak base-shears but larger peak drifts. The trend however is not consistently observed in all the cases. It is possible that the stiffeners are obscuring the effects.

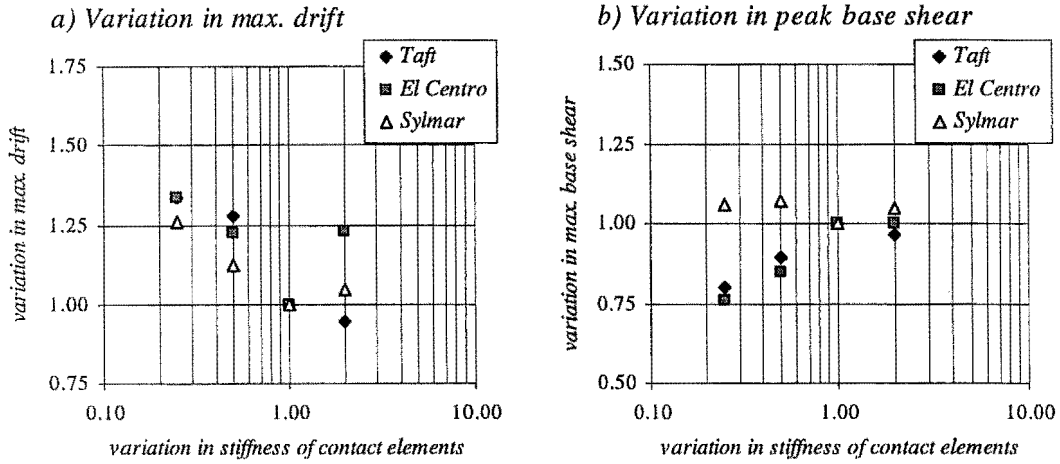

Figure 7-8 Effect of the stiffness of contact elements normalised to the results for the "true" stiffness

The ideal model (without stiffeners) was subjected to the same process and the results are shown in Figure 7-9. The reduction in the peak base shear as the contact elements are softened follows a consistent trend in all cases now. There is however no clear effect in the observed drifts.

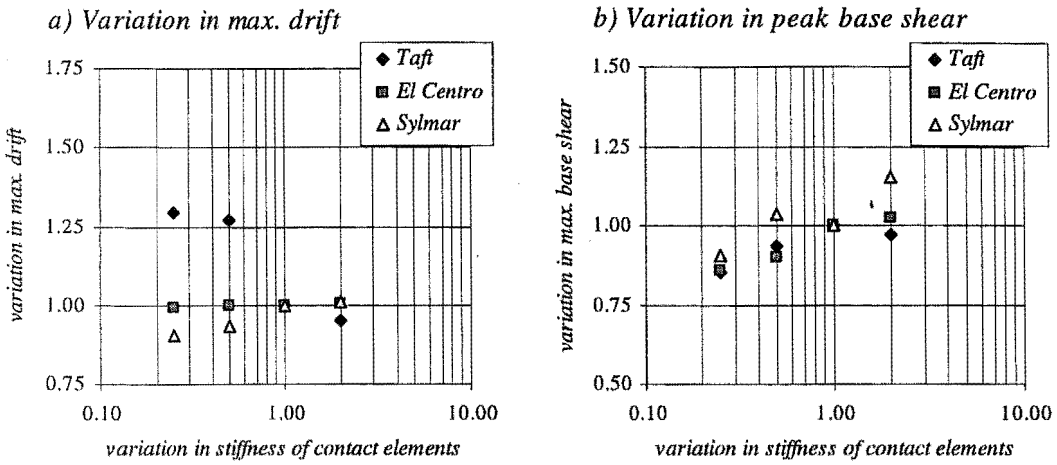

Figure 7-9 Effect of the stiffness of contact elements normalised to the results for the "true" stiffness when the numerical model does not have stiffeners

7.4.2 Effect of Larger Equivalent Viscous Damping (EVD) in the Main Vibration Mode

As it has been discussed in section 7.2.6, the quasi-rigid-body motion of the structural elements during the rocking motion, led to the definition of a very low EVD for the main vibration mode. Furthermore, the best match of the experimental results was obtained when, in the numerical model, the EVD for the first vibration mode was equal to 0%. The numerical model was analysed for EVDs of 0%, 1% , 3% and 5%. The results are presented in Figure 7-10. There is a strong negative correlation between the EVD in main mode and the peak drift. On the other hand, there is no apparent effect of the damping in the peak base shear.

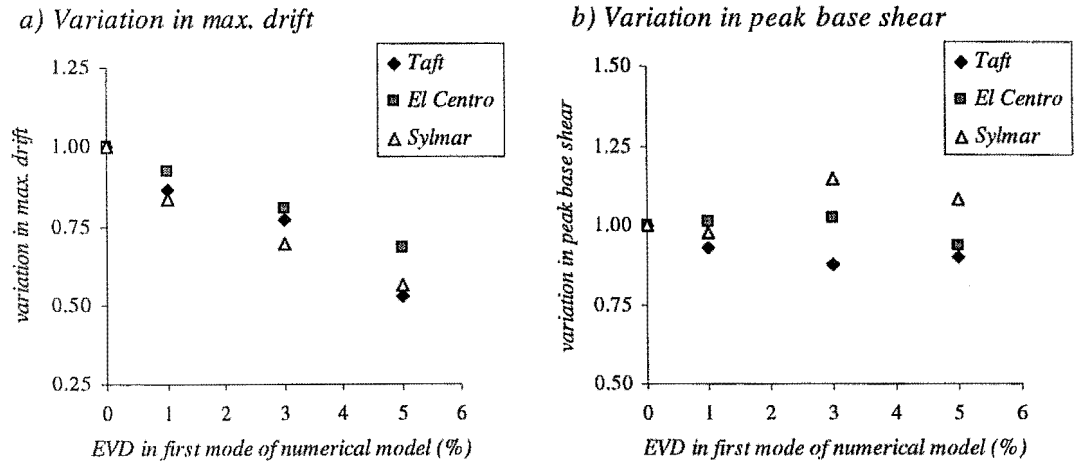

Figure 7-10 Effects of damping in the first-mode normalised to the results in the numerical model with no damping in the first-mode

The beneficial effect of damping in the first mode to control drift is obvious from Figure 7-10. However, one also should be aware of the fact that, in a numerical analysis, allocating damping in the main mode of a rocking system may lead to significant underestimation of the drift. Therefore, if no energy dissipation mechanism is clearly identified in the rest of the structure, one should keep the EVD in the main mode, low.

7.4.3 Effect of the Initial Stiffness of Dissipators

It was discussed in Chapter 4 that dissippators with large initial stiffness would provide larger energy dissipation capacity to the system. This being more evident in the lower levels of seismic demand as it was observed in the results in Table 4-8 . On the other hand, it was also commented that more flexible dissipators appear to reduce the impact actions of the system due to the softening of the main force time-history wave (section 6.6.10). The numerical model was used to investigate the seismic performance of the system with dissipatros with initial stiffness of 0.43, 1.00, 2.14 and 4.29 times the prototype value. The yielding load of the dissipators was kept constant. The results are presented in Figure 7-11. A significant effect in the reduction of the drift, as the stiffness of the dissipator increases, is observed in that figure. No apparent effect is observed in the peak base shear.

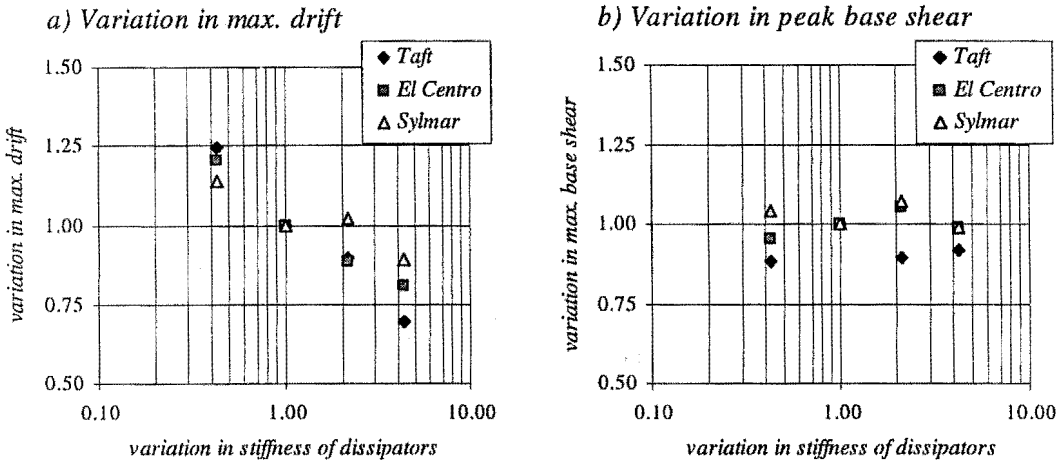

Figure 7-11 Effect of the stiffness of the dissipators, normalised to the results for the numerical model using dissipators with the "true" stiffness

7.4.4 Effect of a Larger Number of Storeys

The experimental results have demonstrated that the assumption of treating the rocking wall as rigid body is reasonable and that the higher modes are not likely to dominate the strength demand in the wall (sections 6.6.36.6.1 and 6.6.3). This however may not be true for taller buildings on which the higher modes may be the dominant aspect of the demand. Three more structures, of 4, 8 and 12 storeys

were analysed and compare with the 3 storey structure to asses their response. Figure 7-12 shows the maximum forces in the masonry struts normalised to the force in the ground floor masonry strut, when the models are subjected to El Centro (Table 6-1). The envelope in the three storey structure follows the expected pattern, dominated by the first mode of oscillation. As the number of storeys increases the effect of higher modes is more significant to the point that, in the 12 storey building, the maximum force is found above the eighth floor.

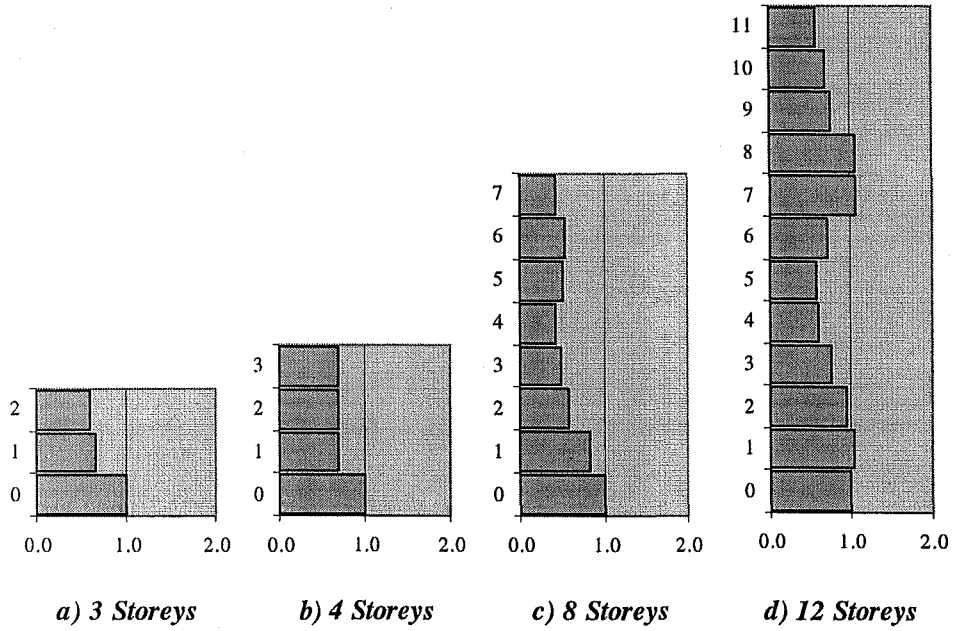

Figure 7-12 Envelope of the forces in the masonry struts normalised to the maximum force in the ground floor masonry strut

The larger flexibility of the taller structures also diminishes the efficiency of the dissipators as the lateral displacement of the rocking wall does not deform the dissipators to the extent that was expected for a quasi-rigid rocking wall. The results of this analysis, for example, showed that the dissipators were deforming only at 70% and 55% of the expected deformation, in the 8 storey structure and the 12 storey building respectively, reducing the expected energy dissipation capacity of the structure. Of course, these taller structures would dissipate more energy in the first mode as they are deforming substantially in that mode, but that is a different scenario. These more flexible walls, therefore, should not be designed using the approach proposed in Chapter 4. The limits for the application of the method, however, cannot be defined simply in terms of number of storeys, as they may vary in mass and stiffness. A practical method could be the use of the static lateral loading of the rocking wall to verify that it is stiff enough to deform the dissipators 90% or more of the deformation expected in a perfectly rigid rocking wall. This, however, requires further investigation.

7.5 Conclusions

- Rocking walls can be numerically modelled with existing inelastic dynamic analysis software. It was found that the software RUAUMOKO had the features required for that modelling.

- The most interesting global aspect of the modelling was the damping. To match the observed results, the EVD in the first mode had to be defined as 0%. Also the damping in the fifth mode, which corresponded to the vertical oscillation of the wall and the contact elements, had to be defined as 4%. The rest of the modes were given a 3% of EVD. Allocating any larger damping in the first mode rendered a highly damped model, more damped than the examples found in the literature review and the specimen tested for this thesis.

- Most aspects of the numerical model could be reasonably well modelled before the experimental results. However, there were some features, like the stiffening and strengthening action of the slab-beams, which could be acceptably modelled only after close calibration against the experimental results.

- The numerical modelling of the specimen showed that the stiffening-strengthening effect of the slab-beams had the potential to corrupt the expected behaviour of the ideal system. That this is the only source of distortion have to be proven experimentally though. A new structure with well defined hinges should be built and tested under similar conditions.

- The numerical modelling of the specimen under different conditions confirmed that the seismic performance can be improved with larger damping in the first mode, larger initial stiffness of the dissipators and a softer impacting region.

- The design approach proposed in Chapter 4 may not be adequate for tall or flexible structures. The strength demand in these structures dominated by higher modes of oscillation rather than the first mode. Also these structures do not meet the requirement of quasi-rigid rotation of the walls, affecting the basic energy dissipation mechanism due to the plastic deformation of the dissipators.

Chapter 8 Conclusions and Recommendations

8.1 Summary

This research was conducted with the idea of expanding the possibilities of masonry structures as reliable aseismic structures. It focused on buildings that use conventional confined masonry shear-walls as their main lateral resistant elements but where the walls are limited in number. These buildings, which are frequently used in developing countries as classrooms, can satisfy a life-safety performance objective, but are likely to suffer damage in moderate to large earthquakes. A major point of this research was to develop an alternative system in a way that minimum or no damage is caused to the structure during such events. More specifically, it was expected that the structure could successfully meet a performance based design environment.

A system based in rocking masonry walls as the main lateral resistant elements was proposed as an alternative to the conventional fixed-base masonry shear-walls described above. It was found that rocking walls have many positive aspects from the seismic point of view. But there were also negative aspects that needed to be addressed. One of the major problems of this system is that rocking walls lack of a reliable source of energy dissipation. To overcome that problem the use of hysteretic energy dissipators has been proposed in the past. Steel bars yielding axially were the elements used for that purpose. In this thesis, however, it was not possible to develop a reliable dissipator of such characteristics. Alternatively, dissipators yielding in flexure were designed and found to have a more reliable performance than those yielding axially. As part of this process, three types of dissipators were designed and tested, one yielding axially (dissipator *D1*) and the other two yielding in flexure (dissipators *D2* and *D3*). All were designed to be attached externally to the rocking wall to ease their inspection and possible replacement after an earthquake. Dissipator *D3* was found to be more reliable and was used in the dynamic test of a reduced scaled model later.

Having a reliable source of energy dissipation allowed the formulation of a seismic design procedure for the system. It was decided that the design procedure should be suited for a performance-based environment. Hence, the design procedure was adapted from the Direct Displacement Method (Priestley and Kowalsky, 2000) which is focused on control of the drift of the structure rather than on strength only. In order to check the viability of the system and the proposed design procedure, a

prototype three-storey structure was defined and designed. The design was conducted using two kinds of dissipators, one with a large initial stiffness and the other with a moderate initial stiffness. It was found that the prototype structure with the dissipators with large initial stiffness could meet the target drifts satisfactorily. The prototype with less stiff dissipators however could meet the target drifts only partially.

A reduced scale model of the prototype was built to be dynamically tested in a shake table. The dissipator used in the model was the less stiff of the ones described in the previous paragraph, because it was not possible to build a reliable dissipator with the characteristics of the stiffer dissipator. This would have been a dissipator yielding axially and it was not possible to build one which avoids early buckling. The less stiff dissipator was of the kind that yields in flexure.

Sixty runs were conducted in the shake table. The ground motions were defined to represent earthquake levels of different intensity, from those regarded as "frequent" earthquakes up to those regarded as "very rare" earthquakes. Some runs were also conducted with the model without dissipators. The system responses were close to the expected responses regarding levels of damage and drift. The masonry was left undamaged and the design capacity of the system was maintained until the final test. However, larger than expected total accelerations, and therefore inertial forces, were observed for large drifts. The problem was due to the strengthening and stiffening influence of the slab-beams rather than to the rocking wall. It was expected to occur but it was thought that after some runs the slabs would soften enough so they would not induce any significant effect in the response. That was not the case.

Finally, a numerical model was prepared using the software RUAUMOKO. The numerical model was able to reproduce the observed behaviour of the specimen but only when the strengthening-stiffening contribution of the slab-beams was included in the model. Without the "beam-stiffeners" the numerical model could not reproduce the observed peak absolute accelerations. The numerical model was then used to assess the response of the structure under different conditions. The effect of the levels of damping, stiffness of the contact elements at the base, stiffness of the dissipators and number of storeys was assessed in the process.

8.2 Conclusions

- The literature review showed that there are many parameters that can affect the quality of masonry. Moreover, these parameters have been found to have a large variability. This creates problems not only on the formulation of theoretical models for masonry but also on the wide application of empirical equations. This makes difficult to achieve one of the basic principles of performance based design: the production of predictable and reliable structures.

- The trend to incorporate performance-based criteria to seismic design is limiting the scope of application of masonry as an aseismic structural material, not only because of what was mentioned above but mainly because of the extensive damage observed in masonry structures in recent destructive earthquakes, particularly in unreinforced masonry and masonry infills. In conventional well engineered MIF and CM buildings, although damage has been observed as well, these structures have met very well the life-safety goal for which they were designed and built. It is believed that the apparent poor seismic performance of masonry is rather due to the ill definition of the expected performance of buildings, which is chiefly focused in life-safety, when the public is growingly more concerned with damageability and functionality of the building stock following earthquakes.

- It has been observed that the deformation capacity of masonry is more stable than its strength capacity. Unfortunately the deformational capacity is very limited and can only be improved at the ultimate drift. The first crack drift has been found to be rather constant. The points discussed above lead to the conclusion that the only way that conventional systems using masonry can satisfy the more demanding seismic performance objectives is avoiding excessive deformation in the masonry. In this context, if masonry is going to be used as the main lateral resisting structural elements, there should be a large enough number of masonry walls to induce only elastic deformations in them.

- Alternative to the restrictive solution described above, it has been observed that the use of innovative structural systems can improve the performance of masonry buildings. Base-isolation is particularly suited due to the relative large stiffness of building with masonry shear walls.

- Rocking is a behaviour that has been observed to protect some structures in the past from damage during earthquakes. Rocking systems have many attractive features from an aseismic point of view. But they also have negative features mainly due to its lack of a reliable source of energy dissipation.

- Hysteretic energy dissipators can provide significant energy dissipation capacity to a rocking wall in a controlled fashion. Energy dissipators yielding in flexure were found to be more reliable than dissipators yielding axially. However, the energy dissipation capacity of the flexural dissipators is smaller than the potential capacity of dissipators yielding axially, and the difference is particularly significant at low to moderate levels of seismic demand. The seismic design technique developed for a structure with rocking walls shows that a much better seismic performance would be obtained at these levels if dissipators with larger initial stiffness were used.

- The Direct Displacement Based Method can be successfully adapted to produce a structure with rocking walls able to match a target displacement. In theory, a number of other features can also be established during the design stage to provide a good picture of the seismic performance of the structure at different levels of demand.

- The dynamic tests showed that rocking can effectively protect masonry walls from damage. It also showed that the hysteretic energy dissipators can provide a reliable source of energy dissipation to the system. Reasonable agreement with the expected drift was also observed in the experimental work. On the other hand, the observed absolute accelerations and, thence the inertial forces, were larger than expected, apparently due to a stiffening mechanism in the structure observed at moderate to large deformations. It seems that failing to detail all the slabs to behave as pinned connections changed the expected seismic behaviour of the structure in that regard. Structural elements other than the rocking wall with energy dissipators should be detailed to transfer only gravity loads and avoid offering resistance to lateral forces. The influence of these other elements will reflect in unnecessary larger total accelerations and therefore larger inertial forces. It is true that they could diminish the lateral displacements of the structure but their contribution is rather unpredictable.

- A system with rocking walls can be numerically modelled with existing inelastic dynamic analysis programs. Most of the features required to numerically model masonry walls can be established reasonably well a priori. There are some features, however, that were found that can alter the expected response and, in our case, could only be modelled after the experimental data was collected. This appears to do mainly with the contribution of elements other than the rocking wall, particularly the slab-beams.

- The response of the structure can be improved with larger modal damping in the first mode, a softer impacting region and stiffer dissipators. On the other hand, during a numerical model of a rocking system, one should be careful in the definition of the damping in the first mode as it was found to be very low and an excessive definition may underestimate the actual drift of the structure.

8.3 Recommendations for further research

- Energy dissipators with large initial stiffness should be developed as they lead to a better seismic performance of the system that uses them. Dissipators yielding axially are the most obvious solution but a technique to avoid a premature buckling should be devised. Friction devices could also be an alternative to study.

- The system that was developed in this thesis provided an energy dissipation capacity that increases with increasing displacement. This behaviour contrasts with the elastic SDOF oscillator used to build response spectra, as these SDOF oscillators have a sustained viscous damping. It would be interesting to study the influence in the seismic response of this characteristic and compare it to the response observed with the conventional SDOF oscillators with constant damping.

- Out of plane behaviour of a rocking wall needs to be addressed to complete the picture of the seismic behaviour of this system.

- It is recommended to build and test a fully articulated model to assess the effect of impact in the system without the interference of any other mechanism. The results here suggest that impact may not create excessive strength demand when dissipators are in place. The results, however, were not conclusive because the impact effects were obscured by the presence of other stiffening mechanisms.

- Because of the limited capacity of the shake table, it was not possible to observe the response of the system subjected to a near-fault type ground motion. It is recommended to investigate this scenario experimentally.

- An important aspect for the practical application of rocking walls is the development of a tridimensional structural system kinematically compatible with the rocking of the walls. Particularly challenging will be the devise of such a structure when rocking walls are expected to rock in more than one direction. Apart from the kinematic compatibility, a key issue is the

definition of adequate detailing so that structural elements other than the rocking walls do not provide any significant lateral resistance to the building.

- It is necessary to develop simplified numerical models that can model the rocking wall in a more concise way. Although the modelling of the rocking walls as assemble of frame elements and contact elements was successfully done in this thesis, a larger structure could demand excessive computational capabilities. It is recommended to reduce the number of contact elements at the base and assess the effects that it brings to the modelling. In our case, it caused excessively large impact actions, but no further investigation was made.

- The efficiency of the use of dissipators at the base for taller (or more flexible) rocking walls should be investigated. In Chapter 7 it was observed that the premise of rigid rocking motion of the rocking wall did not hold when the number of storeys in the prototype was increased to 8 storeys. This led to a shorter than expected deformation in the dissipators and therefore a less than expected hysteretic energy dissipated by the dissipators. It should also be investigated the condition in which the higher modes of lateral oscillation start to dominate the response of the system as the number of storeys alone is not enough to define a limit.

Bibliography

Aguilar, G., Meli, R., Diaz, R. and Vasquez-Del-Mercado, R. (1996). Influence of horizontal reinforcement on the behaviour of confined masonry walls, *Proceedings of the 11th World Conference on Earthquake Engineering*, Acapulco, Mexico, Elsevier Science Ltd., Paper No. 1380.

Alcocer, S. M. and Klinger, R. E. (1994). Masonry research in the Americas, *Masonry in the Americas*, American Concrete Institute, Paper SP 147-5.

Ang, B.G. (1985). *Seismic shear strength of circular bridge piers*, PhD Thesis, Department of Civil Engineering, University of Canterbury, New Zealand.

Aslam, M., Godden, W.G. and Scalise, D.T. (1980), Earthquake rocking response of Rigid Bodies, *Journal of the Structural Division*, ASCE, Vol. 106, No. 2, pp. 377-392.

ASTM (1995). *Annual Book of ASTM Standards,* American Society of Testing and Materials (ASTM), Philadelphia, Pennsylvania.

ATC (1996). *ATC 40 - Seismic evaluation and retrofitting of existing concrete buildings*, Applied Technology Council (ATC), Redwood City, California.

Atkinson, R. H., Amadei, B. P., Saeb, S. and Sture, S. (1989). Response of masonry bed joints in direct shear, *Journal of the Structural Division*, ASCE, Vol. 115, No. 9, pp. 2276-2296.

Bariola, J. (1994). Seismic Resistant and Design of Masonry Structures, *Masonry in the Americas*, American Concrete Institute, Paper SP 147-3.

Bariola, J. (2001). *Earthquake in Arequipa, Peru June 23, 2001*, EERI Special Earthquake Report, http://www.eeri.org/earthquakes/Reconn/Nazca/Nazca1.html

Bariola, J. and Kuroiwa, J. (1996). *The Nazca, Peru, Earthquake of November 12, 1996*, EERI Special Report, Jan. 1997, http://www.eeri.org/earthquakes/Reconn/Nazca/Nazca1.html

Bertero, V. (1996). State-of-the-Art Report on: Design Criteria, *Earthquake Engineering Research at Berkeley 1996*, Report No EERC 96/01.

Brokken, S. and Bertero, V. (1981). *Studies on effects of infills in seismic resistant R/C construction*, University of California , Berkeley, Report No. UBC/EERC-81/12.

Bruneau, M. (1995). Damage to masonry buildings from the 1995 Hanshin-Awaji (Kobe, Japan) earthquake, *Proceedings of the Seventh Canadian Masonry Symposium*, Mc. Master University, Hamilton, Ontario, pp. 84-98.

BSI (2002), *Precast concrete masonry units - BS 607,* British Standards Institution.

Casabone, C. (1994). General description of systems and construction practices, *Masonry in the Americas*, American Concrete Institute, Paper SP 147-2.

Carr, A. (2000). *RUAUMOKO, Software for inelastic dynamic analysis*, Department of Civil Engineering, University of Canterbury, New Zealand.

CEB (1996). *RC frames under earthquake loading: state of the art report*, Comité Euro-international du Béton, T. Telford, London, UK.

CEB (1994). *Behaviour and analysis of reinforced concrete structures under alternate actions inducing inelastic response*, Comité Euro-international du Béton, Bulletin d'Information No.220.

Chik-Sing, Y., Chopra, A., Penzien, J. 1980. Rocking response of rigid bodies to earthquakes. *Earthquake Engineering and Structural Dynamics.* Vol. 8, pp. 565-587.

Chiou, Y. J., Tzeng, J. C. and Liou, Y. W. (1999). Experimental and analytical study of masonry infilled frames, *Journal of Structural Engineering*, ASCE, Vol.125, No. 10, Oct.1999, pp. 1109-1171.

Colombo, A., Negro, P. and Verzeletti, G. (2000) Improving ductility and energy-dissipation capacity of infills by means of polymeric nets, *Proceedings of the 12th World Conference on Earthquake Engineering*, New Zealand Society for Earthquake Engineering, Paper No. 1910.

Cormack, L. G. (1988). The design and construction of the major bridges on the Mangaweka rail deviation, *The Institution of Professional Engineers of New Zealand, Transactions*, Vol. 15, No. 1.

Crisafulli, F. (1997). *Seismic Behaviour Of Reinforced Concrete Structures With Masonry Infills*, Ph.D. Thesis, Department Of Civil Engineering, University Of Canterbury.

Davis, R. O. (1992). Pounding of buildings modelled by an impact oscillator, *Earthquake Engineering and Structural Dynamics,* Vol. 21, pp. 253-274.

Dodd, L.L. and Restrepo-Posada, J.I. (1995). Model for predicting cyclic behaviour of reinforcing steel, *Journal of Structural Engineering*, ASCE, Vol.121, No. 3, Mar.1995, pp. 433-445.

Drysdale, R.G., Hamid, A.A. and Baker, L.R. (1994). *Masonry Structures, Behavior and Design*, Prentice Hall Inc. New Jersey, U.S.A.

Duzuke, A. and Dawe, J. L. (1995). In-plane distortion of unreinforced masonry panels infilling RC frames, *Proceedings of the Seventh Canadian Masonry Symposium*, Mc. Master University, Hamilton, Ontario, pp. 252-262.

Early, M. D. (1989). *Determination of damping in tall buildings*, Central Laboratories Report 89-B92203, Works and Development Services Corporation, New Zealand.

EC8, (1994). *Eurocode 9, Design provisions for earthquake resistance of structures.*

FEMA (1997). *NEHRP Guidelines for the Seismic Rehabilitation of Buildings*, Federal Emergency Management Agency (FEMA), Publication 273, prepared for the Building Seismic Safety Council (BSSC) by the Applied Technology Council (ATC), ATC-33 Project

Fierro, E. (2001). *Initial Report on 23 June 2001 Arequipa, Peru Earthquake*, Wiss, Janney, Elstner Associates Inc., http://www.wje.com/news/arequipa/atico-1.pdf

Gallegos, H. (1994). Masonry in Peru, *Masonry in the Americas*, American Concrete Institute, Paper SP 147-11.

Ghobarah, A. (2001). Performance-based design in earthquake engineering: state of development. *Engineering Structures*, Vol. 23(8) pp. 878-884.

Goldsmith, W. (1960). *Impact: the theory and physical behaviour of colliding solids*. E. Arnold, London.

Hamid, A.A. and Drysdale, R.G., (1982). Effect of strain gradient on tensile strength of concrete blocks, *Masonry: materials, properties and performance*, ASTM STP 778, Edited by J.G. Borchelt.

Harris, H.G., Sabnis, G.M. (1999). *Structural modeling and experimental techniques*, CRC Press, Boca Raton, Florida.

Hendry, A.W. (1990). *Structural Masonry*, Macmillan Education Ltd, U.K.

Hidalgo, P.A. (1994). Seismic behaviour and earthquake-resistant design of masonry buildings in Chile, *Masonry in the Americas*, American Concrete Institute, Paper SP 147-12.

Hildorf, H.K. (1969). Investigation into the failure mechanism of brick masonry loaded in axial compression. *Proceedings of the International Conference on Masonry Structural Systems*, University of Texas at Austin, 1967, Gulf Publishing, 1969, pp. 34-41.

Holden, T., Restrepo, J.I. and Mander, J.B. (2002). Seismic performance of precast reinforced and prestressed concrete walls, *Journal of Structural Engineering*, ASCE, In Press.

Housner G.W. (1956). Limit design of structures to resist earthquakes. *Proceedings of the 1956 World Conference in Earthquake Engineering*. Earthquake Engineering Research Institute.

Housner G.W. (1963). The behavior of inverted pendulum structures during earthquakes, *Bulletin of the Seismological Society of America*, Vol. 53, No. 2, pp. 403-417.

IAEE (1996). *Regulations for seismic design: a world list*, Edited by the International Association for Earthquake Engineering (IAEE), Tokyo, Japan.

ICBO (1997). *Uniform Building Code*, International Conference of Building Officials, Pasadena, California.

Kao, G.C. (1998). *Design and shaking table tests of a four-storey miniature structure built with replaceable plastic hinges*, Master Thesis, Department of Civil Engineering, University of Canterbury, New Zealand.

Kappos, A.J., Stylianidis, K.C. and Michailidis, C.N. (1998), Analytical Models for Brick Masonry Infilled Reinforced Concrete Frames under Lateral Loading, *Journal of Earthquake Engineering*, Vol. 2, No. 1, pp. 59-87.

Kariotis, J.C., Ewing, R.D. and Johnson, A.W. (1985). Strength Determination of Shear Failure Modes of Unreinforced Brick Masonry with Low Strength Mortar, *Proceedings of the 7th International Brick Masonry Conference,* Melbourne, Australia, February, 1985, pp. 1327-1337.

Khoo, C.L. and Hendry, A.W. (1973). Strength tests on brick and mortar under complex stresses for the development of a failure criterion for brickwork in compression, *Proceedings of the British Ceramic Society*, Vol. 21, 1973, pp. 51-66.

Kirtschig, K. (1985). On the failure mechanism of masonry subjected to compression, *Proceedings of the Seventh International Brick Masonry Conference*, Melbourne, Australia, Vol.1, pp. 625-629.

Kramer, S.L. (1996). *Geotechnical Earthquake Engineering*, Prentice Hall, Upper Saddle River, N.J.

Klingner, R. E. (1997). Performance-based design of masonry structures for seismic loads, *The EERC-CUREe Symposium in Honor of Vitelmo V. Bertero*, Earthquake Engineering Research Centre (EERC), University of California, Berkeley, Report No. UCB/EERC-97/05.

Klinger, R. E. and Bertero, V. V. (1976). *Infilled frames in earthquake resistant construction*, Earthquake Engineering Research Centre (EERC), University of California, Berkeley, Report No. EERC 76-32.

Langenbach, R. (1994). Public policy vs. seismic design: cost and performance criteria for seismic rehabilitation of URM infill frame buildings, *Proceedings from the NCEER Workshop on Seismic Response of Masonry Buildings*, Technical Report NCEER-94-0004.

Lee, H.S. and Woo, S.W., (2002) Effect of masonry infills on seismic performance of a 3-storey R/C frame with non-seismic detailing, *Earthquake Engineering and Structural Dynamics.* Vol. 31, pp. 353-378.

Lynch, G. (1994). *Brickwork: history, technology and practice*, Donhead, London.

Madan, A., Reinhorn, A.M., and Mander, J.P (1996). Flexural behaviour of reinforced masonry shear walls with unbonded reinforcement. *The Masonry Society Journal*, Aug. 1996, pp. 87-98.

Madan, A., Reinhord, A.M., Mander, J.P. and Valles, R. E. (1997). Modeling of masonry infill panels for structural analysis. *Journal of Structural Engineering*, ASCE, Vol. 123, No. 10, Oct. 1997, pp. 1295-1302.

Magenes, G. and Calvi, M. (1997). In-plane seismic response of brick masonry walls. *Earthquake Engineering and Structural Dynamics.* Vol. 26, pp. 1091-1112

Makris, N. and Roussos, Y. (1998). *Rocking response and overturning of equipment under horizontal-type pulses*. Report No PEER-98/05 University of California, Berkeley.

Mander, J. B. (2001). Future directions in seismic design and performance based engineering, *Proceedings of the NZSEE Annual Conference 2001,* Wairakei, New Zealand.

Mander, J. B. and Cheng, C. T. (1997). *Seismic resistance of bridge piers based on damage avoidance design*, Technical Report NCEER-97-0014.

Meli, R. (1994). Structural Design of Masonry Buildings: The Mexican Practice, *Masonry in the Americas*, American Concrete Institute, Paper SP 147-8.

Moroni, M., Sarrazin, M., Boroschek, R. Valdebenito R. and Romo, D. (2000) Analysis of Seismic Records Obtained in Isolated Structures, *Proceedings of the 12th World Conference on Earthquake Engineering*, New Zealand Society for Earthquake Engineering.

Muñoz A., Montalbetti, A. and Tinman, M. (1997). *Daños en estructuras de concreto armado ocasionados por el sismo de Nasca en noviembre de 1996*, Publication DI-97-02 Department of Engineering, Civil Engineering Section, Catholic University of Peru.

Naeim, F. and Lew, M. (1995). On the use of design spectrum compatible time histories, *Earthquake Spectra*, Vol 11, Issue 1, pp 111-127.

Nakaki, S.D., Stanton, J.F., Sritharan, S. (1999). An overview of the PRESS five story precast test building, *PCI Journal*, Vol. 44, No.2, pp. 26-39.

NZS New Zealand Standards 4203 (1992). *Code of practice for general structural design, and design loadings for buildings.*

Otani, S. (1997). Development of Performance-Based Design Methodology in Japan, *Seismic Design Methodologies for the Next Generation of Codes*, A. A. Balkema, pp. 59-67.

Paulay, T. and Priestley, M.J.N. (1992). *Seismic design of reinforced concrete and masonry buildings*, John Wiley & Sons Inc., New York.

Priestley. M.J.N., Evison R.J., Carr A.J. (1978). Seismic response of structures free to rock on their foundations, *Bulletin of the New Zealand Society for Earthquake Eng.*, Vol. 11, No. 3, pp. 141-150.

Priestley. M.J.N., Kowalsky, M.J. (2000). Direct displacement-based seismic design of concrete buildings, *Bulletin of the New Zealand Society for Earthquake Eng.*, Vol. 33, No. 4, pp. 421-444.

Priestley, M.J.N., Sritharan, S., Conley, J., Pampanin, S. (1999). Preliminary results and conclusions from the PRESS five-story precast concrete test building, *PCI Journal*, Vol. 44, No.6, pp. 42-67.

Quiun, D., San-Bartolome, A., Torrealva, D. and Zegarra, L. (1997). *The Nasca earthquake of 12-November-1996*, Publication DI-97-01 Catholic University of Peru, Department of Engineering, Civil Engineering Section, Catholic University of Peru.

Rahman, A. and Restrepo, J. (2000). *Earthquake resistant precast concrete buildings: seismic performance of cantilever walls using unbonded tendons*, Research Report No. 2000-5, Department of Civil Engineering, University of Canterbury, Christchurch, New Zealand.

Restrepo, J. I., Mander J. B. and Holden, T. J. (2001). New Generation of Structural Systems for Earthquake Resistance, *Proceedings of the New Zealand Society for Earthquake Engineering 2001 Conference,* Wairakei, New Zealand.

Rodriguez, M. and Rodriguez, V. (2000). Performance-based earthquake-resistant design of confined masonry walls, *Proceedings of the 12th World Conference on Earthquake Engineering*, New Zealand Society for Earthquake Engineering, Paper No. 1955.

Sahlin, S., (1971). *Structural Masonry*, Prentice Hall Inc, New Jersey, U.S.A.

SEOAC (1995). *Report On Performance-Based Seismic Engineering*, Prepared by the Vision 2000 Committee of the Structural Engineers Association of California, SEOAC,

Sharpe, R. D. and Skinner, R. I. (1983). The seismic design of an industrial chimney with rocking base, *Bulletin of the New Zealand Society for Earthquake Enginnering*, Vol. 16, No. 2.

Shultz, A. E. (1994). Performance of masonry structures during extreme lateral loading events, *Masonry in the Americas*, American Concrete Institute, Paper SP 147-4.

Sinha, B.P., (1983). *Factors Affecting the Brick/Mortar Interface Bond Strength*, International Journal of Masonry Construction, Vol. 3, No. 1, pp. 14-18.

Stafford Smith, B. (1962). Lateral stiffness of infilled frames, *Journal of the Structural Division*, ASCE, Vol. 88, No. ST6, pp. 183-199.

Tomazevic, M. (1999). *Earthquake Resistant Design of Masonry Buildings*, Imperial College Press, London, U.K.

Yamin, L.E. and Garcia L.E. (1994). Masonry Materials, *Masonry in the Americas*, American Concrete Institute, Paper SP 147-1

Yeong-Bin Yang, Hsiao-Hui Hung and Meng-Ju He. (2000). Sliding and rocking response of rigid blocks due to horizontal excitation, *Structural Engineering and Mechanics,* Vol. 9, No. 1, pp. 1-16.

Appendix A Expected Drift at other Earthquake Levels

A.1 Closed form Equation for the Expected Drift at Other Earthquake Levels

At this stage, the capacity of the dissipators has been defined and, therefore, the design base-shear of the structure, V, is known. The displacement for any level of demand can be calculated with a closed form equation if the structure is modelled as a SDOF oscillator and the displacement spectra can be represented by a straight line with slope m_d. The process starts by defining:

$$V = K_{eff}\Delta \qquad \text{(Eq. A.1)}$$

$$\Delta = m_d T_{eff} \qquad \text{(Eq. A.2)}$$

comparing these two equations: $V = K_{eff} m_d T_{eff}$ (Eq. A.3)

Now one can develope from the fact that the structure is being assumed to be a SDOF oscillator, defining its effective stiffness , K_{eff}, in terms of its effective mass M_{eff} and its effective period T_{eff}.

but: $$K_{eff} = \frac{4\pi^2}{T_{eff}^2} M_{eff} \qquad \text{(Eq. A.4)}$$

also: $$V = \left(\frac{4\pi^2}{T_{eff}^2} M_{eff} \right) \left(m_d T_{eff} \right)$$

or (as long as $T_{eff} \neq 0$): $$V = m_d \frac{4\pi^2}{T_{eff}} M_{eff} \qquad \text{(Eq. A.5)}$$

and then one can solve T_{eff}: $$T_{eff} = m_d \frac{4\pi^2}{V} M_{eff} \qquad \text{(Eq. A.6)}$$

and finally Δ would be: $$\Delta = m_d T_{eff} = (m_d)^2 \frac{4\pi^2}{V} M_{eff} \qquad \text{(Eq. A.7)}$$

The slope, m_d, depends on the level of damping, ξ, and the level of damping depends on the displacement, Δ. Therefore, this loop needs to be solved. As discussed earlier in Chapter 3, it has been proposed that the displacement for any level of damping can be related to the displacement for the basic 5% damping by the relationship (Priestley and Kowalsky, 2000):

$$\Delta = \left(\frac{7}{2+\xi}\right)^{1/2} \Delta_{5\%} \qquad \text{(Eq. A.7)}$$

In that case, the slopes, m_d, of the straight lines that represent the displacement spectra can also be related by an analogous equation

$$m_d = \left(\frac{7}{2+\xi}\right)^{1/2} m_{d-5\%} \qquad \text{(Eq. A.8)}$$

The spectral displacement, Δ, in a structure with a defined period, T_{eff}, for any earthquake return period can also be related to the spectral displacement expected for a basic earthquake return period of 475 years through a risk factor, RF (NZS4203).

$$\Delta = (RF)\Delta_{475} \qquad \text{(Eq. A. 9)}$$

Again, the slopes can be related as:

$$m_d = (RF)m_{d-475} \qquad \text{(Eq. A.10)}$$

Therefore, it is possible to define the slope of the displacement spectra for any level of damping and any return period, m_d, as a function of the slope of the basic displacement spectra for 5% damping and a return period of 475 years, $m_{d\text{-}475,5\%}$.

$$m_d = \left(\frac{7}{2+\xi}\right)^{1/2} (RF)m_{d-475,5\%} \qquad \text{(Eq. A.11)}$$

and

$$(m_d)^2 = \left(\frac{7}{2+\xi}\right)(RF)^2 (m_{d-475,5\%})^2 \qquad \text{(Eq. A.12)}$$

Now, one can go back to Eq. A.7 and define Δ as a function of the damping, ξ.

and finally

$$\Delta = \left[\left(\frac{7}{2+\xi}\right)(RF)^2 (m_{d-475,5\%})^2\right]\frac{4\pi^2}{V} M_{eff} \qquad \text{(Eq. A.13)}$$

or

$$\Delta = \frac{28\pi^2}{V} M_{eff} (RF)^2 (m_{d-475,5\%})^2 \left(\frac{1}{2+\xi}\right) \qquad \text{(Eq. A.14)}$$

if we define:

$$Q_1 = \frac{28\pi^2}{V} M_{eff} (RF)^2 (m_{d-475,5\%})^2 \qquad \text{(Eq. A.15)}$$

Then delta will be:

$$\Delta = Q_1 \left(\frac{1}{2+\xi}\right) \qquad \text{(Eq. A.16)}$$

Eq. A-16 defines the displacement, Δ, in terms of the damping, ξ, but a component of this damping, the hysteretic damping ξ_h, depends on the lateral displacement Δ, and therefore a loop still exists there. This is addressed next:

Damping is defined as: $$\xi = \xi_o + \xi_i + \xi_h \quad \text{(Eq. 3.89)}$$

or more explicitly: $$\xi = \xi_o + \xi_i + C_1 C_2 C_3 \xi_{h-ideal} \quad \text{(Eq. A.17)}$$

In Eq. A.17, all the terms but C_1 have been found to be relatively independent of the lateral displacement, Δ. The factor C_1 has already been defined in Chapter 3 as follows:

$$C_1 = \sum \left(1 - \frac{2F_y h_{eff}}{\Delta B_i k_d} \right) \quad \text{(Eq. 3.88)}$$

If the number and position of the dissipators is defined, this equation would yield a simpler definition. For example, when two dissipators are used and they are placed near the ends, Eq. 3.88 would be reduced to:

$$C_1 = \frac{Bk_d\Delta - 2F_y h_{eff}}{\Delta B k_d} \quad \text{(Eq. A.18)}$$

therefore one can define $$\xi = \xi_o + \xi_i + \left(\frac{Bk_d\Delta - 2F_y h_{eff}}{\Delta B k_d} \right) C_2 C_3 \xi_{h-ideal} \quad \text{(Eq. A.19)}$$

Back into Eq. A.7:

$$\Delta = Q_1 \left(\frac{1}{2 + \xi_o + \xi_i + \left(\frac{Bk_d\Delta - 2F_y h_{eff}}{\Delta B k_d} \right) C_2 C_3 \xi_{h-ideal}} \right)$$

or: $$\Delta = Q_1 \left(\frac{\Delta B k_d}{(2 + \xi_o + \xi_i)(\Delta B k_d) + (Bk_d\Delta - 2F_y h_{eff})(C_2 C_3 \xi_{h-ideal})} \right)$$

Finally, Δ can be solved from here to be:

$$\Delta = \frac{Q_1 B_d k_d + 2F_y h_{eff} C_2 C_3 \xi_{h-ideal}}{(2 + \xi_o + \xi_i + C_2 C_3 \xi_{h-ideal}) B_d k_d} \quad \text{(Eq. A.20)}$$

A.2 Drift at Other Earthquake Levels when Constant Damping is Assumed

From Fig. A-1, the following relationships can be defined for the secant stiffness, K:

$$K_{RP=475} = V/\Delta_{RP=475} \quad \text{(Eq. A.21)}$$

$$K_{RP\neq475} = V/\Delta_{RP\neq475} \quad \text{(Eq. A.22)}$$

Since the base shear, V, is the same for both cases, one can say that:

$$K_{RP=475}\Delta_{RP=475} = K_{RP\neq475}\Delta_{RP\neq475} \quad \text{(Eq. A.23)}$$

but:

$$K = \frac{4\pi^2}{T_{eff}^2} M_{eff} \quad \text{(Eq. A.24)}$$

Therefore, since the masses are the same in both cases and $4\pi^2$ is a constant, Eq. A.23 can be rewritten in terms of the corresponding effective period, T_{eff}:

$$\frac{\Delta_{RP=475}}{T^2_{eff\ RP=475}} = \frac{\Delta_{RP\neq475}}{T^2_{eff\ RP\neq475}} \quad \text{(Eq. A.25)}$$

or

$$\Delta_{RP\neq475} = \left(\frac{T_{eff\ RP\neq475}}{T_{eff\ RP=475}}\right)^2 \Delta_{RP=475} \quad \text{(Eq. A.26)}$$

From the displ. spectra (Fig. A-1) it is possible to find a new relationship for the periods, T_{eff}:

$$\Delta_{RP=475} = m_{d-475-5\%} T_{eff\ RP=475} \quad \text{(Eq. A.27)}$$

$$\Delta_{RP\neq475} = RF m_{d-475-5\%} T_{eff\ RP\neq475} \quad \text{(Eq. A.28)}$$

From here:

$$\left(\frac{T_{eff\ RP\neq475}}{T_{eff\ RP=475}}\right) = \frac{1}{RF}\frac{\Delta_{RP\neq475}}{\Delta_{RP=475}} \quad \text{(Eq. A.29)}$$

Now, replacing B.9 in B.6:

$$\Delta_{RP\neq475\,years} = (RF)^2 \Delta_{RP=475\,years} \quad \text{(Eq. A.30)}$$

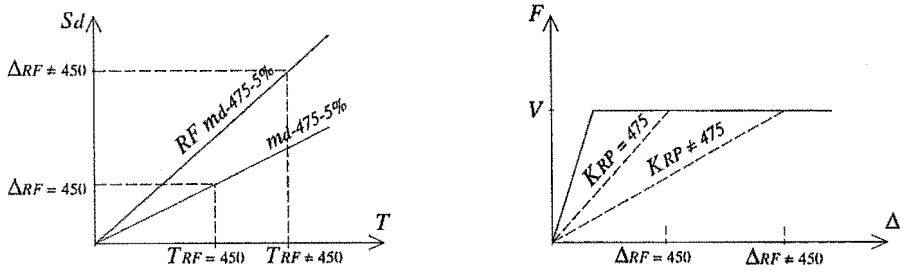

a) Displacement Spectra *b) Secant Stiffness*

Figure A-1 Displacement spectra and definition of secant stiffness for two different earthquakes

Appendix B Input Files for RUAUMOKO

The files that are listed next were the ones used in the numerical analysis described in Chapter 7. They are ModelPH, ModelPHND, ModelSH and ModelSHND. A brief description is given before each file. Figure B-1 shows the numbering of the nodes and members of the basic model ModelPH.

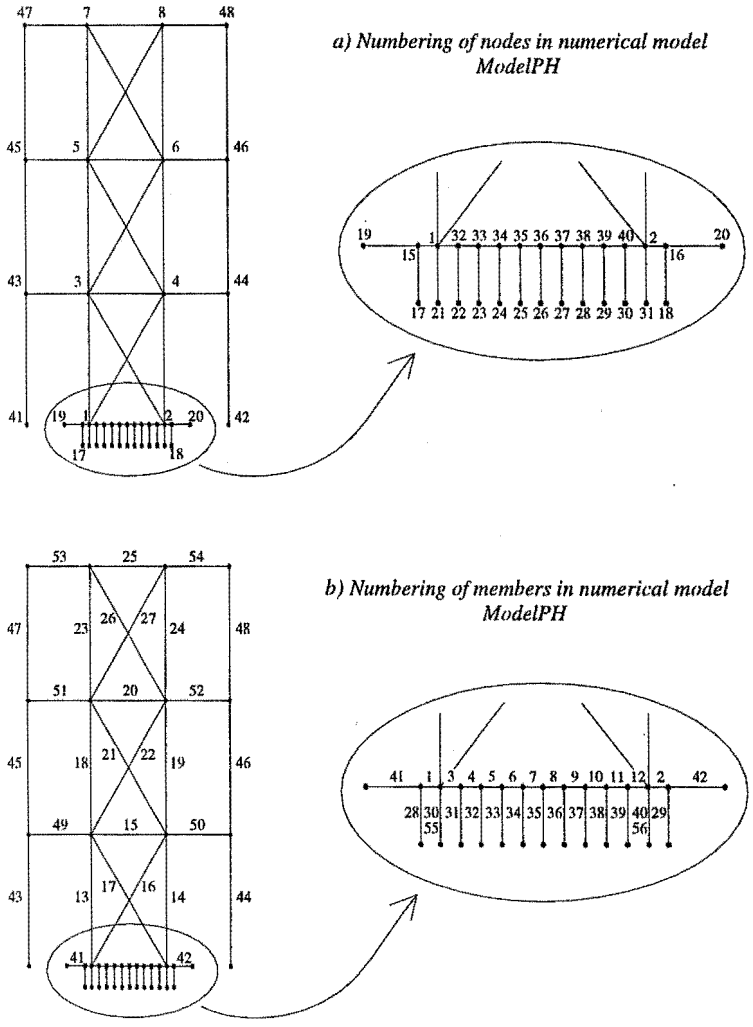

Figure B-1 Numbering of nodes and members in numerical model ModelPH

B.1 ModelPH

This is the basic ideal model. It includes the dissipators but does not incorporate the "stiffeners" in the beams yet. This input file, which is completely listed next, will be used as reference for the description of the input files of the other models.

```
THREE STOREY ONE-BAY REINFORCED CONCRETE FRAME WITH MASONRY INFILLS
2  0  1 1 3 0 1 0 0                          !CONTROL PARAMETERS
48  56  12  8  8  0  9.81  0.0  0.0  0.000020  35  !FRAME AND TIME-HISTORY
0  625 625  0  1  1  0.7  0.1                 !OUTPUT AND PLOTTING OPTIONS
0 0                                          !ITERATION CONTROL
1 0  2 3  3 3  4 3  5 4  6 3  7 3  8 3       !USER SPECIFIED MODAL DAMPING PARAMETERS


NODES
 1      0.000   0.000  0 0 0  0 0 0
 2      0.710   0.000  0 0 0  0 0 0
 3      0.000   1.235  0 0 0  0 0 0
 4      0.710   1.235  0 0 0  0 0 0
 5      0.000   2.495  0 0 0  0 0 0
 6      0.710   2.495  0 0 0  0 0 0
 7      0.000   3.755  0 0 0  0 0 0
 8      0.710   3.755  0 0 0  0 0 0
 9      0.000   5.120  0 0 0  0 0 0
10      0.710   5.120  0 0 0  0 0 0
11      0.000   6.400  0 0 0  0 0 0
12      0.710   6.400  0 0 0  0 0 0
13      0.000   7.680  0 0 0  0 0 0
14      0.710   7.680  0 0 0  0 0 0
15     -0.065   0.000  0 0 0  0 0 0
16      0.775   0.000  0 0 0  0 0 0
17     -0.065  -0.400  1 1 1  0 0 0
18      0.775  -0.400  1 1 1  0 0 0
19     -0.120   0.000  1 1 1  0 0 0
20      0.830   0.000  1 1 1  0 0 0
21      0.000  -0.400  1 1 1  0 0 0
22      0.071  -0.400  1 1 1  0 0 0
23      0.142  -0.400  1 1 1  0 0 0
24      0.213  -0.400  1 1 1  0 0 0
25      0.284  -0.400  1 1 1  0 0 0
26      0.355  -0.400  1 1 1  0 0 0
27      0.426  -0.400  1 1 1  0 0 0
28      0.497  -0.400  1 1 1  0 0 0
29      0.568  -0.400  1 1 1  0 0 0
30      0.639  -0.400  1 1 1  0 0 0
31      0.710  -0.400  1 1 1  0 0 0
32      0.071   0.000  0 0 0  0 0 0
33      0.142   0.000  0 0 0  0 0 0
34      0.213   0.000  0 0 0  0 0 0
35      0.284   0.000  0 0 0  0 0 0
36      0.355   0.000  0 0 0  0 0 0
37      0.426   0.000  0 0 0  0 0 0
38      0.497   0.000  0 0 0  0 0 0
39      0.568   0.000  0 0 0  0 0 0
40      0.639   0.000  0 0 0  0 0 0
```

```
41      -0.595  0.000  1 1 0  0 0 0
42       1.305  0.000  1 1 0  0 0 0
43      -0.595  1.235  0 0 0  0 0 0
44       1.305  1.235  0 0 0  0 0 0
45      -0.595  2.495  0 0 0  0 0 0
46       1.305  2.495  0 0 0  0 0 0
47      -0.595  3.755  0 0 0  0 0 0
48       1.305  3.755  0 0 0  0 0 0

ELEMENTS
 1   5 15   1          !shortbeam
 2   5  2  16          !shortbeam
 3   4  1  32          !base beam
 4   4 32  33          !base beam
 5   4 33  34          !base beam
 6   4 34  35          !base beam
 7   4 35  36          !base beam
 8   4 36  37          !base beam
 9   4 37  38          !base beam
10   4 38  39          !base beam
11   4 39  40          !base beam
12   4 40   2          !base beam
13   6  1   3          !column first level
14   6  2   4          !column first level
15   1  3   4          !confining beam
16   9  1   4          !masonry first level
17   9  2   3          !masonry first level
18   6  3   5          !column second level
19   6  4   6          !column second level
20   1  5   6          !confining beam
21   9  3   6          !masonry second level
22   9  4   5          !masonry second level
23   6  5   7          !column third level
24   6  6   8          !column third level
25   1  7   8          !confining beam
26   9  5   8          !masonry third level
27   9  6   7          !masonry third level
28  10 17  15          !contact vertical
29  10 18  16          !contact vertical
30  10 21   1          !contact vertical
31  10 22  32          !contact vertical
32  10 23  33          !contact vertical
33  10 24  34          !contact vertical
34  10 25  35          !contact vertical
35  10 26  36          !contact vertical
36  10 27  37          !contact vertical
37  10 28  38          !contact vertical
38  10 29  39          !contact vertical
39  10 30  40          !contact vertical
40  10 31   2          !contact vertical
41  11 19  15          !contact horizontal
42  11 20  16          !contact horizontal
43   7 41  43          !exterior column first
44   7 42  44          !exterior column first
45   8 43  45          !exterior column second
46   8 44  46          !exterior column second
47   8 45  47          !exterior column third
```

```
48   8  46  48          !exterior column third
49   2  43   3          !exterior beam first
50   2  44   4          !exterior beam first
51   2  45   5          !exterior beam second
52   2  46   6          !exterior beam second
53   2  47   7          !exterior beam third
54   2  48   8          !exterior beam third
55  12  21   1          !dissipator
56  12  31   2          !dissipator

PROPS
1 FRAME                                          !CONFINING BEAMS
 1 0 0 4 2 1                                     !basic parameters
 20.E9  0.733E9  0.01000  0.01000  2.08e-6  00   !elastic properties
 0.0  0.00  0.4  0.4                             !bi-linear & hinge
 4.16e5  -2.08e6  1344  -1344  1344  -1344       !yield properties
 4  10  0.50  15                                 !strength degradation
 0.1  0.1  1  1                                  !hysteresis (takeda)
 0  0  20  20  20  20                           !ultimate ductilities
2 FRAME                                          !EXTERIOR BEAMS (PINNED)
 1 3 0 0 0 0                                     !basic parameters
 20.E9  0.733E9  0.04  0.04  6e-9 00  0.065  0.065  !elastic properties
3 FRAME                                          !EXTERIOR BEAM STIFFENERS
 1 0 0 37 0 0                                    !basic parameters
 20.E9  0.733E9  0.04  0.04  20e-8 00  0.065  0.065  !elastic properties
 0.00  0.000  0.065  0.065                       !bi-linear & hinge
 4.16e5  -2.08e5  0.10  -0.10  0.10  -0.10       !yield properties
 1.9  1.9  1.9  1.9                              !hysteresis (non-linear elastic power rule)
4 FRAME                                          !ELASTIC BEAM AT THE BASE
 1 0 0 0 0 0                                     !basic parameters
 20.E9  0.733E9  0.01920  0.01920  2.46e-5  00   !elastic properties
5 FRAME                                          !SHORT ELASTIC BASE ELEMENTS
 1 0 0 0 0 0                                     !basic parameters
 20.E9  0.733E9  0.032  0.16  0.00256  00        !elastic properties
6 FRAME                                          !CONFINING COLUMNS
 1 0 0  4 2 1                                    !basic parameters
 20.E9  0.733E9  0.0143  0.0143  1.21e-5  00     !elastic properties
 0.0  0.03  0.3  0.3                             !bi-linear & hinge
 1.02E6  -3.36E6  53120  -53120  53120  -53120   !yield properties
 4  10  0.50  15                                 !strength degradation
 0.1  0.1  1  1                                  !hysteresis (takeda)
 0  0  20  20  20  20                           !ultimate ductilities
7 FRAME                                          !EXTERIOR COLUMNS WITH HINGE AT BASE
 1 0 0  4 2 1                                    !parameters
 20.E9  0.733E9  0.036  0.036  2.59e-5  00       !elastic properties
 0.0  0.003  0.1  0.1                            !bi-linear & hinge
 1.02E6  -3.36E6  267  -267  53120  -53120       !yield properties
 4  10  0.50  15                                 !strength degradation
 0.01  0.001  1  1                               !hysteresis parameters (takeda)
 0  0  20  20  20  20                           !ultimate ductilities
8 FRAME                                          !EXTERIOR COLUMNS IN HIGHER FLOORS
 1 0 0  4 2 1                                    !parameters
 20.E9  0.733E9  0.0036  0.0036  2.59e-5  00     !elastic properties
 0.0  0.001  0.3  0.3                            !bi-linear & hinge
 1.02E6  -3.36E6  53120  -53120  53120  -53120   !yield properties
 4  10  0.50  15                                 !strength degradation
 0.1  0.1  1  1                                  !hysteresis (takeda)
```

```
 0  0  20  20  20  20                                  !ultimate ductilities
9 SPRING                                              !MASONRY
  1  33  0  0  5.00e9   0  0  000  0.01  0  -0  0  0   !basic section proprerties
 -2.00e6  1.00e5  -.003  -.03  .003  12.00e9  2  1.5   !masonry strut hysteresis
  0.033   0.023   -0.0007   -0.0036  0                 !strut data
10 SPRING                                             !VERTICAL CONTACT SPRINGS
  1  19  0 0 1.8e8 0  0  0  0  0  0  0  0  90          !spring parameters
  1  1  1.0  1.1  100 -0.00                            !hertzian contact spring parameters
11 SPRING                                             !HORIZONTAL CONTACT SPRINGS
  1  19  0 0 1.8e8 0  0  0  0  0  0  0  0  00         !spring parameters
  1  1  1.0  1.1  100 -0.00                            !hertzian contact spring parameters
12 SPRING                                             !DISSIPATORS
  1  39  0 0 7e6 0 0 0 0.07  0.07  0  0  0  90        !spring parameters
  12.00e3 -12.00e3 0 0 0 0                            !yield proprties
  0.1   0.2  20000  1.0                               !hysteresis parameters (dodd-restrepo)

WEIGHT 1
 1     0.343e3   0.343e3
 2     0.343e3   0.343e3
 3     6.008e3   6.008e3
 4     6.008e3   6.008e3
 5     6.008e3   6.008e3
 6     6.008e3   6.008e3
 7     5.665e3   5.665e3
 8     5.665e3   5.665e3
 9     0          0          0
42     0          0          0
43     3.636e3   3.636e3
44     3.636e3   3.636e3
45     3.636e3   3.636e3
46     3.636e3   3.636e3
47     3.430e3   3.430e3
48     3.430e3   3.430e3

LOADS
 1     0   -0.343e3   0
 2     0   -0.343e3   0
 3     0   -6.008e3   0
 4     0   -6.008e3   0
 5     0   -6.008e3   0
 6     0   -6.008e3   0
 7     0   -5.665e3   0
 8     0   -5.665e3   0
 9     0    0         0
42     0    0         0
43     0   -3.636e3   0
44     0   -3.636e3   0
45     0   -3.636e3   0
46     0   -3.636e3   0
47     0   -3.430e3   0
48     0   -3.430e3   0


EQUAKE
3  1  0.0  1 -1  0  0  1
```

B.2 ModelPHND

This model modifies the basic ModelPH removing the two dissipators there. The number of elements is therefore reduced from 56 to 54. there are also changes in the section ELEMENTS from the basic file ModelPH.

```
THREE STOREY ROCKING WALL WITHOUT DISSIPATORS AND PERFECT HINGES
...
48  54 12  8  8  0  9.81  0.0  0.0  0.000020  35   !FRAME AND TIME-HISTORY
...
...
ELEMENTS
  1    5  15   1          !shortbeam
  2    5   2  16          !shortbeam
  3    4   1  32          !base beam
  4    4  32  33          !base beam
  5    4  33  34          !base beam
  6    4  34  35          !base beam
  7    4  35  36          !base beam
  8    4  36  37          !base beam
  9    4  37  38          !base beam
 10    4  38  39          !base beam
 11    4  39  40          !base beam
 12    4  40   2          !base beam
 13    6   1   3          !column first level
 14    6   2   4          !column first level
 15    1   3   4          !confining beam
 16    9   1   4          !masonry first level
 17    9   2   3          !masonry first level
 18    6   3   5          !column second level
 19    6   4   6          !column second level
 20    1   5   6          !confining beam
 21    9   3   6          !masonry second level
 22    9   4   5          !masonry second level
 23    6   5   7          !column third level
 24    6   6   8          !column third level
 25    1   7   8          !confining beam
 26    9   5   8          !masonry third level
 27    9   6   7          !masonry third level
 28   10  17  15          !contact vertical
 29   10  18  16          !contact vertical
 30   10  21   1          !contact vertical
 31   10  22  32          !contact vertical
 32   10  23  33          !contact vertical
 33   10  24  34          !contact vertical
 34   10  25  35          !contact vertical
 35   10  26  36          !contact vertical
 36   10  27  37          !contact vertical
 37   10  28  38          !contact vertical
 38   10  29  39          !contact vertical
 39   10  30  40          !contact vertical
 40   10  31   2          !contact vertical
 41   11  19  15          !contacthorizontal
```

```
42  11  20  16          !contacthorizontal
43   7  41  43          !exterior column first
44   7  42  44          !exterior column first
45   8  43  45          !exterior column second
46   8  44  46          !exterior column second
47   8  45  47          !exterior column third
48   8  46  48          !exterior column third
49   2  43   3          !exterior beam first
50   2  44   4          !exterior beam first
51   2  45   5          !exterior beam second
52   2  46   6          !exterior beam second
53   2  47   7          !exterior beam third
54   2  48   8          !exterior beam third

PROPS
...
...
EQUAKE
3  1  0.0  1 -1  0  0  1
```

B.3 ModelSH

This model is similar to the basic ModelPH but incorporates the "stiffeners" in parallel to the slab-beams. The number of elelements, therefore is increased from 56 to 62 and the section Elements is changed as well.

```
THREE STOREY ROCKING WALL WITH DISSIPATORS AND STIFFENERS
...
48  62  12  8  8  0  9.81  0.0  0.0  0.000020  35        !FRAME AND TIME-HISTORY
...

ELEMENTS
 1   5  15   1          !shortbeam
 2   5   2  16          !shortbeam
 3   4   1  32          !base beam
 4   4  32  33          !base beam
 5   4  33  34          !base beam
 6   4  34  35          !base beam
 7   4  35  36          !base beam
 8   4  36  37          !base beam
 9   4  37  38          !base beam
10   4  38  39          !base beam
11   4  39  40          !base beam
12   4  40   2          !base beam
13   6   1   3          !column first level
14   6   2   4          !column first level
15   1   3   4          !confining beam
```

```
16   9   1   4        !masonry first level
17   9   2   3        !masonry first level
18   6   3   5        !column second level
19   6   4   6        !column second level
20   1   5   6        !confining beam
21   9   3   6        !masonry second level
22   9   4   5        !masonry second level
23   6   5   7        !column third level
24   6   6   8        !column third level
25   1   7   8        !confining beam
26   9   5   8        !masonry third level
27   9   6   7        !masonry third level
28  10  17  15        !contact vertical
29  10  18  16        !contact vertical
30  10  21   1        !contact vertical
31  10  22  32        !contact vertical
32  10  23  33        !contact vertical
33  10  24  34        !contact vertical
34  10  25  35        !contact vertical
35  10  26  36        !contact vertical
36  10  27  37        !contact vertical
37  10  28  38        !contact vertical
38  10  29  39        !contact vertical
39  10  30  40        !contact vertical
40  10  31   2        !contact vertical
41  11  19  15        !contact horizontal
42  11  20  16        !contact horizontal
43   7  41  43        !exterior column first
44   7  42  44        !exterior column first
45   8  43  45        !exterior column second
46   8  44  46        !exterior column second
47   8  45  47        !exterior column third
48   8  46  48        !exterior column third
49   2  43   3        !exterior beam first
50   2  44   4        !exterior beam first
51   2  45   5        !exterior beam second
52   2  46   6        !exterior beam second
53   2  47   7        !exterior beam third
54   2  48   8        !exterior beam third
55  12  21   1        !dissipator
56  12  31   2        !dissipator
57   3  43   3        !stiffener exterior beam first
58   3  44   4        !stiffener exterior beam first
59   3  45   5        !stiffener exterior beam second
60   3  46   6        !stiffener exterior beam second
61   3  47   7        !stiffener exterior beam third
62   3  48   8        !stiffener exterior beam third
...
EQUAKE
3  1  0.0  1 -1  0  0  1
```

B.4 ModelSHND

This model incorporates the "stiffeners" but removes the dissipators. The number of elements is now 60.

```
THREE STOREY ROCKING WALL WITHOUT DISSIPATORS AND WITH STIFFENERS
...
48 60 12 8 8 0 9.81 0.0 0.0 0.000020 35          !FRAME AND TIME-HISTORY
...
...
ELEMENTS
 1  5 15  1          !shortbeam
 2  5  2 16          !shortbeam
 3  4  1 32          !base beam
 4  4 32 33          !base beam
 5  4 33 34          !base beam
 6  4 34 35          !base beam
 7  4 35 36          !base beam
 8  4 36 37          !base beam
 9  4 37 38          !base beam
10  4 38 39          !base beam
11  4 39 40          !base beam
12  4 40  2          !base beam
13  6  1  3          !column first level
14  6  2  4          !column first level
15  1  3  4          !confining beam
16  9  1  4          !masonry first level
17  9  2  3          !masonry first level
18  6  3  5          !column second level
19  6  4  6          !column second level
20  1  5  6          !confining beam
21  9  3  6          !masonry second level
22  9  4  5          !masonry second level
23  6  5  7          !column third level
24  6  6  8          !column third level
25  1  7  8          !confining beam
26  9  5  8          !masonry third level
27  9  6  7          !masonry third level
28 10 17 15          !contact vertical
29 10 18 16          !contact vertical
30 10 21  1          !contact vertical
31 10 22 32          !contact vertical
32 10 23 33          !contact vertical
33 10 24 34          !contact vertical
34 10 25 35          !contact vertical
35 10 26 36          !contact vertical
36 10 27 37          !contact vertical
37 10 28 38          !contact vertical
38 10 29 39          !contact vertical
39 10 30 40          !contact vertical
40 10 31  2          !contact vertical
41 11 19 15          !contacthorizontal
42 11 20 16          !contacthorizontal
43  7 41 43          !exterior column first
44  7 42 44          !exterior column first
```

```
45   8  43  45          !exterior column second
46   8  44  46          !exterior column second
47   8  45  47          !exterior column third
48   8  46  48          !exterior column third
49   2  43   3          !exterior beam first
50   2  44   4          !exterior beam first
51   2  45   5          !exterior beam second
52   2  46   6          !exterior beam second
53   2  47   7          !exterior beam third
54   2  48   8          !exterior beam third
55   3  43   3          !stiffener exterior beam first
56   3  44   4          !stiffener exterior beam first
57   3  45   5          !stiffener exterior beam second
58   3  46   6          !stiffener exterior beam second
59   3  47   7          !stiffener exterior beam third
60   3  48   8          !stiffener exterior beam third

PROPS
...
EQUAKE
3  1  0.0  1 -1  0  0  1
```

Appendix C Results from the Dynamic Tests

In the next pages, selected plots are presented from all the significant dynamic tests conducted as described in Chapter 5. From the 60 runs conducted, 54 are shown here. The other six runs are cases where the specimen was either hit or displaced very slowly to acquire some preliminary information. Some relevant information is also presented along with the plots of each test. A concise summary of all the tests can be found in Chapter 6. The scale of the plots has been tried to maintain constant to ease the comparison between different tests. Only run 54, which was the case where the specimen reached its larger lateral displacement, has greater limits in the plots.

RUN # 5

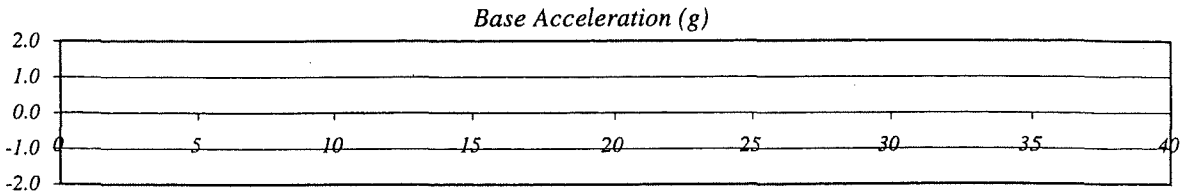

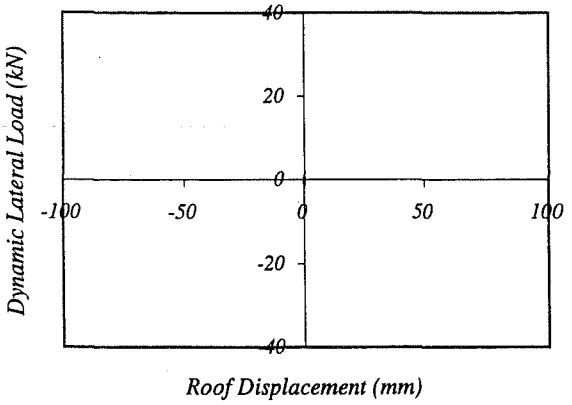

Wall with 1st set of dissipators

Basic Input Ground Motion (BIGM):	*White Noise 1*
Scaling Factor for BIGM:	0.10
Expected Peak Table Acceleration:	0.01 g
Measured Peak Table Acceleration:	0.03 g
Peak Roof Hor. Acceleration:	0.06 g
Peak Roof Vert. Acceleration:	0.03 g
Peak Roof Displacement:	1 mm
Peak Average Drift:	0.02 %
Residual Roof Displacement:	0 mm
Max. Total Inertial Lat. Load:	1.89 kN

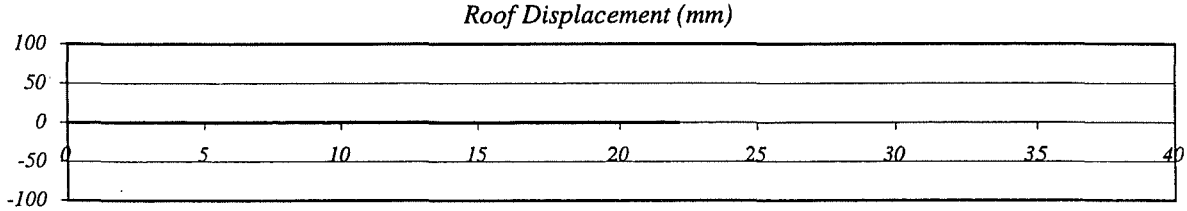

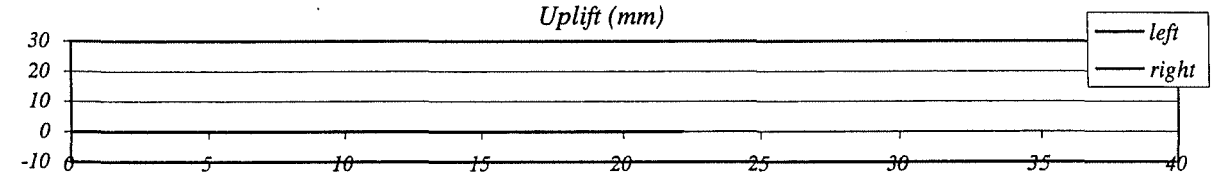

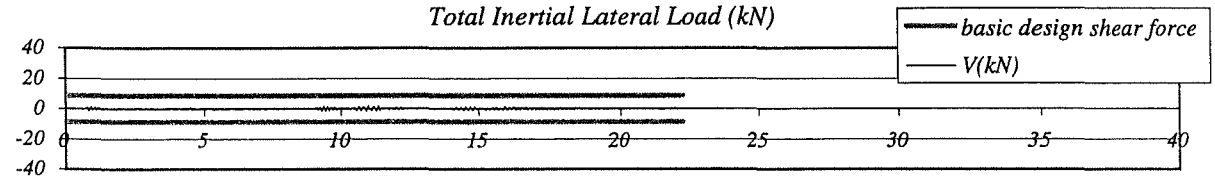

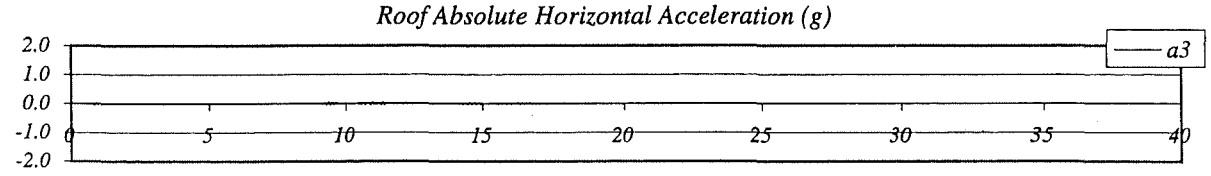

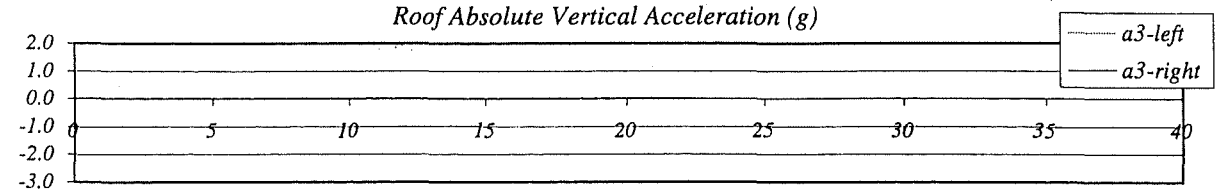

RUN # 6

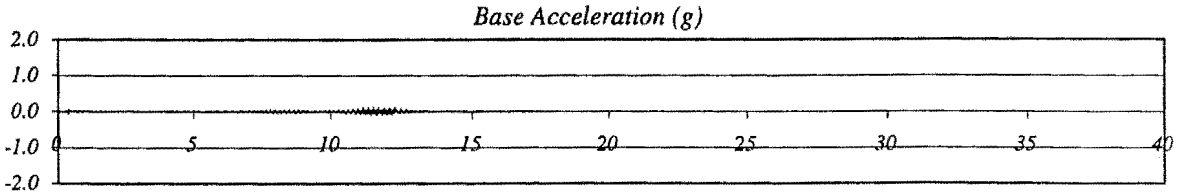

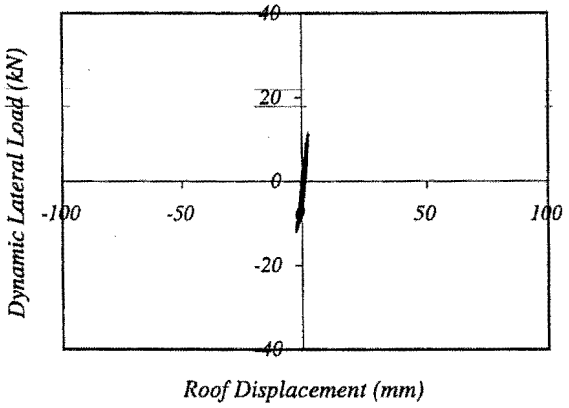

Wall with 1st set of dissipators

Basic Input Ground Motion (BIGM):	*White Noise 1*
Scaling Factor for BIGM:	0.50
Expected Peak Table Acceleration:	0.03 g
Measured Peak Table Acceleration:	0.14 g
Peak Roof Hor. Acceleration:	0.33 g
Peak Roof Vert. Acceleration:	0.15 g
Peak Roof Displacement:	3 mm
Peak Average Drift:	0.08 %
Residual Roof Displacement:	0 mm
Max. Total Inertial Lat. Load:	12.17 kN

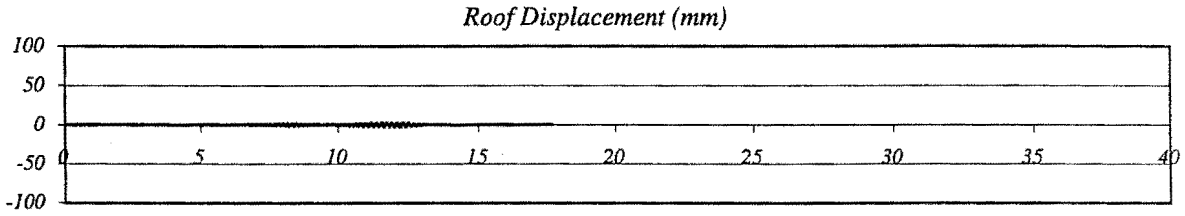

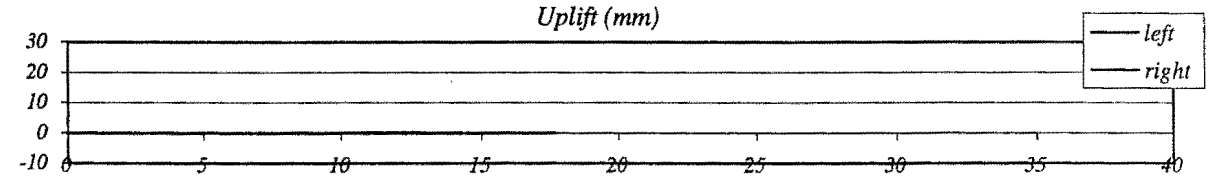

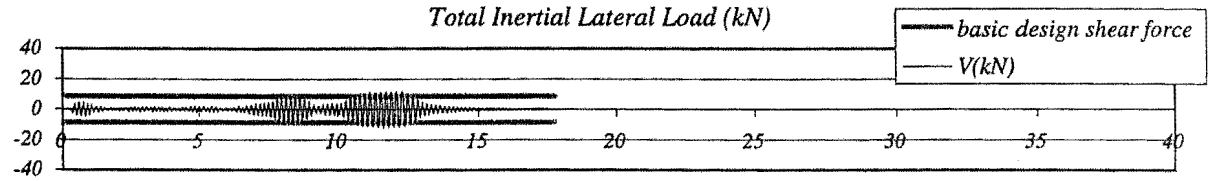

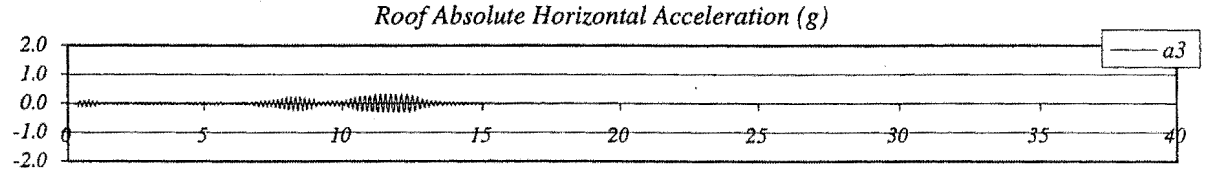

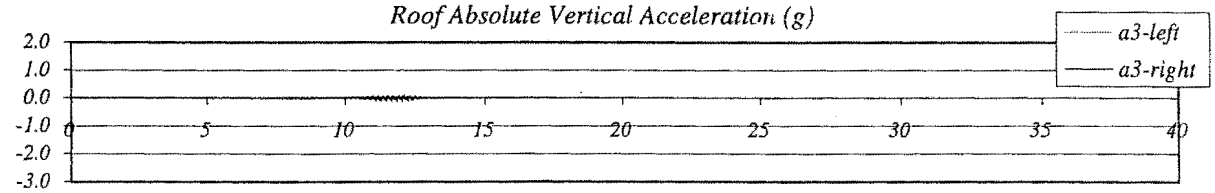

RUN # 7

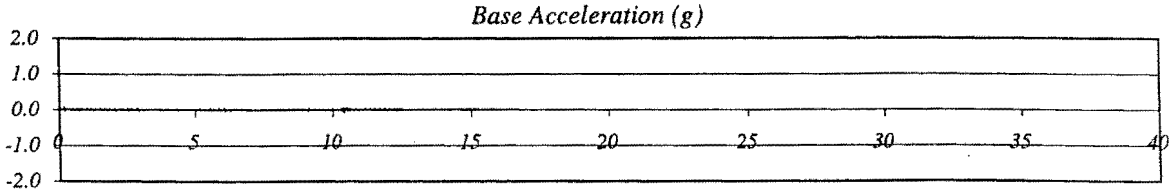

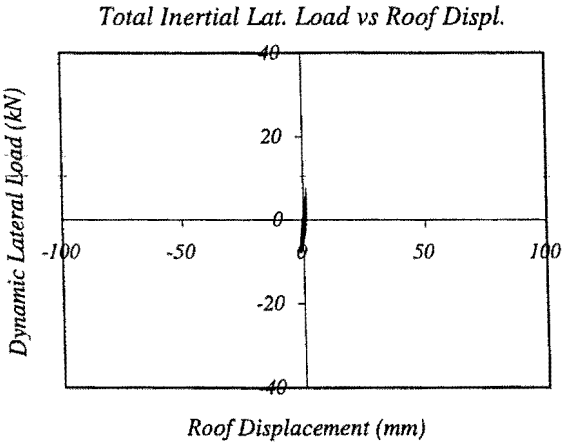

Wall with 1st set of dissipators

Basic Input Ground Motion (BIGM):	*White Noise 2*
Scaling Factor for BIGM:	0.50
Expected Peak Table Acceleration:	0.03 g
~~Measured Peak Table Acceleration:~~	~~0.09 g~~
Peak Roof Hor. Acceleration:	0.22 g
Peak Roof Vert. Acceleration:	0.04 g
Peak Roof Displacement:	1 mm
Peak Average Drift:	0.04 %
Residual Roof Displacement:	0 mm
Max. Total Inertial Lat. Load:	7.93 kN

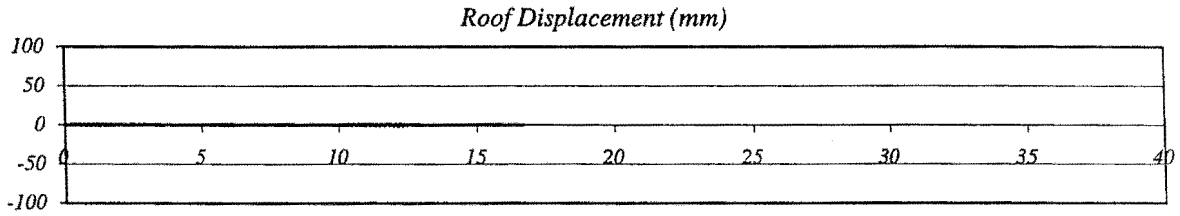

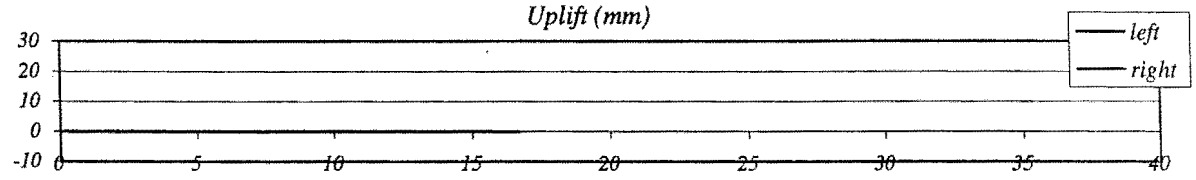

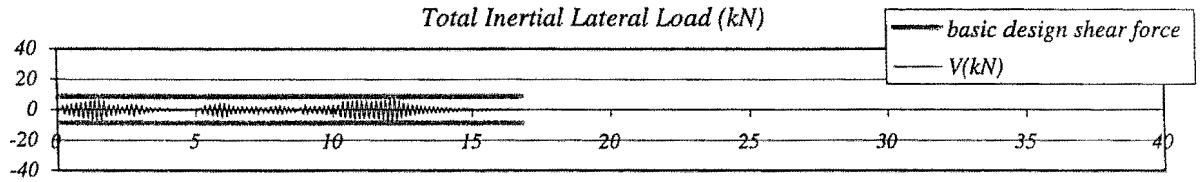

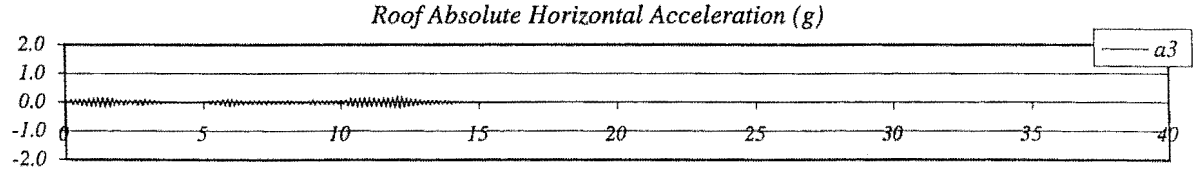

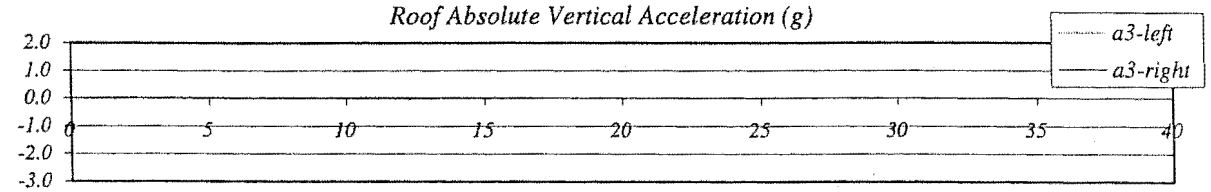

RUN # 8

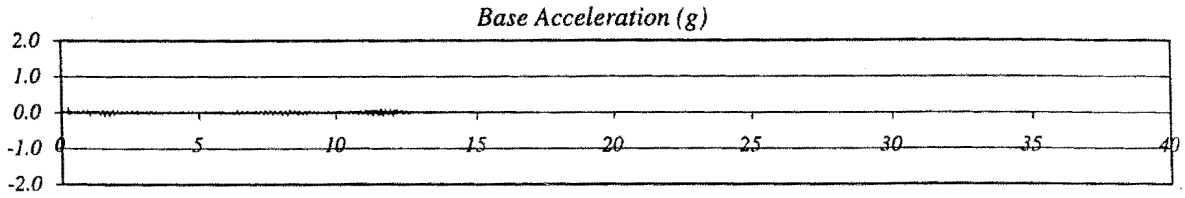

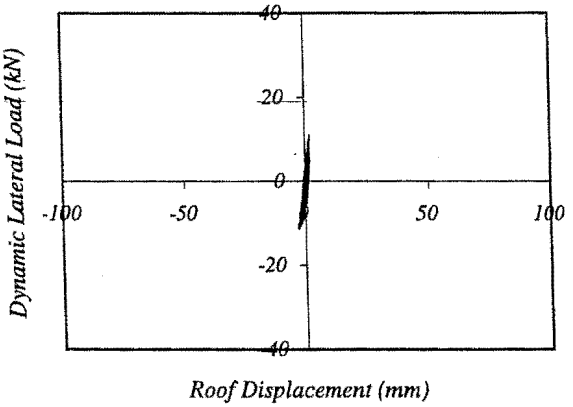

Wall with 1st set of dissipators

Basic Input Ground Motion (BIGM):	*White Noise 2*
Scaling Factor for BIGM:	1.00
~~Expected Peak Table Acceleration:~~	~~0.05 g~~
Measured Peak Table Acceleration:	0.13 g
Peak Roof Hor. Acceleration:	0.30 g
Peak Roof Vert. Acceleration:	0.14 g
Peak Roof Displacement:	3 mm
Peak Average Drift:	0.08 %
Residual Roof Displacement:	0 mm
Max. Total Inertial Lat. Load:	11.52 kN

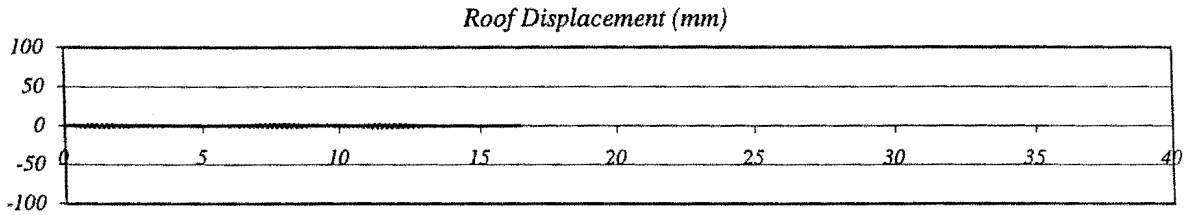

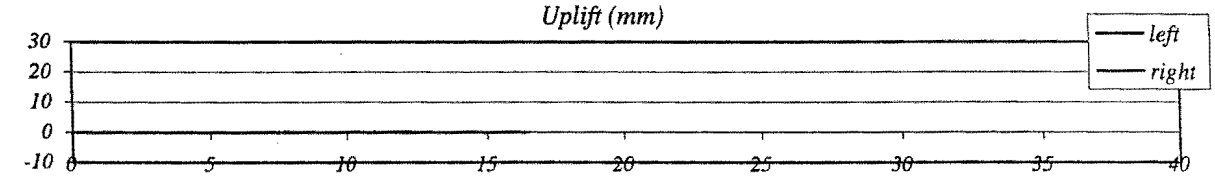

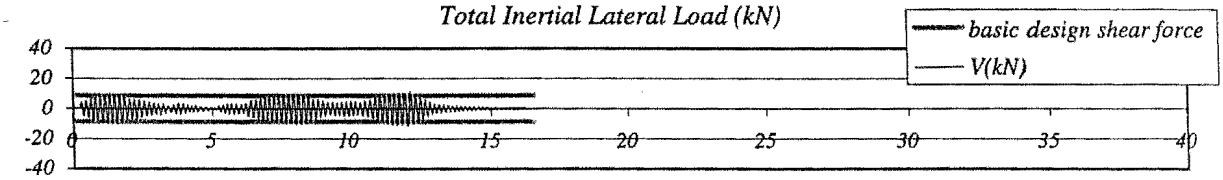

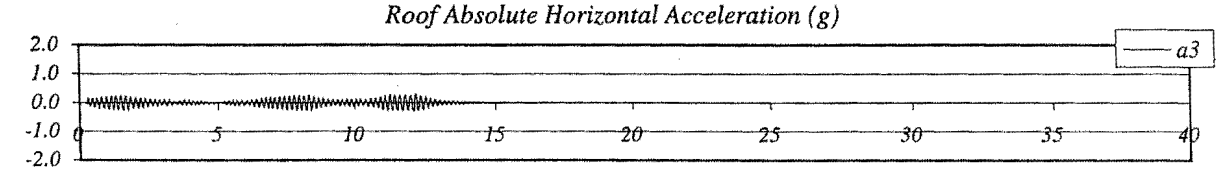

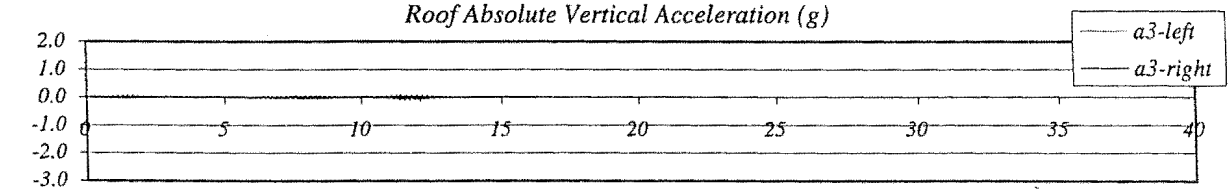

RUN # 9

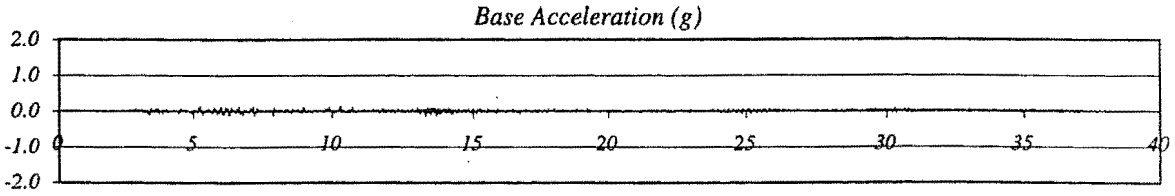

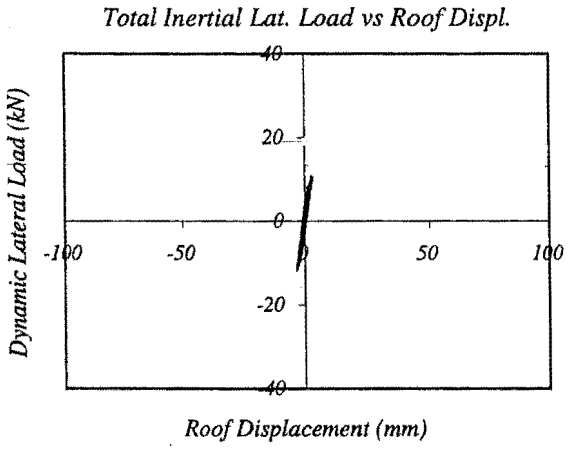

Wall with 1st set of dissipators

Basic Input Ground Motion (BIGM):	*Taft 111*
Scaling Factor for BIGM:	0.50
Expected Peak Table Acceleration:	0.09 g
Measured Peak Table Acceleration:	0.14 g
Peak Roof Hor. Acceleration:	0.34 g
Peak Roof Vert. Acceleration:	0.15 g
Peak Roof Displacement:	4 mm
Peak Average Drift:	0.10 %
Residual Roof Displacement:	0 mm
Max. Total Inertial Lat. Load:	11.91 kN

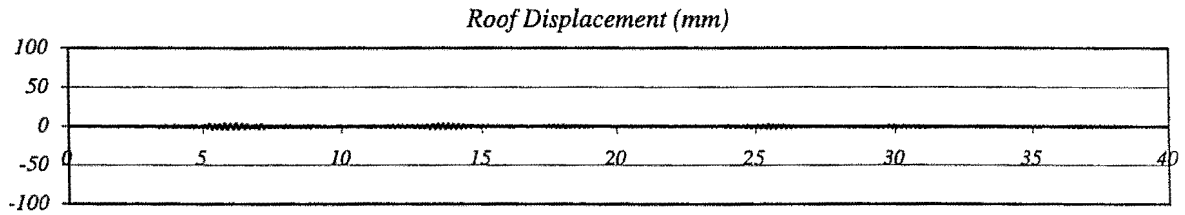

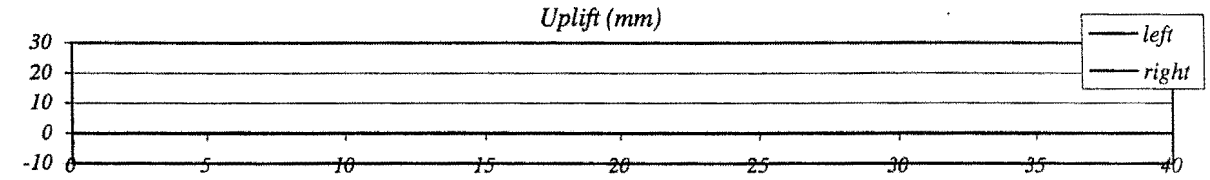

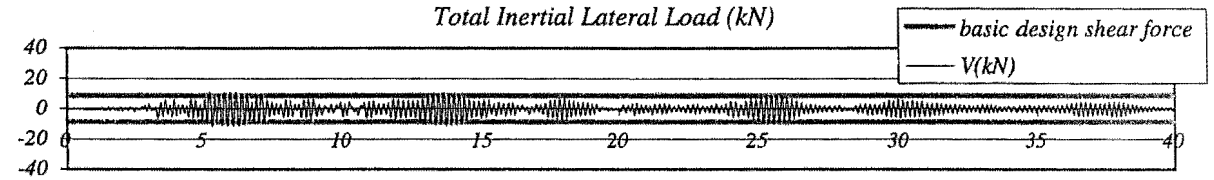

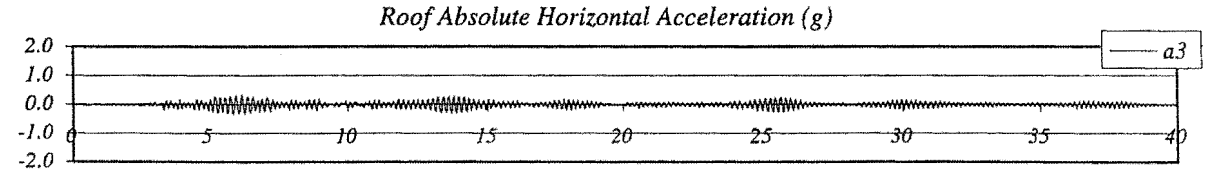

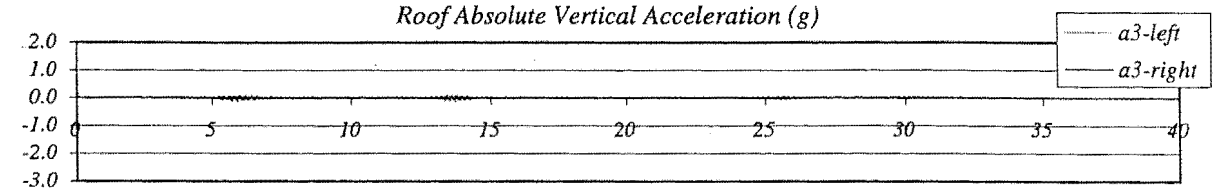

RUN # 12

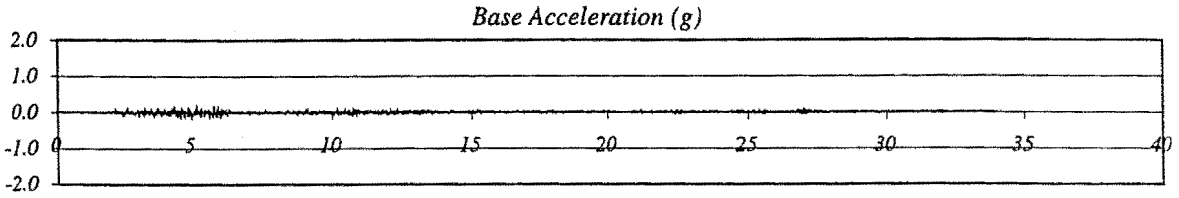

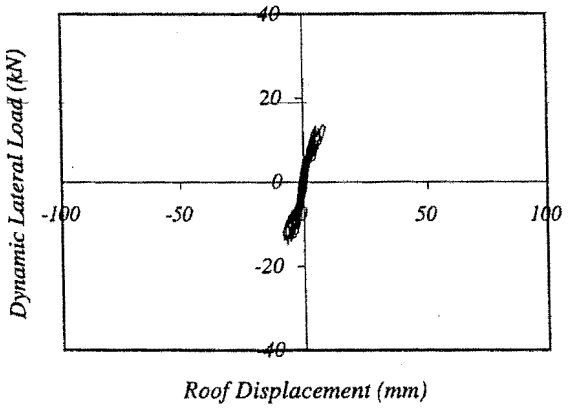

Wall with 1st set of dissipators

Basic Input Ground Motion (BIGM):	*Taft 021*
Scaling Factor for BIGM:	0.50
~~Expected Peak Table Acceleration:~~	~~0.08 g~~
Measured Peak Table Acceleration:	0.22 g
Peak Roof Hor. Acceleration:	0.47 g
Peak Roof Vert. Acceleration:	0.38 g
Peak Roof Displacement:	9 mm
Peak Average Drift:	0.25 %
Residual Roof Displacement:	1 mm
Max. Total Inertial Lat. Load:	14.85 kN

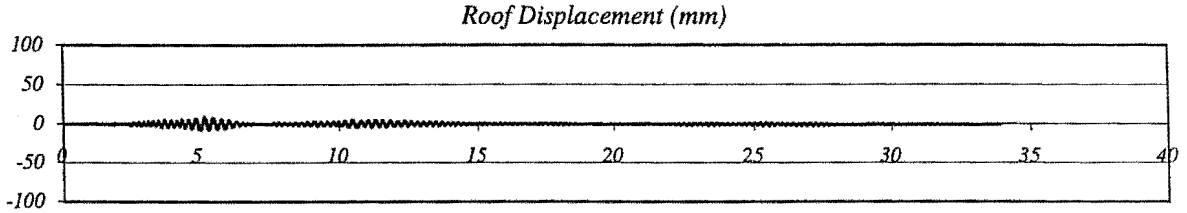

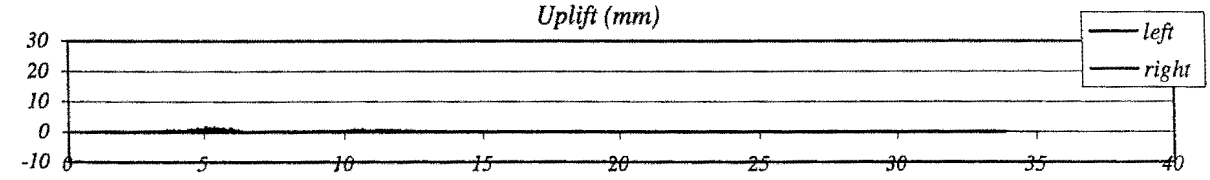

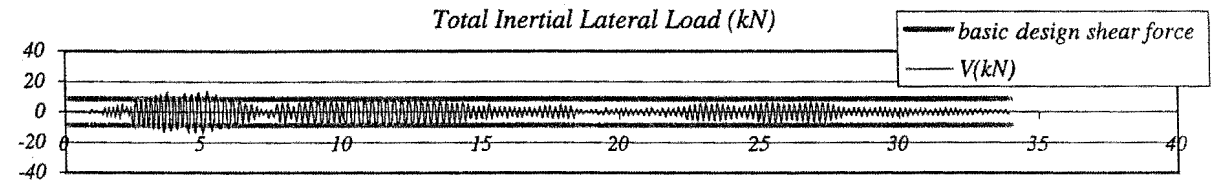

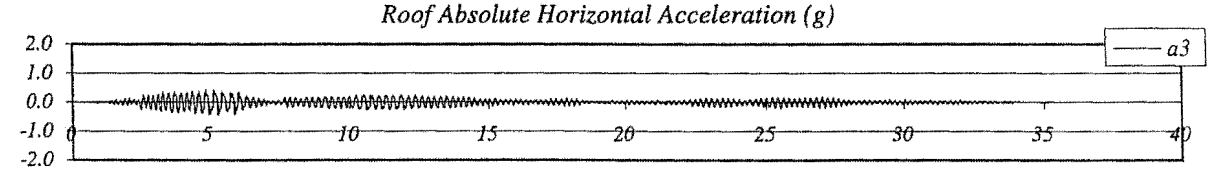

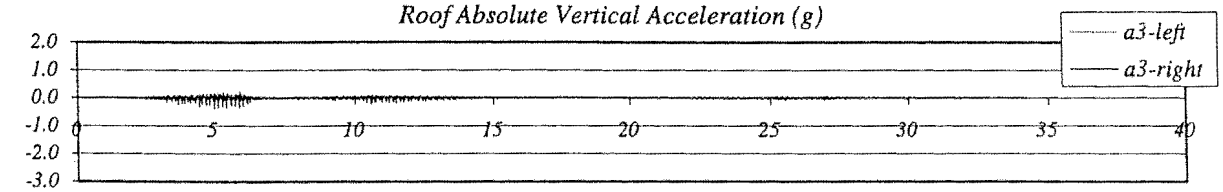

RUN # 13

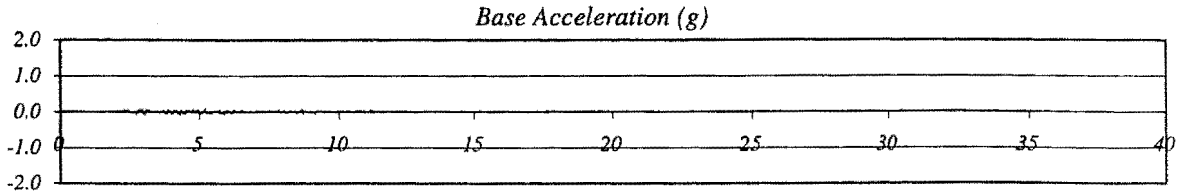

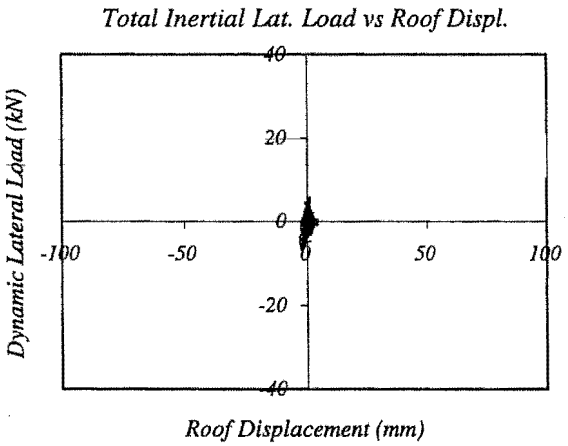

Wall with 1st set of dissipators

Basic Input Ground Motion (BIGM):	*Saticoy 000*
Scaling Factor for BIGM:	0.10
Expected Peak Table Acceleration:	0.05 g
Measured Peak Table Acceleration:	0.10 g
Peak Roof Hor. Acceleration:	0.21 g
Peak Roof Vert. Acceleration:	0.06 g
Peak Roof Displacement:	5 mm
Peak Average Drift:	0.13 %
Residual Roof Displacement:	2 mm
Max. Total Inertial Lat. Load:	7.20 kN

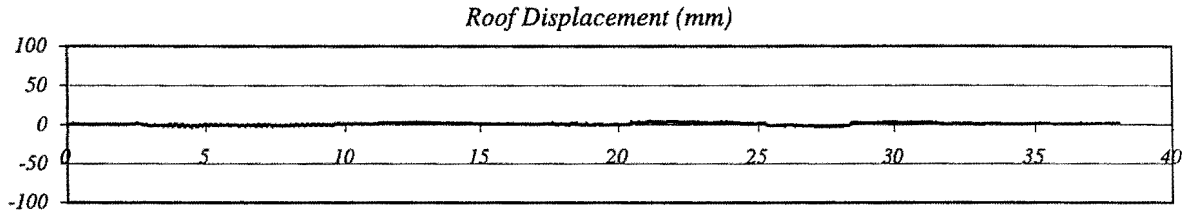

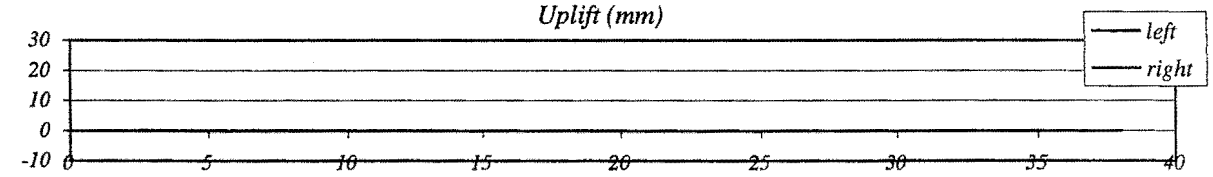

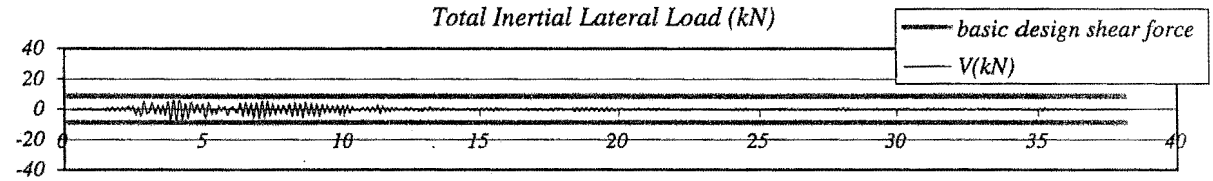

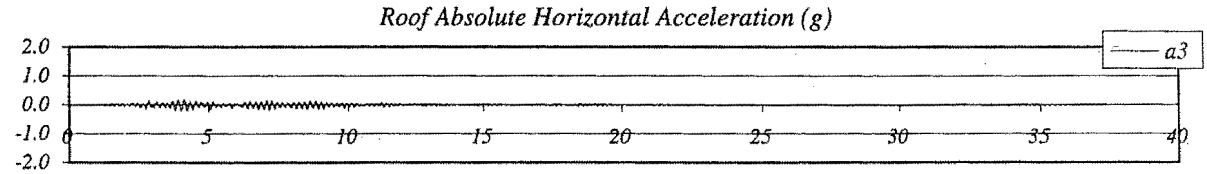

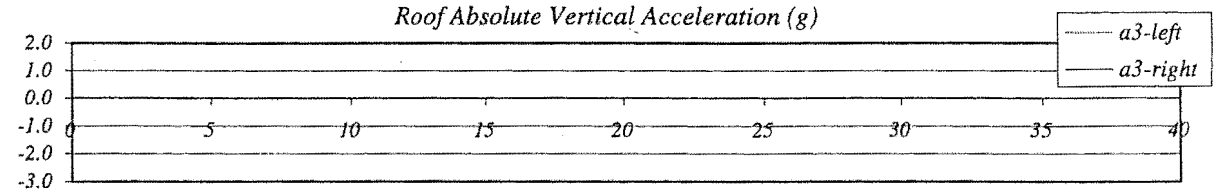

RUN # 14

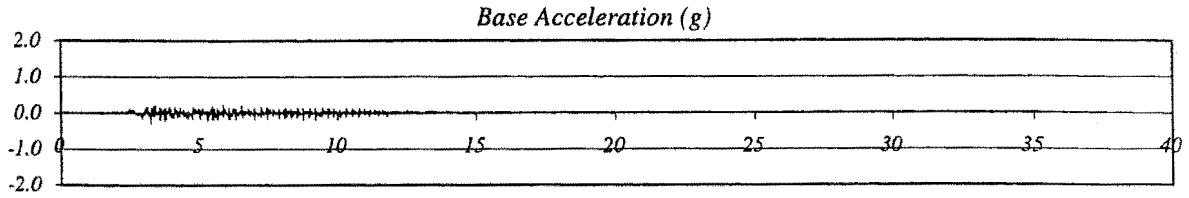

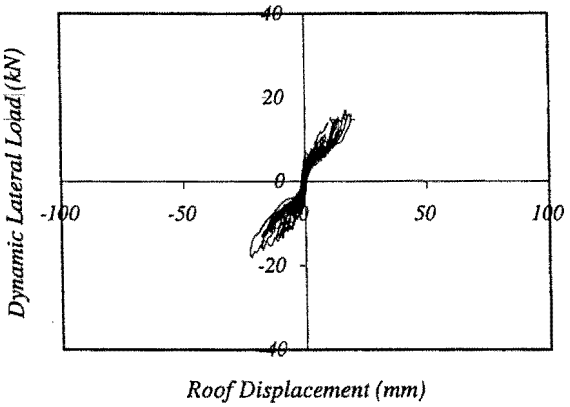

Wall with 1st set of dissipators

Basic Input Ground Motion (BIGM):	*Saticoy 000*
Scaling Factor for BIGM:	0.25
Expected Peak Table Acceleration:	0.11 g
Measured Peak Table Acceleration:	0.29 g
Peak Roof Hor. Acceleration:	0.53 g
Peak Roof Vert. Acceleration:	0.63 g
Peak Roof Displacement:	23 mm
Peak Average Drift:	0.62 %
Residual Roof Displacement:	0 mm
Max. Total Inertial Lat. Load:	18.04 kN

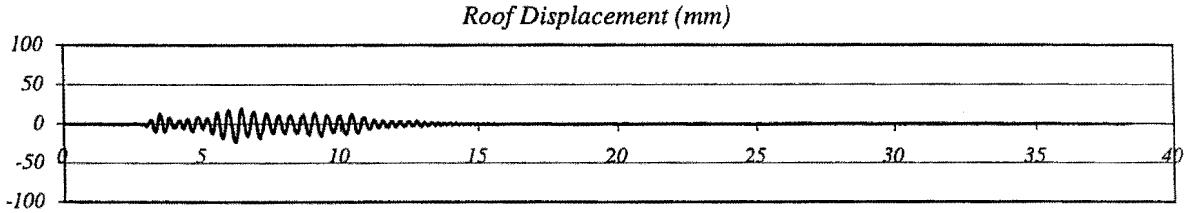

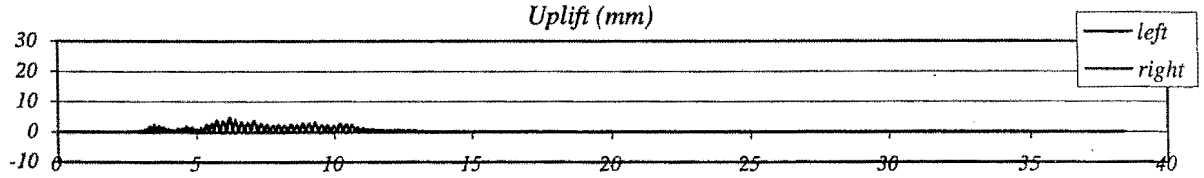

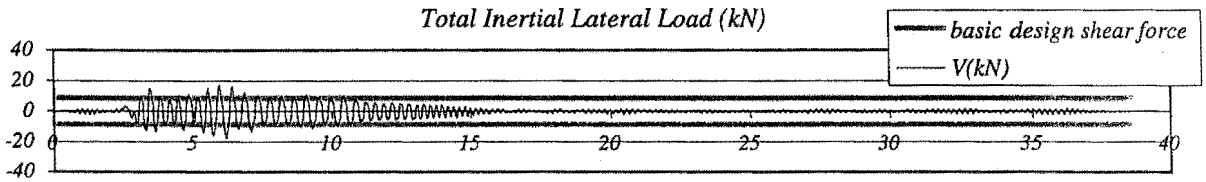

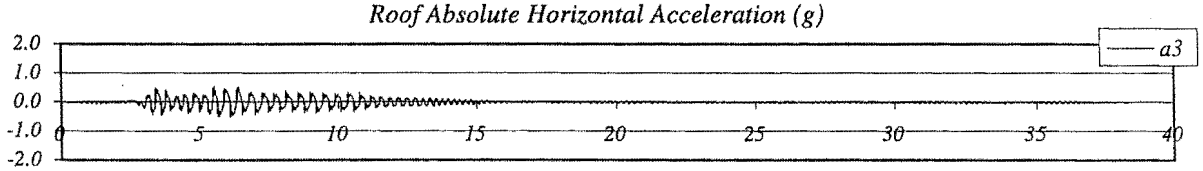

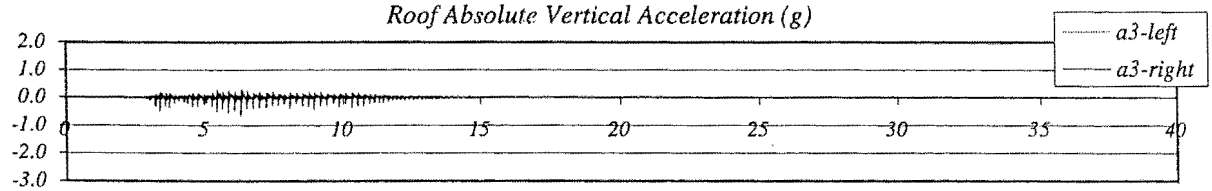

RUN # 15

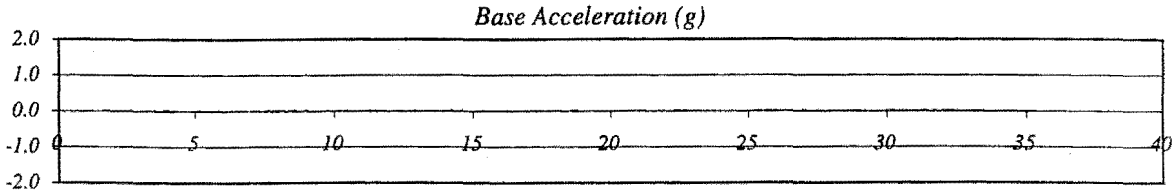

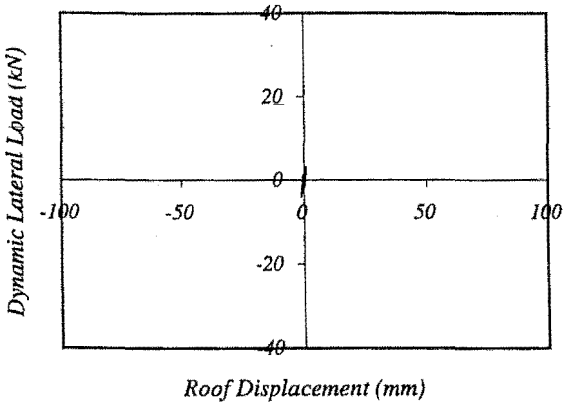

Wall with 1st set of dissipators

Basic Input Ground Motion (BIGM):	*Taft 111*
Scaling Factor for BIGM:	0.10
Expected Peak Table Acceleration:	0.02 g
Measured Peak Table Acceleration:	0.05 g
Peak Roof Hor. Acceleration:	0.12 g
Peak Roof Vert. Acceleration:	0.04 g
Peak Roof Displacement:	1 mm
Peak Average Drift:	0.03 %
Residual Roof Displacement:	0 mm
Max. Total Inertial Lat. Load:	4.11 kN

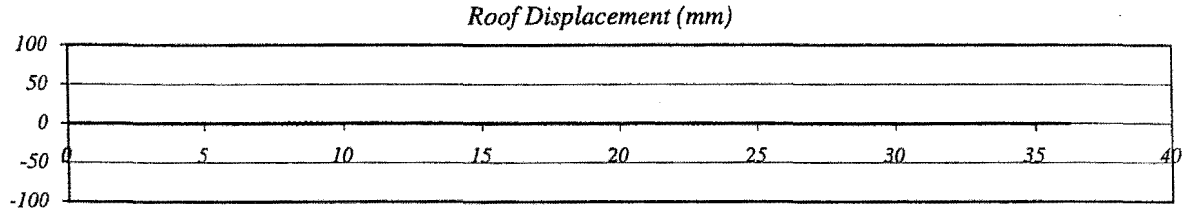

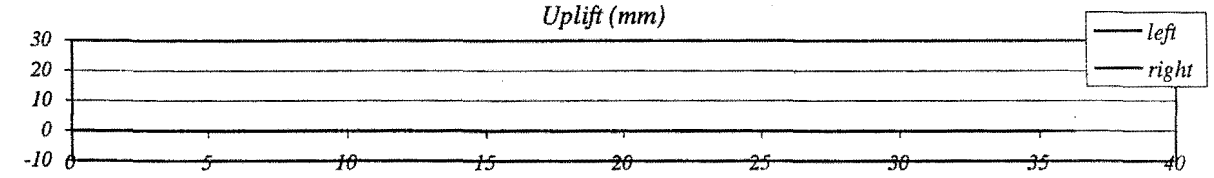

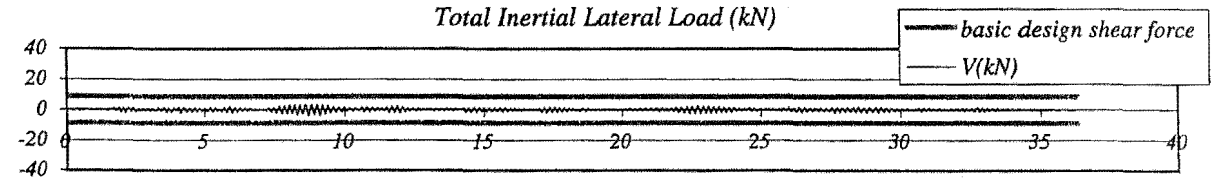

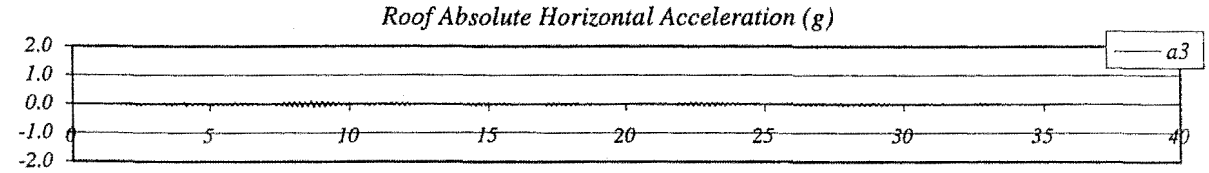

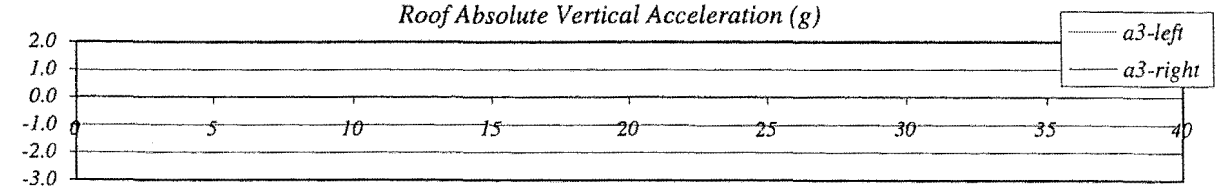

RUN # 16

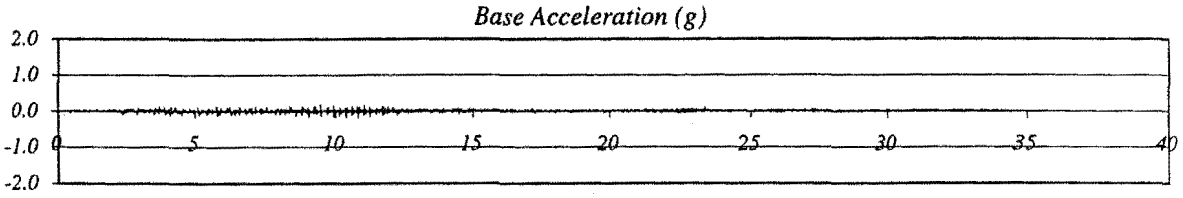

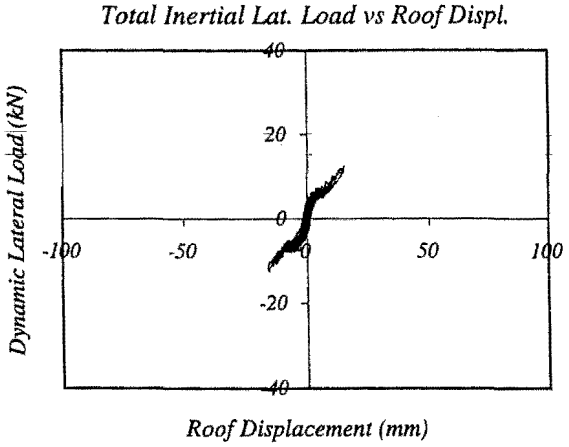

Wall with 1st set of dissipators

Basic Input Ground Motion (BIGM):	*Taft 111*
Scaling Factor for BIGM:	0.50
Expected Peak Table Acceleration:	0.10 g
Measured Peak Table Acceleration:	0.20 g
Peak Roof Hor. Acceleration:	0.48 g
Peak Roof Vert. Acceleration:	0.43 g
Peak Roof Displacement:	16 mm
Peak Average Drift:	0.44 %
Residual Roof Displacement:	0 mm
Max. Total Inertial Lat. Load:	12.59 kN

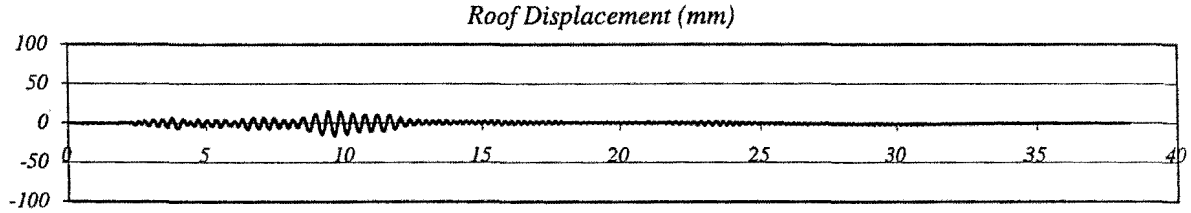

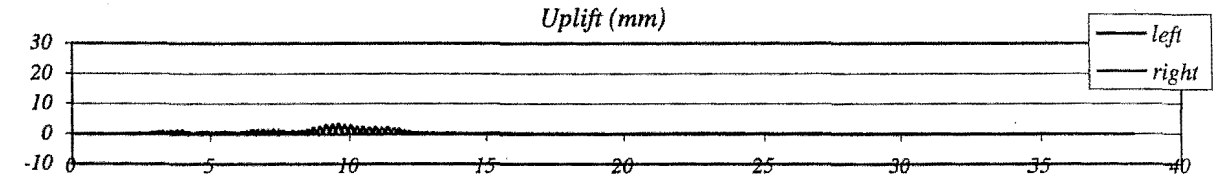

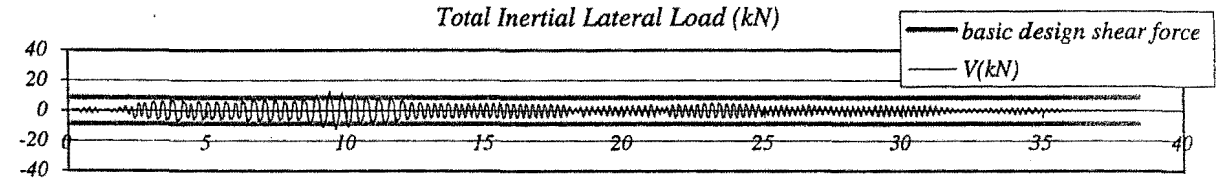

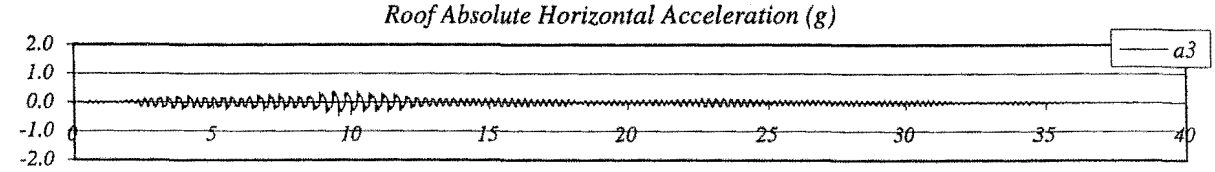

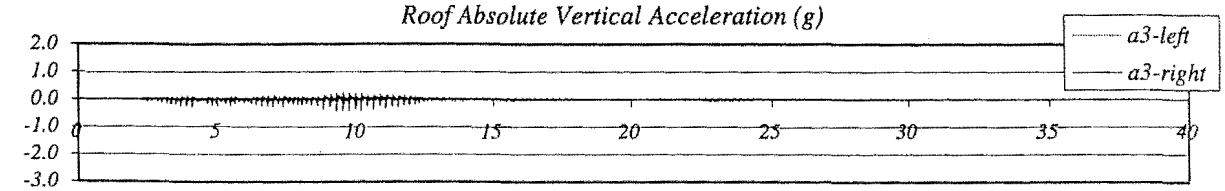

RUN # 17

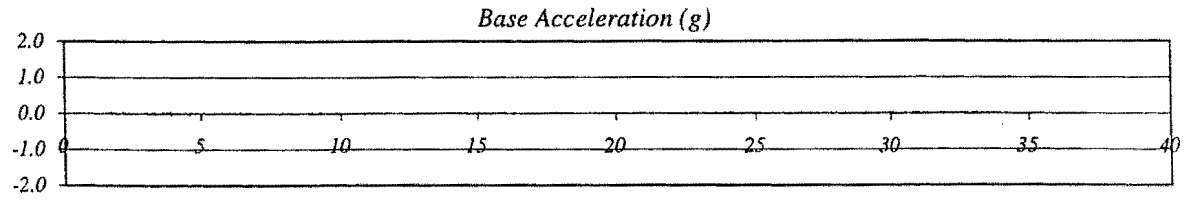

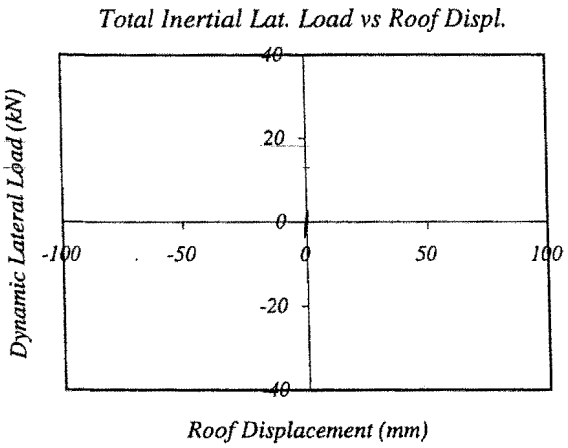

Wall with 1st set of dissipators

Basic Input Ground Motion (BIGM):	*Taft 021*
Scaling Factor for BIGM:	0.10
Expected Peak Table Acceleration:	0.02 g
Measured Peak Table Acceleration:	0.06 g
Peak Roof Hor. Acceleration:	0.12 g
Peak Roof Vert. Acceleration:	0.03 g
Peak Roof Displacement:	1 mm
Peak Average Drift:	0.03 %
Residual Roof Displacement:	0 mm
Max. Total Inertial Lat. Load:	3.75 kN

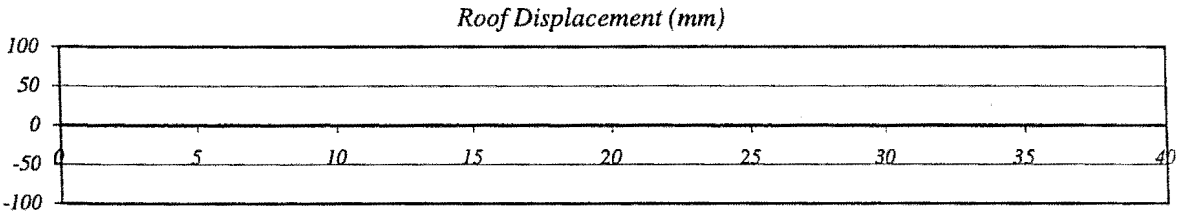

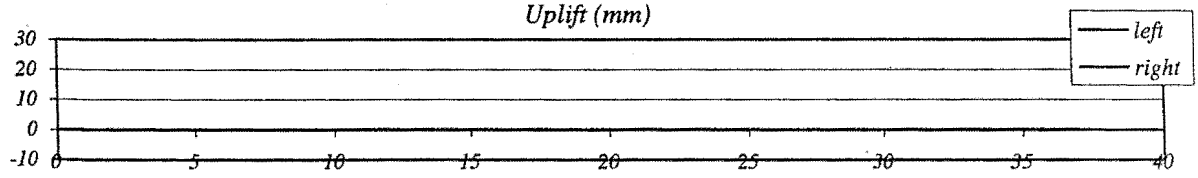

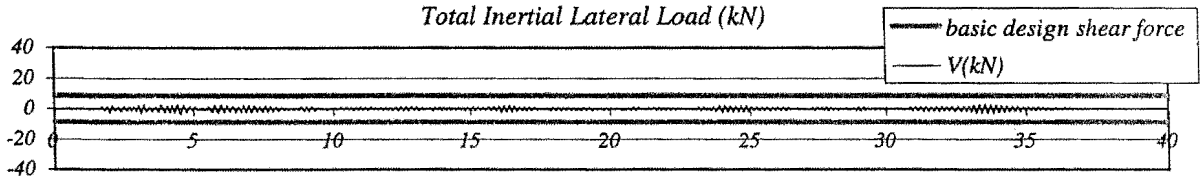

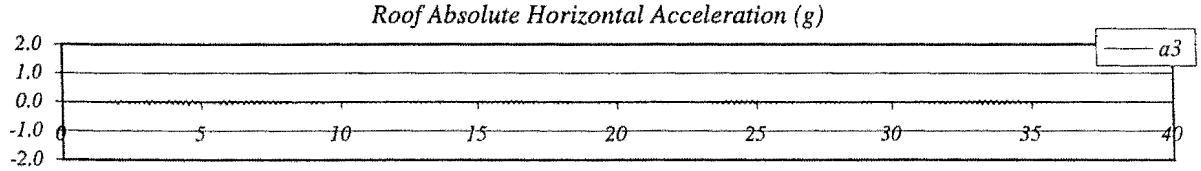

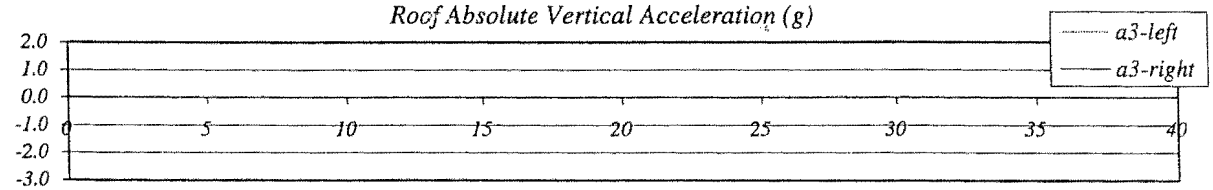

RUN # 18

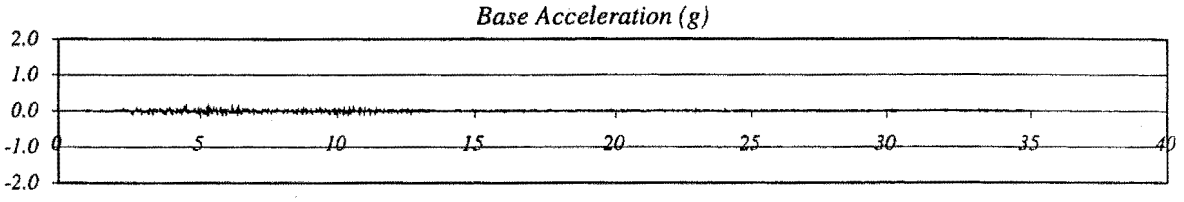

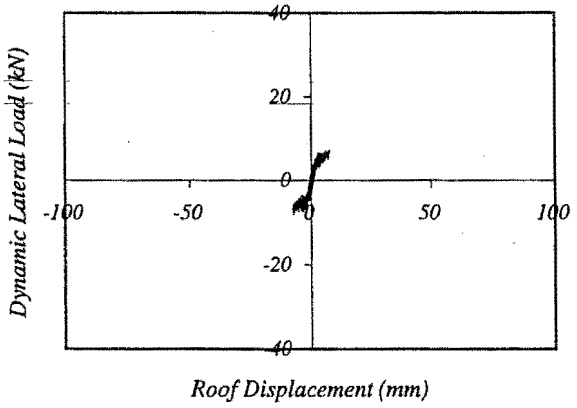

Wall with 1st set of dissipators

Basic Input Ground Motion (BIGM):	*Taft 021*
Scaling Factor for BIGM:	0.50
Expected Peak Table Acceleration:	0.08 g
Measured Peak Table Acceleration:	0.20 g
Peak Roof Hor. Acceleration:	0.31 g
Peak Roof Vert. Acceleration:	0.31 g
Peak Roof Displacement:	8 mm
Peak Average Drift:	0.21 %
Residual Roof Displacement:	0 mm
Max. Total Inertial Lat. Load:	8.12 kN

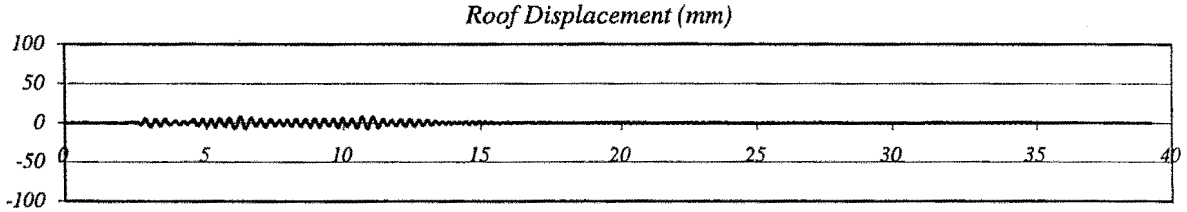

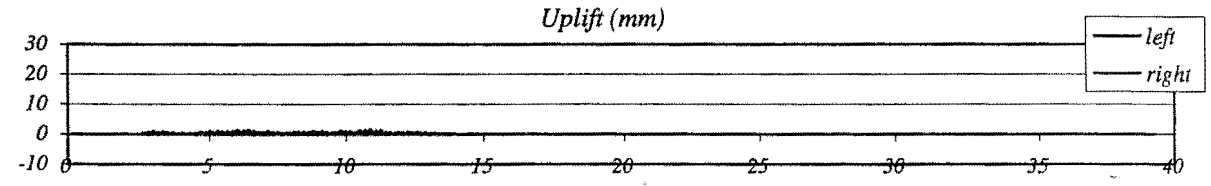

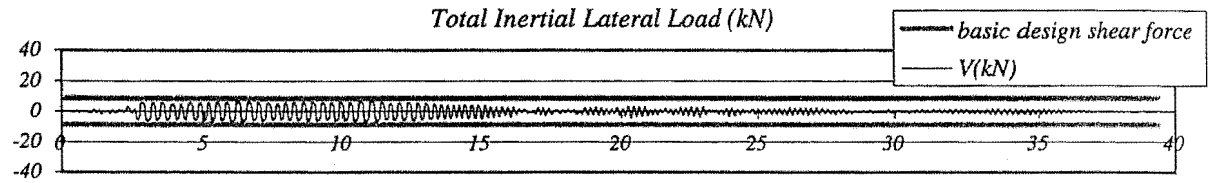

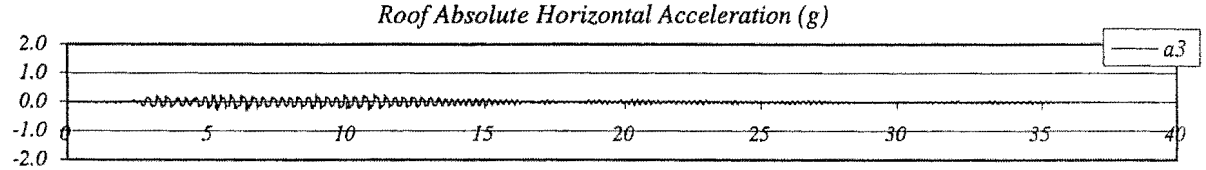

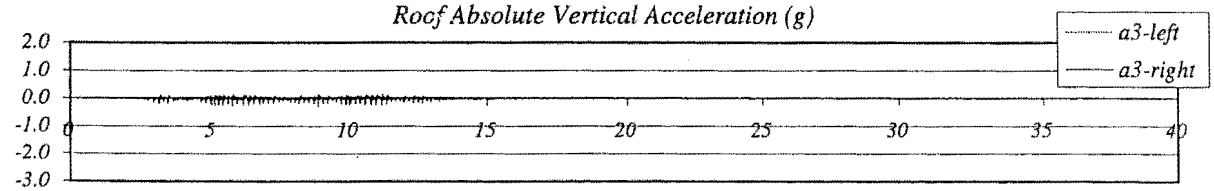

RUN # 19

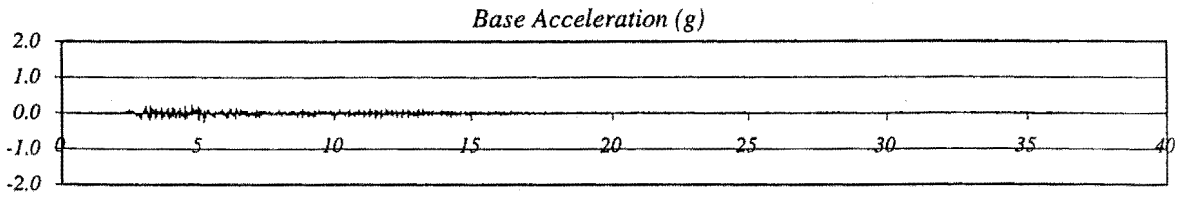

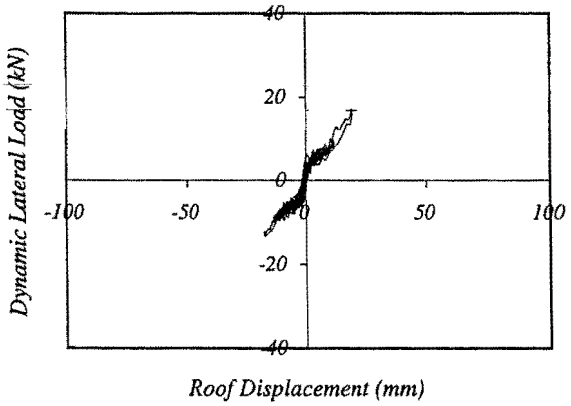

Wall with 1st set of dissipators

Basic Input Ground Motion (BIGM):	*Saticoy 000*
Scaling Factor for BIGM:	0.25
Expected Peak Table Acceleration:	0.11 g
Measured Peak Table Acceleration:	0.26 g
Peak Roof Hor. Acceleration:	0.47 g
Peak Roof Vert. Acceleration:	0.45 g
Peak Roof Displacement:	19 mm
Peak Average Drift:	0.51 %
Residual Roof Displacement:	0 mm
Max. Total Inertial Lat. Load:	17.11 kN

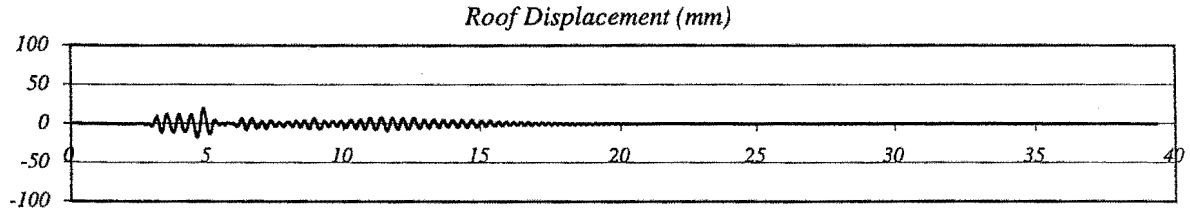

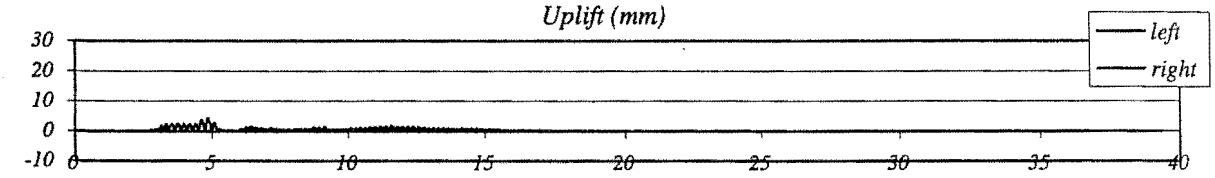

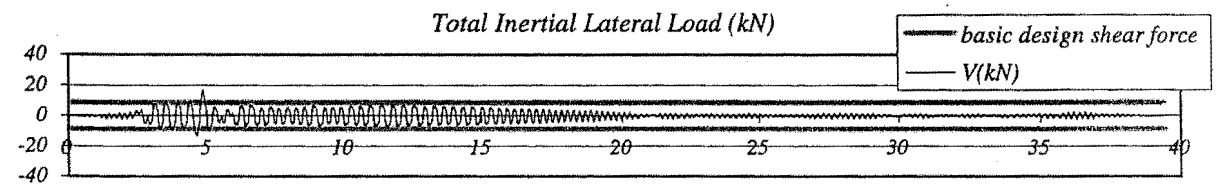

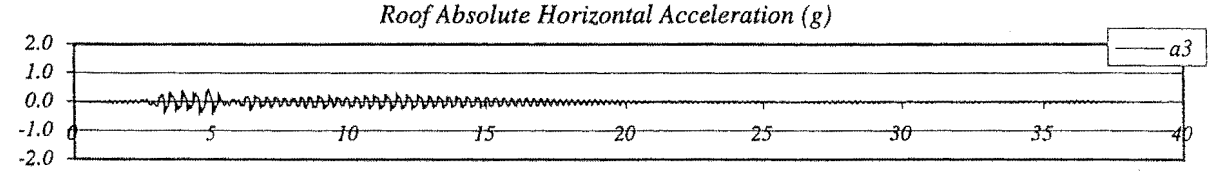

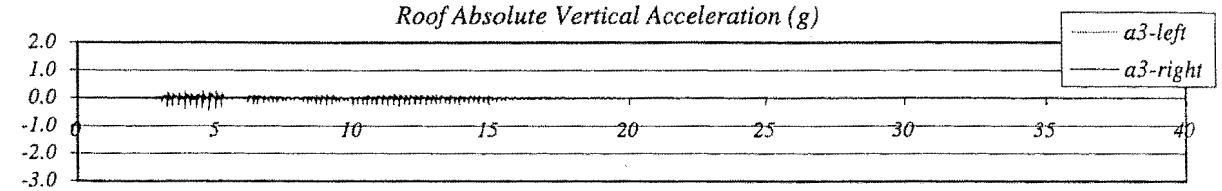

RUN # 20

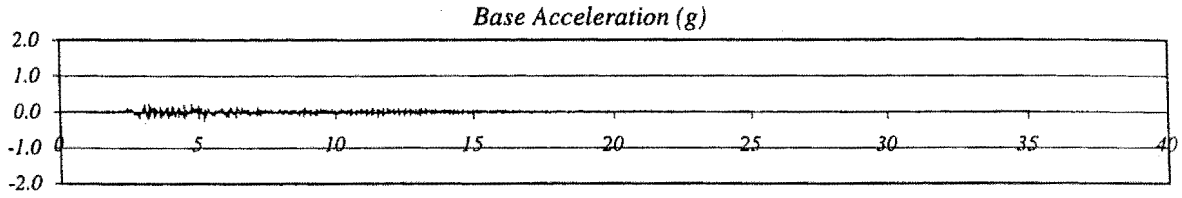

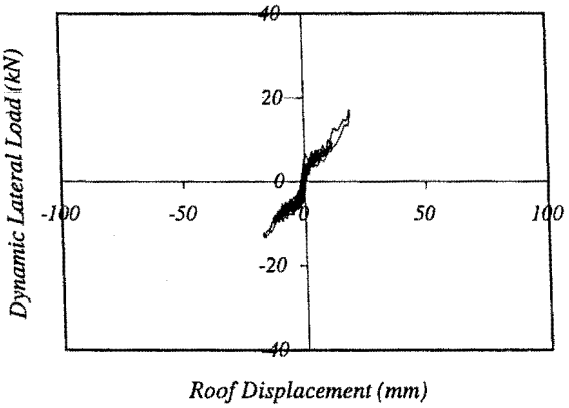

Wall with 1st set of dissipators

Basic Input Ground Motion (BIGM):	*El Centro 180*
Scaling Factor for BIGM:	0.10
Expected Peak Table Acceleration:	0.04 g
Measured Peak Table Acceleration:	0.08 g
Peak Roof Hor. Acceleration:	0.13 g
Peak Roof Vert. Acceleration:	0.04 g
Peak Roof Displacement:	2 mm
Peak Average Drift:	0.04 %
Residual Roof Displacement:	1 mm
Max. Total Inertial Lat. Load:	4.91 kN

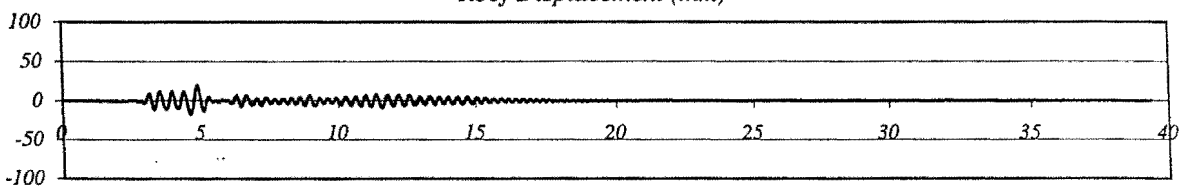

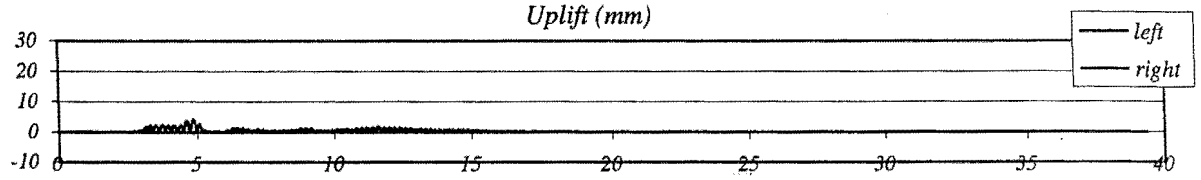

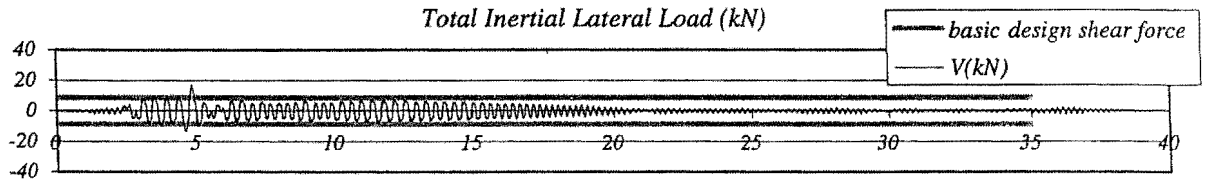

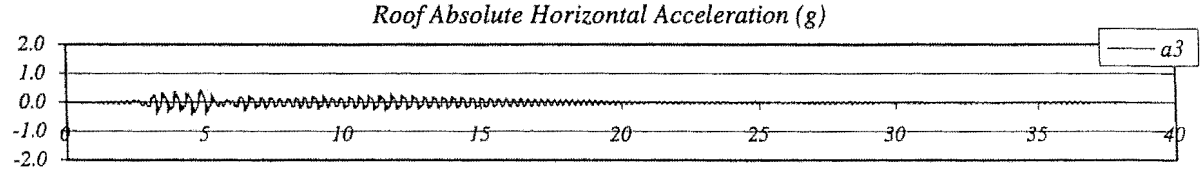

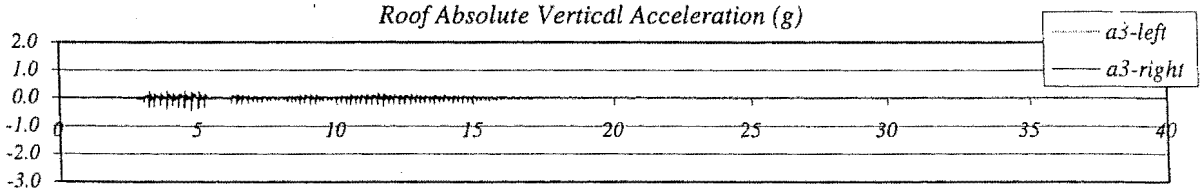

RUN # 21

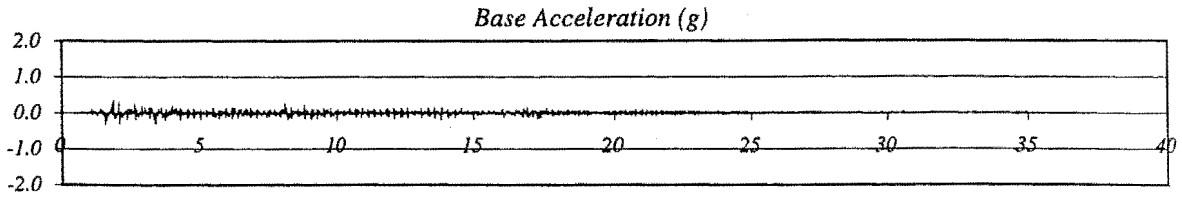

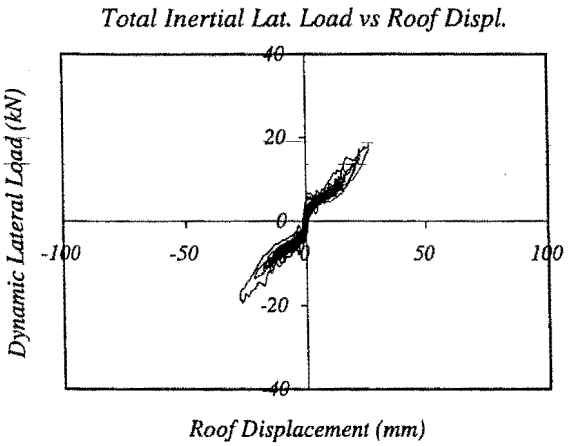

Wall with 1st set of dissipators

Basic Input Ground Motion (BIGM):	*El Centro 180*
Scaling Factor for BIGM:	0.56
Expected Peak Table Acceleration:	0.20 g
Measured Peak Table Acceleration:	0.35 g
Peak Roof Hor. Acceleration:	0.56 g
Peak Roof Vert. Acceleration:	0.82 g
Peak Roof Displacement:	28 mm
Peak Average Drift:	0.74 %
Residual Roof Displacement:	0 mm
Max. Total Inertial Lat. Load:	19.40 kN

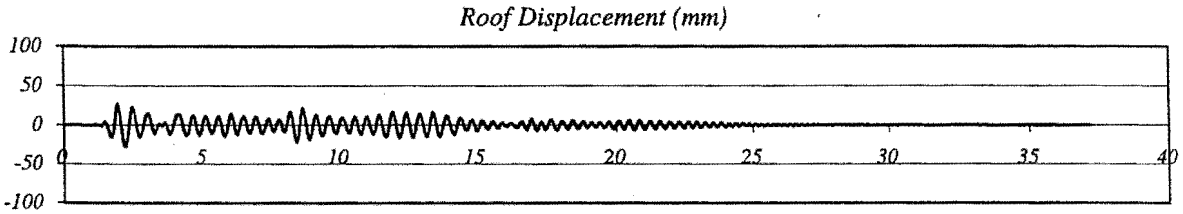

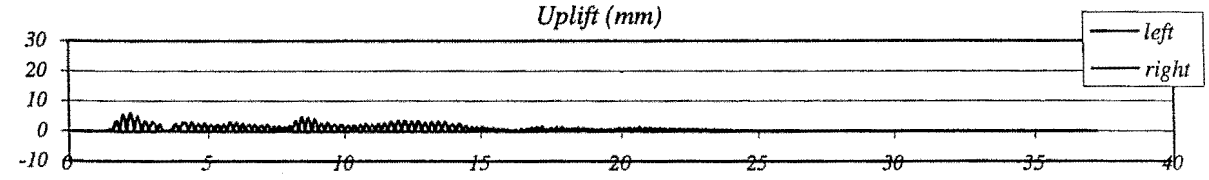

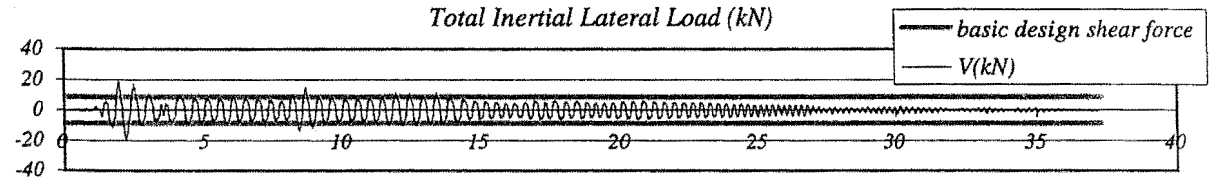

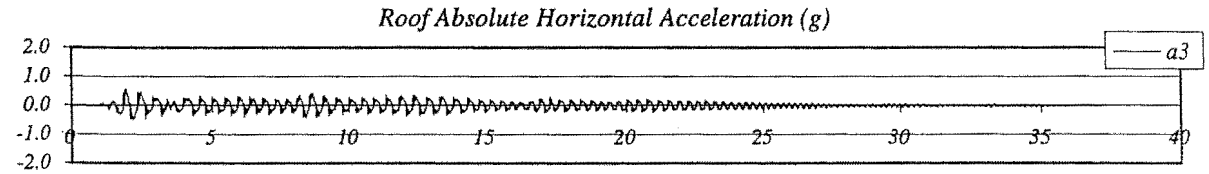

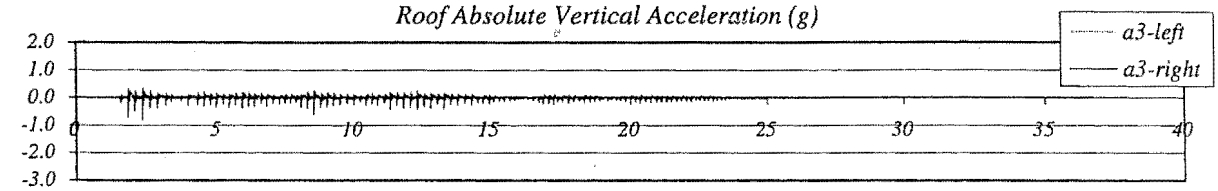

RUN # 22

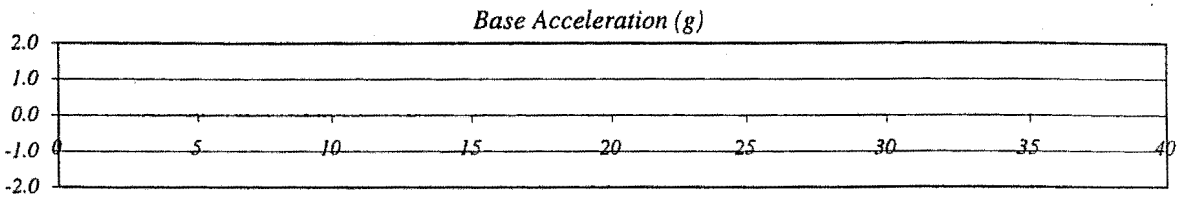

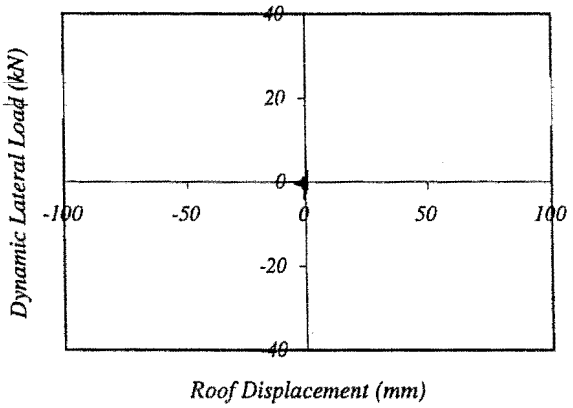

Wall with 1st set of dissipators

Basic Input Ground Motion (BIGM):	*Taft 111*
Scaling Factor for BIGM:	0.10
Expected Peak Table Acceleration:	0.02 g
Measured Peak Table Acceleration:	0.04 g
Peak Roof Hor. Acceleration:	0.11 g
Peak Roof Vert. Acceleration:	0.03 g
Peak Roof Displacement:	4 mm
Peak Average Drift:	0.12 %
Residual Roof Displacement:	4 mm
Max. Total Inertial Lat. Load:	4.17 kN

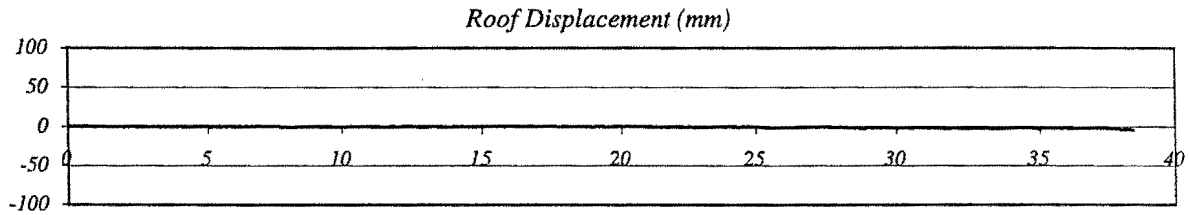

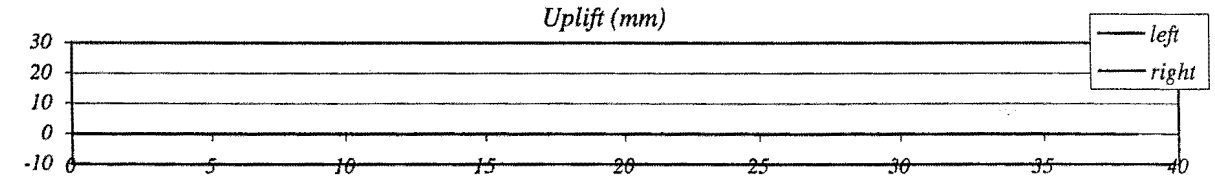

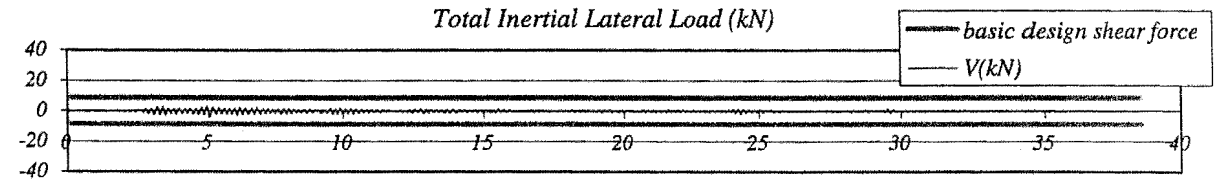

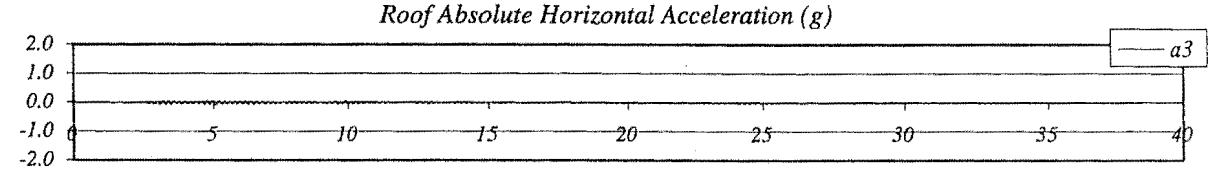

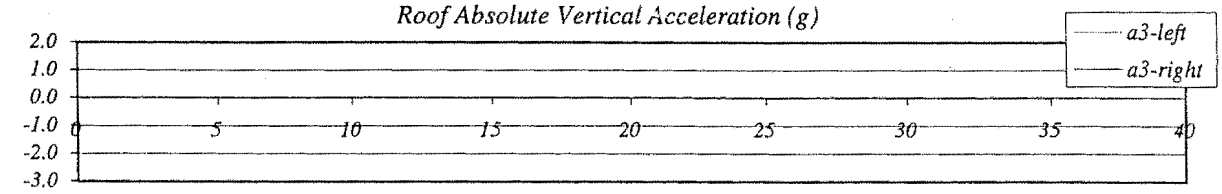

RUN # 23

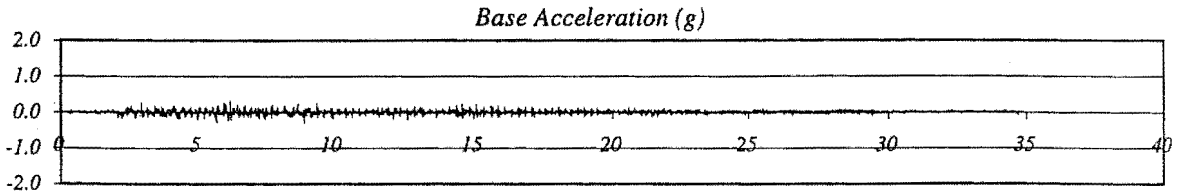

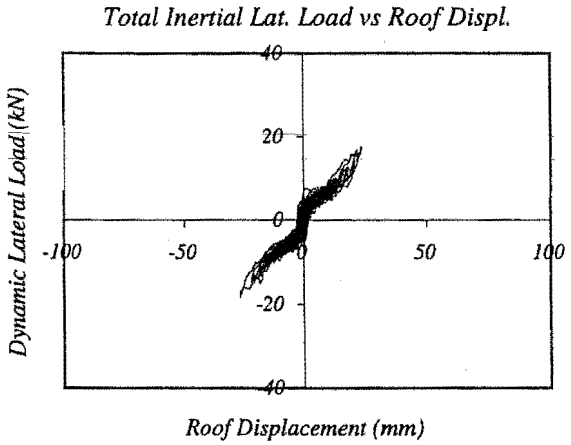

Wall with 1st set of dissipators

Basic Input Ground Motion (BIGM):	*Taft 111*
Scaling Factor for BIGM:	1.13
~~Expected Peak Table Acceleration:~~	~~0.20 g~~
Measured Peak Table Acceleration:	0.32 g
Peak Roof Hor. Acceleration:	0.56 g
Peak Roof Vert. Acceleration:	0.83 g
Peak Roof Displacement:	26 mm
Peak Average Drift:	0.70 %
Residual Roof Displacement:	1 mm
Max. Total Inertial Lat. Load:	18.47 kN

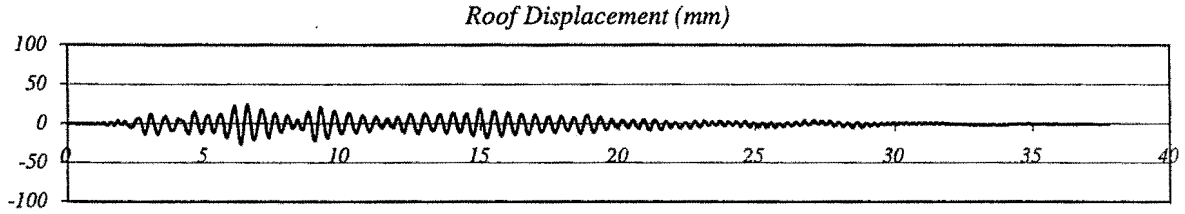

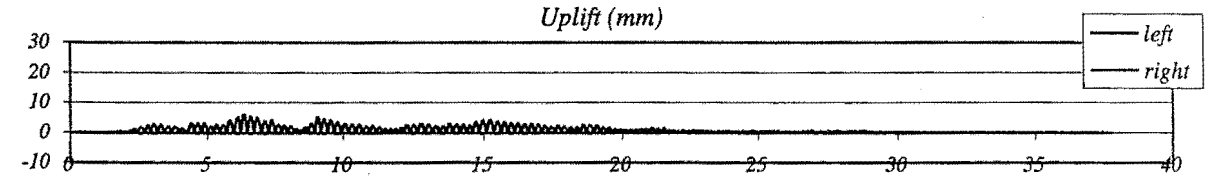

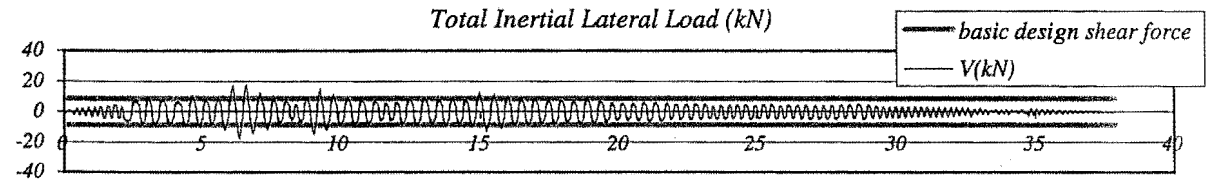

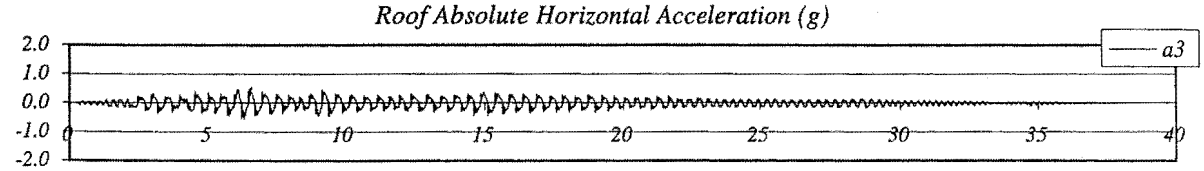

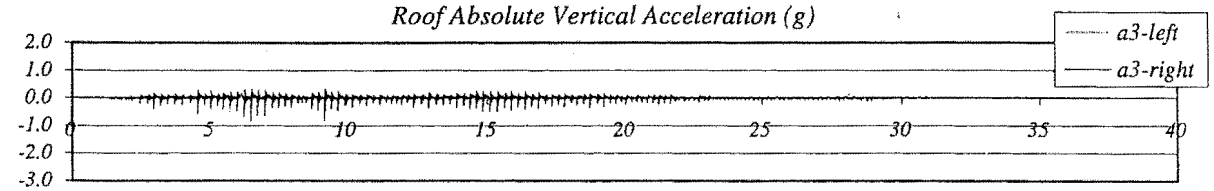

RUN # 24

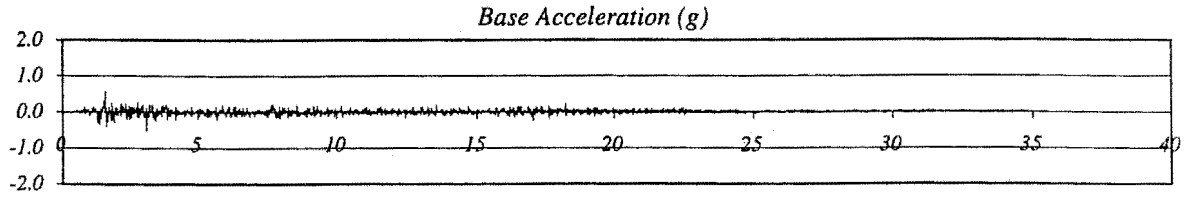

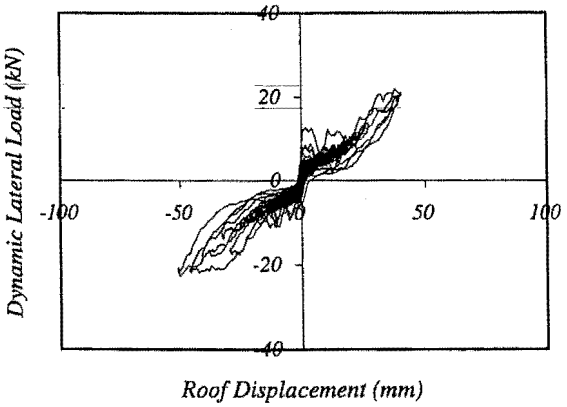

Wall with 1st set of dissipators

Basic Input Ground Motion (BIGM):	*El Centro 180*
Scaling Factor for BIGM:	0.84
Expected Peak Table Acceleration:	0.30 g
Measured Peak Table Acceleration:	0.57 g
Peak Roof Hor. Acceleration:	0.89 g
Peak Roof Vert. Acceleration:	1.54 g
Peak Roof Displacement:	51 mm
Peak Average Drift:	1.38 %
Residual Roof Displacement:	0 mm
Max. Total Inertial Lat. Load:	22.76 kN

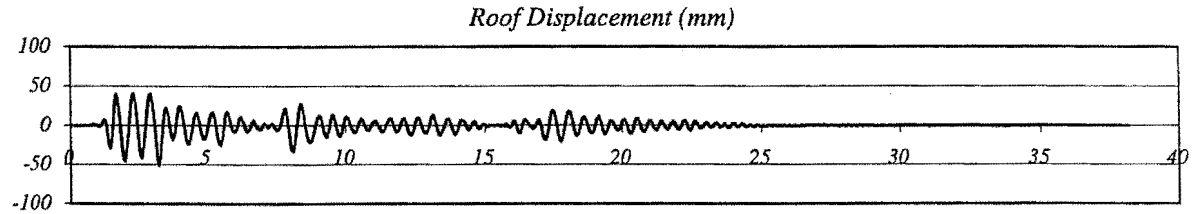

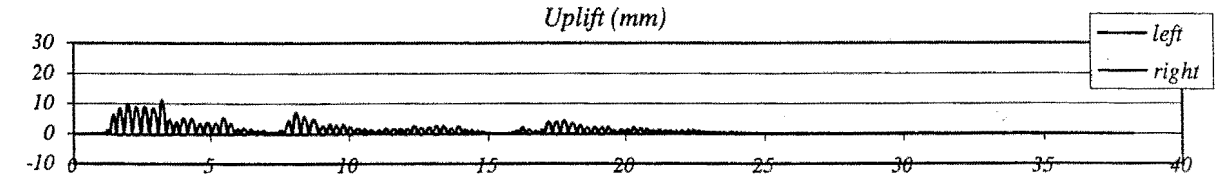

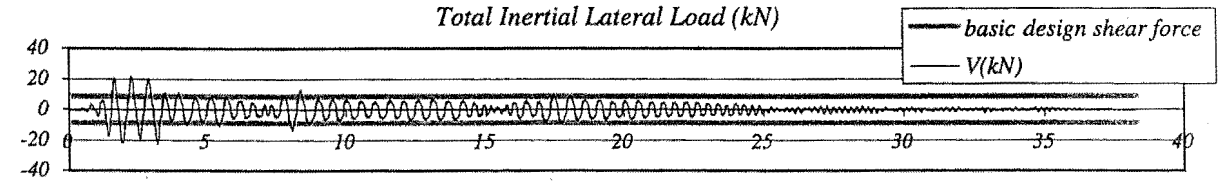

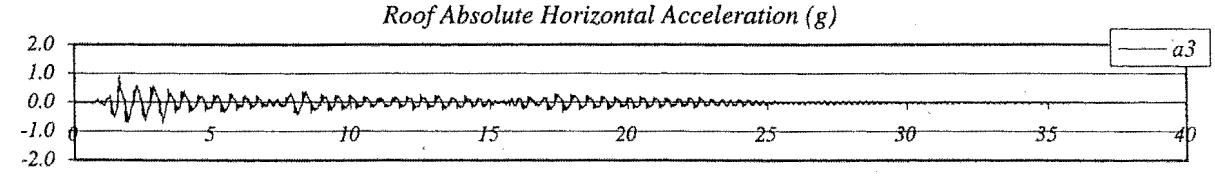

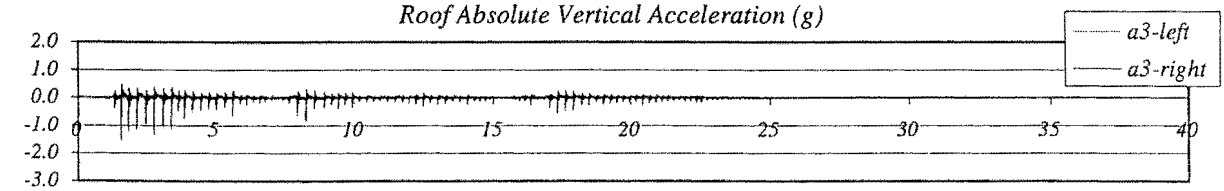

RUN # 25

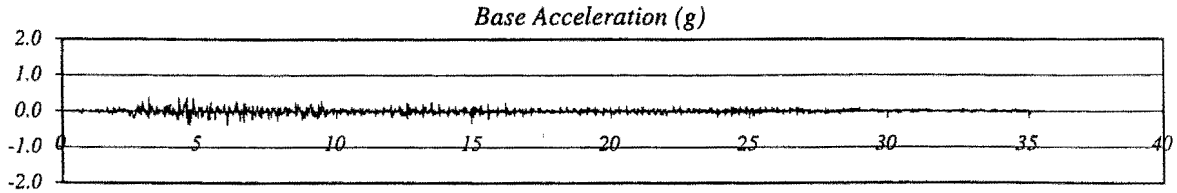

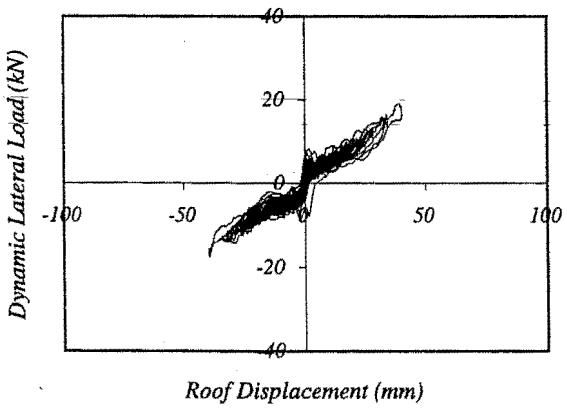

Wall with 1st set of dissipators

Basic Input Ground Motion (BIGM):	*Taft 111*
Scaling Factor for BIGM:	1.69
~~Expected Peak Table Acceleration:~~	~~0.30 g~~
Measured Peak Table Acceleration:	0.38 g
Peak Roof Hor. Acceleration:	0.65 g
Peak Roof Vert. Acceleration:	1.34 g
Peak Roof Displacement:	40 mm
Peak Average Drift:	1.07 %
Residual Roof Displacement:	0 mm
Max. Total Inertial Lat. Load:	19.57 kN

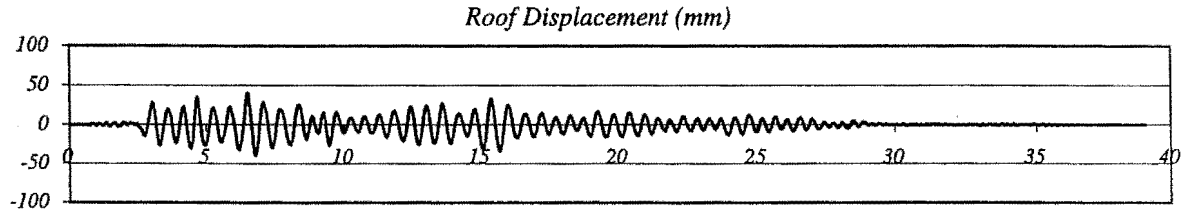

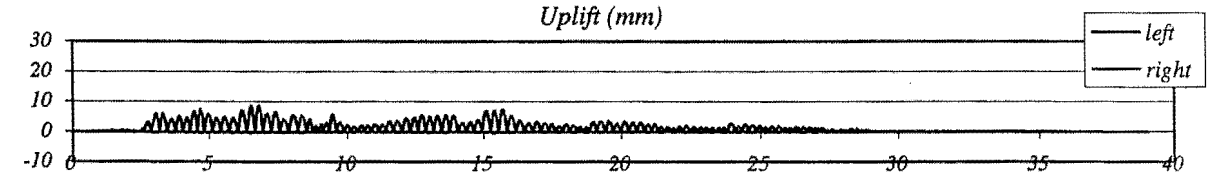

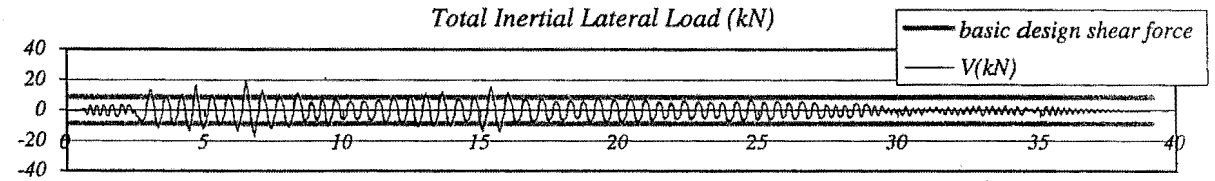

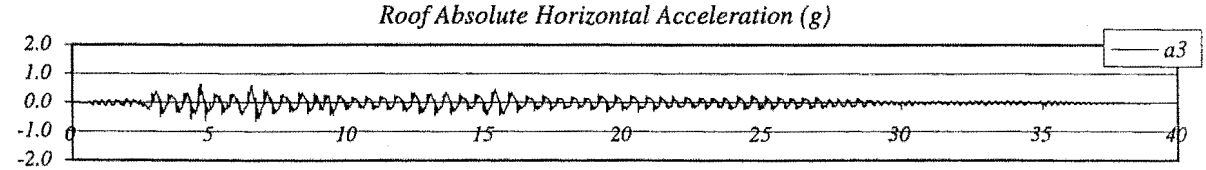

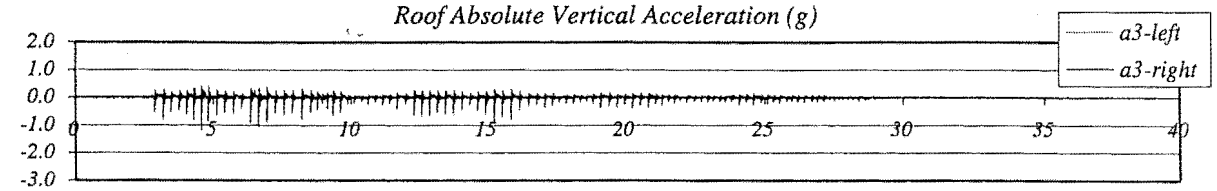

RUN # 26

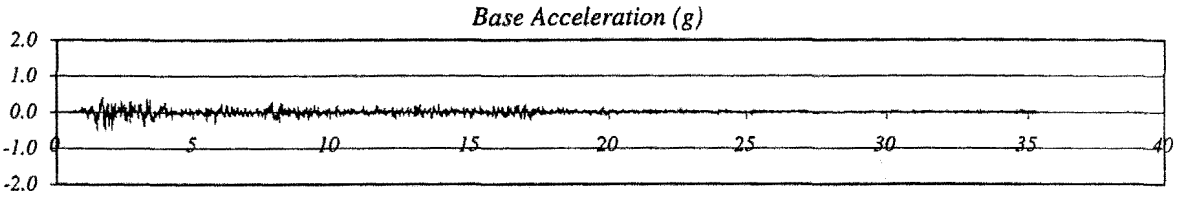

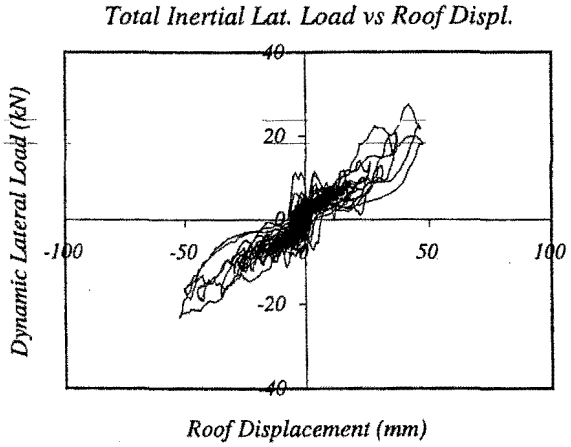

Wall with 1st set of dissipators

Basic Input Ground Motion (BIGM):	*El Centro 180*
Scaling Factor for BIGM:	1.12
Expected Peak Table Acceleration:	0.40 g
Measured Peak Table Acceleration:	0.50 g
Peak Roof Hor. Acceleration:	0.84 g
Peak Roof Vert. Acceleration:	2.14 g
Peak Roof Displacement:	52 mm
Peak Average Drift:	1.41 %
Residual Roof Displacement:	3 mm
Max. Total Inertial Lat. Load:	27.50 kN

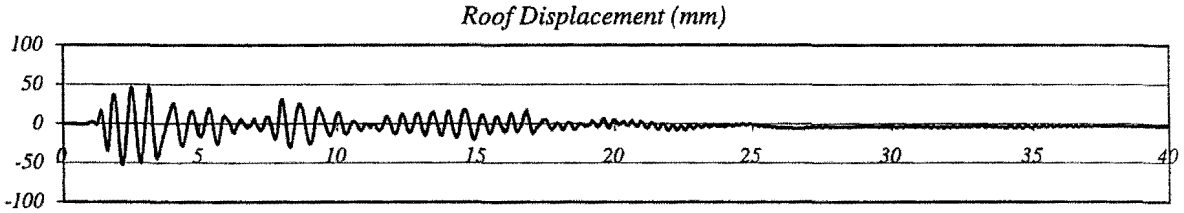

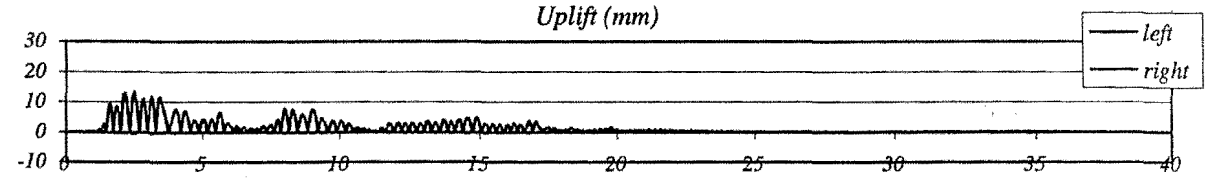

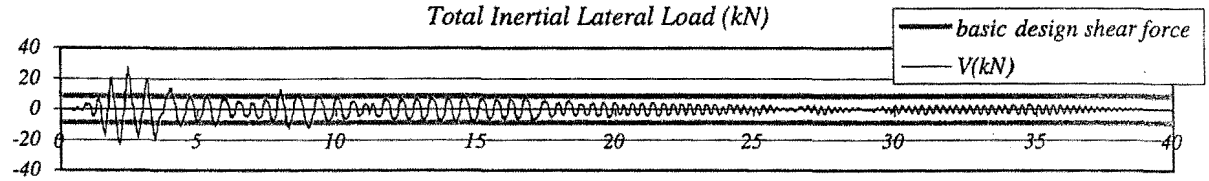

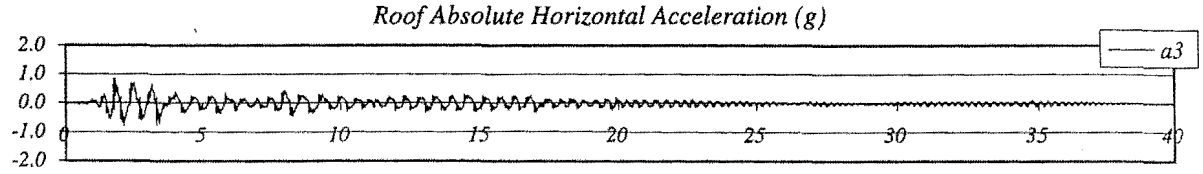

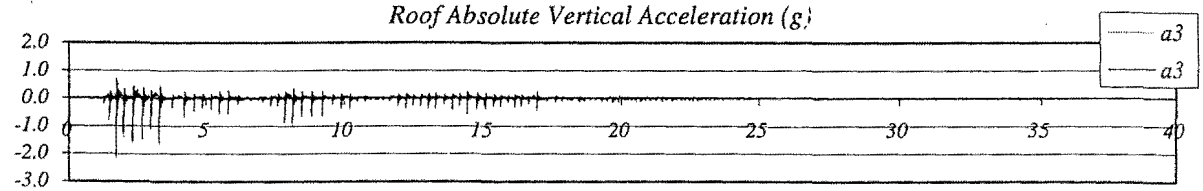

RUN # 27

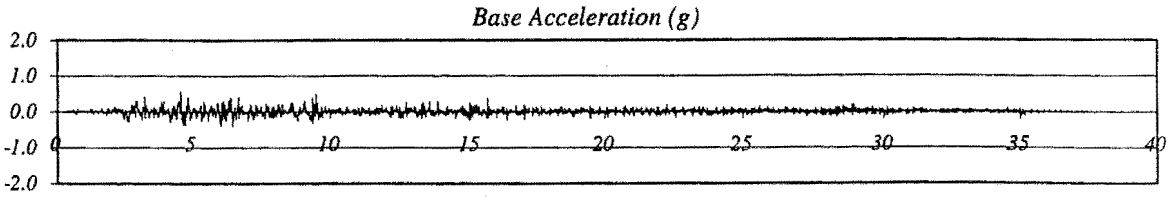

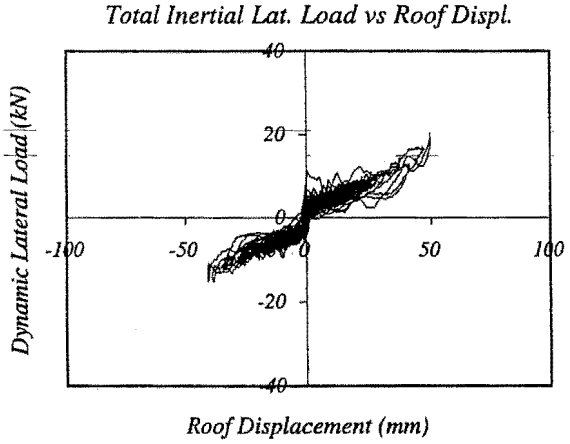

Wall with 1st set of dissipators

Basic Input Ground Motion (BIGM):	*Taft 111*
Scaling Factor for BIGM:	2.26
Expected Peak Table Acceleration:	0.40 g
Measured Peak Table Acceleration:	0.57 g
Peak Roof Hor. Acceleration:	0.65 g
Peak Roof Vert. Acceleration:	1.59 g
Peak Roof Displacement:	50 mm
Peak Average Drift:	1.33 %
Residual Roof Displacement:	0 mm
Max. Total Inertial Lat. Load:	20.24 kN

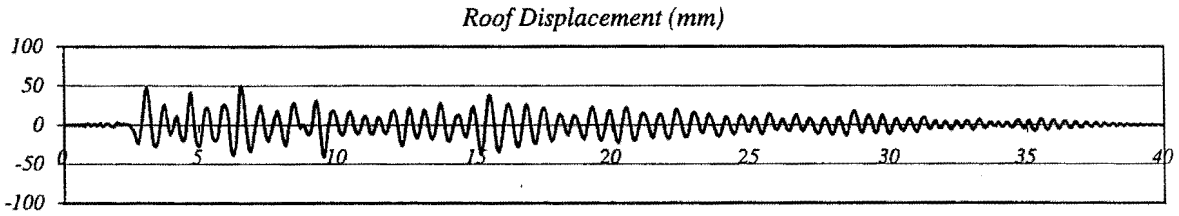

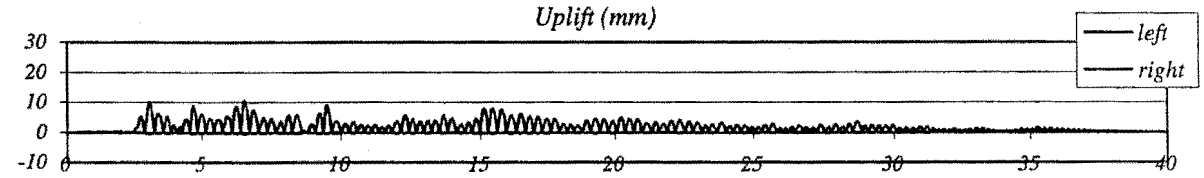

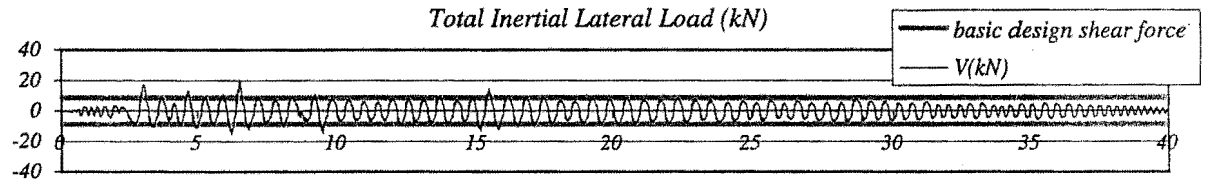

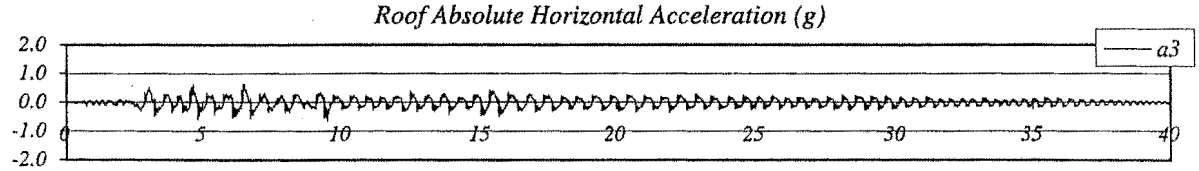

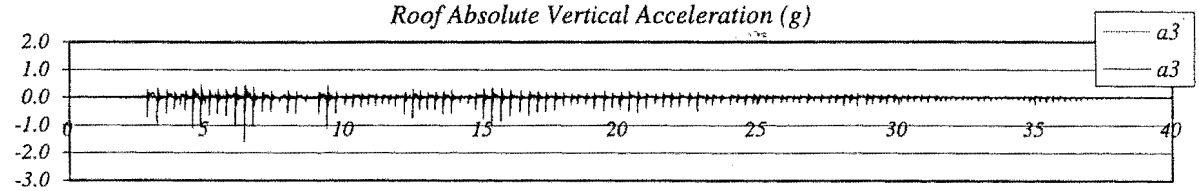

RUN # 28

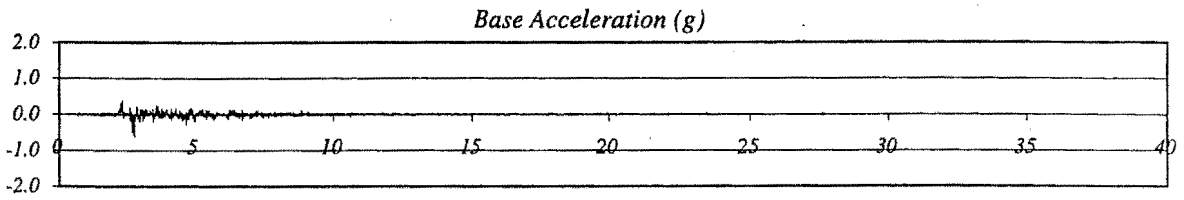

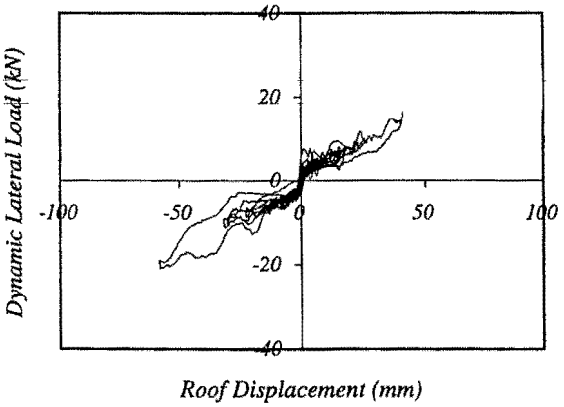

Wall with 1st set of dissipators

Basic Input Ground Motion (BIGM):	*Sylmar 000*
Scaling Factor for BIGM:	0.50
Expected Peak Table Acceleration:	0.40 g
Measured Peak Table Acceleration:	0.61 g
Peak Roof Hor. Acceleration:	0.67 g
Peak Roof Vert. Acceleration:	1.23 g
Peak Roof Displacement:	58 mm
Peak Average Drift:	1.56 %
Residual Roof Displacement:	0 mm
Max. Total Inertial Lat. Load:	21.00 kN

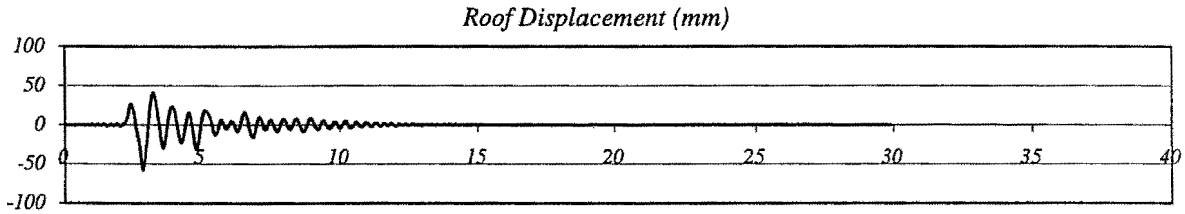

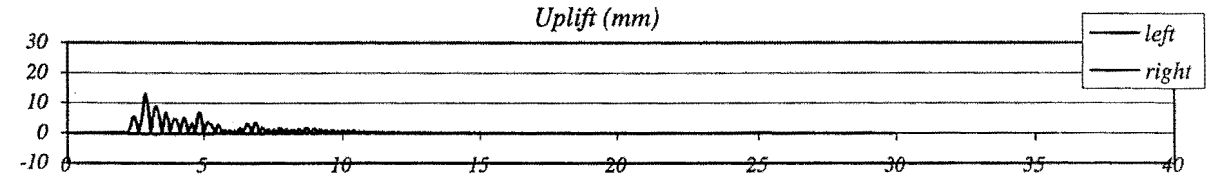

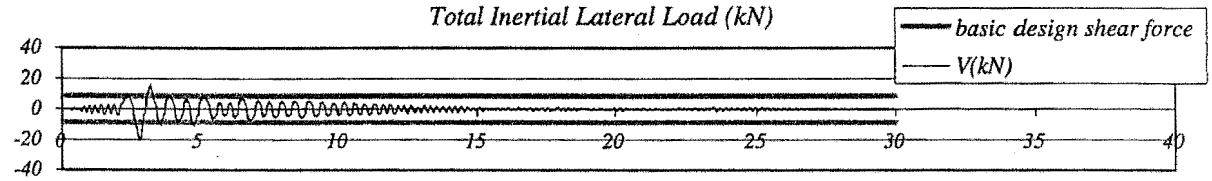

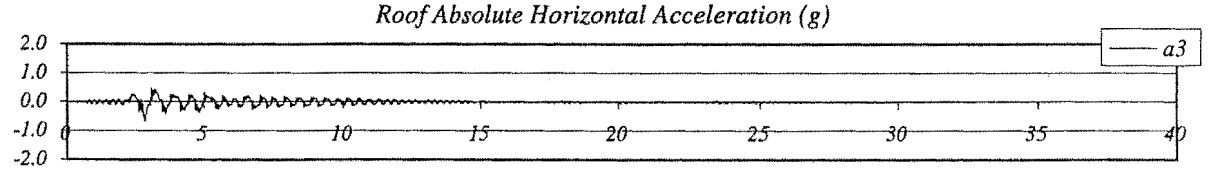

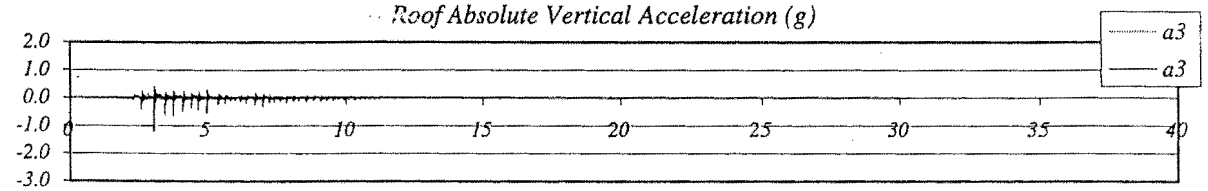

RUN # 29

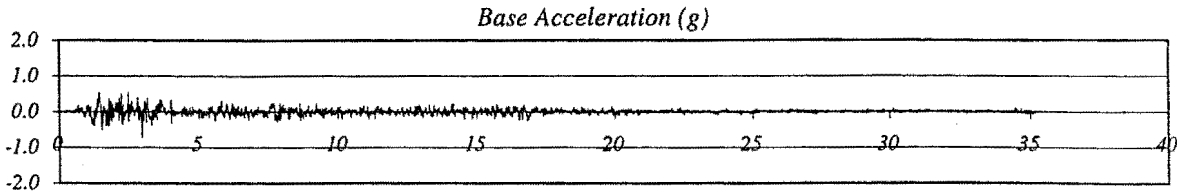

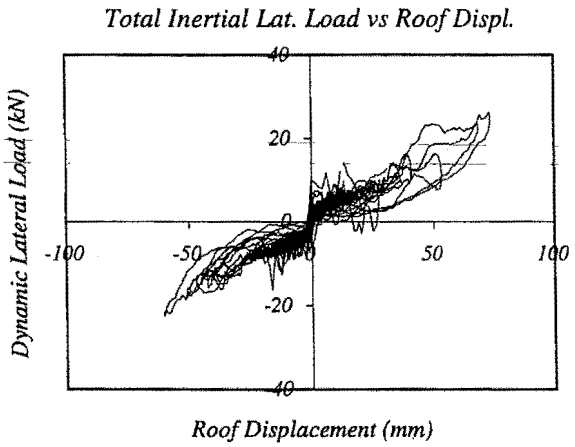

Wall with 1st set of dissipators

Basic Input Ground Motion (BIGM):	*El Centro 180*
Scaling Factor for BIGM:	1.40
Expected Peak Table Acceleration:	0.50 g
Measured Peak Table Acceleration:	0.74 g
Peak Roof Hor. Acceleration:	0.95 g
Peak Roof Vert. Acceleration:	2.13 g
Peak Roof Displacement:	74 mm
Peak Average Drift:	1.98 %
Residual Roof Displacement:	0 mm
Max. Total Inertial Lat. Load:	26.16 kN

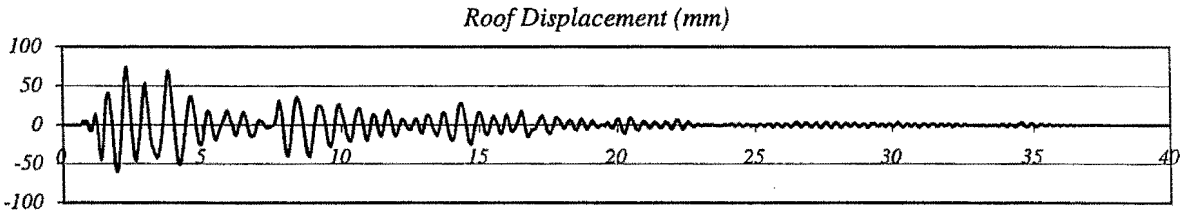

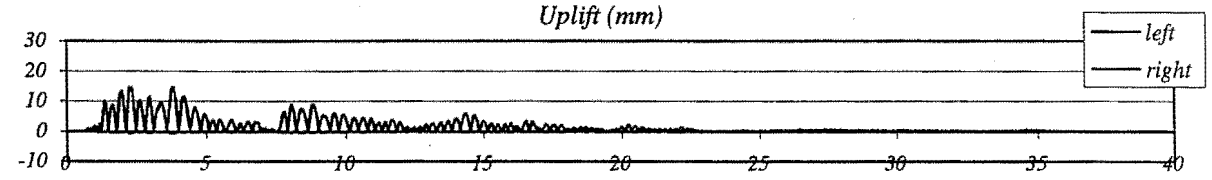

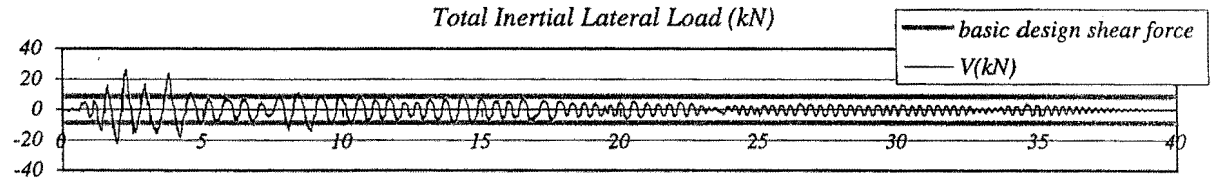

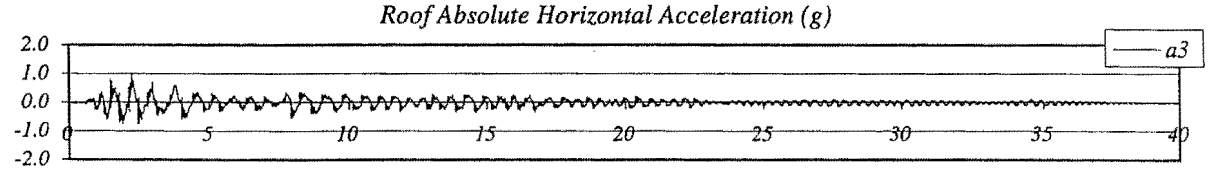

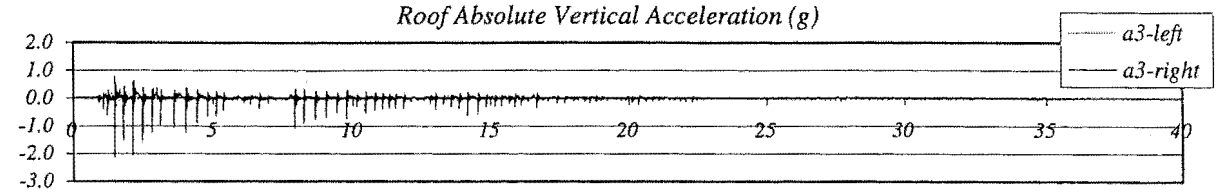

RUN # 30

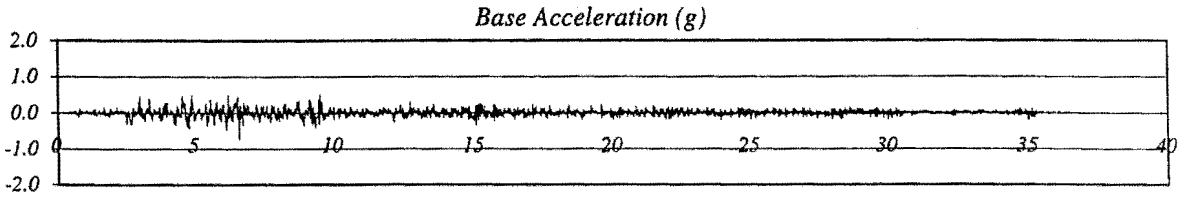

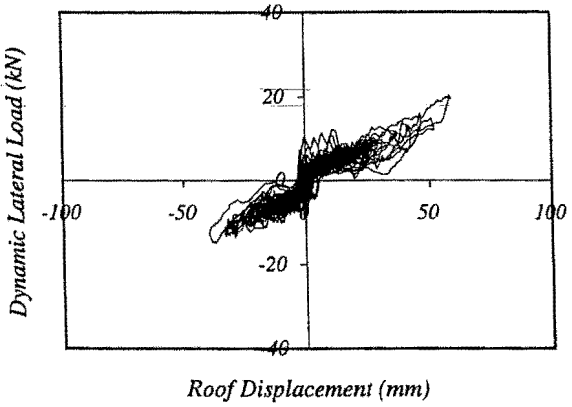

Wall with 1st set of dissipators

Basic Input Ground Motion (BIGM):	*Taft 111*
Scaling Factor for BIGM:	2.83
Expected Peak Table Acceleration:	0.50 g
Measured Peak Table Acceleration:	0.73 g
Peak Roof Hor. Acceleration:	0.86 g
Peak Roof Vert. Acceleration:	1.92 g
Peak Roof Displacement:	59 mm
Peak Average Drift:	1.58 %
Residual Roof Displacement:	1 mm
Max. Total Inertial Lat. Load:	20.30 kN

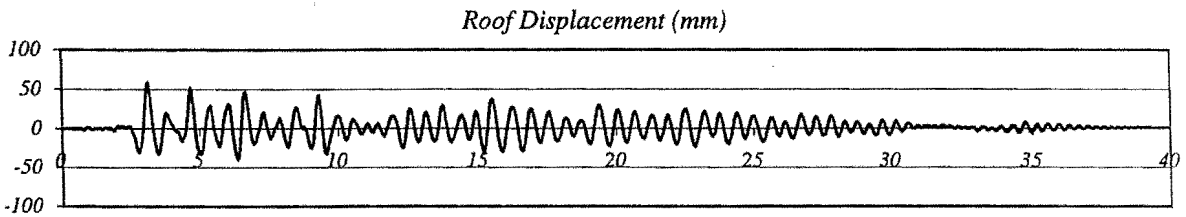

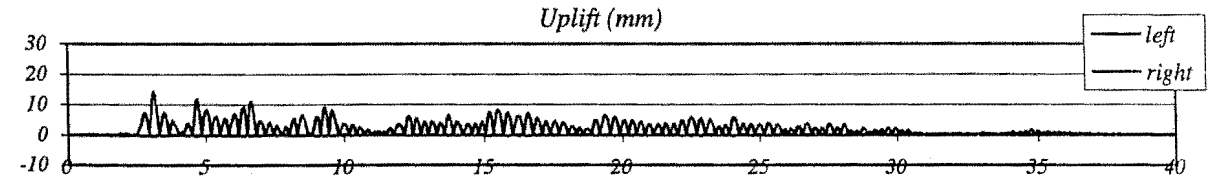

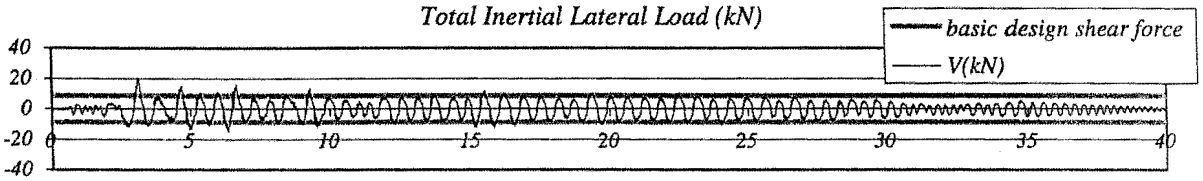

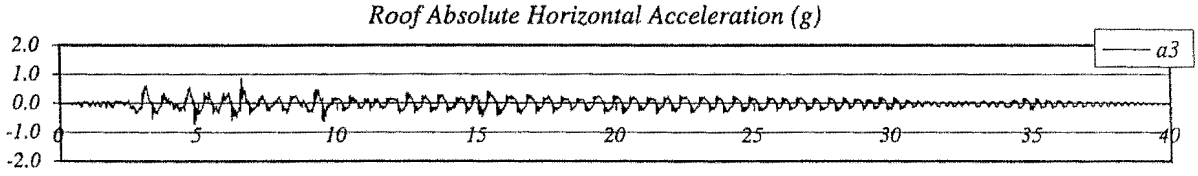

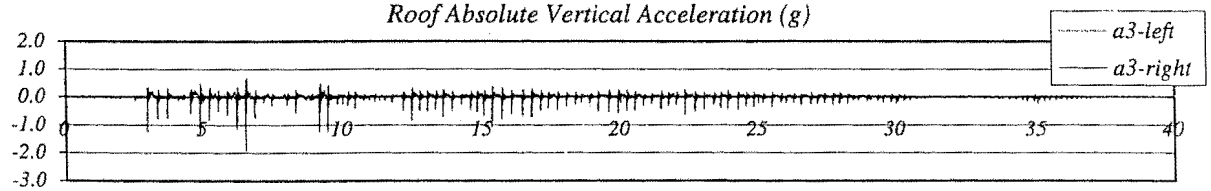

RUN # 31

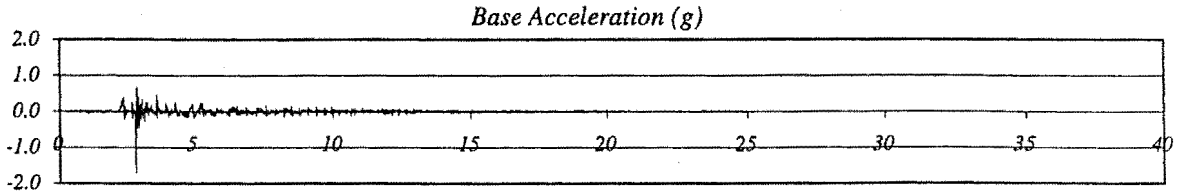

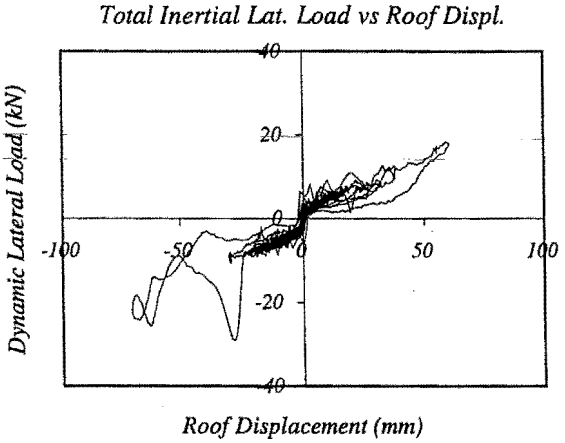

Wall with 1st set of dissipators

Basic Input Ground Motion (BIGM):	*Sylmar 000*
Scaling Factor for BIGM:	0.63
Expected Peak Table Acceleration:	0.50 g
Measured Peak Table Acceleration:	1.70 g
Peak Roof Hor. Acceleration:	0.90 g
Peak Roof Vert. Acceleration:	1.33 g
Peak Roof Displacement:	70 mm
Peak Average Drift:	1.88 %
Residual Roof Displacement:	0 mm
Max. Total Inertial Lat. Load:	29.15 kN

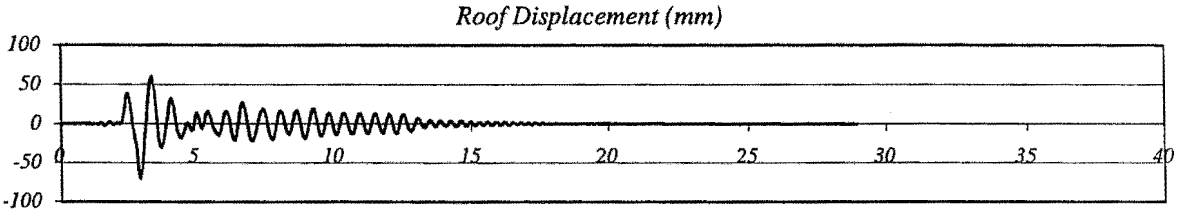

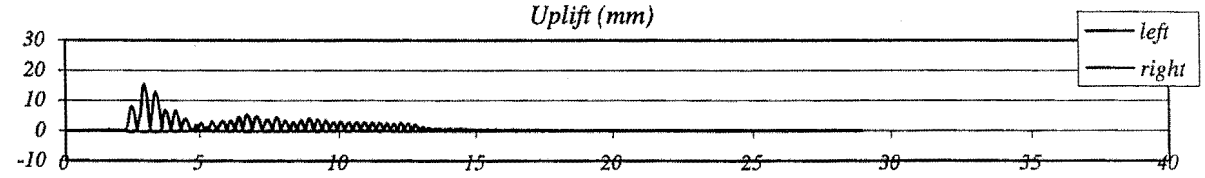

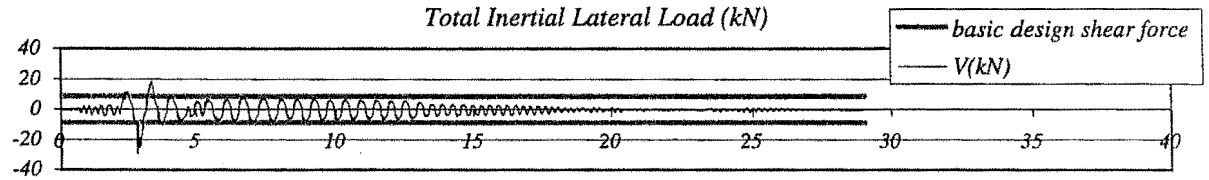

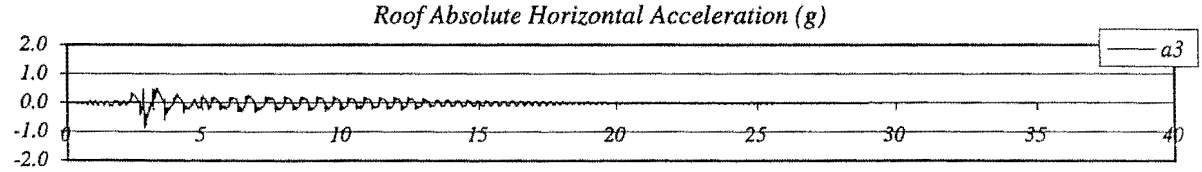

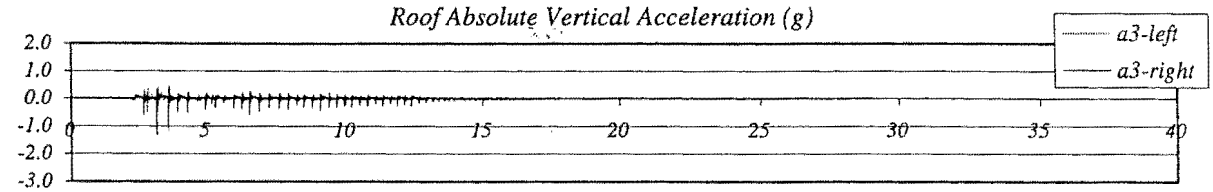

RUN # 32

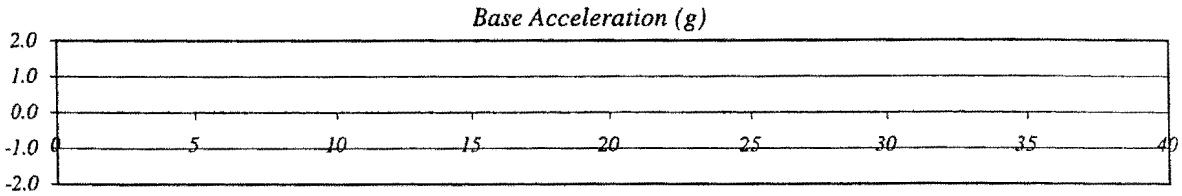

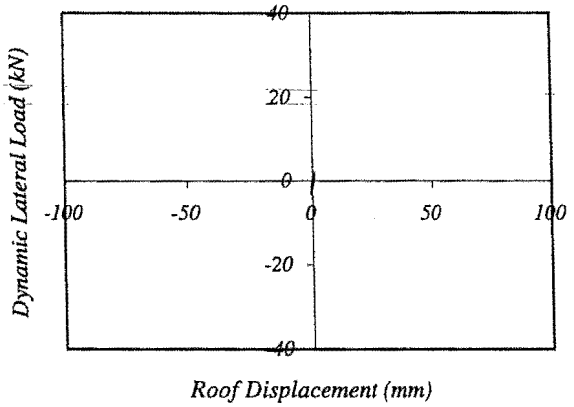

Wall with 1st set of dissipators

Basic Input Ground Motion (BIGM):	*Taft 111*
Scaling Factor for BIGM:	0.10
Expected Peak Table Acceleration:	0.02 g
Measured Peak Table Acceleration:	0.04 g
Peak Roof Hor. Acceleration:	0.09 g
Peak Roof Vert. Acceleration:	0.04 g
Peak Roof Displacement:	1 mm
Peak Average Drift:	0.03 %
Residual Roof Displacement:	0 mm
Max. Total Inertial Lat. Load:	3.37 kN

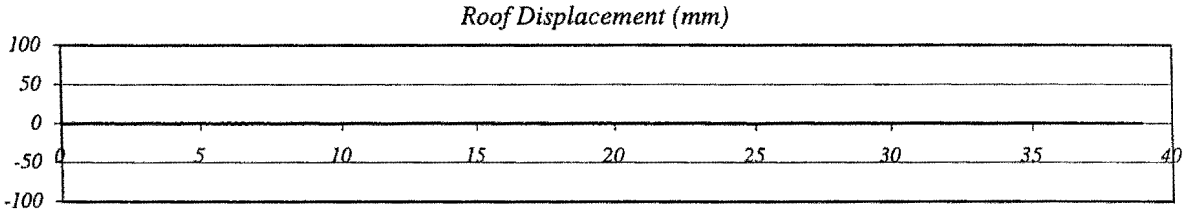

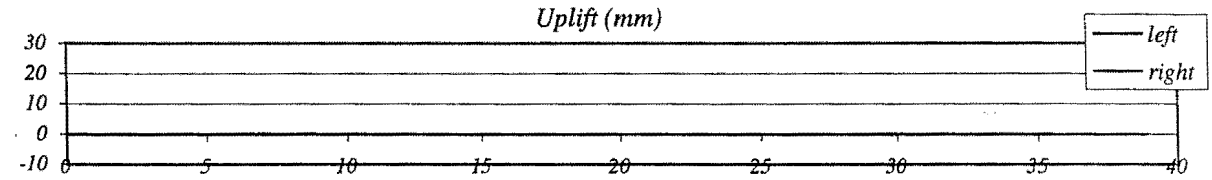

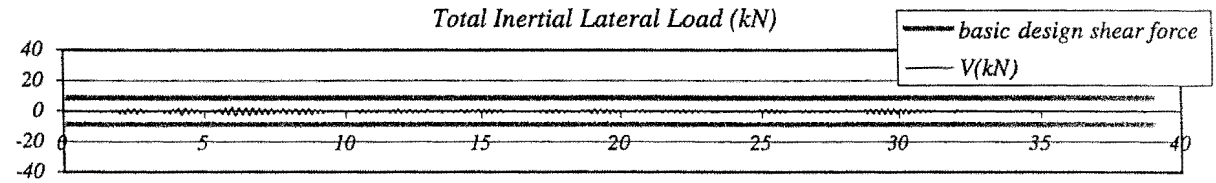

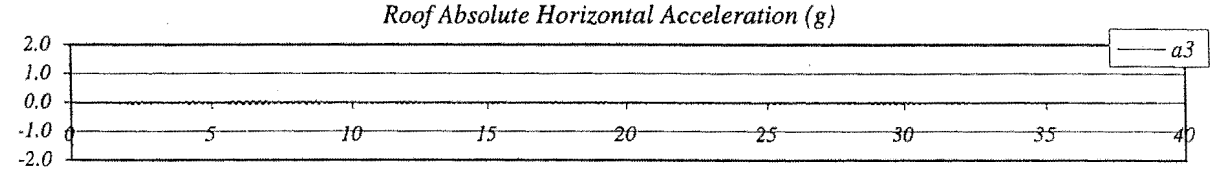

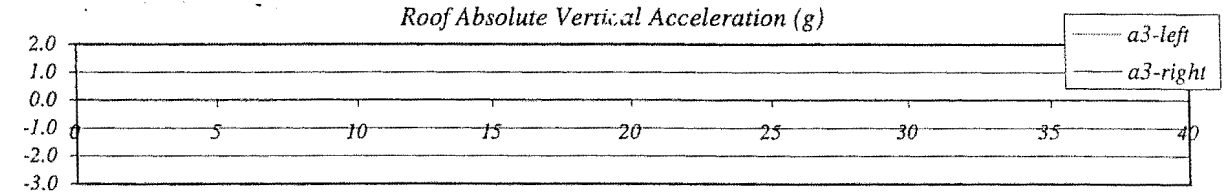

RUN # 33

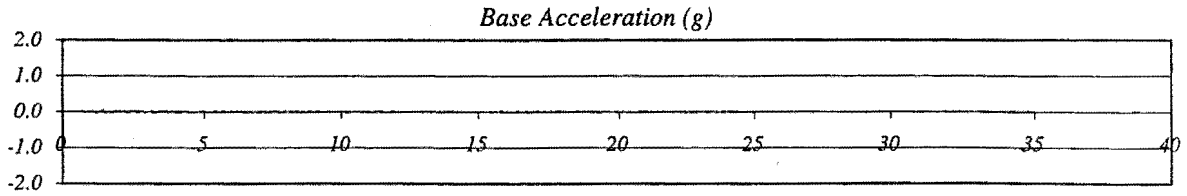

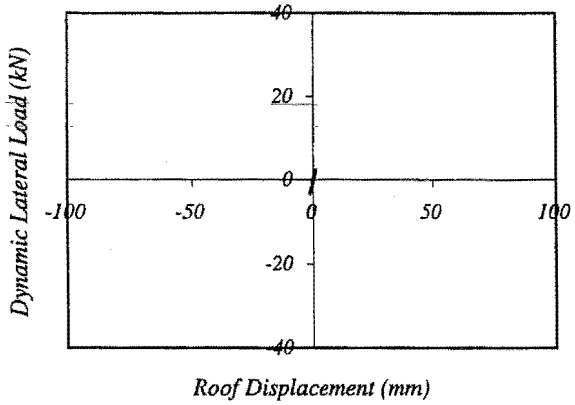

Wall with 1st set of dissipators

Basic Input Ground Motion (BIGM):	*El Centro 180*
Scaling Factor for BIGM:	0.10
Expected Peak Table Acceleration:	0.04 g
Measured Peak Table Acceleration:	0.08 g
Peak Roof Hor. Acceleration:	0.11 g
Peak Roof Vert. Acceleration:	0.05 g
Peak Roof Displacement:	2 mm
Peak Average Drift:	0.05 %
Residual Roof Displacement:	0 mm
Max. Total Inertial Lat. Load:	3.75 kN

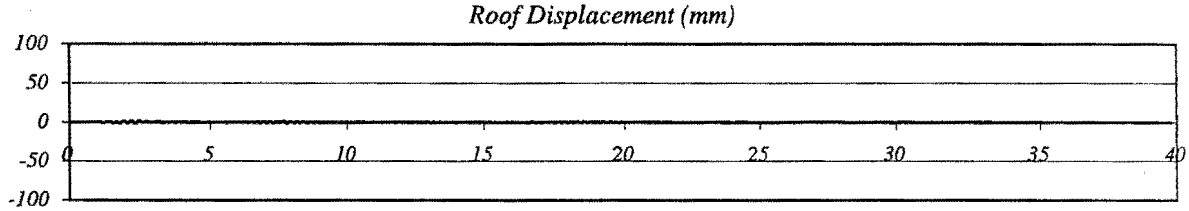

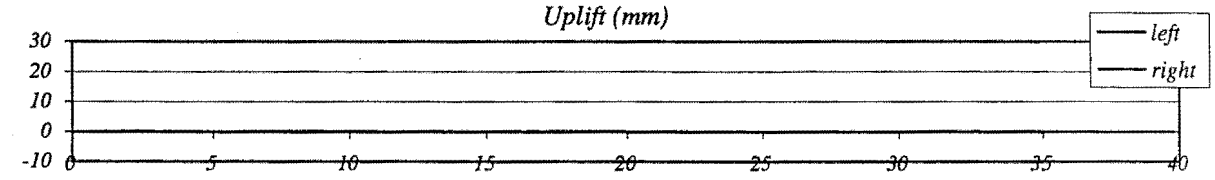

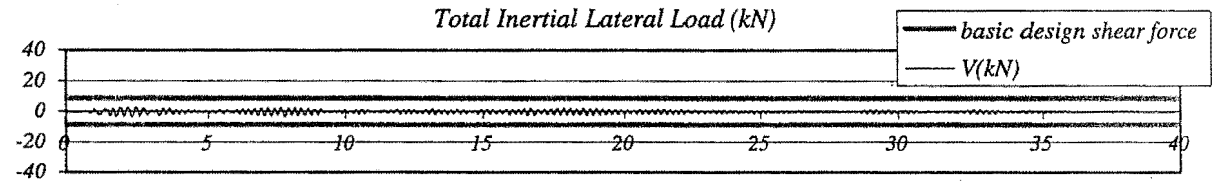

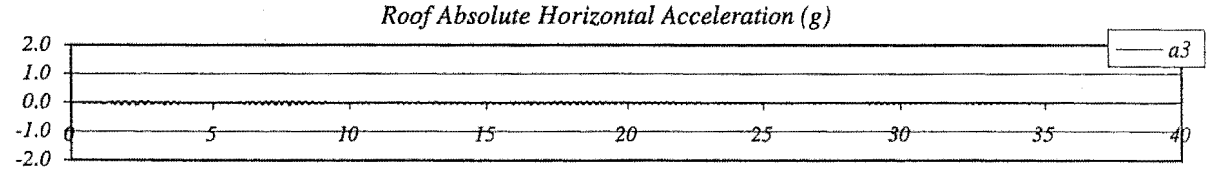

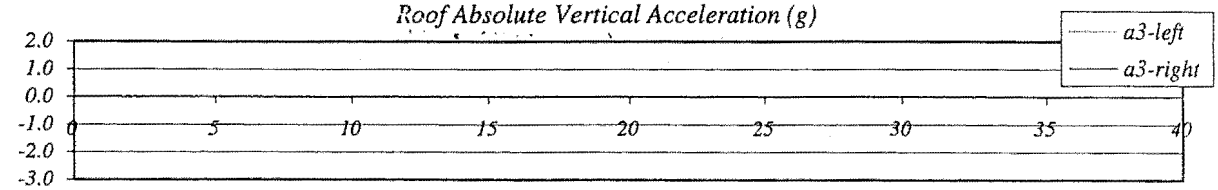

RUN # 34

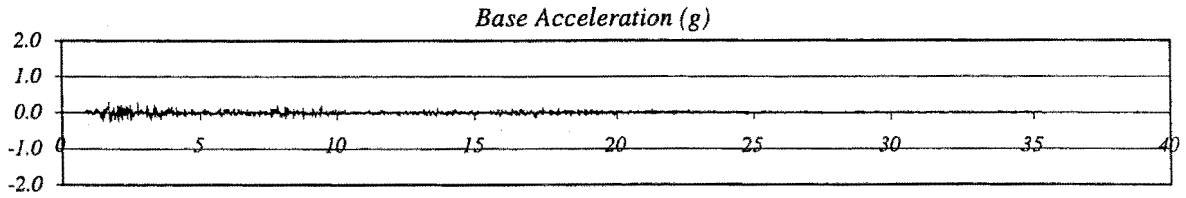

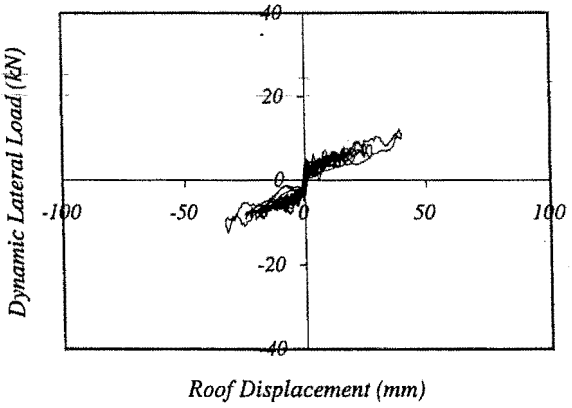

Wall with 1st set of dissipators

Basic Input Ground Motion (BIGM):	*El Centro 180*
Scaling Factor for BIGM:	0.56
Expected Peak Table Acceleration:	0.20 g
Measured Peak Table Acceleration:	0.28 g
Peak Roof Hor. Acceleration:	0.51 g
Peak Roof Vert. Acceleration:	0.98 g
Peak Roof Displacement:	40 mm
Peak Average Drift:	1.08 %
Residual Roof Displacement:	0 mm
Max. Total Inertial Lat. Load:	12.68 kN

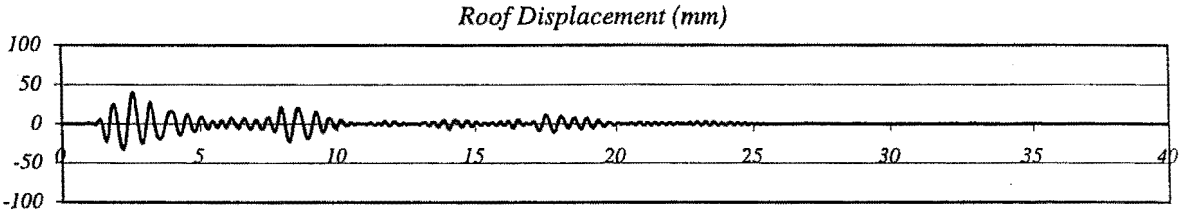

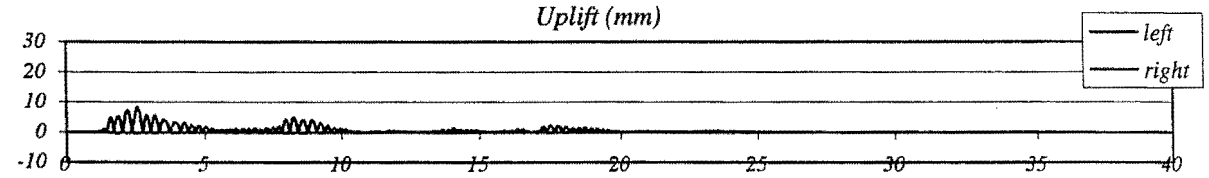

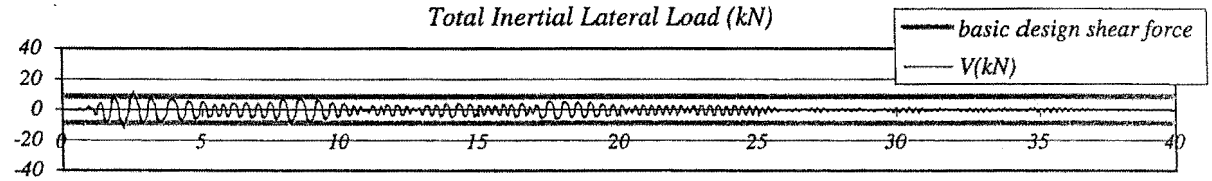

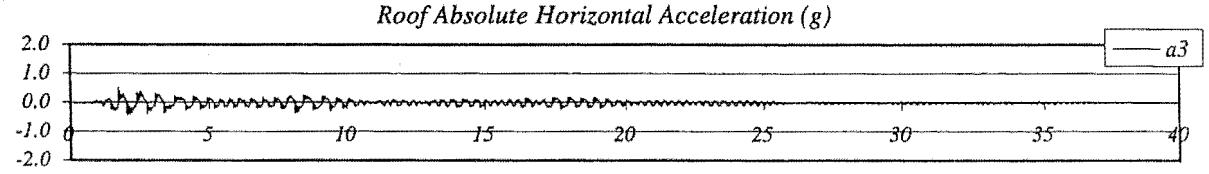

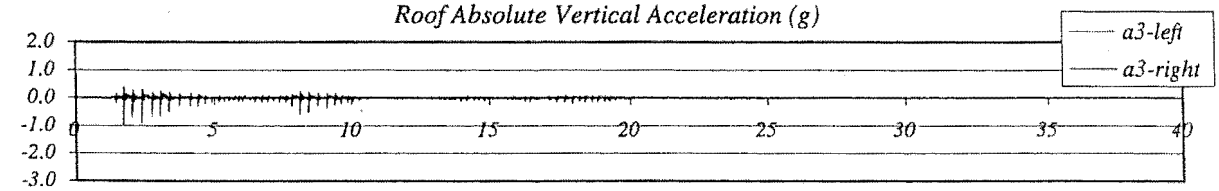

RUN # 35

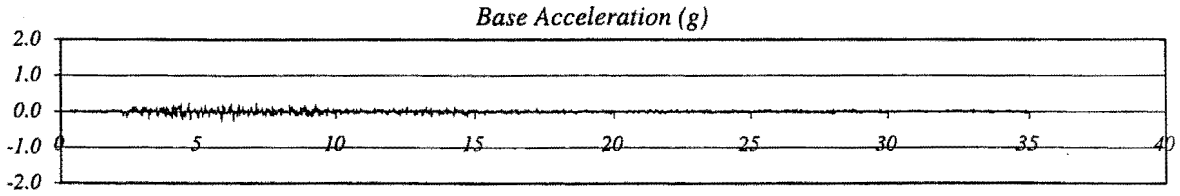

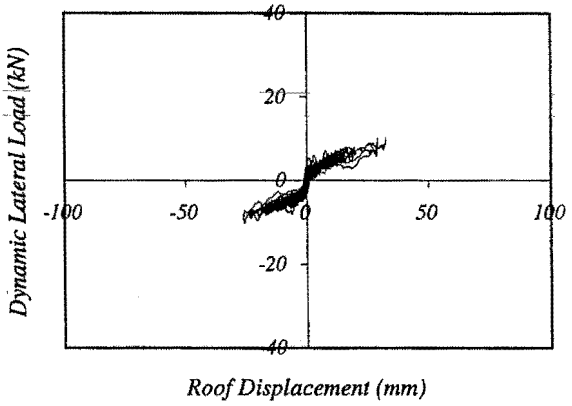

Wall with 1st set of dissipators

Basic Input Ground Motion (BIGM):	*Taft 111*
Scaling Factor for BIGM:	1.13
Expected Peak Table Acceleration:	0.20 g
Measured Peak Table Acceleration:	0.28 g
Peak Roof Hor. Acceleration:	0.40 g
Peak Roof Vert. Acceleration:	0.88 g
Peak Roof Displacement:	33 mm
Peak Average Drift:	0.88 %
Residual Roof Displacement:	0 mm
Max. Total Inertial Lat. Load:	10.31 kN

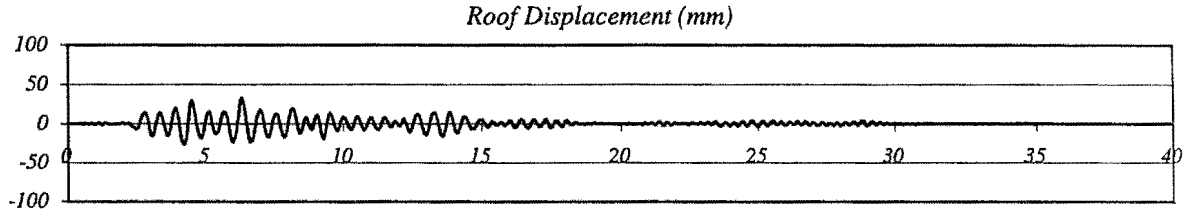

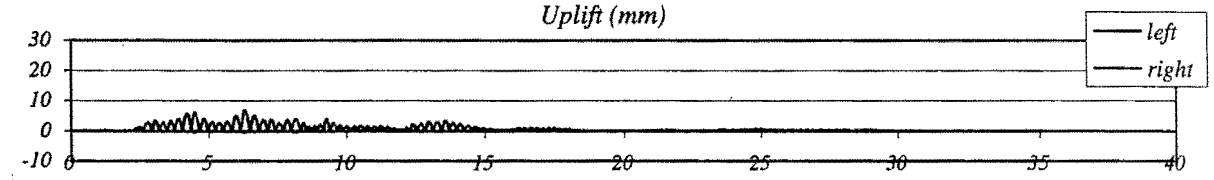

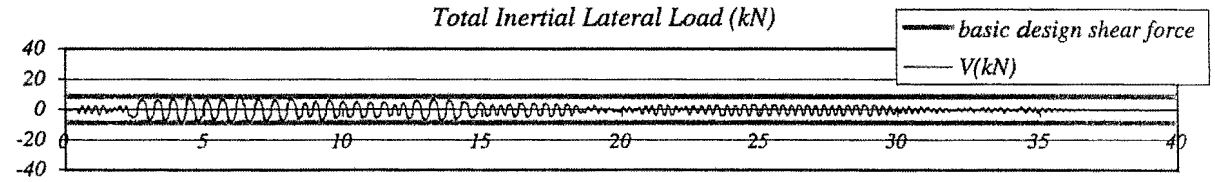

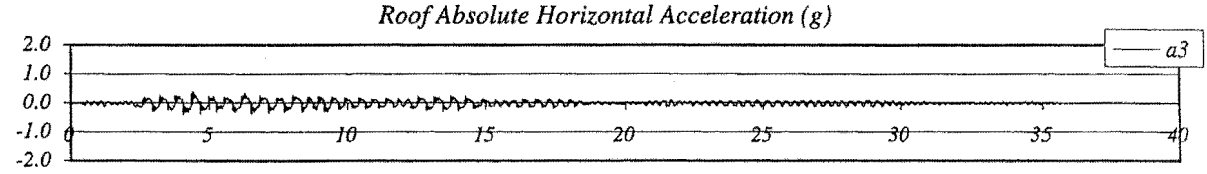

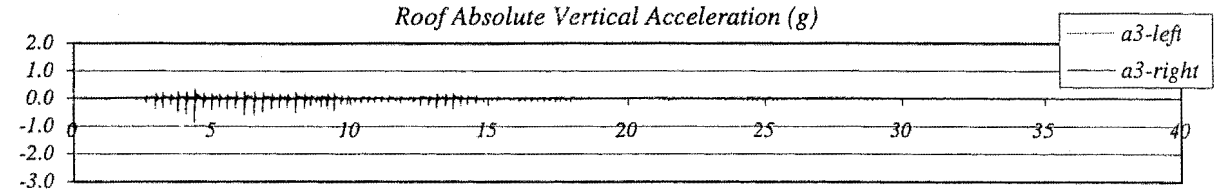

RUN # 36

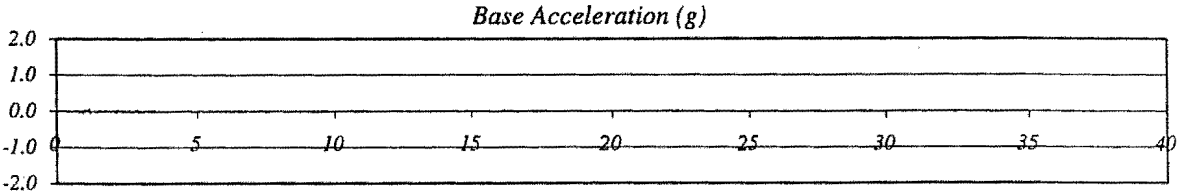

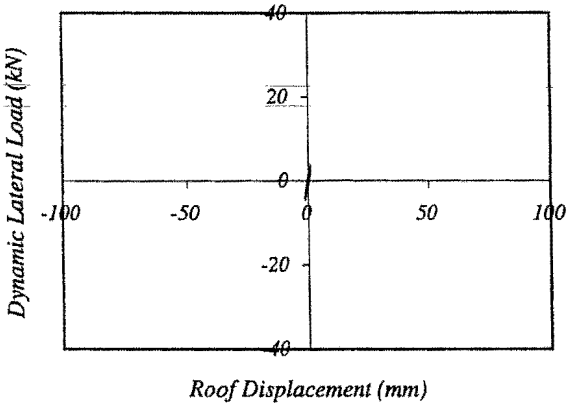

Wall with 2nd set of dissipators

Basic Input Ground Motion (BIGM):	*El Centro 180*
Scaling Factor for BIGM:	0.10
Expected Peak Table Acceleration:	0.04 g
Measured Peak Table Acceleration:	0.07 g
Peak Roof Hor. Acceleration:	0.13 g
Peak Roof Vert. Acceleration:	0.03 g
Peak Roof Displacement:	2 mm
Peak Average Drift:	0.04 %
Residual Roof Displacement:	0 mm
Max. Total Inertial Lat. Load:	4.69 kN

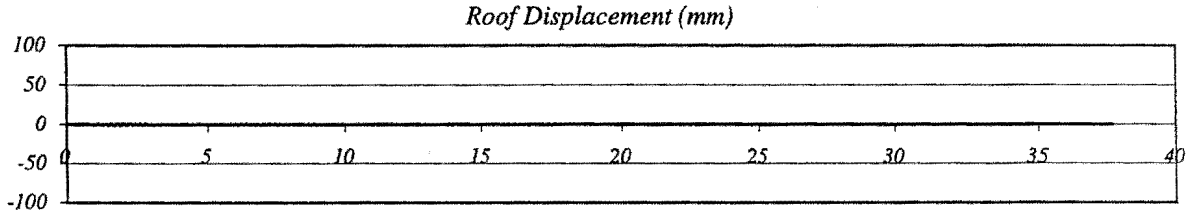

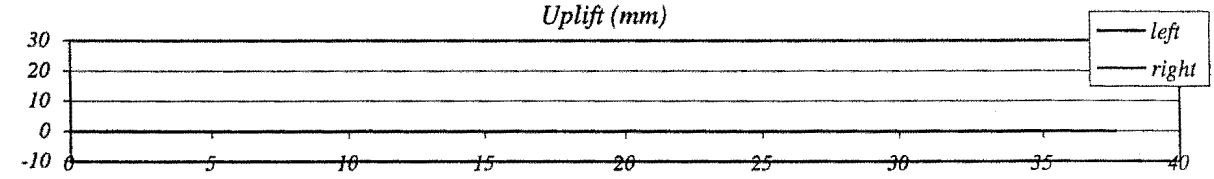

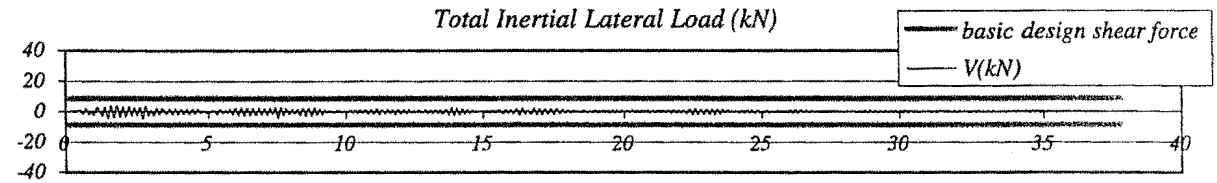

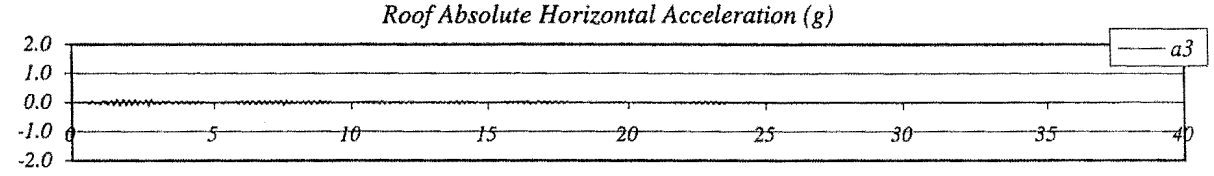

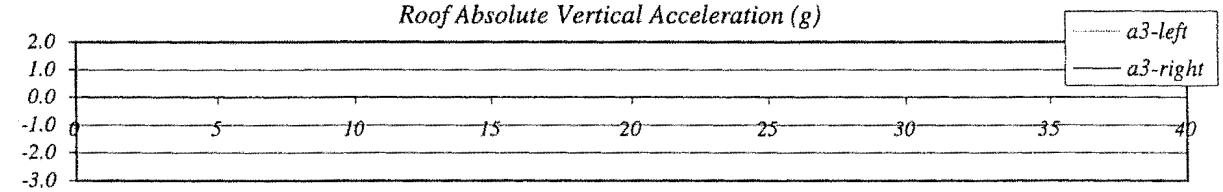

RUN # 37

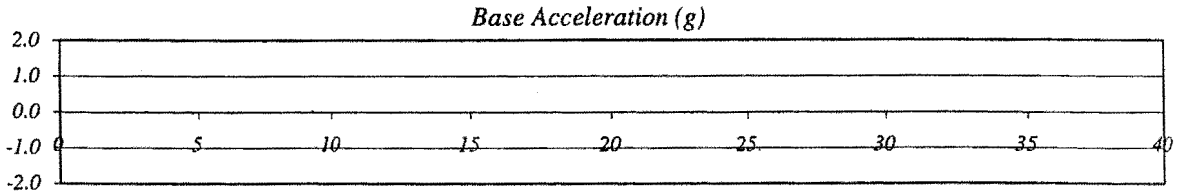

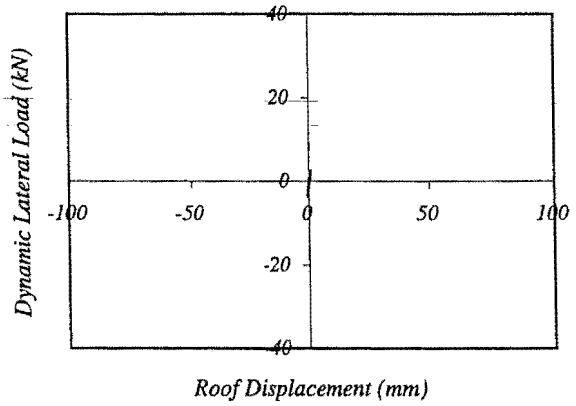

Wall with 2nd set of dissipators

Basic Input Ground Motion (BIGM):	*Taft 111*
Scaling Factor for BIGM:	0.10
Expected Peak Table Acceleration:	0.02 g
Measured Peak Table Acceleration:	0.04 g
Peak Roof Hor. Acceleration:	0.11 g
Peak Roof Vert. Acceleration:	0.03 g
Peak Roof Displacement:	1 mm
Peak Average Drift:	0.03 %
Residual Roof Displacement:	0 mm
Max. Total Inertial Lat. Load:	3.93 kN

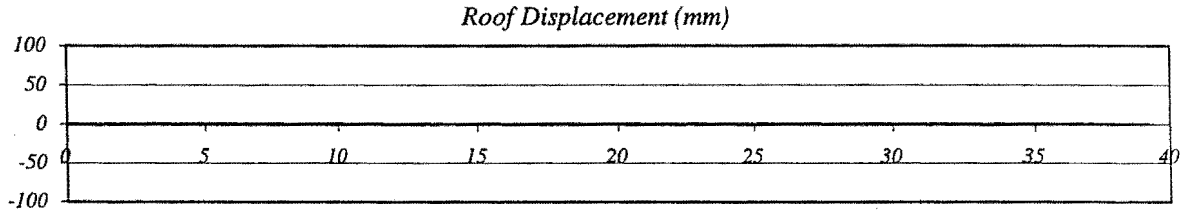

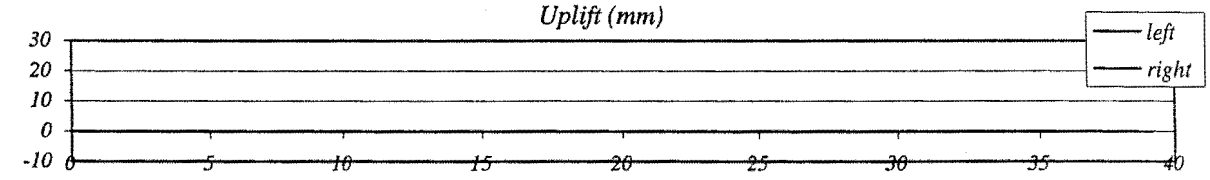

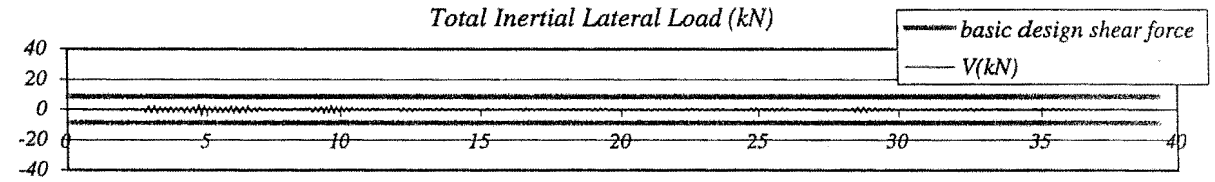

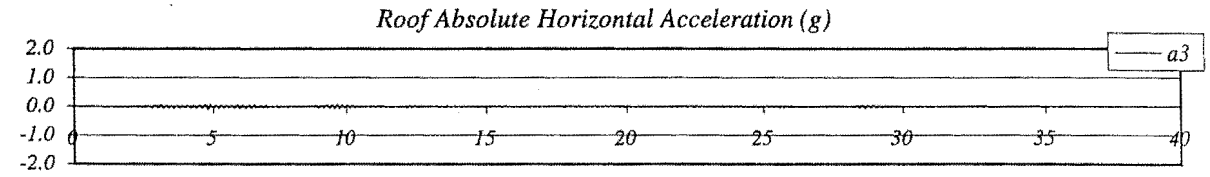

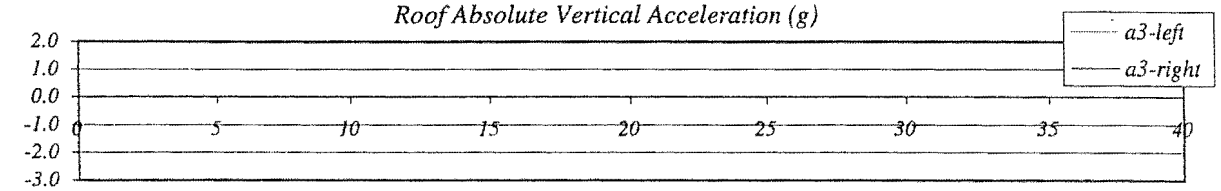

RUN # 38

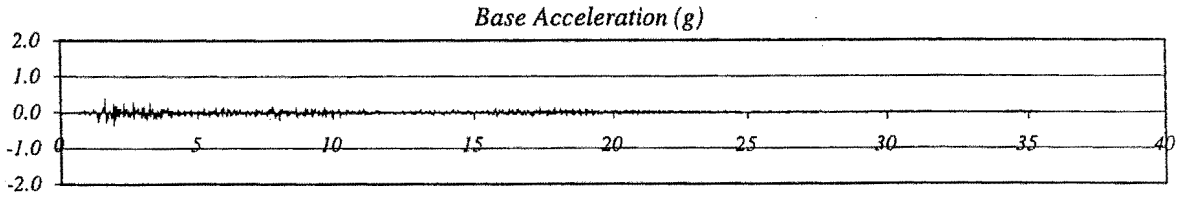

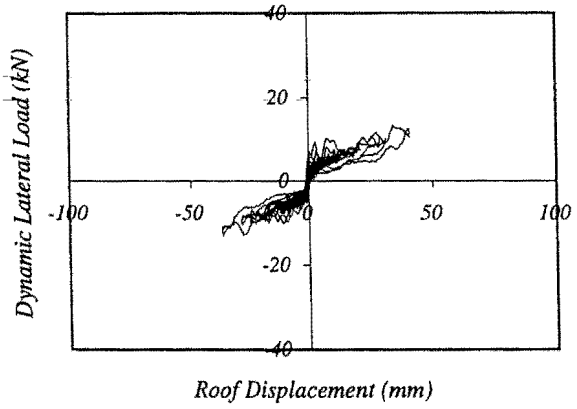

Wall with 2nd set of dissipators

Basic Input Ground Motion (BIGM):	*El Centro 180*
Scaling Factor for BIGM:	0.56
Expected Peak Table Acceleration:	0.20 g
Measured Peak Table Acceleration:	0.40 g
Peak Roof Hor. Acceleration:	0.51 g
Peak Roof Vert. Acceleration:	0.89 g
Peak Roof Displacement:	41 mm
Peak Average Drift:	1.10 %
Residual Roof Displacement:	0 mm
Max. Total Inertial Lat. Load:	13.34 kN

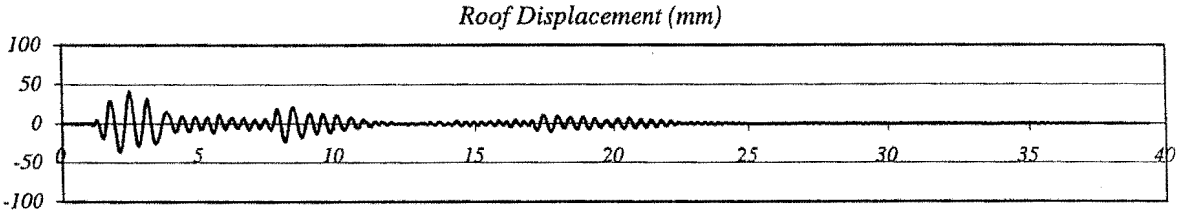

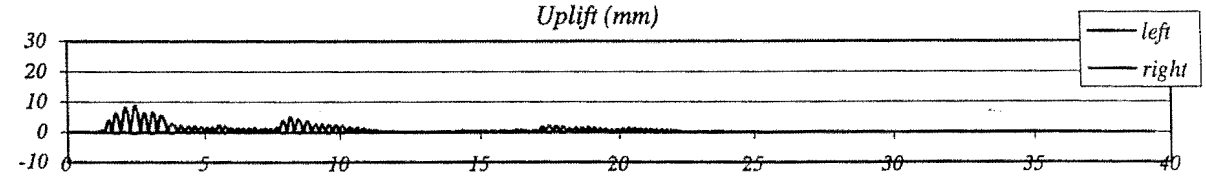

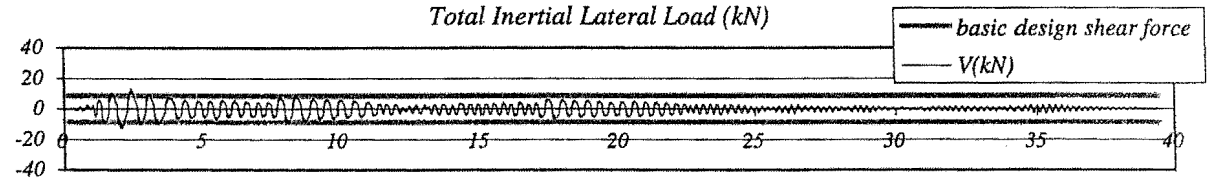

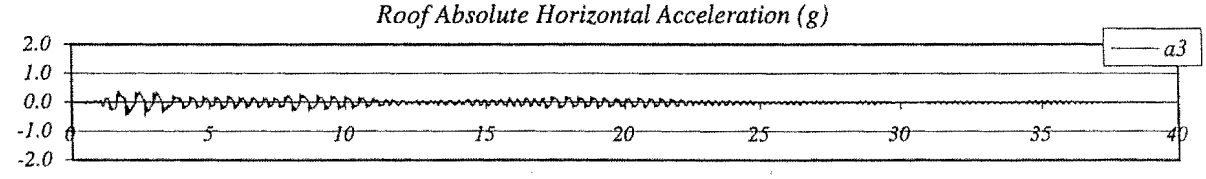

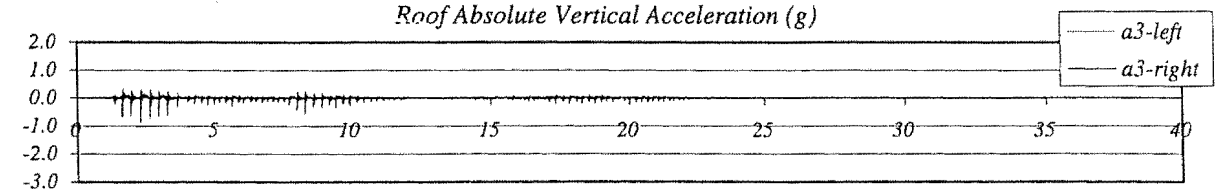

RUN # 39

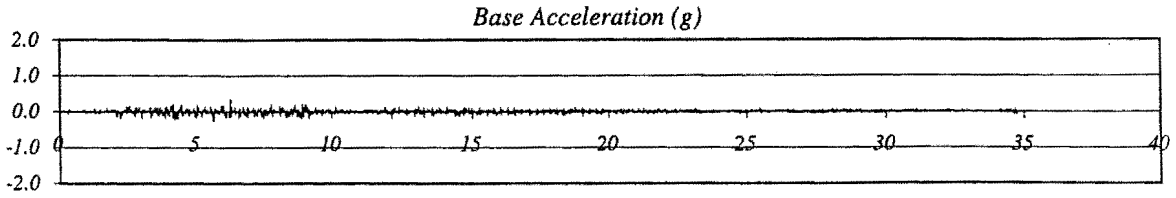

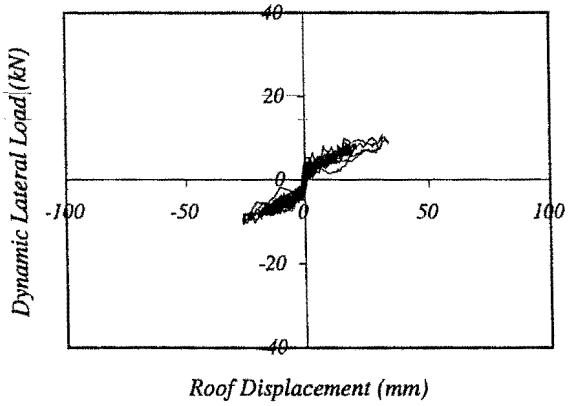

Wall with 2nd set of dissipators

Basic Input Ground Motion (BIGM):	*Taft 111*
Scaling Factor for BIGM:	1.13
Expected Peak Table Acceleration:	0.20 g
Measured Peak Table Acceleration:	0.35 g
Peak Roof Hor. Acceleration:	0.42 g
Peak Roof Vert. Acceleration:	0.96 g
Peak Roof Displacement:	34 mm
Peak Average Drift:	0.91 %
Residual Roof Displacement:	0 mm
Max. Total Inertial Lat. Load:	11.21 kN

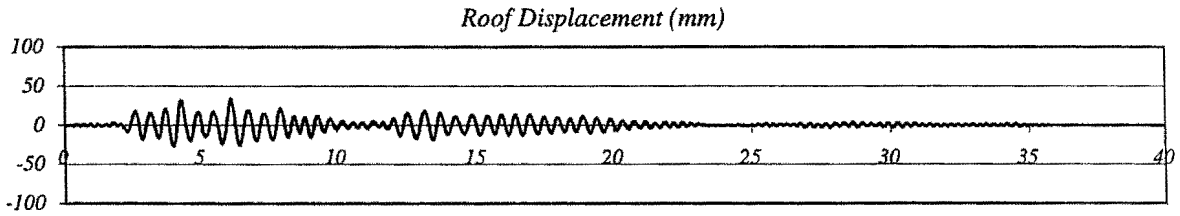

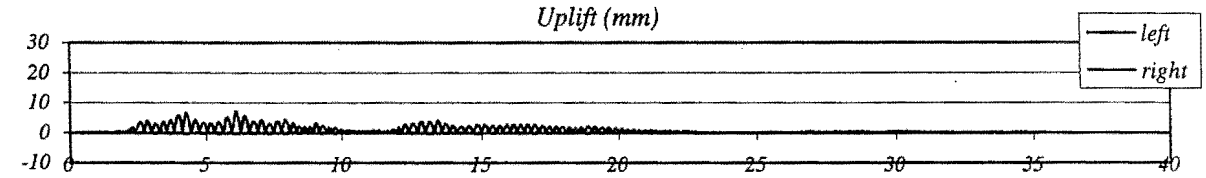

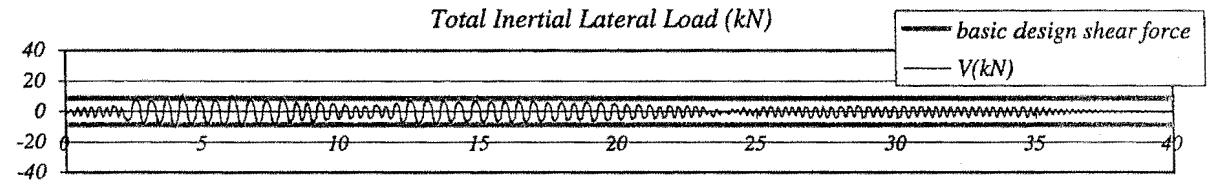

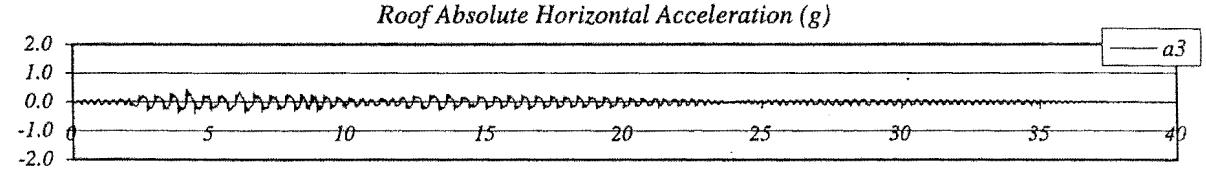

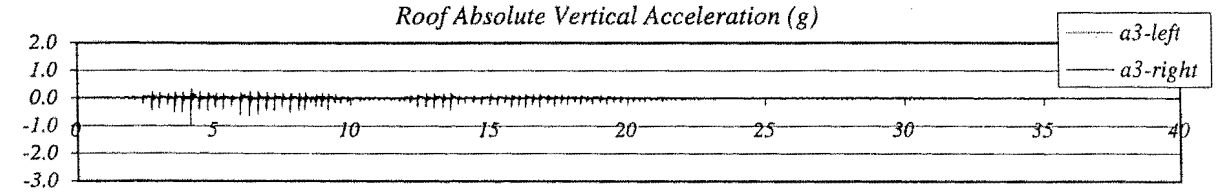

RUN # 40

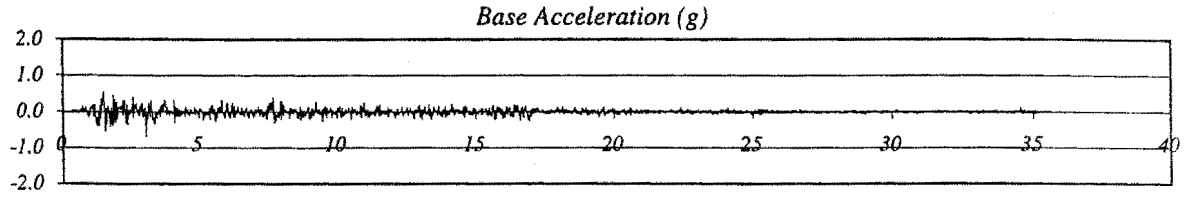

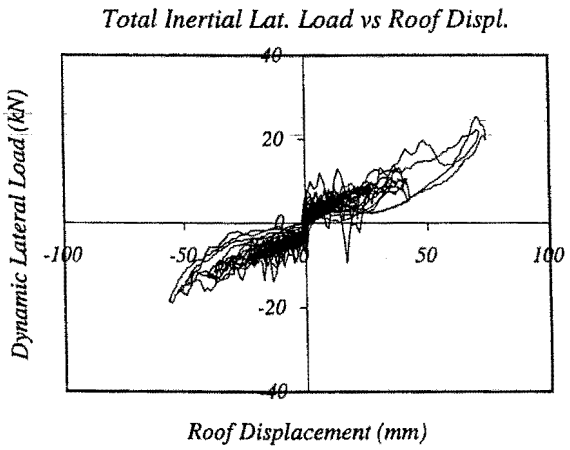

Wall with 2nd set of dissipators

Basic Input Ground Motion (BIGM):	*El Centro 180*
Scaling Factor for BIGM:	1.40
Expected Peak Table Acceleration:	0.50 g
Measured Peak Table Acceleration:	0.69 g
Peak Roof Hor. Acceleration:	0.77 g
Peak Roof Vert. Acceleration:	1.98 g
Peak Roof Displacement:	74 mm
Peak Average Drift:	1.98 %
Residual Roof Displacement:	0 mm
Max. Total Inertial Lat. Load:	25.23 kN

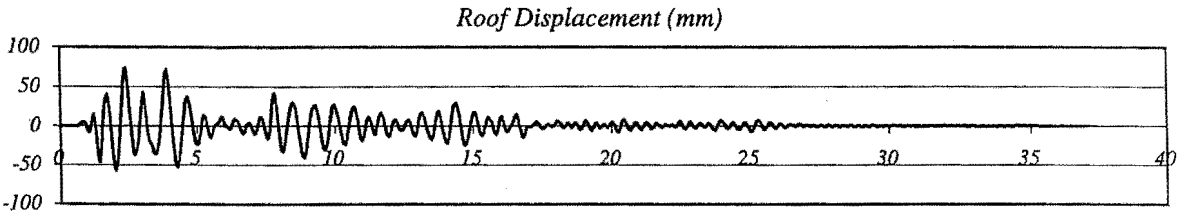

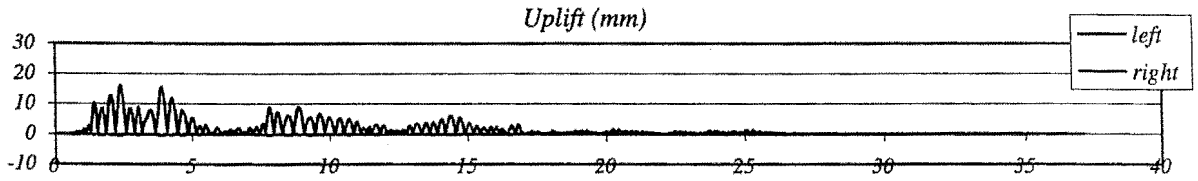

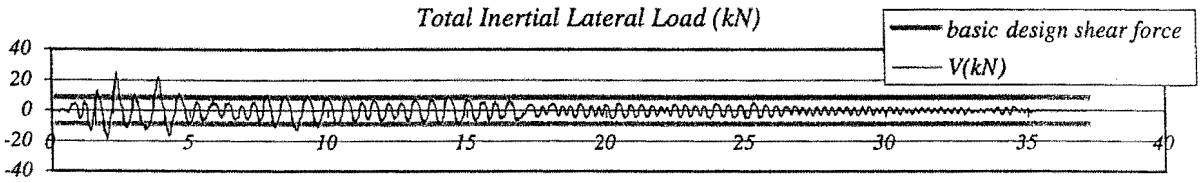

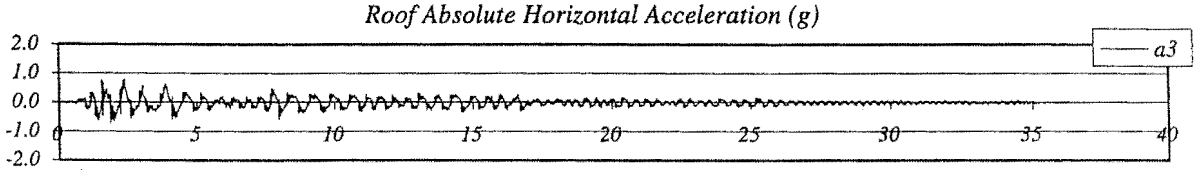

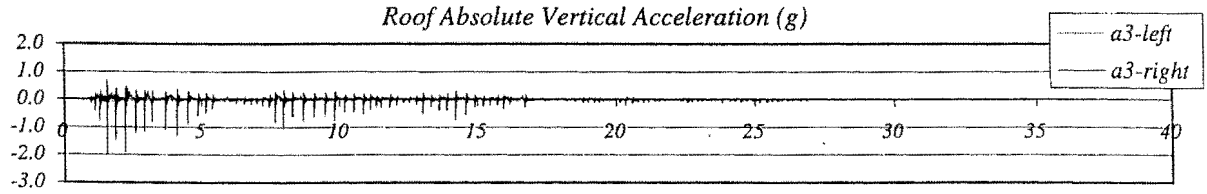

RUN # 41

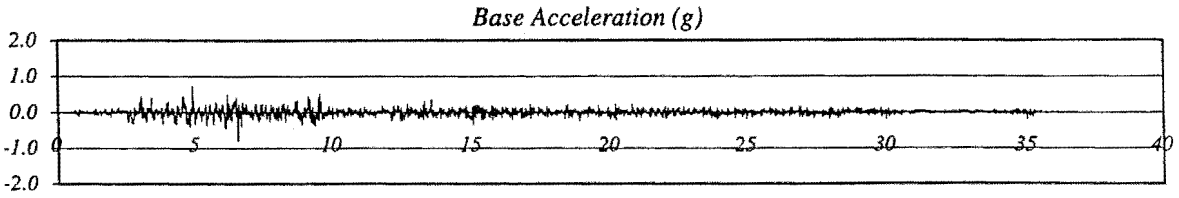

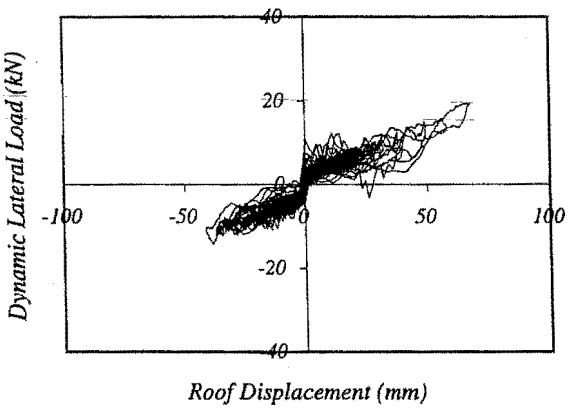

Wall with 2nd set of dissipators

Basic Input Ground Motion (BIGM):	*Taft 111*
Scaling Factor for BIGM:	2.83
Expected Peak Table Acceleration:	0.50 g
Measured Peak Table Acceleration:	0.80 g
Peak Roof Hor. Acceleration:	0.86 g
Peak Roof Vert. Acceleration:	1.75 g
Peak Roof Displacement:	68 mm
Peak Average Drift:	1.81 %
Residual Roof Displacement:	0 mm
Max. Total Inertial Lat. Load:	19.45 kN

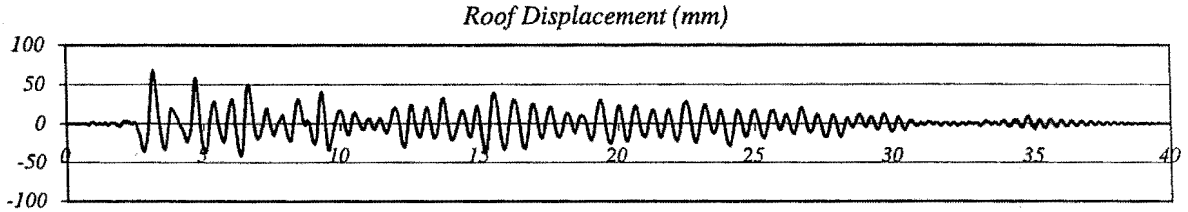

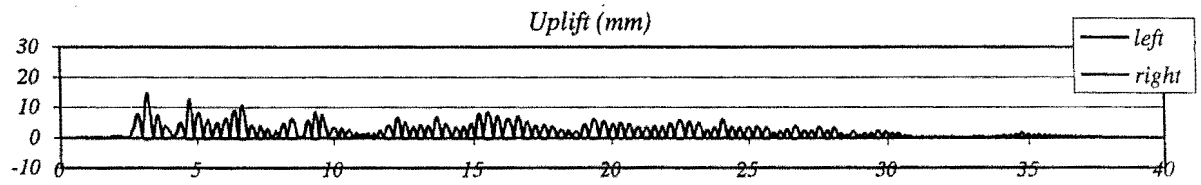

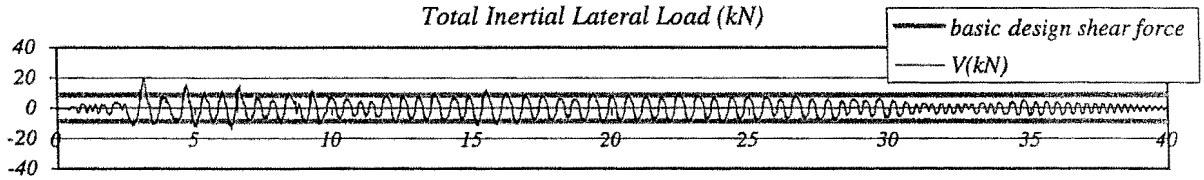

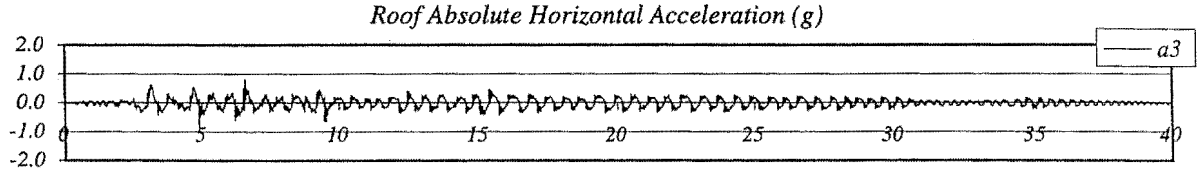

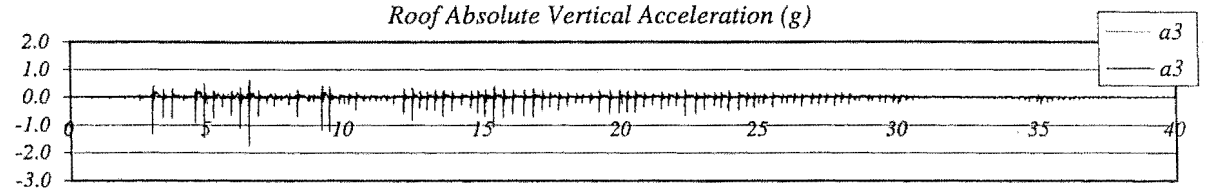

RUN # 42

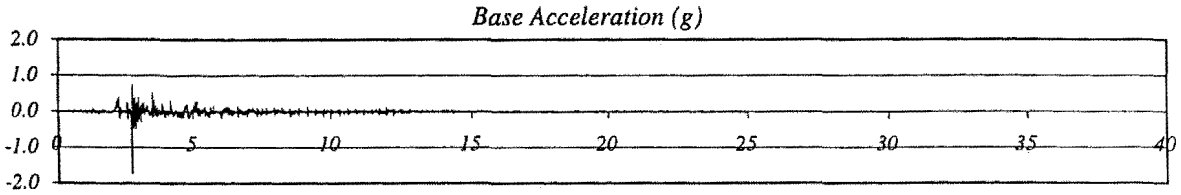

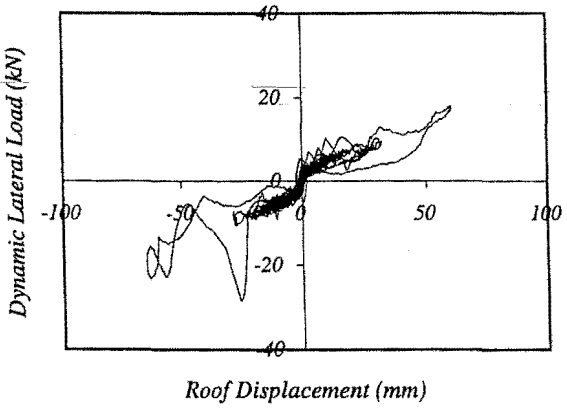

Wall with 2nd set of dissipators

Basic Input Ground Motion (BIGM):	*Sylmar 000*
Scaling Factor for BIGM:	0.63
Expected Peak Table Acceleration:	0.50 g
Measured Peak Table Acceleration:	1.75 g
Peak Roof Hor. Acceleration:	0.79 g
Peak Roof Vert. Acceleration:	1.19 g
Peak Roof Displacement:	64 mm
Peak Average Drift:	1.73 %
Residual Roof Displacement:	0 mm
Max. Total Inertial Lat. Load:	28.52 kN

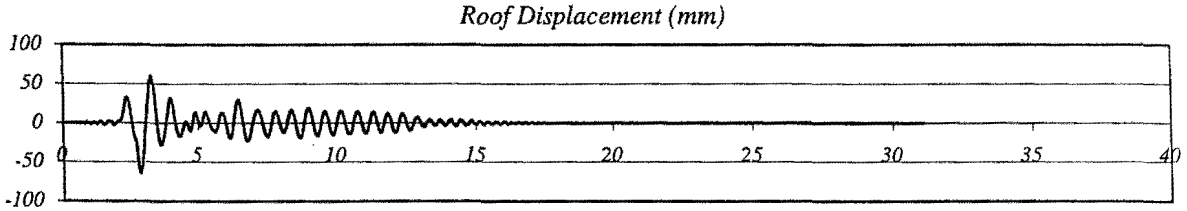

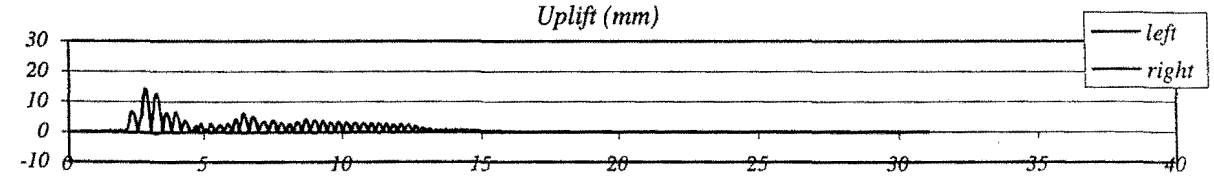

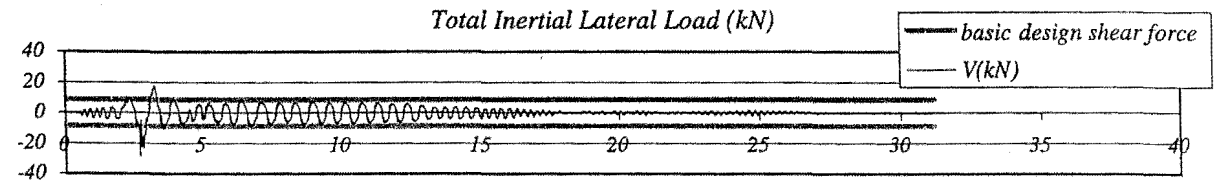

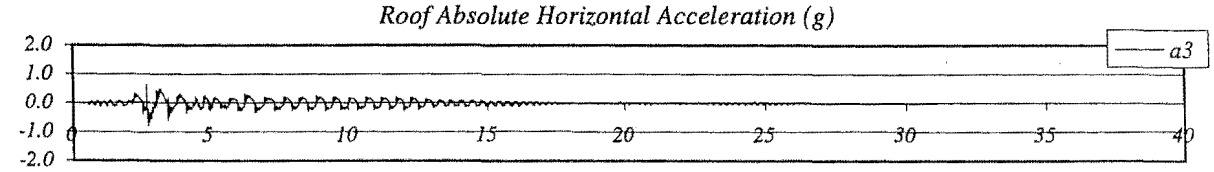

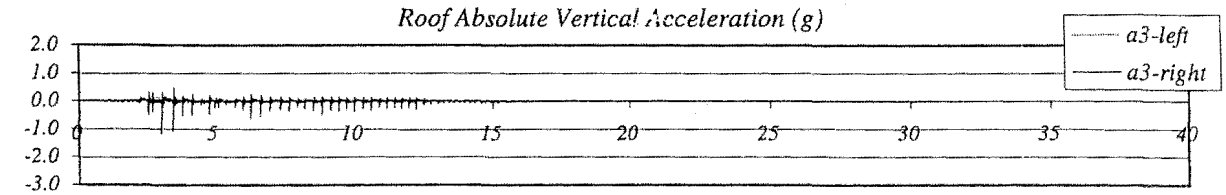

RUN # 43

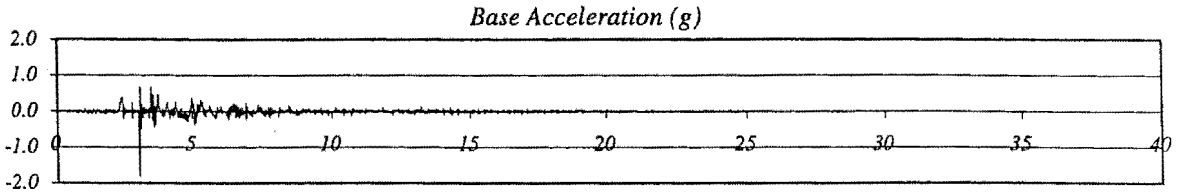

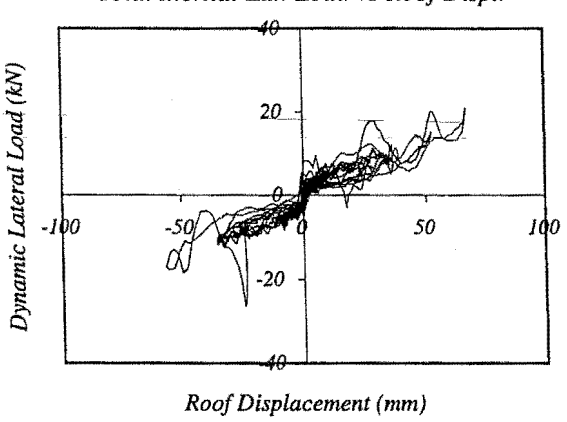

Wall with 2nd set of dissipators

Basic Input Ground Motion (BIGM):	*Sylmar 000*
Scaling Factor for BIGM:	1.00
Expected Peak Table Acceleration:	0.80 g
Measured Peak Table Acceleration:	1.82 g
Peak Roof Hor. Acceleration:	0.87 g
Peak Roof Vert. Acceleration:	1.54 g
Peak Roof Displacement:	66 mm
Peak Average Drift:	1.78 %
Residual Roof Displacement:	0 mm
Max. Total Inertial Lat. Load:	26.32 kN

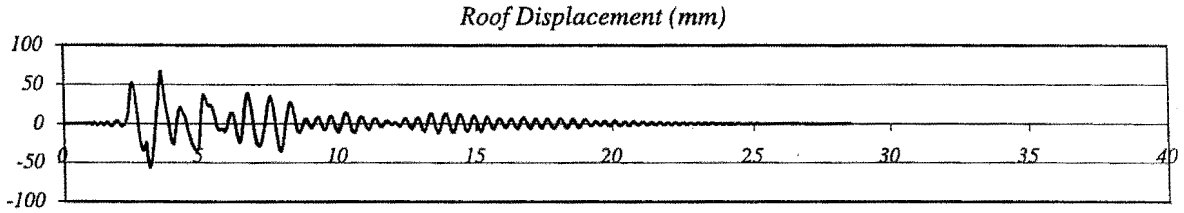

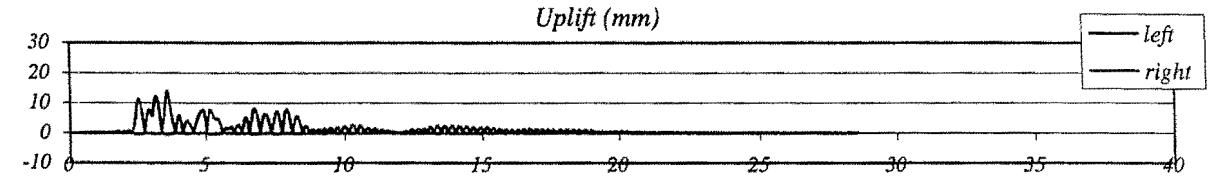

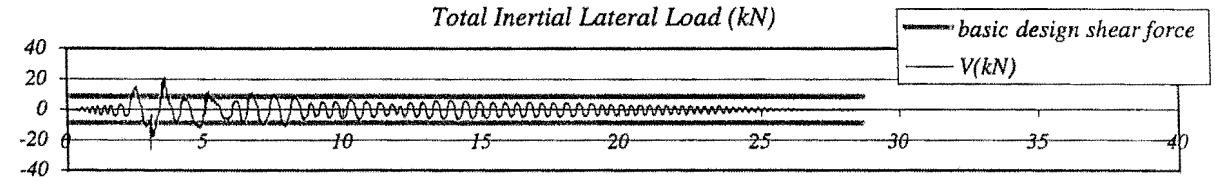

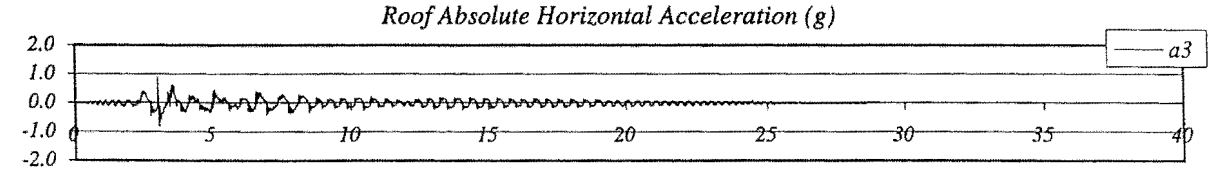

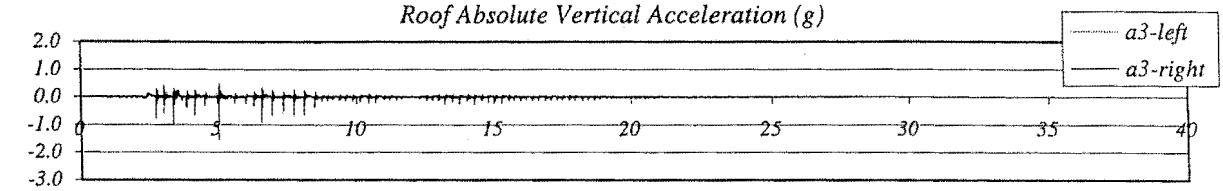

RUN # 44

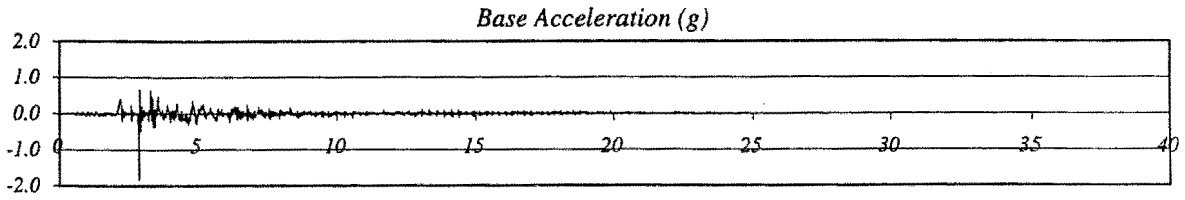

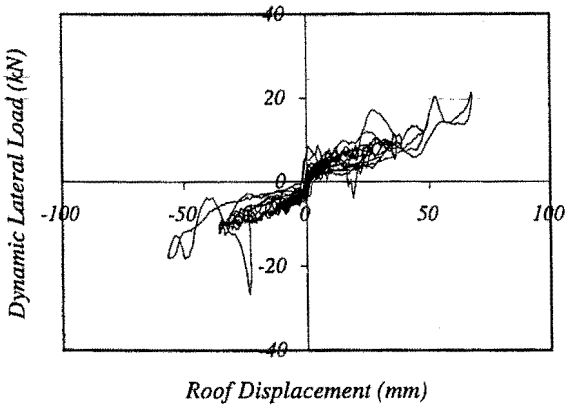

Wall with 2nd set of dissipators

Basic Input Ground Motion (BIGM):	*Sylmar 000*
Scaling Factor for BIGM:	1.00
Expected Peak Table Acceleration:	0.80 g
Measured Peak Table Acceleration:	1.84 g
Peak Roof Hor. Acceleration:	0.88 g
Peak Roof Vert. Acceleration:	1.48 g
Peak Roof Displacement:	67 mm
Peak Average Drift:	1.80 %
Residual Roof Displacement:	0 mm
Max. Total Inertial Lat. Load:	26.64 kN

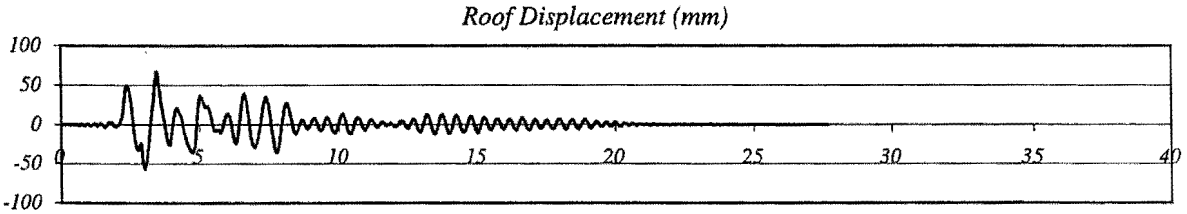

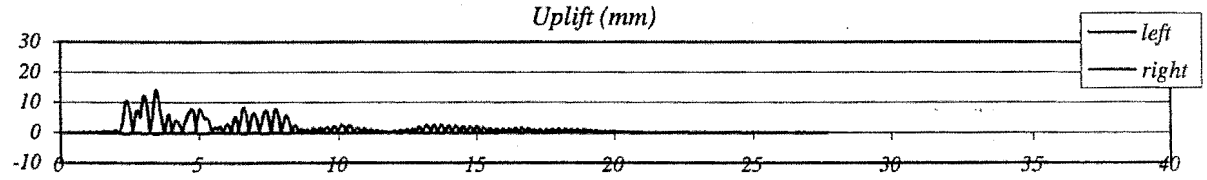

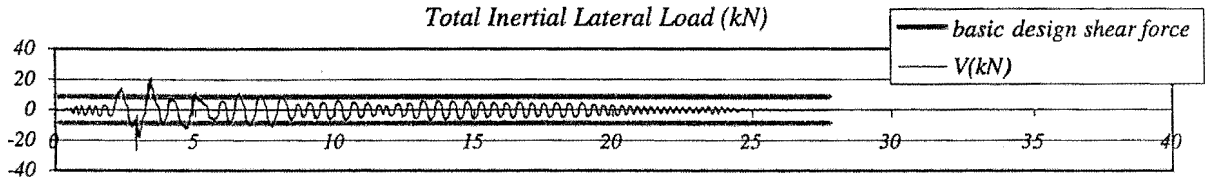

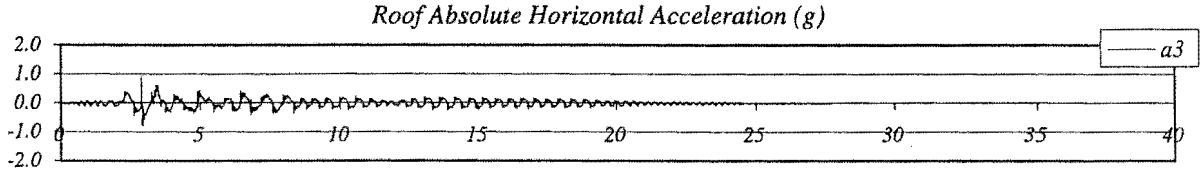

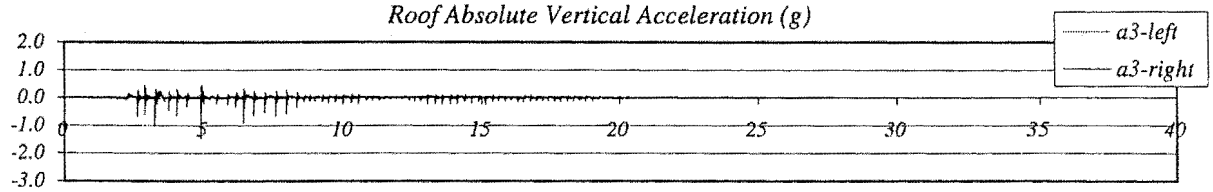

RUN # 45

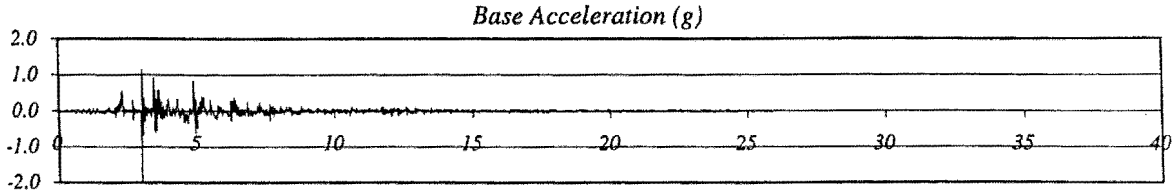

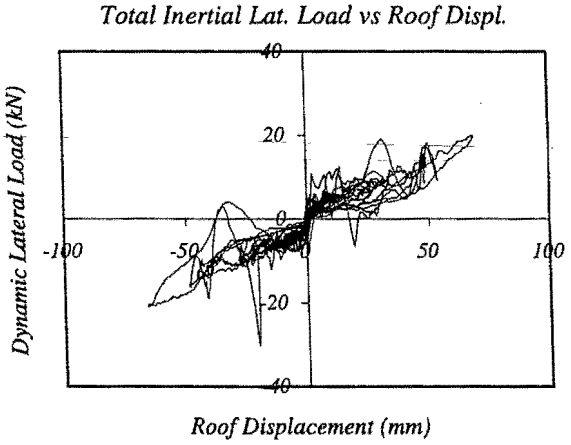

Wall with 2nd set of dissipators

Basic Input Ground Motion (BIGM):	*Sylmar 000*
Scaling Factor for BIGM:	1.25
Expected Peak Table Acceleration:	1.00 g
Measured Peak Table Acceleration:	2.17 g
Peak Roof Hor. Acceleration:	1.30 g
Peak Roof Vert. Acceleration:	2.08 g
Peak Roof Displacement:	69 mm
Peak Average Drift:	1.85 %
Residual Roof Displacement:	0 mm
Max. Total Inertial Lat. Load:	30.14 kN

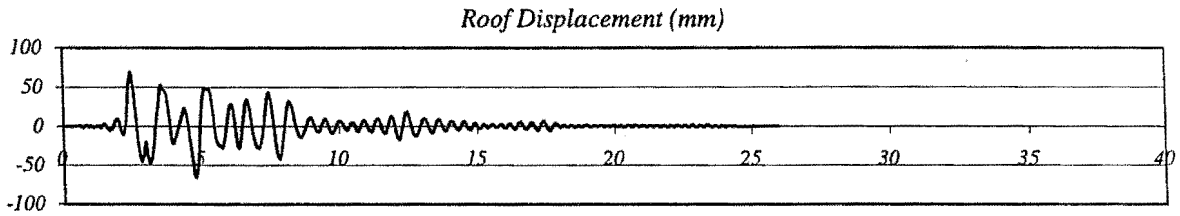

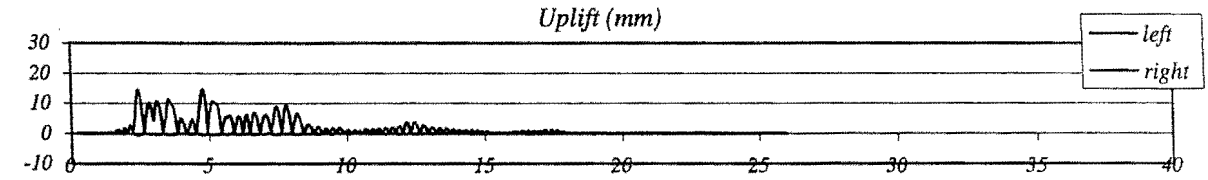

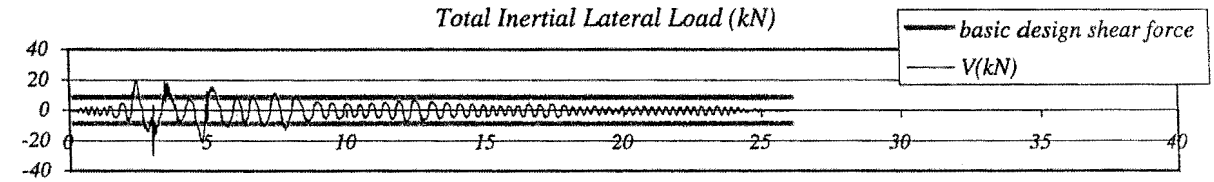

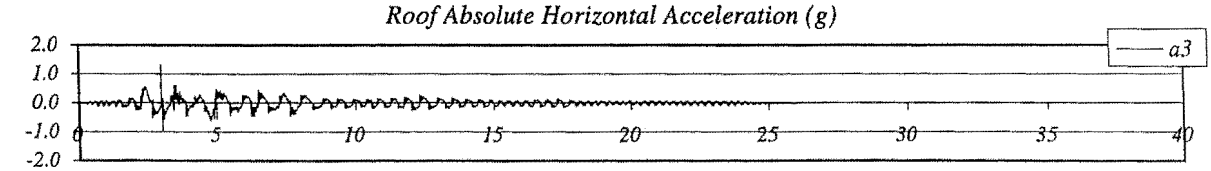

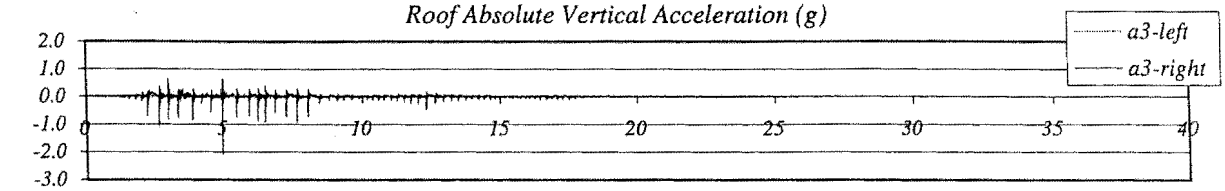

RUN # 46

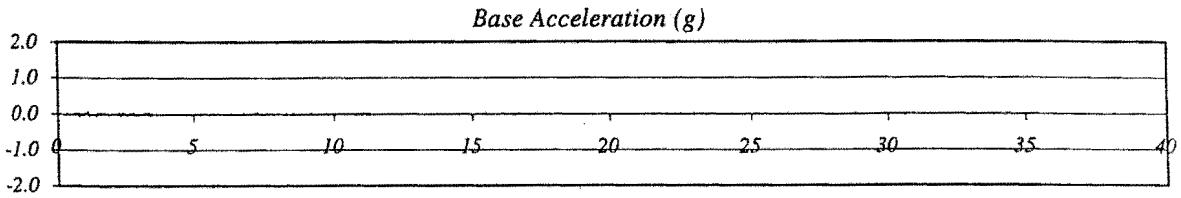

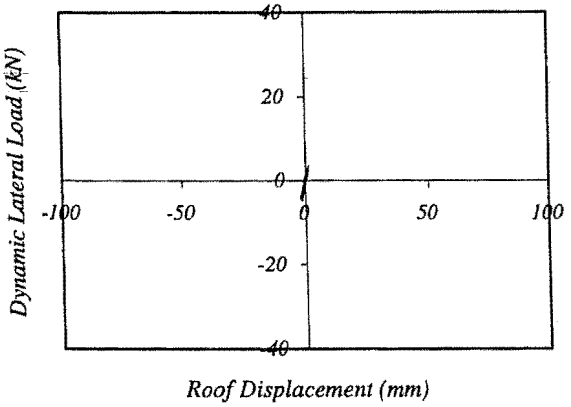

Wall without dissipators

Basic Input Ground Motion (BIGM):	*El Centro 180*
Scaling Factor for BIGM:	0.10
Expected Peak Table Acceleration:	0.04 g
Measured Peak Table Acceleration:	0.08 g
Peak Roof Hor. Acceleration:	0.13 g
Peak Roof Vert. Acceleration:	0.05 g
Peak Roof Displacement:	2 mm
Peak Average Drift:	0.05 %
Residual Roof Displacement:	0 mm
Max. Total Inertial Lat. Load:	4.73 kN

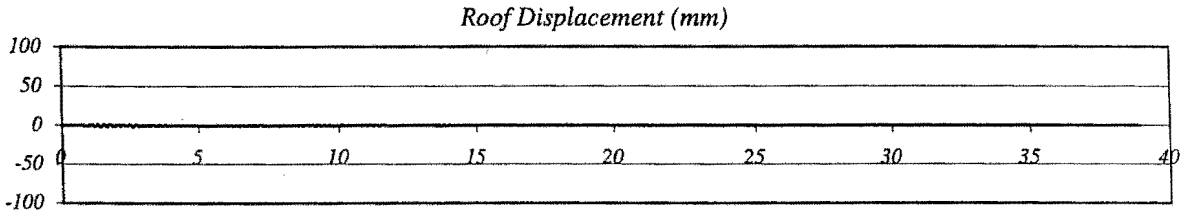

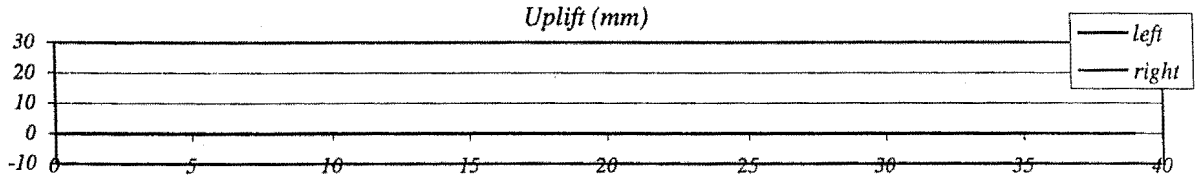

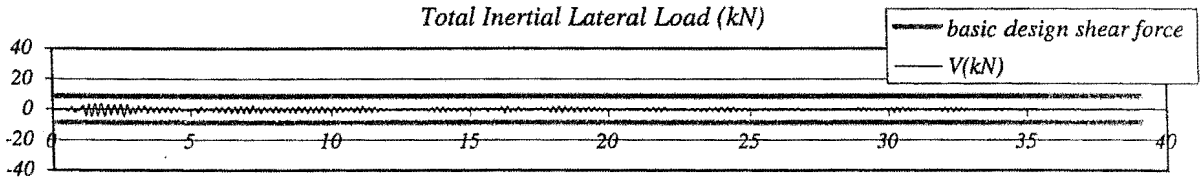

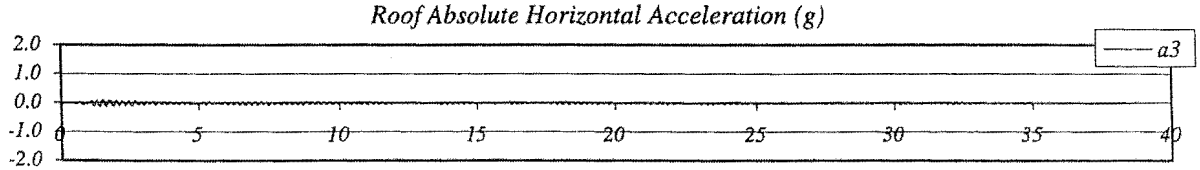

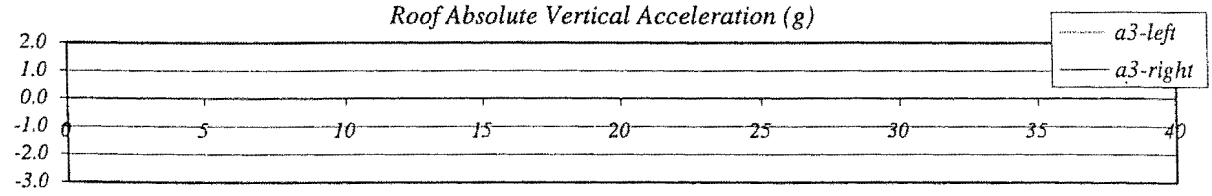

RUN # 47

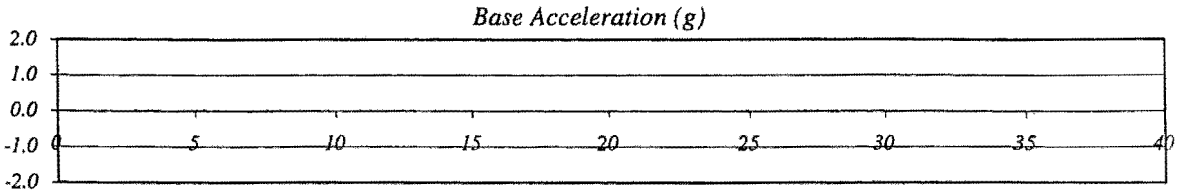

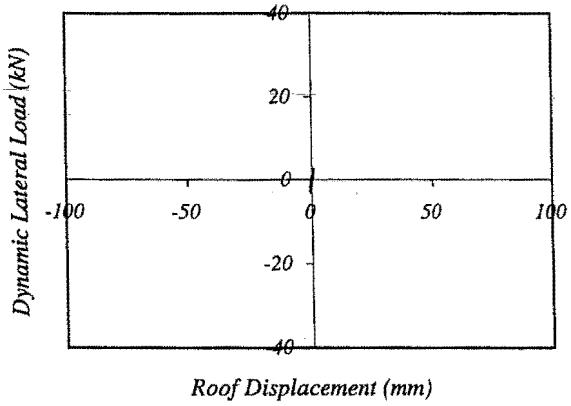

Wall without dissipators

Basic Input Ground Motion (BIGM):	*Taft 111*
Scaling Factor for BIGM:	0.10
Expected Peak Table Acceleration:	0.02 g
Measured Peak Table Acceleration:	0.04 g
Peak Roof Hor. Acceleration:	0.11 g
Peak Roof Vert. Acceleration:	0.03 g
Peak Roof Displacement:	1 mm
Peak Average Drift:	0.02 %
Residual Roof Displacement:	0 mm
Max. Total Inertial Lat. Load:	3.35 kN

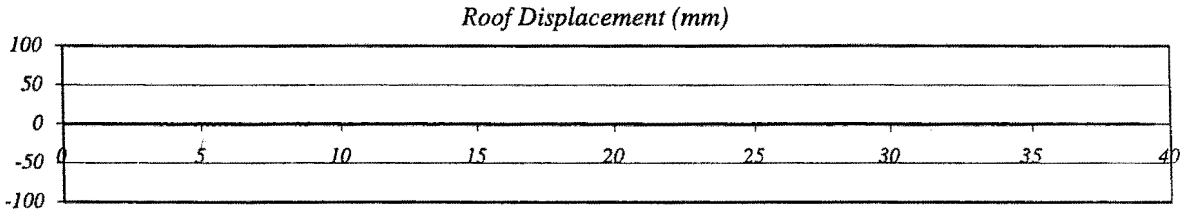

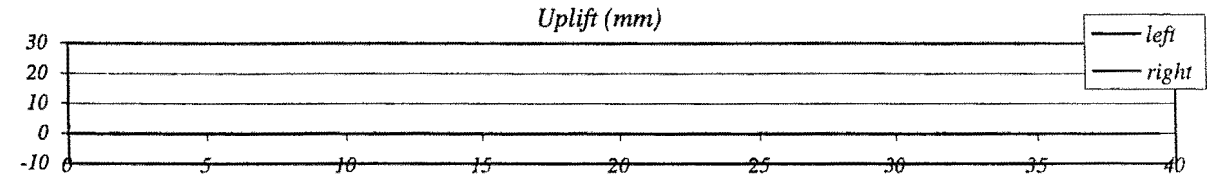

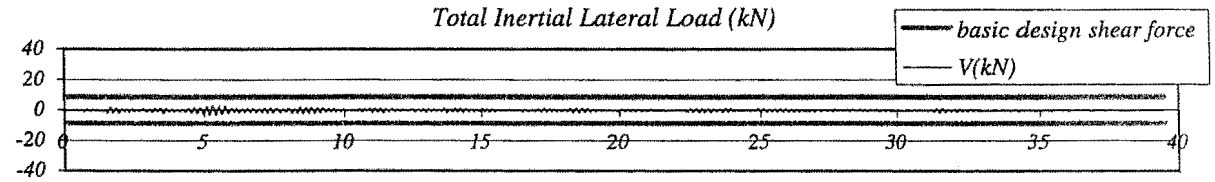

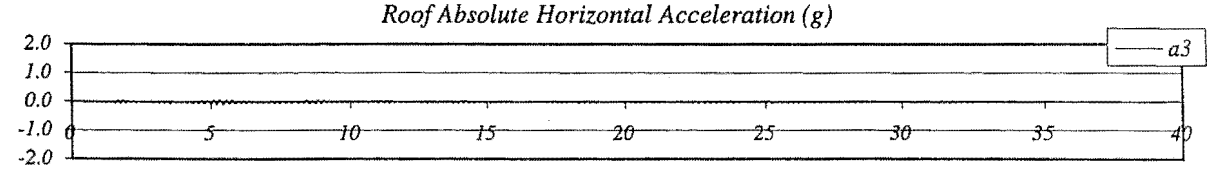

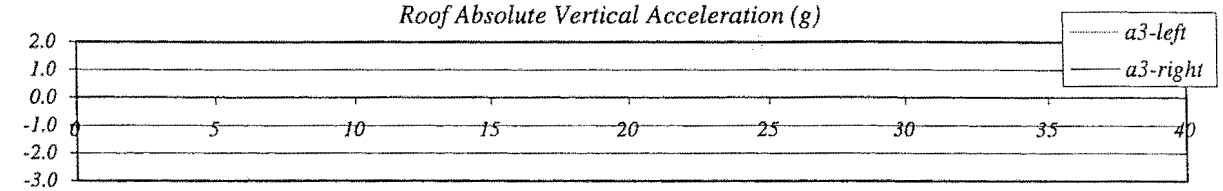

RUN # 48

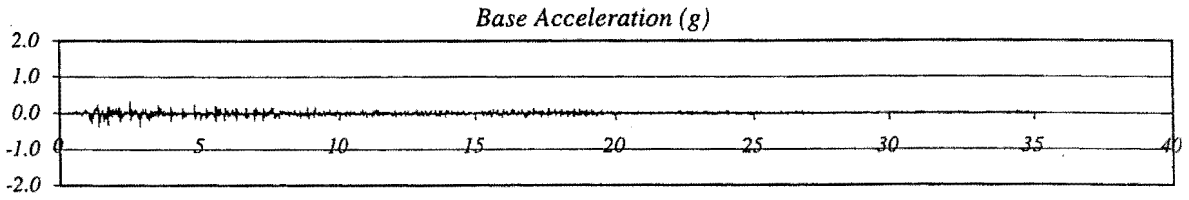

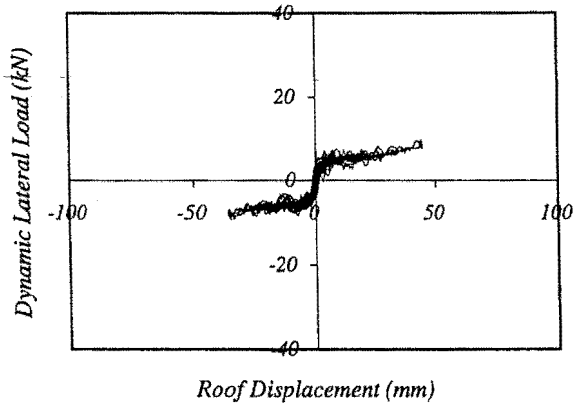

Wall without dissipators

Basic Input Ground Motion (BIGM):	*El Centro 180*
Scaling Factor for BIGM:	0.56
Expected Peak Table Acceleration:	0.20 g
Measured Peak Table Acceleration:	0.37 g
Peak Roof Hor. Acceleration:	0.52 g
Peak Roof Vert. Acceleration:	0.85 g
Peak Roof Displacement:	45 mm
Peak Average Drift:	1.20 %
Residual Roof Displacement:	0 mm
Max. Total Inertial Lat. Load:	9.75 kN

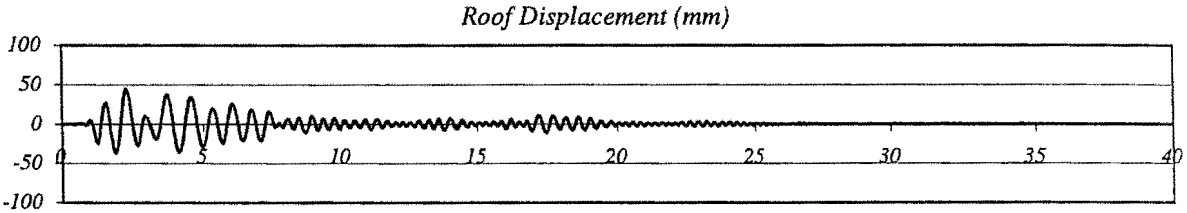

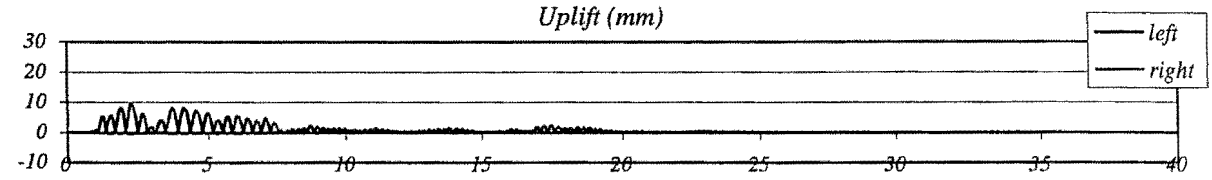

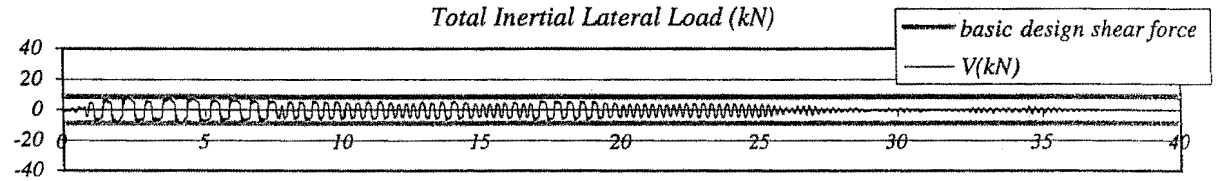

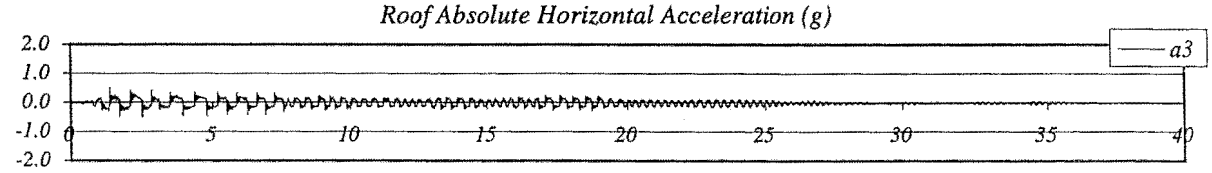

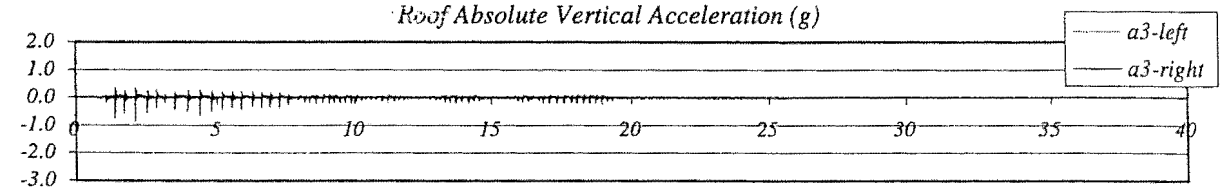

RUN # 49

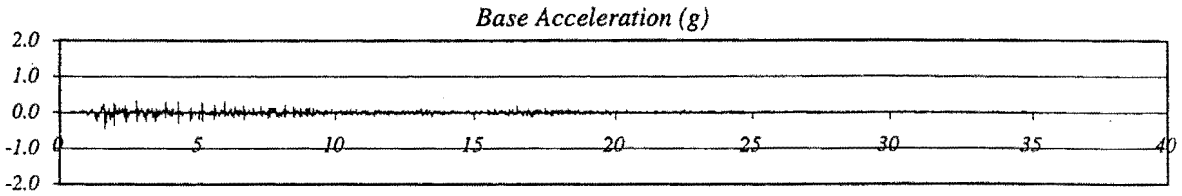

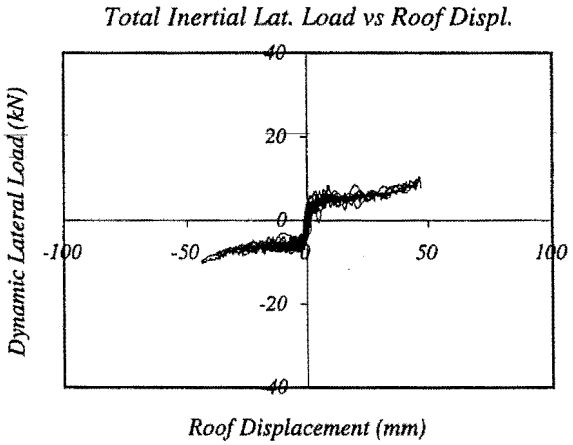

Wall without dissipators

Basic Input Ground Motion (BIGM):	*El Centro 180*
Scaling Factor for BIGM:	0.56
Expected Peak Table Acceleration:	0.20 g
Measured Peak Table Acceleration:	0.45 g
Peak Roof Hor. Acceleration:	0.65 g
Peak Roof Vert. Acceleration:	0.83 g
Peak Roof Displacement:	47 mm
Peak Average Drift:	1.26 %
Residual Roof Displacement:	1 mm
Max. Total Inertial Lat. Load:	10.51 kN

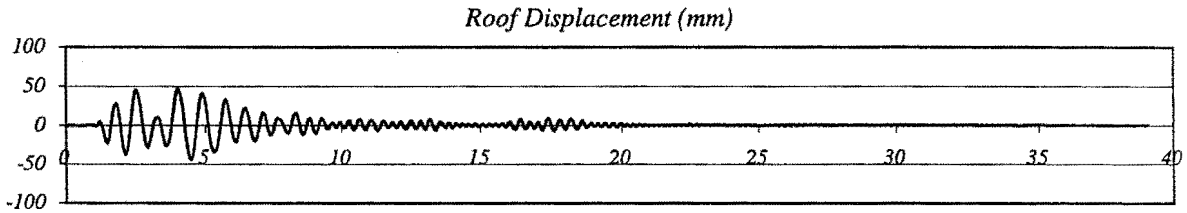

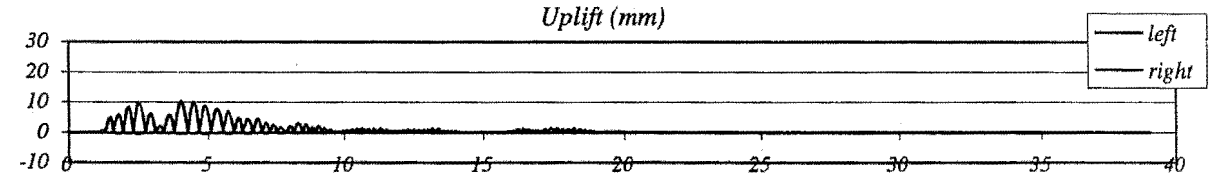

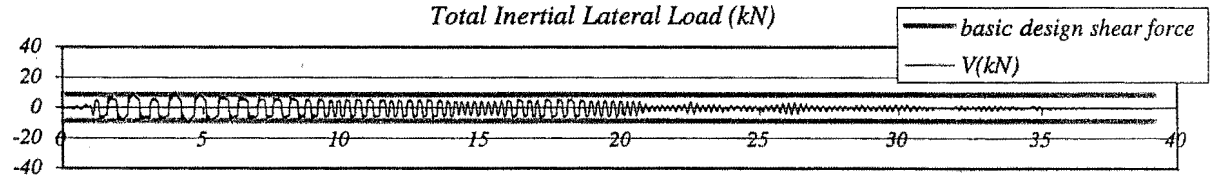

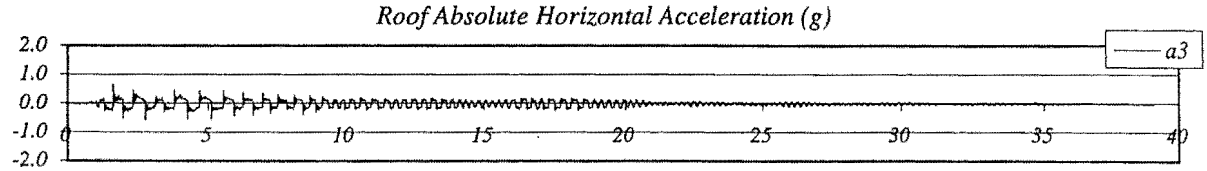

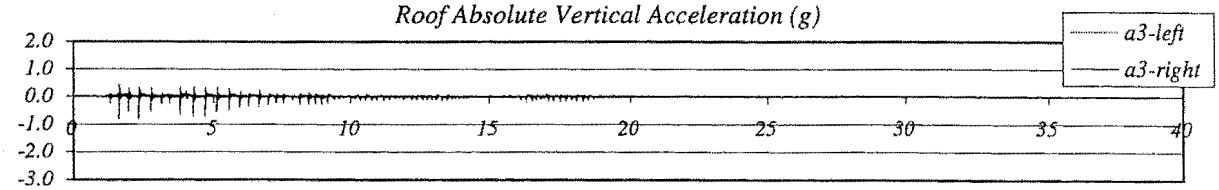

RUN # 50

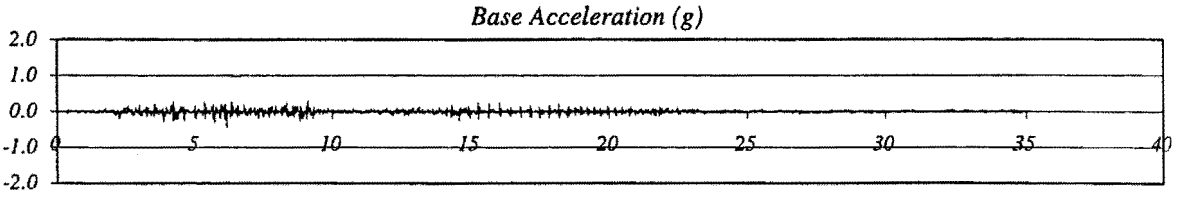

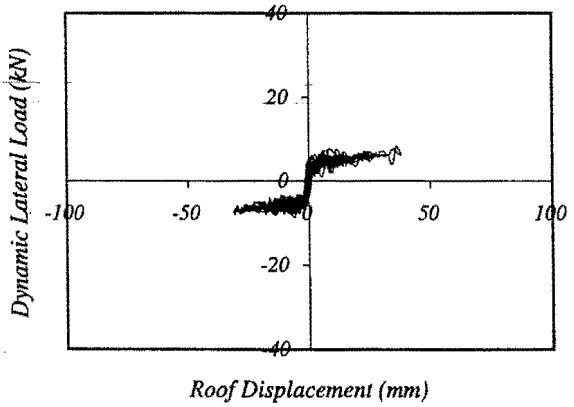

Wall without dissipators

Basic Input Ground Motion (BIGM):	*Taft 111*
Scaling Factor for BIGM:	1.13
Expected Peak Table Acceleration:	0.20 g
Measured Peak Table Acceleration:	0.44 g
Peak Roof Hor. Acceleration:	0.56 g
Peak Roof Vert. Acceleration:	0.84 g
Peak Roof Displacement:	38 mm
Peak Average Drift:	1.03 %
Residual Roof Displacement:	0 mm
Max. Total Inertial Lat. Load:	8.73 kN

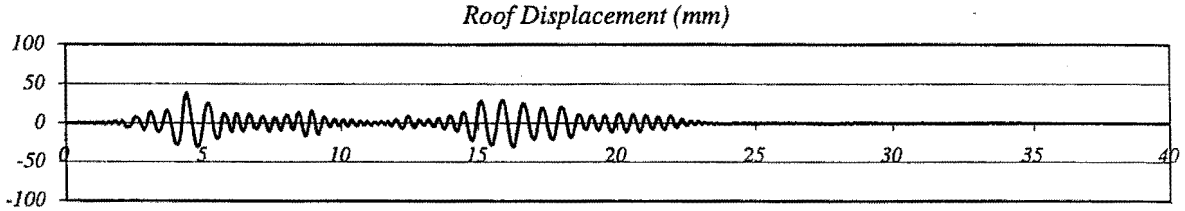

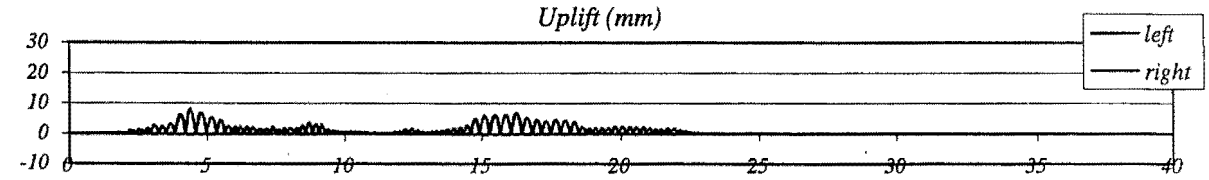

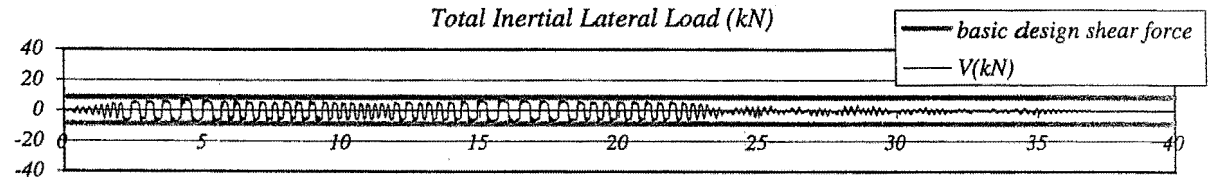

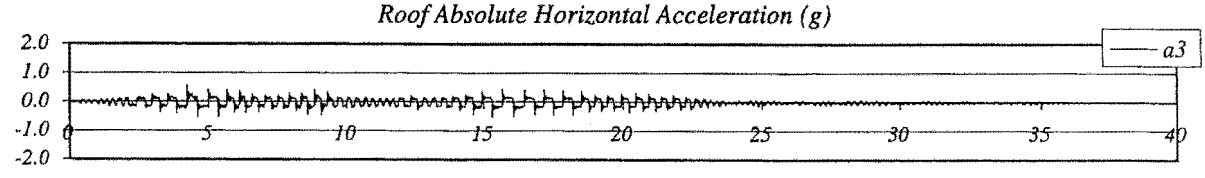

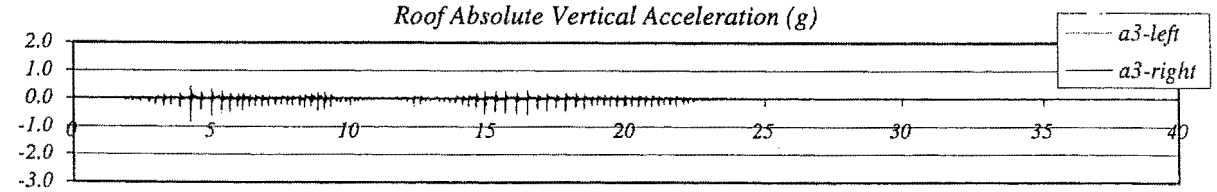

RUN # 51

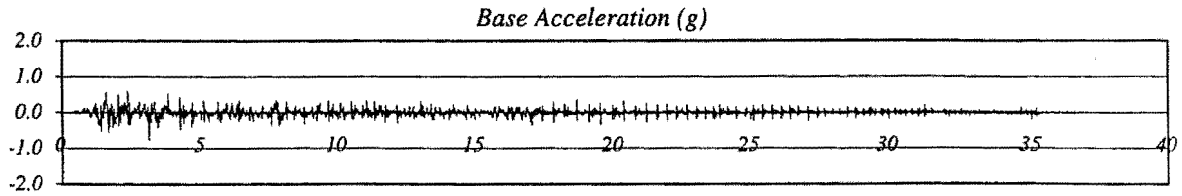

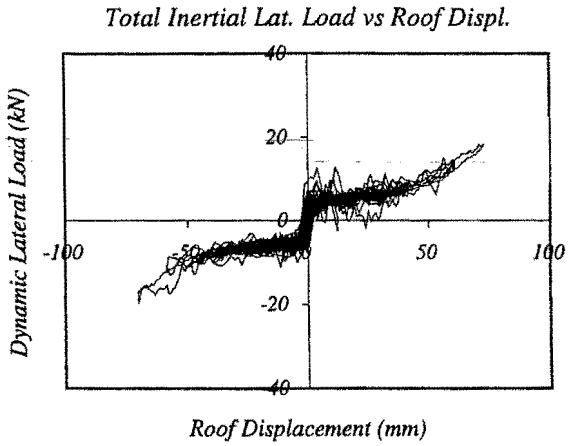

Wall without dissipators

Basic Input Ground Motion (BIGM):	*El Centro 180*
Scaling Factor for BIGM:	1.40
Expected Peak Table Acceleration:	0.50 g
Measured Peak Table Acceleration:	0.79 g
Peak Roof Hor. Acceleration:	0.76 g
Peak Roof Vert. Acceleration:	1.38 g
Peak Roof Displacement:	73 mm
Peak Average Drift:	1.96 %
Residual Roof Displacement:	0 mm
Max. Total Inertial Lat. Load:	19.93 kN

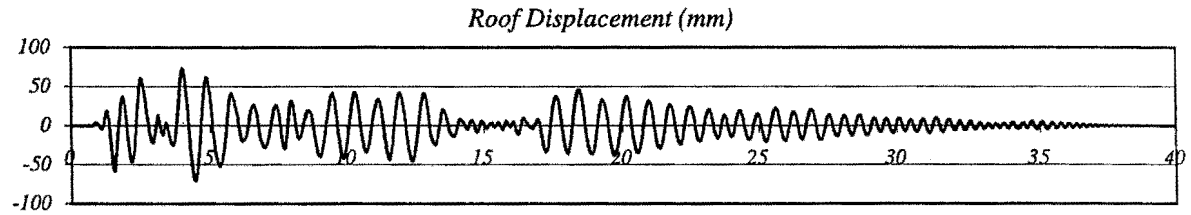

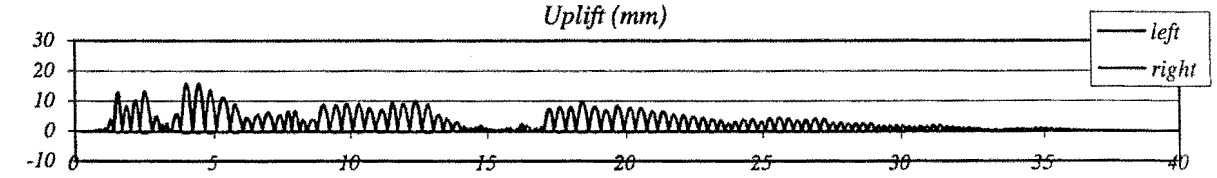

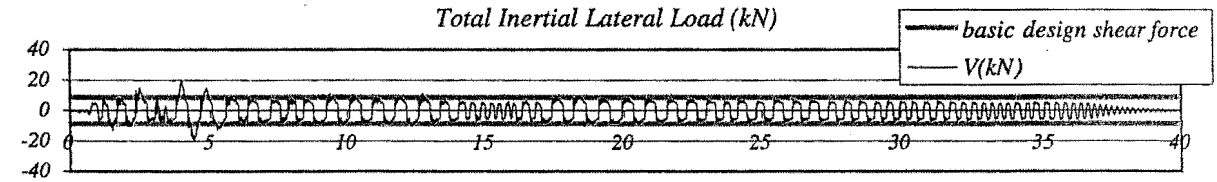

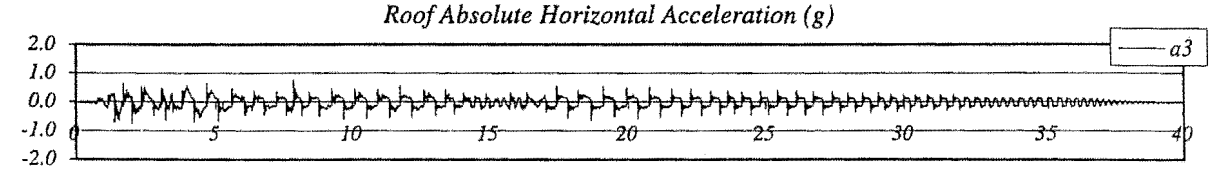

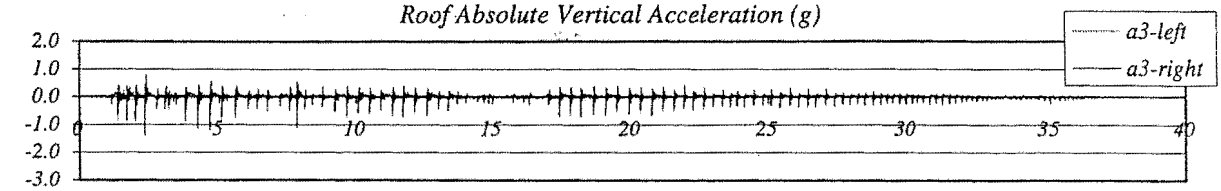

RUN # 52

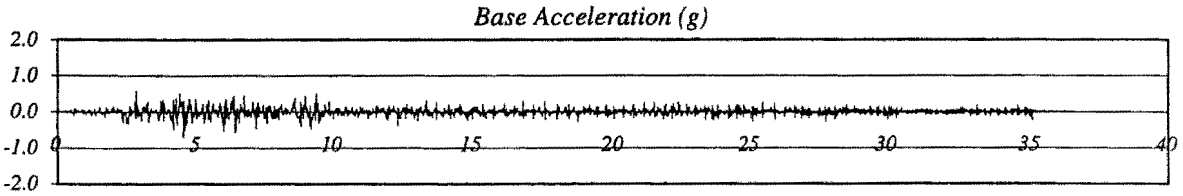

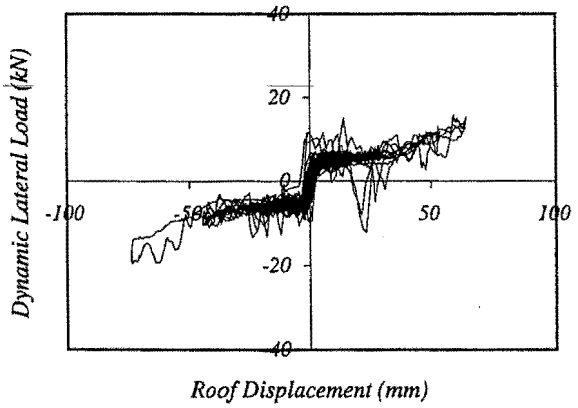

Wall without dissipators

Basic Input Ground Motion (BIGM):	*Taft 111*
Scaling Factor for BIGM:	2.83
Expected Peak Table Acceleration:	0.50 g
Measured Peak Table Acceleration:	0.71 g
Peak Roof Hor. Acceleration:	0.95 g
Peak Roof Vert. Acceleration:	2.16 g
Peak Roof Displacement:	73 mm
Peak Average Drift:	1.96 %
Residual Roof Displacement:	0 mm
Max. Total Inertial Lat. Load:	19.60 kN

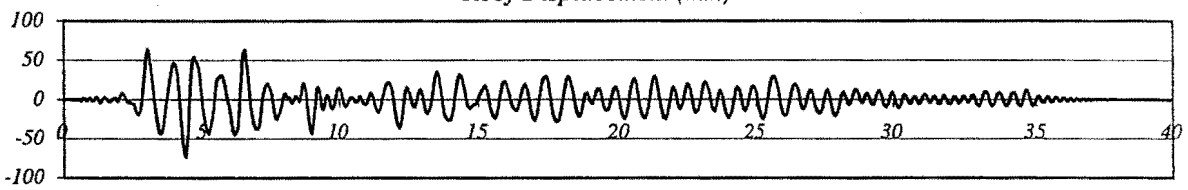

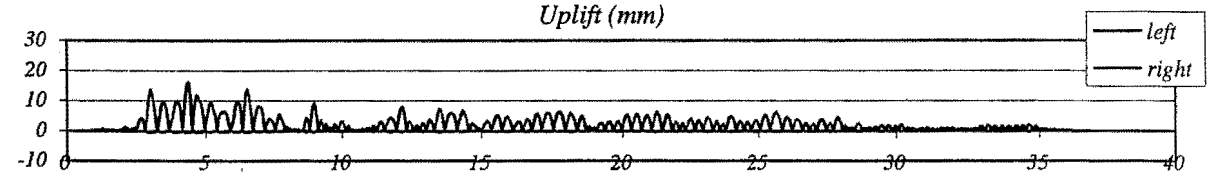

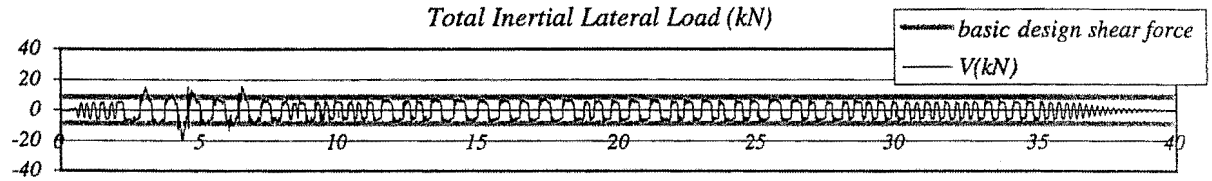

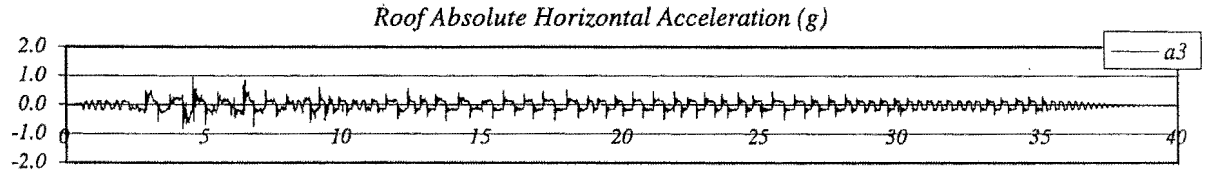

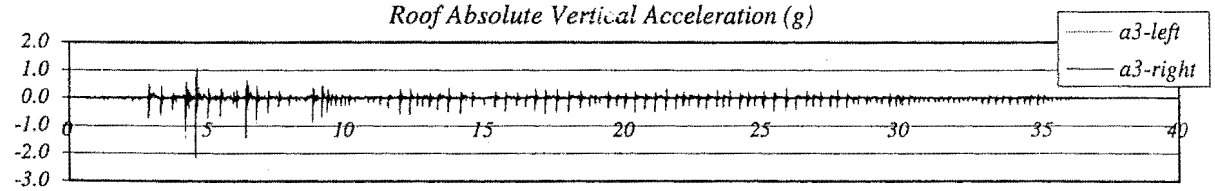

RUN # 53

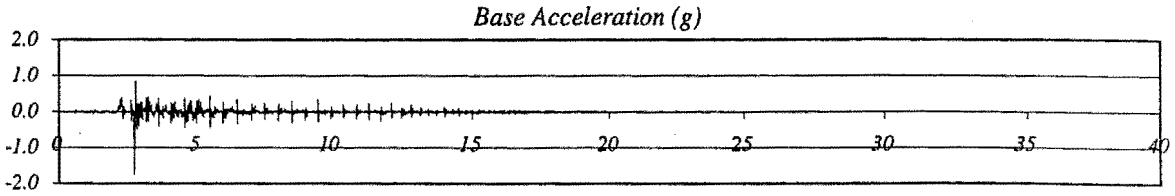

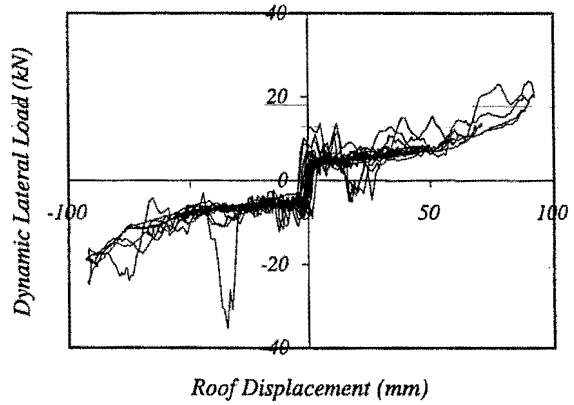

Wall without dissipators

Basic Input Ground Motion (BIGM):	*Sylmar 000*
Scaling Factor for BIGM:	0.63
Expected Peak Table Acceleration:	0.50 g
Measured Peak Table Acceleration:	1.77 g
Peak Roof Hor. Acceleration:	1.43 g
Peak Roof Vert. Acceleration:	1.81 g
Peak Roof Displacement:	93 mm
Peak Average Drift:	2.50 %
Residual Roof Displacement:	0 mm
Max. Total Inertial Lat. Load:	35.33 kN

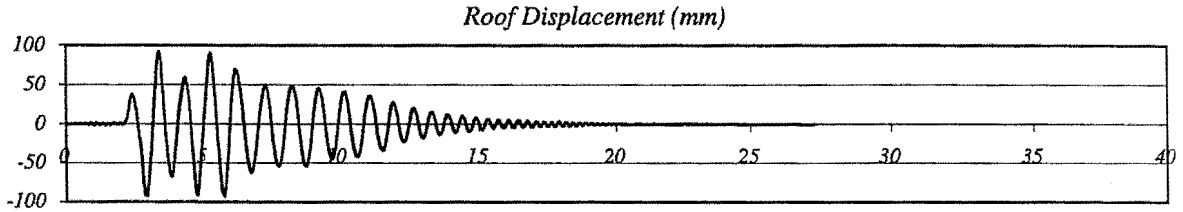

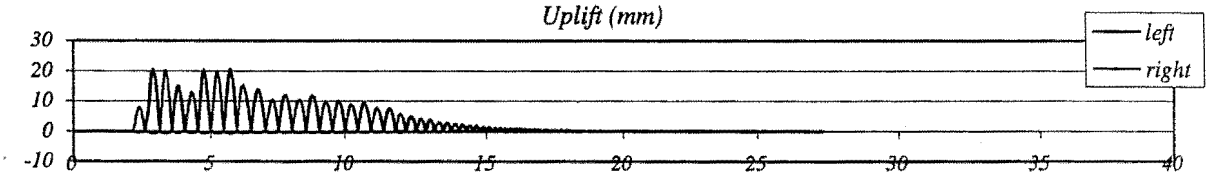

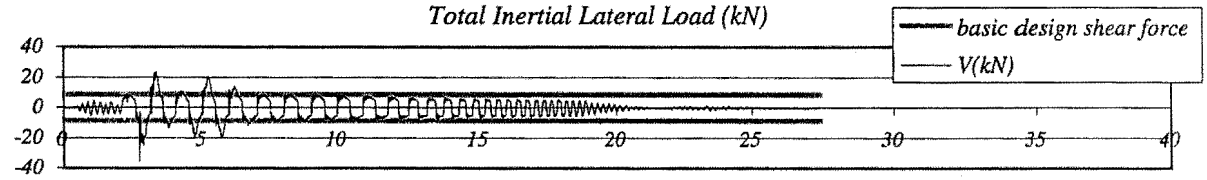

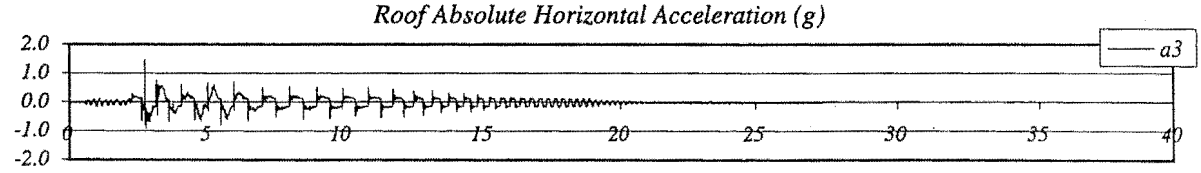

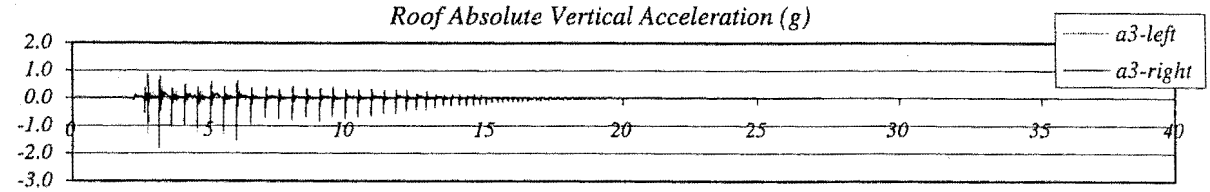

RUN # 54

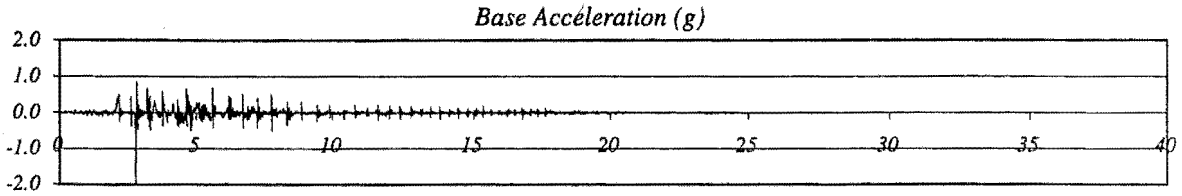

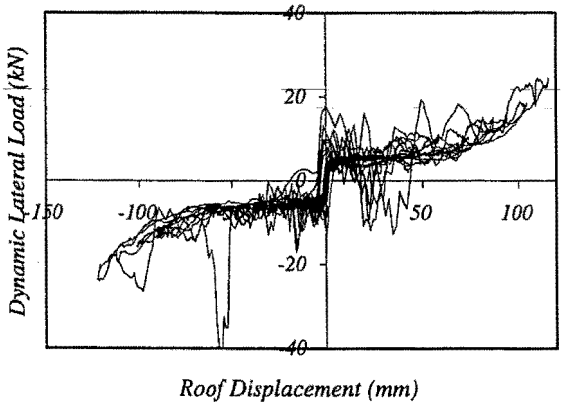

Wall without dissipators

Basic Input Ground Motion (BIGM):	*Sylmar 000*
Scaling Factor for BIGM:	1.00
Expected Peak Table Acceleration:	0.80 g
Measured Peak Table Acceleration:	2.00 g
Peak Roof Hor. Acceleration:	1.69 g
Peak Roof Vert. Acceleration:	2.69 g
Peak Roof Displacement:	122 mm
Peak Average Drift:	3.28 %
Residual Roof Displacement:	0 mm
Max. Total Inertial Lat. Load:	42.14 kN

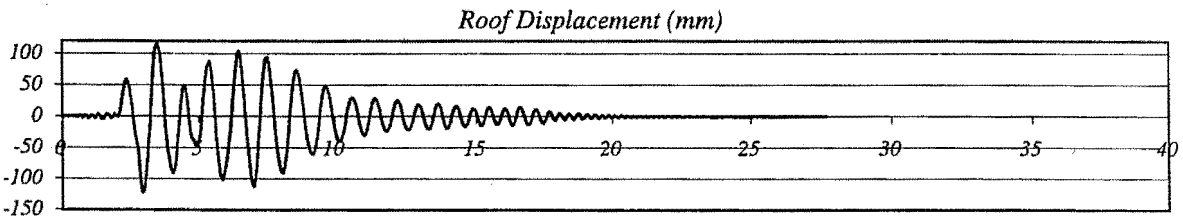

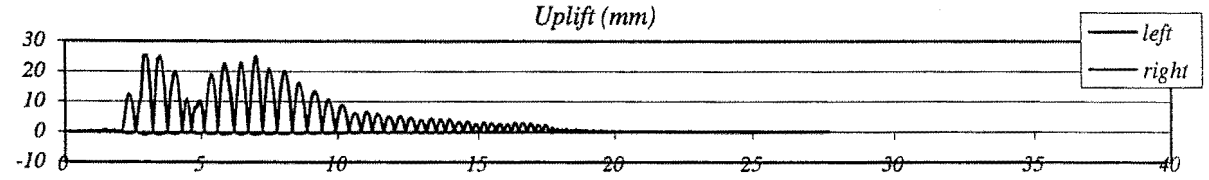

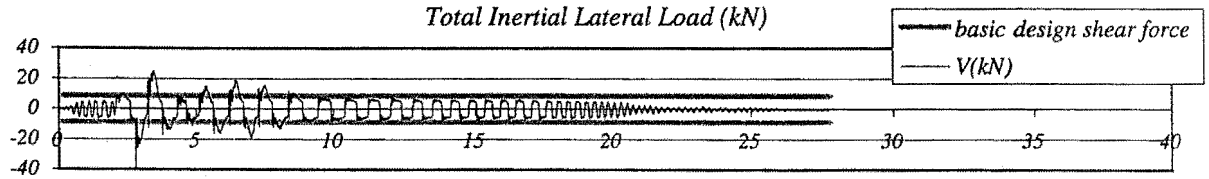

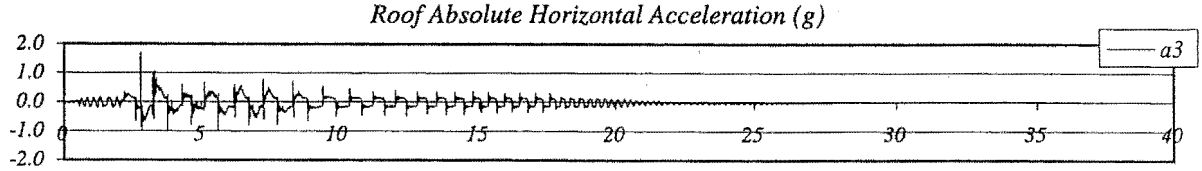

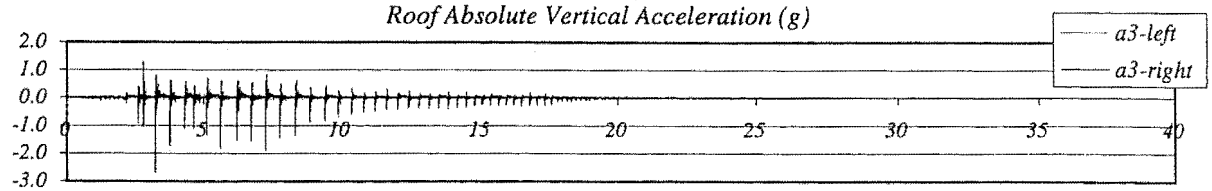

RUN # 55

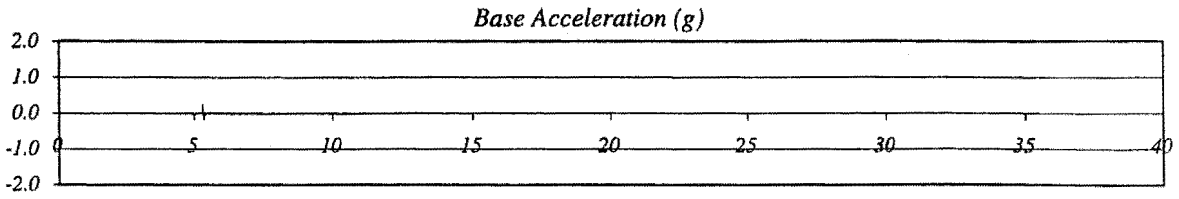

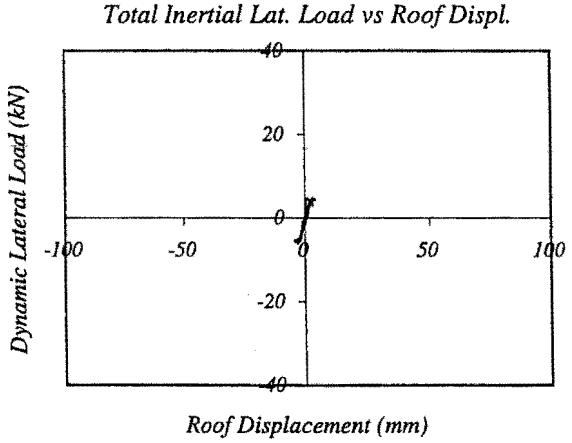

Wall without dissipators

Basic Input Ground Motion (BIGM):	*Half Sine Pulse*
Scaling Factor for BIGM:	NA
Expected Peak Table Acceleration:	NA g
Measured Peak Table Acceleration:	0.23 g
Peak Roof Hor. Acceleration:	0.20 g
Peak Roof Vert. Acceleration:	0.12 g
Peak Roof Displacement:	4 mm
Peak Average Drift:	0.11 %
Residual Roof Displacement:	0 mm
Max. Total Inertial Lat. Load:	6.29 kN

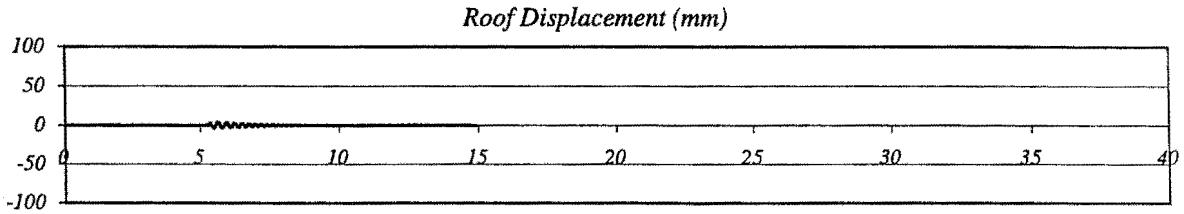

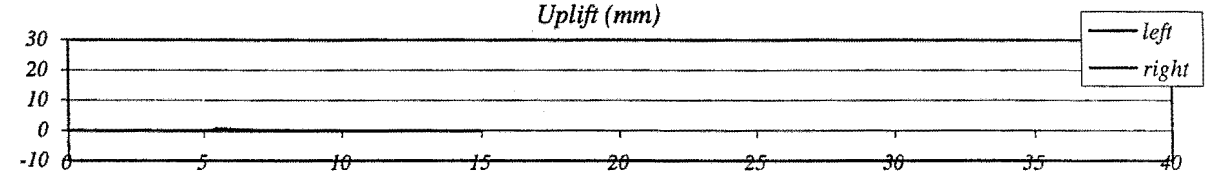

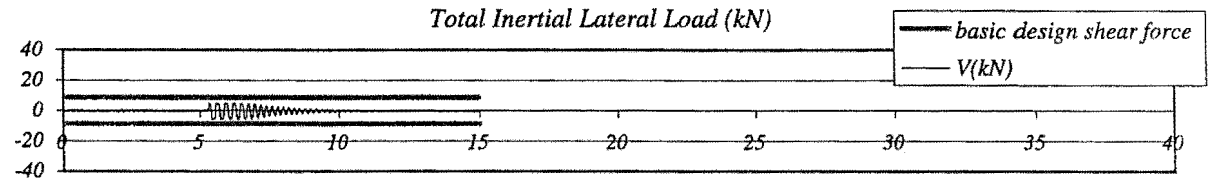

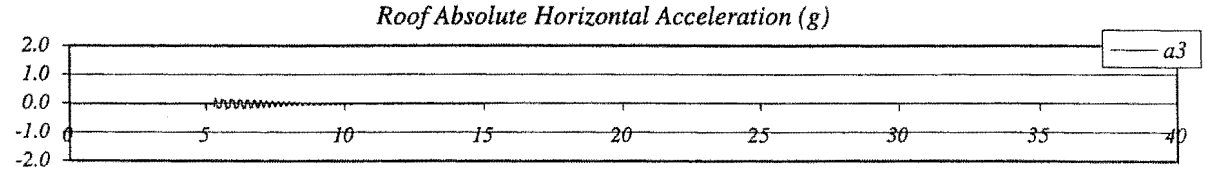

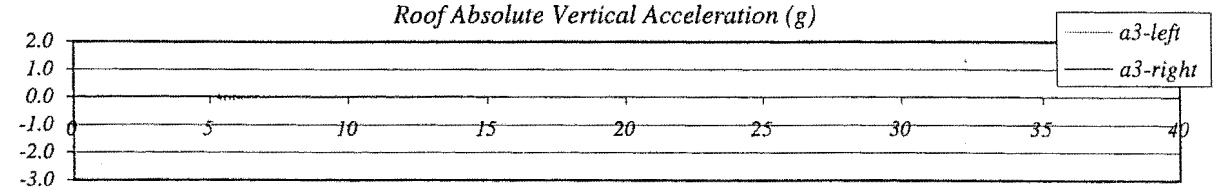

RUN # 56

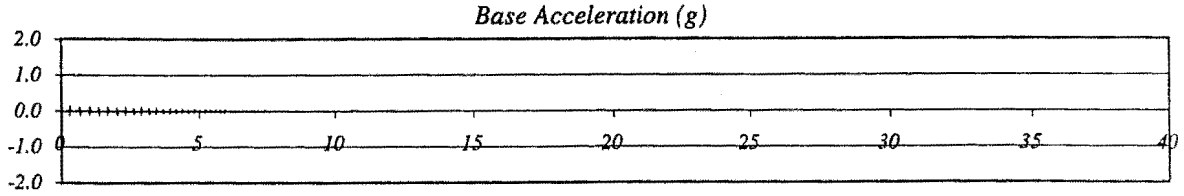

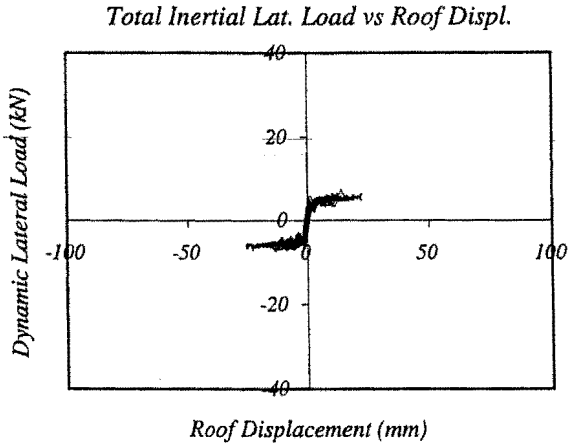

Wall without dissipators

Basic Input Ground Motion (BIGM):	*Half Sine Pulse*
Scaling Factor for BIGM:	NA
Expected Peak Table Acceleration:	NA g
Measured Peak Table Acceleration:	0.15 g
Peak Roof Hor. Acceleration:	0.45 g
Peak Roof Vert. Acceleration:	0.50 g
Peak Roof Displacement:	25 mm
Peak Average Drift:	0.67 %
Residual Roof Displacement:	0 mm
Max. Total Inertial Lat. Load:	7.43 kN

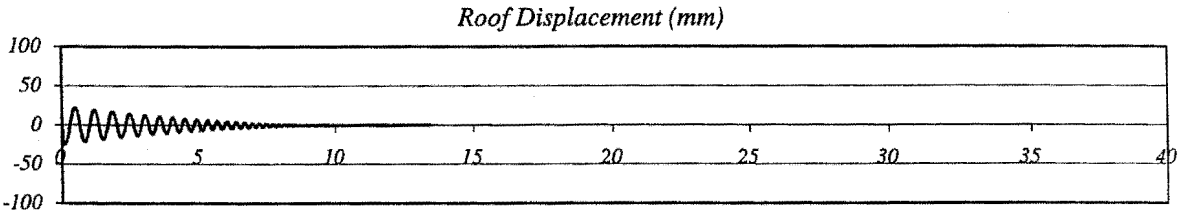

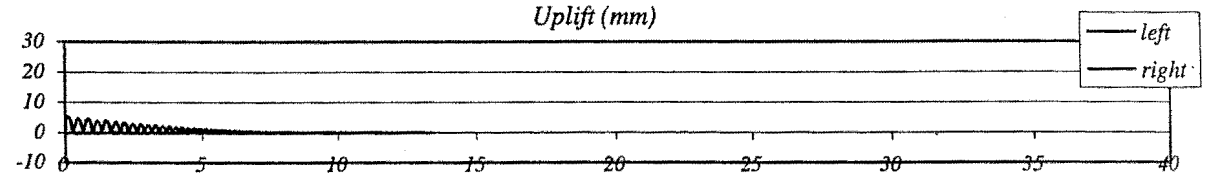

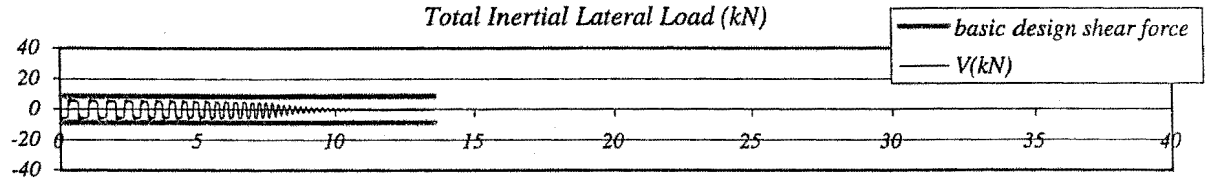

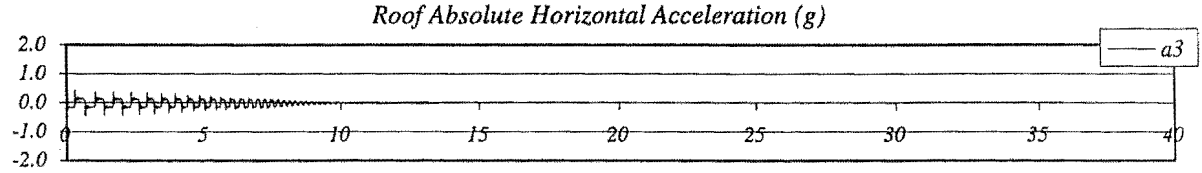

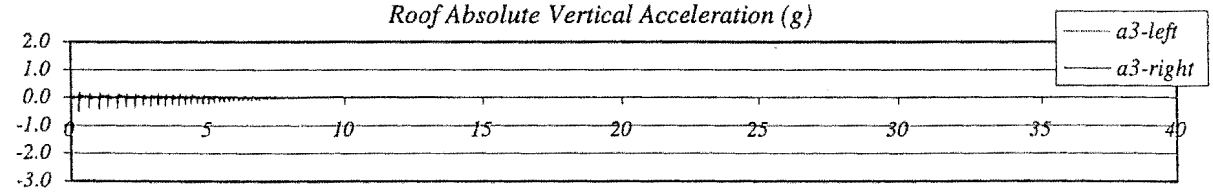

RUN # 57

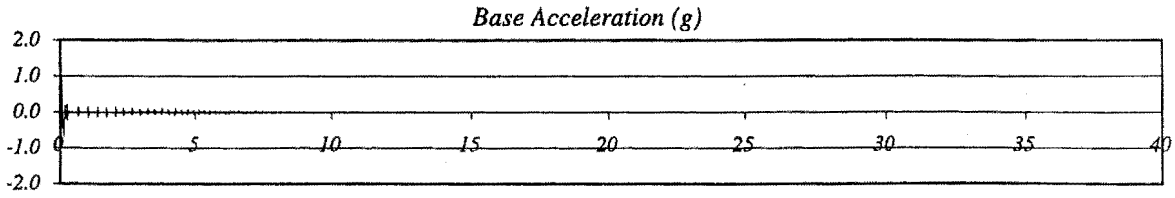

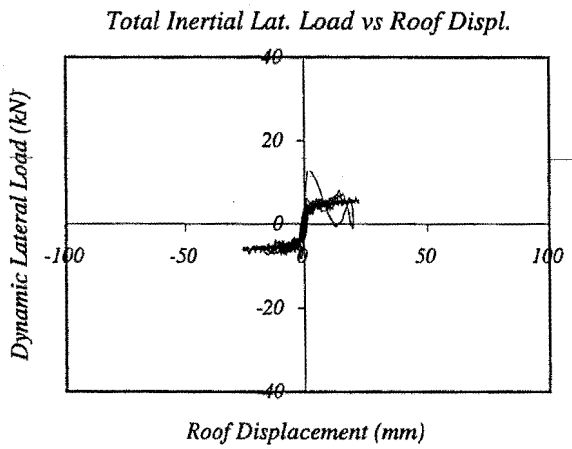

Wall without dissipators

Basic Input Ground Motion (BIGM):	*Half Sine Pulse*
Scaling Factor for BIGM:	NA
Expected Peak Table Acceleration:	NA g
Measured Peak Table Acceleration:	1.02 g
Peak Roof Hor. Acceleration:	0.49 g
Peak Roof Vert. Acceleration:	0.57 g
Peak Roof Displacement:	25 mm
Peak Average Drift:	0.68 %
Residual Roof Displacement:	0 mm
Max. Total Inertial Lat. Load:	13.53 kN

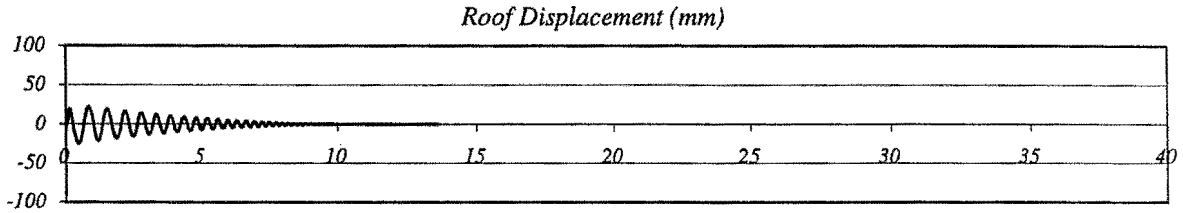

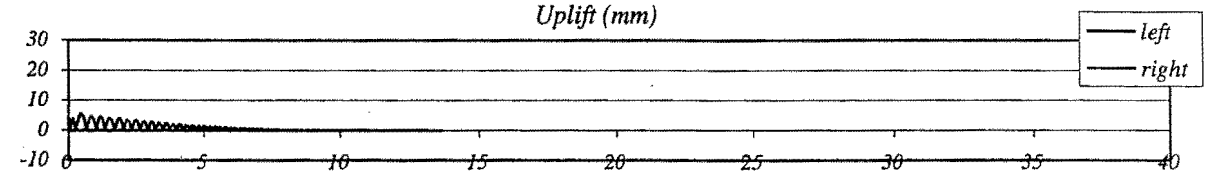

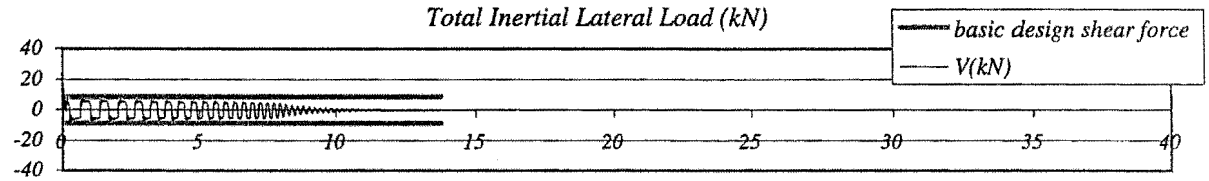

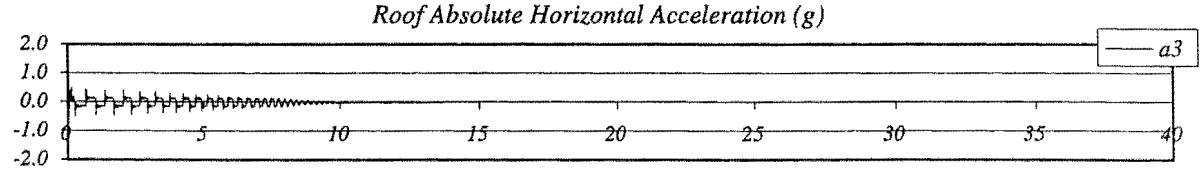

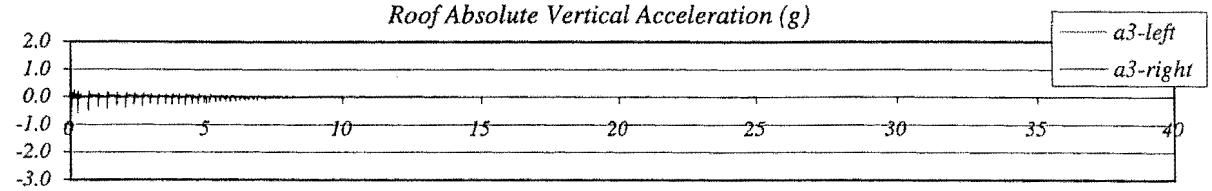

RUN # 58

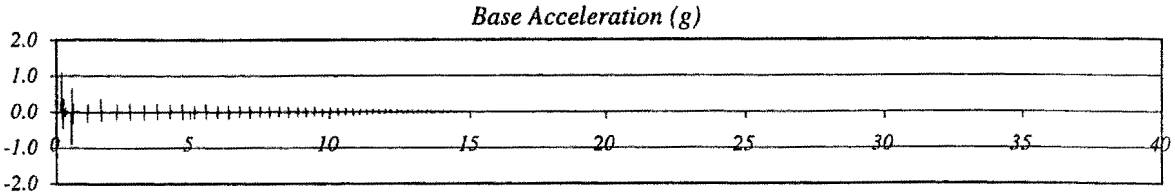

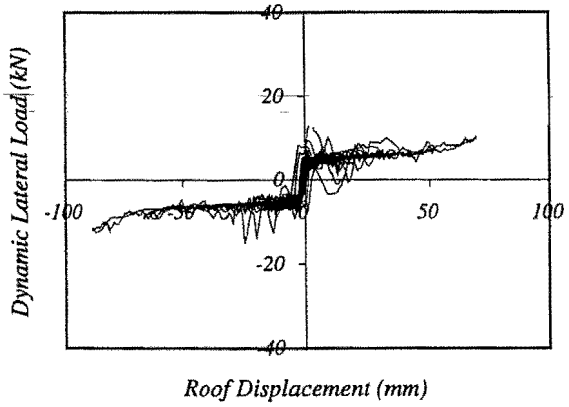

Wall without dissipators

Basic Input Ground Motion (BIGM):	*Half Sine Pulse*
Scaling Factor for BIGM:	NA
~~Expected Peak Table Acceleration:~~	~~NA g~~
Measured Peak Table Acceleration:	1.09 g
Peak Roof Hor. Acceleration:	1.04 g
Peak Roof Vert. Acceleration:	1.46 g
Peak Roof Displacement:	89 mm
Peak Average Drift:	2.38 %
Residual Roof Displacement:	1 mm
Max. Total Inertial Lat. Load:	15.05 kN

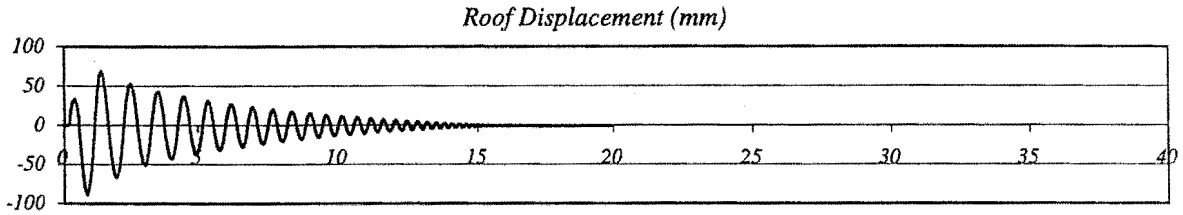

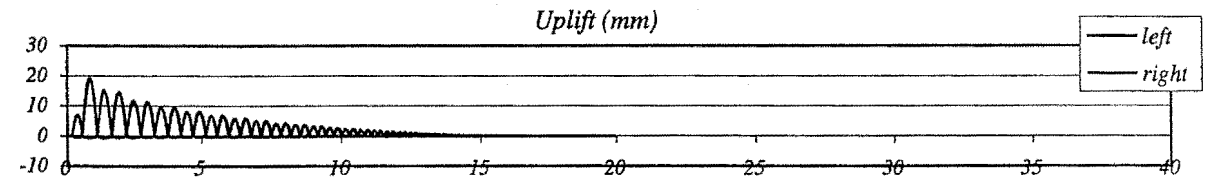

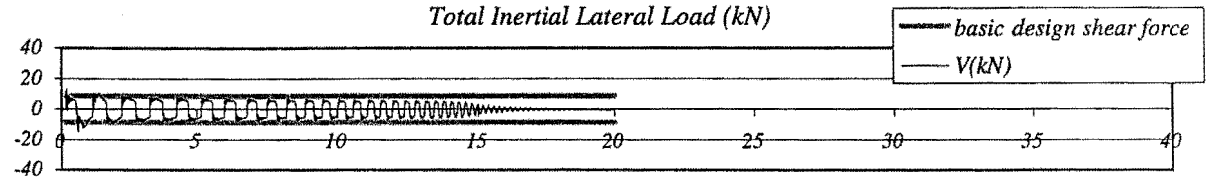

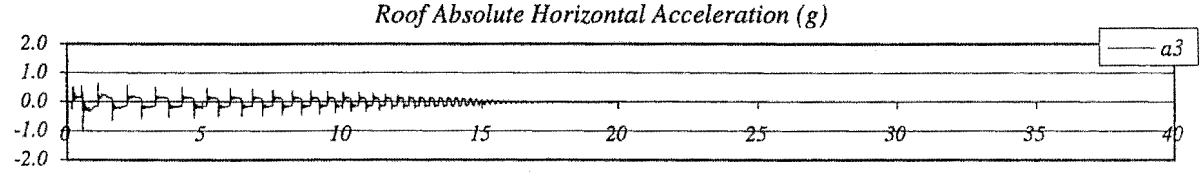

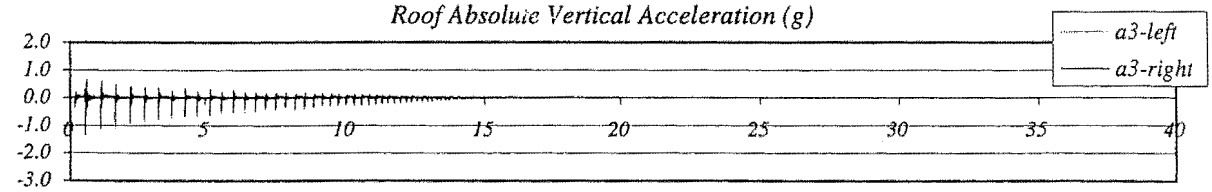

RUN # 59

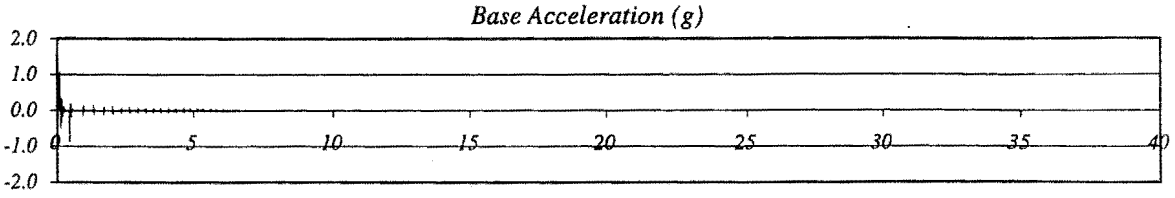

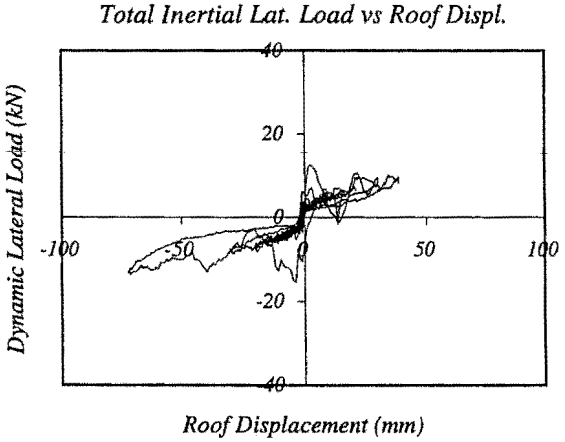

Wall with 2nd set of dissipators

Basic Input Ground Motion (BIGM):	*Half Sine Pulse*
Scaling Factor for BIGM:	NA
Expected Peak Table Acceleration:	NA g
Measured Peak Table Acceleration:	1.08 g
Peak Roof Hor. Acceleration:	0.47 g
Peak Roof Vert. Acceleration:	1.11 g
Peak Roof Displacement:	71 mm
Peak Average Drift:	1.92 %
Residual Roof Displacement:	1 mm
Max. Total Inertial Lat. Load:	15.42 kN

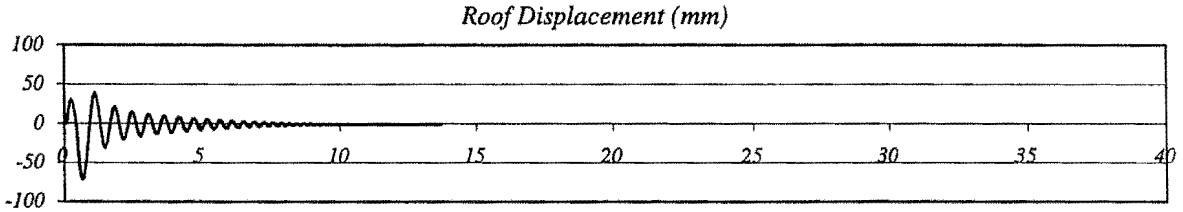

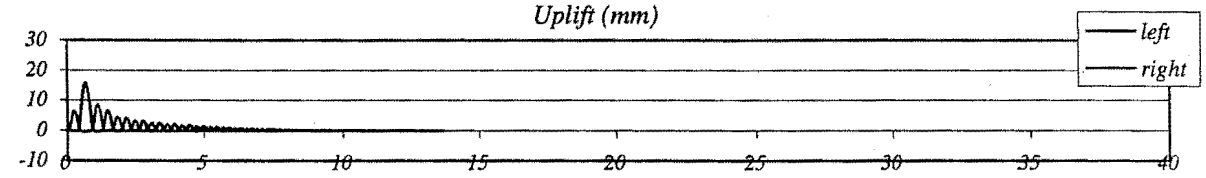

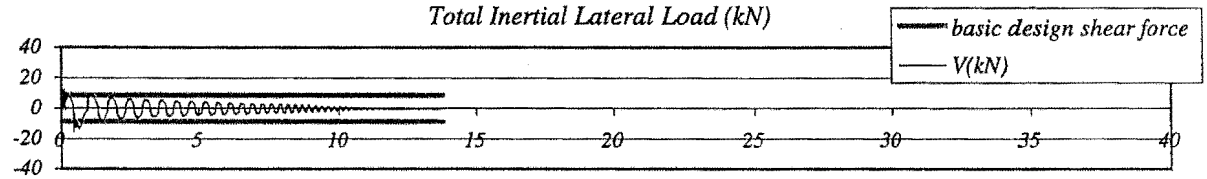

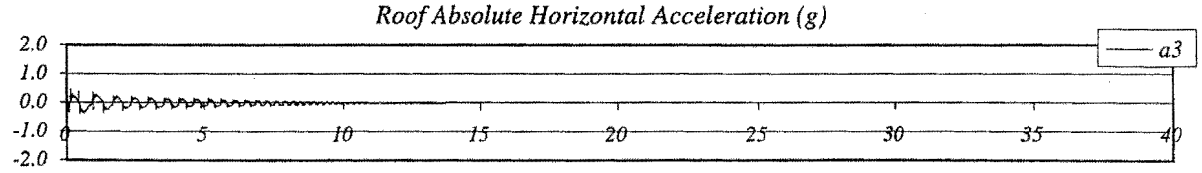

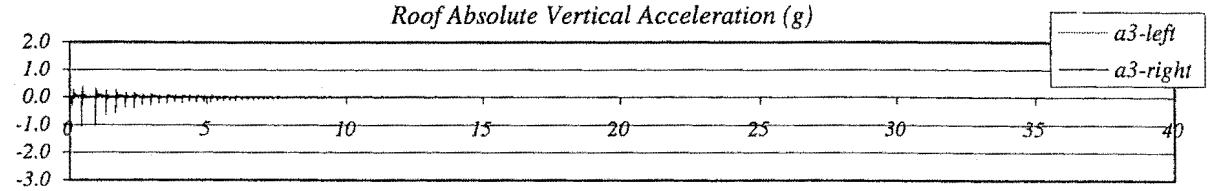

RUN # 60

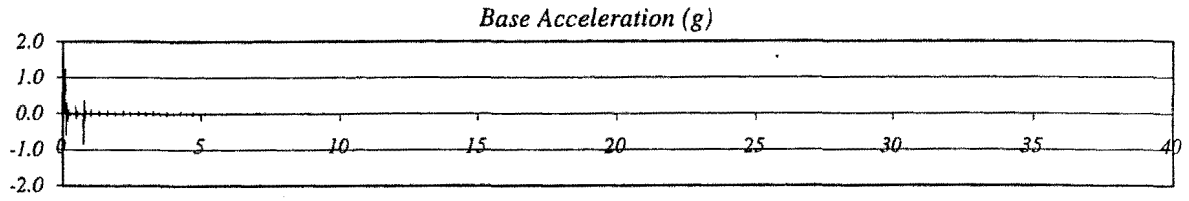

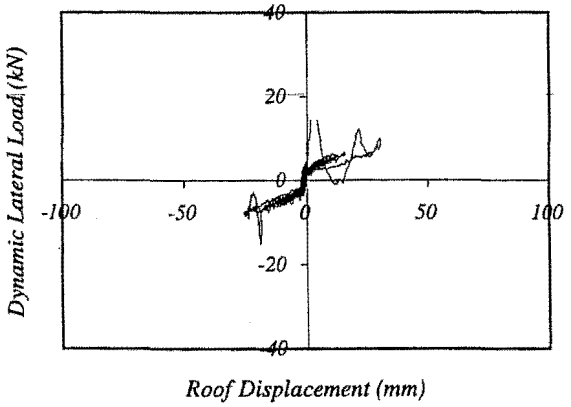

Wall with 2nd set of dissipators

Basic Input Ground Motion (BIGM):	*Half Sine Pulse*
Scaling Factor for BIGM:	NA
Expected Peak Table Acceleration:	NA g
Measured Peak Table Acceleration:	1.25 g
Peak Roof Hor. Acceleration:	0.54 g
Peak Roof Vert. Acceleration:	0.56 g
Peak Roof Displacement:	31 mm
Peak Average Drift:	0.82 %
Residual Roof Displacement:	1 mm
Max. Total Inertial Lat. Load:	16.03 kN